Seismic Assessment of Basement Walls in British Columbia

by

Elnaz Amirzehni

B.Sc., Civil Engineering, University of Tehran, Iran, 2006

M.Sc., Geotechnical Engineering, University of Tehran, Iran, 2009

A THESIS SUBMITTED IN PARTIAL FULFILLMENT
OF THE REQUIREMENTS FOR THE DEGREE OF

DOCTOR OF PHILOSOPHY

in

THE FACULTY OF GRADUATE AND POSTDOCTORAL STUDIES

(Civil Engineering)

The University of British Columbia

(Vancouver)

April 2016

Abstract

The current state of practice for seismic design of basement walls in Vancouver is based on the Mononobe-Okabe (M-O) method using a Peak Ground Acceleration (PGA) mandated by the National Building Code of Canada (NBCC, 2010). Because there is a little evidence of any significant damage to basement walls during major earthquakes, the Structural Engineers Association of British Columbia (SEABC) became concerned about designing the walls under the code-mandated PGA and set up a task force to review the current procedure for seismic design of basement walls in British Columbia. The University of British Columbia (UBC) was asked to carry out this investigation. This thesis aims to provide solid base for designing the basement walls using an appropriate fraction of the code-mandated PGA in the M-O analyses. To this end, a series of dynamic nonlinear soil–structure interaction analyses are conducted to examine the seismic resistance of typical basement walls designed according to current practice in BC, for different fractions of the code-mandated PGA (100% to 50%). The seismic responses of the walls are evaluated by subjecting them to ensembles of ground motions comprised of shallow crustal, deep subcrustal, interface earthquakes from a Cascadia subduction events and near-fault earthquake motions. Input motions are matched to the intensity of the seismic hazard using both spectral and linear scaling techniques. Representative 4-level and 6-level basement walls are analyzed. The nonlinear hysteretic response of the foundation soil is characterized in order to obtain realistic estimates of an interaction between the basement wall and the surrounding soil. In addition, the effects of the local site conditions in terms of geometrical and geological structure of soil deposits underlying the basement structure on the seismic performance of the basement walls are evaluated. The analyses show that current

engineering practice for designing basement walls based on the M-O method and using 100% PGA is too conservative. The analyses suggest that a wall designed using 50% to 60% PGA results in an acceptable performance in terms of drift ratio.

Preface

In 2010, the Structural Engineers Association of British Columbia (SEABC) initiated a voluntary task force to review current seismic design procedure for deep basement walls and the University of British Columbia (UBC) was asked to carry out this research. Prof. Finn and Drs. DeVall and Taiebat are members of this voluntary task force and together with Prof. Ventura are the members of the supervisory committee of this thesis. The present study aims to evaluate the performance of basement walls designed following the current state of practice in Vancouver and provide a basis for recommending an acceptable reduced design loads for basement wall. The seismic design of the basement walls presented was done by Dr. DeVall, R. H., senior consultant structural engineering at Read Jones Christoffersen Ltd., Vancouver, who is also a member of technical committee on basement walls at SEABC. The outputs of this thesis aid the advancement of the state of practice in this area.

I, Elnaz Amirzehni, am the principle contributor to all seven chapters of this thesis. I was responsible for all major areas of concept formation, data collection and analysis, and wiring the chapters. Some parts of the findings of this thesis have been published in a journal and three conferences so far.

- Amirzehni, E., Taiebat, M., Finn, W. D. L., and DeVall, R. H. (2015), "Ground motion scaling/matching for nonlinear dynamic analysis of basement walls", Proceedings of the 11th Canadian Conference on Earthquake Engineering. Victoria, BC, Canada, p. 10 pages.

  This paper includes a version of some sections in Chapter 6. I conducted all the numerical analyses and wrote the first draft of the manuscript. Prof. Finn and Dr. DeVall provided guidance throughout the evolution of the project and manuscript edits.

- Amirzehni, E., Taiebat, M., Finn, W. D. L., and DeVall, R. H. (2015), “Seismic performance of deep basement walls”, Proceedings of the 6th International Conference on Earthquake Geotechnical Engineering. Christchurch, New Zealand, p. Paper ID: 194, 8 pages.

  This paper includes a version of Section 5.4 in Chapter 5. I conducted all the numerical analyses and wrote the first draft of the manuscript. Prof. Finn and Drs. DeVall and Taiebat provided guidance throughout the evolution of the project and manuscript edits.

- Taiebat, M., Amirzehni, E., and Finn, W. D. L. (2014), “Seismic design of basement walls: evaluation of the current practice in British Columbia”, Canadian Geotechnical Journal, vol. 51, no. 9, pp. 1004-1020.

  This paper includes a version of some sections in Chapters 3 and 4. I conducted all the numerical analyses and wrote the first draft of the manuscript. Prof. Finn and Drs. Taiebat and DeVall provided guidance throughout the evolution of the project and manuscript edits.

- Amirzehni, E., Taiebat, M., Finn, W. D. L., and DeVall, R. H. (2013), “Effect of near-fault ground motions on seismic response of deep basement walls”, Proceedings of the 4th International Conference on Computational Methods in Structural Dynamics & Earthquake Engineering (COMPDYN 2013). Kos Island, Greece, p. 11 pages.

  This paper includes a version of some sections in Chapters 6. I conducted all the numerical analyses and wrote the first draft of the manuscript. Prof. Finn and Drs. Taiebat and DeVall provided guidance throughout the evolution of the project and manuscript edits.

  Additional papers are under preparation to publish the remainder of the thesis findings.

Table of Contents

List of Tables

List of Figures

Acknowledgments

Though only my name appears on the cover of this dissertation, a great many people have contributed to its production. I owe my gratitude to all those people who have made this dissertation possible and because of whom my graduate experience has been one that I will cherish forever.

Firstly, I would like to express my deepest gratitude to my research supervisor Prof. W.D. Liam Finn for his continuous support, patience, motivation, and immense knowledge. I have been amazingly fortunate to have an advisor who gave me the freedom to explore on my own, and at the same time the guidance to recover when my steps faltered. I could not have imagined having a better advisor and mentor and he is the one teacher who truly made a difference in my life.

I take this opportunity to sincerely acknowledge the support of Dr. John Howie for providing necessary infrastructure and resources to accomplish my research work. I am very much thankful to him for picking me up as a student at the critical stage of my Ph.D. program.

Besides my supervisor, I would like to thank the members of my thesis advisory committee: Dr. Ronald H. DeVall from Read Jones Christoffersen Consultants Ltd. and Prof. Carlos Ventura for their deep interest, support, dedication, passion, and insightful comments and encouragement, but also for the questions which incented me to widen my research from various perspectives. I am honored of having the opportunity of working with them. I would like to thank Prof. Geoffrey R. Martin from the Faculty of Civil and Environmental Engineering at the University of Southern California, Dr. Gregory A. Lawrence, from the Faculty of Civil Engineering at the University of British Columbia and Dr. Davide Elmo from the Norman B. Keevil Institute of Mining Engineering at the University of British Columbia for taking time out from their busy schedule to serve as my examiners.

Dr. Taiebat's insightful comments and constructive criticisms at different stages of my research were thought-provoking and they helped me focus my ideas. I am grateful to him for holding me to a high research standard and enforcing strict validations for each research result.

Most of the results described in this thesis would not have been obtained without a close collaboration with some people from early days of my research. My thanks go in particular to Dr. Ernest Naesgaard and Dr. Ali Amini from Naesgaard-Amini Geotechnical Ltd., Prof. Donald Anderson, and Prof. Peter Byrne with whom I started this work and many rounds of discussions on my project with them helped me a lot. I owe a great deal of appreciation and gratitude to Mr. Doug Wallis from Levelton Consultants Ltd. for his suggestions and guidance in geotechnical aspects of the project. Thanks also goes out to Dr. Armin Bebamzadeh for sharing his knowledge and experience.

I am ever indebted to Prof. Perry Adebar, Head of the Civil Engineering Department at the University of British Columbia, who helped me at the time of critical need and his moral support. Appreciation also goes out to Ms. Glenda Levins and Ms. Sylvia Margraff for all the instances in which their assistance helped me along the way.

My appreciation extends to all of my colleagues and friends who helped me immensely during the four-year Ph.D. journey. I am very grateful to my office-mates: Amin Rahmani, Sajjad Fayyazi, Speideh Ashtari, Gaziz Seidalinov, Andres Barrero, and Boris Kolev for our exchanges of knowledge, skills, and venting of frustration during my graduate program, which helped enrich the experience.

Most importantly, none of this would have been possible without the love and patience of my family. My family to whom this dissertation is dedicated to, has been a constant source of love, concern, support and strength all these years. I would like to express my heart-felt gratitude to my parents and my brother for their unconditional trust, timely encouragement, and endless patience and their generosity with their love and support despite the long distance between us. Last but not least, my loving, supportive, encouraging, and patient husband, Hessam, whose faithful support during the different stages of this Ph.D. is so appreciated.

Finally, I recognize that this research would not have been possible without the financial assistance of the Natural Sciences and Engineering Research Council of Canada (NSERC- PGS D and NSERC- CGS M), the Office of Graduate and Postdoctoral Studies at the University of British Columbia (Four Year Doctoral Fellowship), and the Department of Civil Engineering at the University of British Columbia (teaching assistantships, research assistantships, and Thurber Engineering Graduate Scholarship in Civil Engineering), and express my gratitude to those agencies.

Chapter 1

Introduction

Design is not just what it looks like and feels like. Design is how it works.
— Steve Jobs (1955-2011)

1.1 Overview

Deep basement walls constructed to utilize the underground parking, constitute an essential part of buildings and should be designed to resist the static and seismic induced lateral earth pressures during earthquakes. The seismic performance of basement walls is a complex soil–structure interaction problem that depends on many different parameters such as the nature of the earthquake ground motion, dynamic response of the backfill soil, and the flexural response of the wall.

The current state of practice for seismic design of basement walls in the United States (Lew, 2012; Lew et al., 2010b; Psarropoulos et al., 2005) as well as in British Columbia, Canada (DeVall et al., 2010) is generally based on the studies of Okabe (1924) and Mononobe and Matsuo (1929) known as the Mononobe-Okabe (M-O) method and incorporating the modification suggested by Seed and Whitman (1970) for estimating seismic pressures on the walls. In this limit-equilibrium force method, the earthquake thrust acting on the wall is a function of the Peak Ground Acceleration (PGA). The Mononobe-Okabe method is simple to use, but the validity and applicability of the method and its limiting assumptions have been questioned by researchers. Despite the limitations and uncertainties of the M-O method, it has been and continues to be widely used in practice for designing basement walls.

The seismic hazard level for design of buildings in an earlier version of the National Building Code of Canada (NBCC, 1995) had a probability of exceedance of 10% in 50 years (the 475 year earthquake), resulting in a PGA of 0.24 g for Vancouver. The more recent editions of the NBCC (2005, 2010) mandate a considerably different seismic hazard level with the probability of exceedance of 2% in 50 years (the 2475 year earthquake). Under the current code, the design PGA is about 0.46 g, almost double that of NBCC (1995). Adopting higher PGA leads the designers who have been using the M-O method for estimating the seismic lateral pressures to very large seismic forces that make the resulting structures expensive.

Lew et al. (2010a) and Sitar et al. (2012) reported on the performance of basement walls during past earthquake events inside and outside the United States and show that the failure is rare even though no particular seismic design was implemented. Based on their research no report of any damage to building basement walls has been found for the San Fernando (1971), Whittier Narrows (1987), Loma Prieta (1989), and Northridge (1994) earthquakes in the United States.

Due to the fact that there is no reported damage to the basement walls during the recent major earthquake events, the Structural Engineers Association of British Columbia (SEABC) became concerned about whether basement walls are being over-designed against the NBCC (2010) seismic hazard with the present design procedure. This led the SEABC to set up a task force to review current seismic design procedures for deep basement walls and the University of British Columbia was asked to carry out this research. This study was initiated in response to the SEABC request. The main purpose of this study is to capture the essential features of the seismic behavior of the basement wall systems and determine an appropriate fraction of PGA for Vancouver to be used in the M-O analysis to ensure a satisfactory performance in terms of moment and shear capacity and drift ratio along the height of the wall.

Various researchers have proposed the use of a reduced seismic coefficient less than the peak ground acceleration for the design of basement walls (Arulmoli, 2001; Lew et al., 2010b; Seed and Whitman, 1970; Sitar et al., 2012). Recent centrifuge modeling work by Al Atik (2008); Al-Atik and Sitar (2007, 2009) on model cantilever walls showed that estimating seismic lateral pressures utilizing the full peak ground acceleration overestimates the seismic earth pressure on cantilever retaining walls. To expand upon the work by Al-Atik and Sitar, additional centrifuge experiments were reported by Geraili Mikola (2012) at the University of California, Berkeley on non-displacing cross-braced basement wall structures founded on dry medium-dense sand. These results also confirm that the M-O pressures calculating using PGA are considerably higher than measured pressures and using the full PGA leads to very large seismic forces and very conservative design.

1.2 Objectives and scope

The first objective of this study is to develop a full-scale two-dimensional continuum model of soil–basement wall system, in which the walls are designed using the M-O procedure for various fractions of the NBCC (2010) PGA. The goal is to provide benchmark data for evaluating the state of practice for dynamic analysis of braced basement walls and to provide a basis for recommending an acceptable fraction of PGA for their seismic design. To this aim, a series of plane-strain nonlinear dynamic analyses have been conducted, taking into an account the flexibility and potential yielding of the wall components, to study the seismic performance of the basement walls designed for different fractions of PGA. This requires a comprehensive understanding of the interaction between the basement wall structure and the surrounding soil.

More specific components and features of this study are as follows:

- A 4-level basement wall structure is designed by members of the SEABC committee following the state of practice for six different values of the pseudo-static horizontal seismic coefficient varying from 100% down to 50% of the NBCC (2010) PGA (=0.46g). This results in a total of six walls.

- The designed walls and the surrounding soil domain are modeled in a fully coupled manner using a finite difference code, FLAC 7.0 (Itasca, 2012). Dynamic nonlinear soil–structure interaction analyses are then conducted on computational models of these basement walls to explore the capacity of the walls under seismic demand corresponding to an exceedance rate of 2% in 50 years for Vancouver.

- The soil layers of the computational model are simulated using the Mohr–Coulomb material model with non-associated flow rule. With insight from equivalent linear analyses of the soil system in the far field, degraded elastic modulus and equivalent damping ratios are also employed for a better representation of the soil system response in seismic loading.

- A suite of crustal ground motions are selected and the spectral matching method is used to modify the earthquake time histories to become compatible with the NBCC (2010) uniform hazard spectrum for Vancouver. In this fashion the variance of the structural responses is reduced and a platform to estimate the robust mean value of the response with fewer numbers of analyses is provided. Later on, the results will be compared with additional sensitivity analyses conducted using different linear scaling methods. The results show that spectral matching gives good estimates of the mean values.

- The seismic performance of the basement walls is presented in terms of the time history and envelope of lateral earth pressures along the height of the walls, lateral earth forces on the walls, envelopes of the bending moments and shear forces, and envelopes of lateral displacements and drift ratios. The results indicate that flexibility and deflection of the wall have important effects on the distribution of the seismic lateral pressures on the wall. The results of these analyses are used to evaluate an appropriate fraction of PGA to be used in the M-O analysis to have a satisfactory performance in terms of the resulting drift ratio along the height of the wall.

- A number of sensitivity analyses on different input parameters are also conducted, and the results are presented and discussed.

The second objective of this thesis is to provide additional analyses for further evidence to evaluate the recommended fraction of code mandated PGA that may be used with the M-O method for acceptable seismic performance of basement walls. To this end the following specific components and features are investigated:

- A more advanced constitutive model is used instead of a simple Mohr–Coulomb, to simulate nonlinear behavior of soils undergoing time-varying deformations caused by earthquake ground motions.

- Dynamic soil–structure interaction effects in the form of local site condition and the corresponding local amplification of strong ground motions due to shallow soft soil layers are investigated. The importance of the impedance contrast of underlying soil deposits and the depth of the underlying stiff soil layers on the seismic performance of the embedded structures are studied.

- The effect of geometric parameters of the basement wall structures on their seismic performance is investigated. To this aim two new sets of deep basement walls with different heights, thickness and configurations are designed for different fractions of code PGA and their performance under the full seismic demand in Vancouver are evaluated.

- In addition to shallow crustal earthquakes, deep subcrustal earthquakes and interface earthquakes from the Cascadia subduction event are added to the database to reflect three dominant seismic mechanisms in the Lower Mainland, Vancouver. Also the effect of near-fault pulse-like ground motions, which contain a short-duration pulse with high amplitude is investigated.

- In addition to the spectrally matched accelerograms used in benchmark analyses to estimate the robust mean values of the seismic response, different linear scaling methods are adopted to capture the inherent motion-to-motion variability of the basement wall responses subjected to a suites of earthquake ground motions under the seismic demand adopted by NBCC (2010) for Vancouver. The seismic performance of the basement walls in the form of drift ratio are evaluated and the level of variability of the response, quantified by a standard deviation, are presented. The results of these analyses using different scaling/matching techniques are compared to facilitate a decision on the more reliable scaling/matching technique to use for this problem.

1.3 Organization of dissertation

This dissertation consists of seven Chapters. Chapters two, three and four address the first aforementioned objective and Chapters five and six cover the second objective discussed in the previous section. The organization of the thesis for fulfilling the research objectives are as follows:

Chapter 2, The state-of-the-art for seismic design of the basement walls based on the current state of practice in British Columbia is presented in this chapter. The performance of basement walls during past major earthquake events as well as a summary of the building code provisions requirements for seismic design of basement walls are discussed. Also the assumptions and limitations of the M-O method are reviewed.

Chapter 3, A seismic design of a typical 4-level basement wall structure according to the state of practice in Vancouver for different fractions of the code PGA is described in this chapter. In order to assess the seismic performance of these walls, a series of two-dimensional nonlinear dynamic analyses have been set up using a finite difference platform, FLAC 7.0 (Itasca, 2012). Elements of the computational model, including the model building procedure, boundary conditions, interface elements, applied ground motions, and soil properties used in these analyses are described.

Chapter 4, The seismic performance of the 4-level basement walls described in Chapter 3 are evaluated using nonlinear dynamic analyses and are set as benchmark analyses. Typical results such as the time history and envelope of lateral earth pressures and lateral earth forces along the height of the walls, envelope of the bending moments, shear forces, lateral displacements and drift ratios are presented and discussed. Based on the results of these analyses, an appropriate fraction of PGA to be used in the M-O analysis is recommended to ensure a satisfactory cost-effective performance based on the limiting drift ratio along the height of the wall. In addition, the sensitivity of the findings to variations of adopted system parameters is evaluated.

Chapter 5, The 4-level basement wall described in Chapter 4 is analyzed using a more sophisticated and representative constitutive model than the simple

Mohr–Coulomb model which was used initially. Also this chapter provides an insight into dynamic soil–structure interaction effects as well as the local site effects on the seismic performance of basement walls. The effect of local site conditions defined by various shear wave velocity profiles on the seismic performance of the designed basement walls is investigated. This chapter also offers an evaluation on the influence of the wall geometry in terms of the wall's height, thickness and configuration on the seismic performance of basement walls by investigating a 4-level basement wall with a higher top level and a 6-level basement wall.

Chapter 6, This chapter provides an insight into the selection and scaling of a suite of earthquake accelerograms for time history analyses. This is one of the most important steps in any nonlinear dynamic history analysis and governs the result and amount of uncertainty in seismic design. Five intensity-based linear scaling methods, which preserve the variety of each ground motion are introduced and the full distribution of the structural responses in the form of standard deviation are presented. In this chapter four ground motion ensembles are considered; shallow crustal earthquakes, deep subcrustal earthquakes, interface earthquakes from a Cascadia subduction event and the near-fault pulse-like ground motions. The result of this study indicates that the spectrum matched results compare well (both mean and scatter) with reasonable and established linear scaling methods. The results also indicate that several other linear scaling methods introduce amounts of scatter viewed as unreasonable.

Chapter 7, A summary of key results and conclusions drawn from this research are presented in this chapter. Suggestions for future research are also provided.

Chapter 2

Literature review

If I have seen further it is by standing on the shoulders of Giants.
— Isaac Newton (1643–1727)

2.1 Introduction

The problem of evaluating seismically induced lateral earth pressures on retaining structures was first addressed in Japan after the Great Kanto Earthquake (1923) by Okabe (1926) and followed by Mononobe and Matsuo (1929). The Mononobe-Okabe (M-O) method is based on Mononobe and Matsuo's experimental studies on a small scale cantilever wall with a dry, medium dense cohesionless granular backfill excited by a one gravity ($1g$) sinusoidal excitation on a shaking table.

The M-O computational method was originally developed for gravity non-yielding walls retaining cohesionless backfill materials. It follows the procedure developed by the Coulomb (1776) theory of static soil pressures and is today, the most common approach in determining seismically induced lateral earth pressures due to its simplicity. Despite the uncertainties associated with this method, the current state of practice in British Columbia (DeVall et al., 2010) as well as in the United States (Lew, 2012; Lew et al., 2010b; Psarropoulos et al., 2005) is to use the M-O method incorporating the modification suggested by Seed and Whitman (1970) for estimating seismic pressures on the walls.

This Chapter summarizes the performance of basement walls during past major earthquake events in Section 2.2. A summary of the building code provisions in Canada as well as the United States for seismic design of basement walls are reported in Section 2.3. The state of practice in British Columbia for evaluation of seismic earth pressures on building basement walls as well as the applicability of the M-O method are discussed in Section 2.4. The areas of confusion and deficiency of the M-O method is covered in Section 2.5.

2.2 Performance of basement walls during past earthquake events

An extensive summary of reports on basement wall behavior under recent major earthquakes inside and outside the United States is presented in Lew et al. (2010a) and Sitar et al. (2012). The performance of basement walls during past earthquake events shows that the failure is rare even if the structures were not explicitly designed for earthquake loading.

Based on a search of literature by Lew et al. (2010a) and Sitar et al. (2012), the engineered building basement walls did not experience any damage in the major recent United States earthquakes. No reports of any damage to building basement walls have been found for the San Fernando (1971), Whittier Narrows (1987), Loma Prieta (1989), and Northridge (1994) earthquakes in the United States based on the documents published by Benuska (1990); Hall (1995); Holmes and Somers (1996); Lew et al. (1995); Murphy (1973); Stewart et al. (1994); Whitman (1991).

During the magnitude 7.0 Kobe earthquake (1995) in Japan no evidence of damage to building basement walls was reported (Lew et al., 2010a). Also damage to building basement walls were not reported during Kocaeli, Turkey (1999) earthquake by Youd et al. (2000). Huang (2000), Tokida et al. (2001) and Abrahamson et al. (1999) reported different types of retaining structures (gravity-type walls, geosynthetics-reinforced retaining walls, cantilever walls) damages during Chi-Chi, Taiwan (1999) earthquakes, but there is no report of failure or damage of building basement walls. As reported by Sitar et al. (2012), no significant damages or failures of retaining structures occurred in the Wenchuan earthquake in China (1998), or in the recent great subduction zone generated earthquakes in Chile

(2010) and Japan (2011).

2.3 Building code provisions requirement

The current edition of the National Building Code of Canada (NBCC, 2010), International Building Code (IBC, 2009) and the Minimum Design Loads for Building and Other Structures (ASCE/SEI 7-05, 2005; ASCE/SEI 7-10, 2010) require that basement walls be designed to resist increased lateral pressure associated with earthquake ground motions and the geotechnical investigation report shall include the determination of lateral pressures on basement walls due to earthquake motions.

The National Cooperative Highway Research Program (NCHRP) report (Anderson et al., 2008), European Standards for Design of Structures for Earthquake Resistance (Eurocode8-EN1998-5, 2004) and Canadian Highway Bridge Design Code (CAN/CSA-S6-06, 2014) refer to the work of Mononobe and Matsuo (1929) and Okabe (1924) for the design of cantilever walls. Also the current edition of the American Association of State Highway Officials for the Load and Resistance Factor Design for bridges (AASHTO LRFD, 2012) suggests allowing reduction in the seismic coefficient by 50% in the design of cantilever walls.

The NBCC (2010) Commentary J recommended the use of the M-O method for the design of basement walls and stated that these walls are normally considered non-yielding due to the restraints at the top and bottom of these walls, which prevent the small amount of movement required to develop minimum active earth pressures. NBCC (2010) refers to the National Earthquake Hazards Reduction Program report (NEHRP, 2000) for the seismic design of the basement walls. The latest editions of NEHRP Recommended Provisions for Seismic Regulations for New Buildings and Other Structures, NEHRP (2003) and NEHRP (2009) also known as FEMA 450 and FEMA 750 reports, respectively, provide a discussion of the seismic earth pressures on retaining structures for two main categories of walls:

- Yielding walls, which can move sufficiently to develop minimum active earth pressures. The amount of 0.002 times the wall height movement at the top of the wall is typically sufficient to develop the minimum active earth pressure. The simplified Mononobe-Okabe seismic coefficient analysis reasonably represents the dynamic lateral earth pressure increment for yielding retaining walls (Mononobe and Matsuo, 1929; Okabe, 1924).

- Non-yielding walls are rigid, fixed at the base and do not satisfy the movement condition. For these walls, NEHRP Recommended Seismic Provisions presents an elastic solution developed by Wood (1973) for a rigid non-yielding wall retaining a homogeneous linear elastic soil and connected to a rigid base. The dynamic thrust, ΔP_E, is calculated using the following equation with the point of application at a height of 0.6H above the base of the wall:

$$\Delta P_E = k_h \gamma H^2 \tag{2.1}$$

where γ is the unit weight of soil , H is the retaining wall height, and k_h in the horizontal ground acceleration divided by gravitational accelaration.

The two aforementioned methods cover two extreme cases. One is the limit-equilibrium method assumes rigid plastic behavior, while the other one is the elastic approach that treats the soil as a visco-elastic continuum. NEHRP Recommended Seismic Provisions refers to the work of Ostadan (2005) and suggests that dynamic earth pressure solutions would lead to the results that correspond in magnitude to the Mononobe-Okabe solution as a lower bound and the Wood (1973) solution as an upper bound, which is as much as 2 to 2.5 times greater than the M-O approach.

The earlier versions of the National Earthquake Hazards Reduction Program (NEHRP, 2000, 2003) and the more recent edition (NEHRP, 2009) refer to the works of Lam and Martin (1986), Veletsos and Younan (1994*a*), Veletsos and Younan (1994*b*), and Ostadan (2005) among others, which argue that the earth pressures acting on the walls of partially embedded structures (e.g., basement walls) during earthquakes are primarily governed by soil–structure interaction, and thus these walls should not be treated as non-yielding. Sitar et al. (2012) argued that deep basement walls constructed in open excavations that are generally shored, cause the retained backfill soil to be in a yielded (active) condition already. In addition centrifuge tests of Sitar et al. (2012) confirm that the solutions provided for non-yielding walls, such as the one by Wood (1973), grossly overestimate the seismic pressures on basement-type walls and would result in wall designs that are much thicker with more steel reinforcement than those commonly used.

Veletsos and Younan (1997) and Younan and Veletsos (2000) conducted a study on dynamic response of flexible cantilever retaining walls and state that the flexibility of the wall and the rotational compliance at its base are the main reasons for a substantial drop of resultant force from a rigid solution. Gazetas et al. (2004) addressed a couple of other phenomena which lead to a further reduction of dynamic thrust acting on several types of flexible retaining systems. One is the elastic non-homogeneity of the backfill soil which results in a reduction of soil stiffness due to its softening in large shearing and the nonlinear soil–wall interface behavior. Inelastic soil behavior and the frequency content of the ground motion are another reasons for a further reduction of dynamic wall pressure to the values which may only be a fraction of the M-O. For all these reasons along with its simplicity, the M-O method became the most widely used method of analysis of seismic earth pressure in practice.

In the light of the fact that there is no evidence of basement wall failure during the recent major earthquake events, the review of literature suggest that using PGA as a seismic coefficient in the M-O method is overly conservative. However codes have not recommended values less than PGA. This maybe because most of the researches which support the reduction by using fraction of PGA are fairly recent and have not been generally embraced by practice yet. For example the FEMA 450 and FEMA 750 limited the M-O method to yielding walls and suggest using Wood (1973) formula for calculating pressures against non-yielding walls such as basement walls, but neither one of them suggest reducing seismic pressure by reducing PGA. The present study, which is conducted using nonlinear dynamic analyses, examines the seismic resistance of basement walls designed according to current practice in British Columbia, but using fractions of the code PGA (100% to 50%) as a seismic coefficient. The seismic response of all these walls are all evaluated by subjecting them to ensembles of earthquake motions comprise of crustal, subcrustal, subduction and near-fault earthquake ground motions that match the hazard intensity of the current Building Code (NBCC, 2010). The prime objective of this study is to provide solid bases for designing the basement walls using an appropriate fraction of the code PGA in the M-O analyses.

2.4 State of practice in British Columbia

The current state of practice for the seismic design of basement walls in British Columbia is generally based on the M-O method but incorporating the modification advanced by Seed and Whitman (1970), which is referred to as ”the modified M-O method” in this study.

The M-O method is a limit-equilibrium force approach, developed by including the inertial forces due to ground motions into the Coulomb (1776) theory of static earth pressure on retaining walls. This method was developed for dry cohesionless materials. It is assumed that a rigid wall moves sufficiently to produce minimum active (or maximum passive) pressures. The M-O method does not consider the kinematic and dynamic behavior of the structure, backfill and foundation soil due to the earthquake excitation and instead the complex transient ground shaking is represented by pseudo-static accelerations in horizontal and vertical directions. It is assumed that the soil behind the wall behaves as a rigid body so the pseudo-static acceleration can be applied uniformly throughout the mass. Therefore, in addition to the forces that exist under static conditions, the wedge is also acted upon by horizontal and vertical pseudo-static forces whose magnitudes are related to the mass of the wedge by the pseudo-static accelerations: $a_h = k_h g$ and $a_v = k_v g$, where k_h and k_v are the horizontal and vertical components of an earthquake excitation, respectively.

The forces acting on an active wedge in a dry, cohesionless backfill are shown in Figure 2.1. By applying pseudo-static accelerations to a Coulomb active wedge, the pseudo-static soil thrust is calculated from force equilibrium of the wedge. The total (static + dynamic) active lateral force during earthquake, P_{AE}, is expressed as:

$$P_{AE} = 0.5\gamma H^2 K_{AE}(1 - k_v) \tag{2.2}$$

where γ is the unit weight of soil and H is the retaining wall height. The dynamic active earth pressure coefficient, K_{AE}, is given in textbooks on soil dynamics (Kramer, 1996; Prakash, 1981; Towhata, 2008) as:

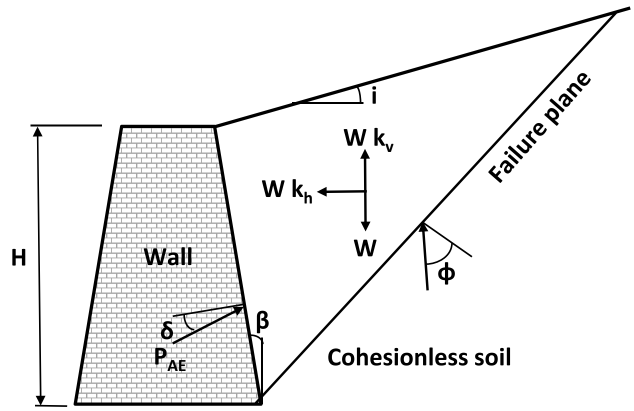

Figure 2.1: Forces considered in the Mononobe-Okabe analysis.

$$K_{AE} = \frac{\cos^2(\phi-\psi-\beta)}{\cos^2\beta\cos\psi\cos(\delta+\beta+\psi)\left(1+\sqrt{\frac{\sin(\delta+\phi)\sin(\phi-\psi-i)}{\cos(\delta+\beta+\psi)\cos(i-\beta)}}\right)^2} \tag{2.3}$$

In this equation ϕ and δ represent the angle of internal friction of the backfill soil and the angle of interface friction between the wall and the soil, respectively. i is the slope of the ground surface behind wall and β is the slope of the back of the wall with respect to vertical alignment. ψ is calculated as $\psi = \arctan[k_h/(1-k_v)]$ with the limitation of $\phi - \beta \geq \psi$. In this equation k_h and k_v are the horizontal and vertical ground acceleration divided by gravitational acceleration, respectively. If the pseudo-static accelerations are set to zero, Equations 2.2 and 2.3 will give the Coulomb static active lateral force, P_A, and the static active earth coefficient, K_A, respectively.

The M-O method provides only the magnitude of the total lateral force during an earthquake, P_{AE}. This method does not give the distribution of lateral earth pressure and the point of application of the seismic force. Several analytical and experimental studies have been conducted to investigate the distribution of the lateral earth pressures and its corresponding point of application due to earthquake loading. (Al Atik, 2008; Bolton and Steedman, 1985; Gazetas et al., 2004; Geraili Mikola, 2012; Ichihara and Matsuzawa, 1973; Lam and Martin, 1986; Ortiz et al., 1983; Prakash and Basavanna, 1969; Seed and Whitman, 1970; Sherif and Fang, 1984; Sherif et al., 1982; Sitar et al., 2012; Stadler, 1996; Steedman and Zeng, 1990; Whitman, 1991).

For practical purposes, Seed and Whitman (1970) proposed to separate the total (static + dynamic) active lateral force, P_{AE}, into two components: the initial active static component, P_A, and the dynamic increment due to the base motion, ΔP_{AE}, where $P_{AE} = P_A + \Delta P_{AE}$ as illustrated in Figure 2.2. The static thrust calculated from the Coulomb theory is applied at $H/3$ from the base of the wall, resulting in a triangular distribution of pressure. As Seed and Whitman (1970) stated, most of the investigators agree that the increase in lateral pressure due to the shaking, $\Delta p_{AE}(z)$, is greater near the top of the wall and the resultant increment in force acts at a height varying from $H/2$ to $2H/3$ above the base of the wall. Seed and Whitman (1970) in particular recommended that the resultant dynamic thrust be applied at $0.6H$ above the base of the wall (i.e., inverted triangular pressure distribution). It is worth to mention that in this approach dry cohesionless backfill material is assumed.

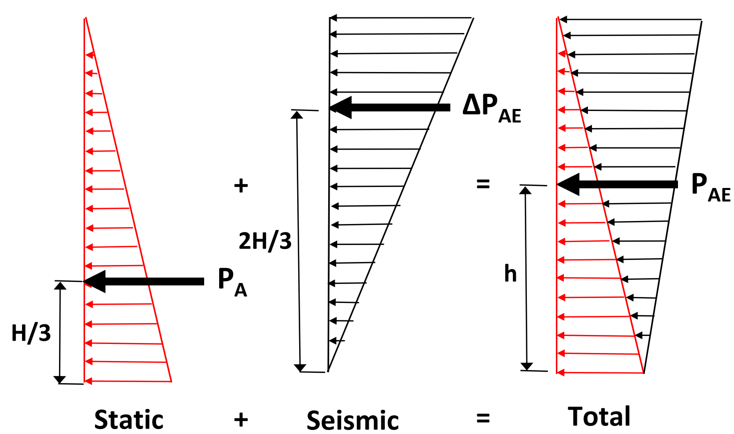

Figure 2.2: State of practice for seismic design of the basement walls in British Columbia using the modified M-O method.

The state of practice in British Columbia (DeVall et al., 2010) is to apply the ΔP_{AE} at height $2H/3$ above the base of the wall, resulting in an inverted triangular distribution of pressure. On this basis, the total thrust will act at a height $h = [P_A(H/3) + \Delta P_{AE}(2H/3)]/P_{AE}$ above the base of the wall. The value of h depends on the relative magnitudes of P_A and ΔP_{AE}, and it often ends up near the mid-height of the wall. This method as presented in Figure 2.2 hereinafter will be referred to as "the modified M-O method".

As presented in Equations 2.2 and 2.3, the earthquake thrust acting on the wall is a function of the horizontal and vertical ground seismic coefficients. The M-O analyses show that k_v, when taken as one-half to two-thirds the value of k_h, affects P_{AE} by less than 10% (Kramer, 1996). As stated by Seed and Whitman (1970), for most earthquakes *"the horizontal acceleration components are considerably greater than the vertical acceleration components"*, thus the vertical component (k_v) could be neglected for practical purposes. Another reason for neglecting vertical loading is attributed to the fact that the *"higher frequency vertical accelerations will be out of phase with the horizontal accelerations and will have positive and negative contributions to wall pressures, which on average can reasonably be neglected for design"* as stated in the National Cooperative Highway Research Program (NCHRP) report (Anderson et al., 2008). Gazetas et al. (2004) concluded that even simultaneous vertical acceleration does not have any noticeable effect on the distribution of the dynamic pressure and consequently the resultant deformation on the wall. Due to all these facts the current state of practice in British Columbia is to use the PGA as the horizontal acceleration and ignore the vertical acceleration in the M-O method.

Finally it should be noted that consideration of a passive pressure cut–off would change the design pressure distribution on the wall near the ground surface. However, according to the Structural Engineers Association of British Columbia (SEABC) pressure cut–off is not being used among practitioners in current design practice of basement walls in British Columbia. As this study is focused on the evaluation of basement walls designed based on the current practice, pressure cut–off is ignored in their seismic design.

The M-O method is a simple and powerful tool for evaluating the seismic earth pressure, but it is based on an experimental study of a small scale cantilever wall with a dry, medium dense cohesionless granular backfill excited by 1g sinusoidal excitation on shaking table and does not scale very well with the size of actual walls. Numerical studies conducted by Green et al. (2003) on cantilever retaining wall-soil system using the FLAC modeling tool showed that at very low levels of acceleration, the seismic earth pressures are in agreement with the M-O predictions, whereas at high levels of acceleration the M-O method may lead to unconservative estimates of the dynamic earth pressures. On the other hand, Gazetas et al. (2004) performed a series of finite element analyses on different types of flexible retaining walls subjected to earthquake motions of either high or moderately low dominant frequencies with PGA of 0.40 g and relatively short duration. They analytical studies and field observations suggested that the M-O method is conservative, if not overly conservative. Brandenberg et al. (2015) addressed these conflicting findings based on different approaches and assumptions regarding system behavior and conducted a kinematic soil–structure interaction using spring models for evaluating seismic earth pressures on buried rigid U-shaped structure.

There are number of concerns associated with the M-O approach which raise questions about the applicability of this method for evaluating the seismic earth pressures on the basement walls (Lew, 2012; NEHRP, 2009; Ostadan and White, 1998). For instance, in basement walls the horizontal movements are often limited due to the presence of floor slabs and the fact that the development of limit-state condition is unlikely. Besides since most deep basement walls are not cantilevered but braced, the applicability of the M-O method can be questioned. In this method the PGA is the only representative of the frequency content of the ground motion, which is not a good indicator of the characteristics and energy content of the motion especially at important frequencies. Arulmoli (2001) recommended the use of the M-O method and stated its unrealistic seismic earth pressure estimation in the case of large ground acceleration. In addition, in this method the dynamic nonlinear behavior of the soil undergoing time-varying deformations caused by earthquake ground motions are not considered and appropriate dynamic properties of the soil, such as the shear wave velocity, are not taken into an account.

Another major area of deficiency in the M-O method is that it is just applicable to the cohesionless soils. The National Cooperative Highway Research Program (NCHRP) report (Anderson et al., 2008) provides design charts and guidelines to account for cohesion in practical design problems. Candia (2013) conducted scaled centrifuge tests on braced U-shaped wall or basement-type wall and a freestanding cantilever wall founded in low plasticity cohesive soils. It was concluded that even a small amount of cohesion can reduce the seismic pressure acting on the wall significantly and proposed that the horizontal ground acceleration can be reduced by one-half to two-third of the PGA, depending on the different wall configuration.

Despite all these concerns about the M-O method, this approach has been used widely in practice and has been recommended by documents such as the NEHRP (2000, 2003, 2009).

2.5 Seismic coefficient in basement wall design

The M-O equation is used by practitioners for a pseudo-static analysis of all types of retaining walls including basement walls. Despite the recent advances in computational technology, sophisticated and time consuming dynamic analysis may not be feasible for routine design practice and professionals may continue to use the simple M-O approach for seismic design of basement structures. Hence the key question to be addressed is: what seismic coefficient k_h should be used in the M-O method to obtain a reasonable and acceptable performance.

Over time there have been studies suggesting that the M-O method may lead to conservative estimates of the dynamic earth pressures (Al Atik, 2008; Clough and Fragaszy, 1977; Gazetas et al., 2004; Koseki et al., 1998; Lew et al., 2010b). By increasing the awareness of seismic risks and moving towards the performance-based design, the practitioners found that designing the walls using the M-O seismic forces would result in an expensive and over-conservative design. There are some well-documented case histories that confirm retaining structures designed only for static loading can stand remarkably well under seismic loading with PGA up to 0.5 g (Clough and Fragaszy, 1977; Gazetas et al., 2004). Similar conclusion were made by Seed and Whitman (1970) that the wall designed to a reasonable static factor of safety (e.g. 1.5) should be able to resist seismic loads up to 0.3 g. They observed that the peak ground acceleration occurs for only one instant of time and does not have sufficient duration to cause significant wall movements. Therefore an effective acceleration equal to 85% of the peak value was suggested to be used in wall design. Seed and Whitman (1970) also stated that "*many walls adequately designed for static earth pressures will automatically have the capacity to withstand earthquake ground motions of substantial magnitudes and in many cases, special seismic earth pressure provisions may not be needed.*"

The major challenge for design is to select an appropriate seismic coefficient. Based on the evidence from shaking table and centrifuge tests reported by Whitman (1991) and subsequent regulatory guidance from documents such as the NEHRP (2000, 2003, 2009), it is recommended that except where structures were founded at a sharp interface between soil and rock, the M–O method should be used with an actual expected PGA that is consistent with the design earthquake ground motions. NEHRP (2009) states that *"... In the past, it was common practice for geotechnical engineers to reduce the instantaneous peak by a factor from 0.5 to 0.7 to represent an average seismic coefficient for determining the seismic earth pressure on a wall. The reduction factor was introduced in a manner similar to the method used in a simplified liquefaction analyses to convert a random acceleration record to an equivalent average series of cyclic loads. This approach can result in confusion on the magnitude of the seismic active earth pressure and, therefore, is not recommended. Any further reduction to represent average rather than instantaneous peak loads is a structural decision and must be an informed decision made by the structural designer...*".

Further justification for the use of a reduced seismic coefficient comes from the Federal Highway Administration (FHWA) (1997) for the design of highway structures. This document states that "*...for retaining walls wherein limited amounts of seismic deformation are acceptable, use of a seismic coefficient between one-half to two-thirds of the peak horizontal ground acceleration divided by gravity would appear to provide a wall design that will limit deformations in the design earthquake to small values...*". Arulmoli (2001) commented on the use of the M-O method and stated that the M-O method *"blows up"* for cases of large ground acceleration. Lew et al. (2010b) in his report mentioned that "*... in practice, many geotechnical engineers have been using a seismic coefficient that is less than the expected peak ground acceleration for the design of building basement walls and other walls...*". Seed and Whitman (1970) suggested 0.85 PGA as an effective acceleration in their paper.

In practice many geotechnical engineers have been using a horizontal acceleration less than the PGA for the design of basement walls. The seismic coefficient of one-half and 0.67 of the horizontal peak ground acceleration are used by practitioners for designing the walls with limited deformations as reported by Lew et al. (2010b) and Sitar et al. (2012), respectively. Lew et al. (2010b) associated the reduction to the fact that the M-O method is a pseudo-static approach of analysis that uses a pseudo-static coefficient to represent earthquake loading. Also in order to take into an account the repeatable nature of ground motions, Lew et al. (2010b) suggested a reduction based upon the use of an effective ground acceleration rather than an isolated peak ground acceleration. They also proposed to take into an effect a reduction to account for the averaging of the lateral forces on the retaining wall over the height of the wall.

The M-O method was originally developed for a medium dense cohesionless backfill soil. As in the real world even the most natural cohesionless soils have some fine content that often contributes to cohesion (Anderson et al., 2008) which would have a significant effect in reducing the dynamic active pressure for design.

The results of the dynamic centrifuge tests conducted over the past decades on model retaining walls with dry cohesionless backfills were compared with the results of the original M-O method by Bolton and Steedman (1985); Conti et al. (2012); Dewoolkar et al. (2001); Ortiz et al. (1983); Stadler (1996); Steedman and Zeng (1991). Most of these researchers concluded that the earth pressure determined by the M-O method gives adequate results, whereas the point of application of the dynamic thrust has been the subject of a continuing discussion. Stadler (1996) concluded that the incremental dynamic lateral earth pressure profile ranges between triangular and rectangular and suggested using a modified magnitude of seismic coefficient by reducing them to magnitudes ranging from 20% to 75% of the M-O method.

Recent centrifuge modeling works by Al Atik (2008) and Al-Atik and Sitar (2007) on stiff and flexible model cantilever walls with medium dense dry sand backfill suggested that estimating seismic lateral pressures using the M-O method and utilizing the full peak ground acceleration overestimates the seismic earth pressure forces for some structures. Later on Al-Atik and Sitar (2009, 2010) developed relationships for the dynamic increment in earth pressure coefficient (ΔK_{ae}) computed from the dynamic earth pressures at the time of maximum wall moments. Their experimental data suggest that seismic loads higher than 0.4 g could be resisted by cantilever walls designed to an adequate factor of safety and the dynamic earth pressures are insignificant for low levels of shaking (PGA less than 0.4 g). This observation is consistent with the observations and analyses performed by Clough and Fragaszy (1977) who concluded that conventionally designed cantilever walls with granular backfill could be reasonably expected to resist seismic loads at accelerations up to 0.5 g. Lew et al. (2010b) also reported on the work of Al-Atik and Sitar (2009) and proposed a horizontal ground acceleration of 25% PGA, 50% PGA and 67% PGA for cohesionless backfill soil with peak ground accelerations of 0.4 g, 0.6 g and 1.0 g, respectively.

To expand upon the work by Al Atik (2008); Al-Atik and Sitar (2007, 2009, 2010), additional centrifuge experiments. The experiments were conducted on two stiff and flexible U-shaped structures with two levels of internal struts to model basement type rigid structures founded on dry medium-dense sand (Geraili Mikola, 2012; Sitar et al., 2012). The resultant incremental dynamic earth pressure data show that the Seed and Whitman (1970) approximation using the PGA, represents a reasonable upper bound for the value of the seismic earth pressure increment for cross-braced basement type walls. The use of 0.85 PGA in the same analysis produces values very close to the mean of the experimental data. However, the M-O solution is considerably higher than measured values at accelerations above 0.4 g. Also it was concluded from these centrifuge tests that the seismic earth pressure increments exerted on the basement walls do not support the use of Wood (1973) solution for rigid or non-yielding walls as suggested by documents such as NEHRP (2000, 2003, 2009).

It is important to note that the proposed reduction factors by the researchers in the United States (Al-Atik and Sitar, 2009, 2010; Geraili Mikola, 2012; Lew et al., 2010b; Sitar et al., 2012) are applicable to the walls designed using the International Building Code (IBC, 2009) load combinations, where the tests were conducted (Lew et al., 2010b; SEAOC, 2013). Considering the load combinations in IBC (2009), it appears that the basement walls in California are designed using at rest pressures with a 1.6 loading factor in static design, which seems adequate for even seismic earth pressure loading. For seismic design, if the M-O analysis is used to determine the seismic loads, the total lateral seismic pressure should consist of the static active earth pressure and the dynamic increment of earth pressure with a load factor of 1.6 and 1.0, respectively. This is while the National Building Code of Canada (NBCC, 2010) proposed lower lateral pressures which are being used by practitioners for seismic design of walls in British Columbia. This recommendation prescribed 1.5 times an active Coulomb pressure for static design and the lateral total seismic pressure consists of the static active earth pressure and the dynamic increment of earth pressure, each with a loading factor of 1.0 for the seismic design.

Based on aforementioned facts it can be concluded that walls designed in the United States following the IBC (2009) load combinations are considerably stronger both in static and dynamic than the similar structures designed in British Columbia using the NBCC (2010) load factors. Therefore, the reduction factors proposed by researchers in United States might not be applicable for the case of basement walls designed in British Columbia and a separate study is required, which is a prime objective of this dissertation.

Chapter 3

Development of the computational model of a basement wall

Software is a great combination between artistry and engineering.
— Bill Gates

3.1 Introduction

This chapter introduces the methodologies used to better approximate the interactions between the basement wall structure and the surrounding soil. First a 4-level basement wall structure is designed following the state of practice for different fractions of the pseudo-static horizontal seismic coefficient as presented in Section 3.2. A commercially available, two-dimensional, finite difference program, FLAC 2D (Itasca, 2012), is used for the analysis in Section 3.3. The interaction of the basement wall and the adjoining soil is treated as a plane-strain problem, which is the condition associated with long structures perpendicular to the analysis plane (e.g., retaining wall systems). Elements of the computational model such as boundary conditions, interface elements, structural and soil properties and applied ground motions are described in detail in this Chapter.

3.2 Seismic design of the typical 4-level basement wall

The prototype model of the 4-level basement wall with a total height of 11.7 m is designed according to the state of practice in Vancouver (see Section 2.4) by the SEABC structural engineers. To determine an appropriate value of the horizontal seismic coefficient to be used in the M-O method, six basement walls are designed for different values of $k_h g$ varying from 100% down to 50% of the NBCC (2010) PGA ($= 0.46g$). Each wall is subjected to the dynamic analyses using ground motions corresponding to 1/2475 hazard levels of NBCC (2010).

Following the state of practice in British Columbia, the structural engineers used two load combinations prescribed by the National Building Code of Canada (NBCC, 2010), for seismic designing the basement walls:

(1) $1.5p_A(z)$, which $p_A(z)$ is not less than 20 kPa compaction/surcharge pressure.

(2) $p_{AE}(z) = p_A(z) + \Delta p_{AE}(z)$

where $p_{AE}(z)$ is the total active lateral pressure consists of $p_A(z)$, the static lateral active pressure and $\Delta p_{AE}(z)$, the dynamic increment of the lateral earth pressure acting on the wall.

Figure 3.1 depicts the distribution of the pressure along the height of the 11.7 m wall based on the factored static load, which comprises 1.5 times static active Coulomb pressure plus compaction pressure at the top. The construction process has a considerable impact on earth pressure distribution of the backfill soil. Therefore the induced lateral earth pressures due to compaction of soil in layers can be significantly higher than those predicted by conventional earth pressure theory. Large number of laboratory and full scale tests (Clayton and Symons, 1992; Duncan and Seed, 1986) have been conducted to investigate the compaction-induced lateral earth pressures on the wall. Clayton and Symons (1992) suggested that in the case of granular backfill, compaction-induced pressures do not normally exceed 20-30 kPa and the effective depth to which compaction pressures are significant will not exceed 3-4 m. The Canadian Highway Bridge Design Code (CAN/CSA-S6-06, 2014) Clause 6.9.3 also provides rough estimations for the lateral force caused by compaction for retained backfill placed and compacted in layers. Based on this recommendation a lateral pressure varying linearly from minimum of 12 *kPa* at the fill surface to 0 *kPa* at a depth of 1.7 to 2.0 m below the surface, depending on the internal friction angle of the soil, shall be added to the lateral earth pressure.

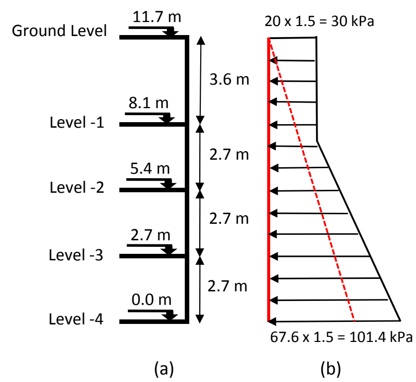

Figure 3.1: (a) Floor heights in the 4-level basement wall and (b) the calculated lateral earth pressure distributions from the first load combination.

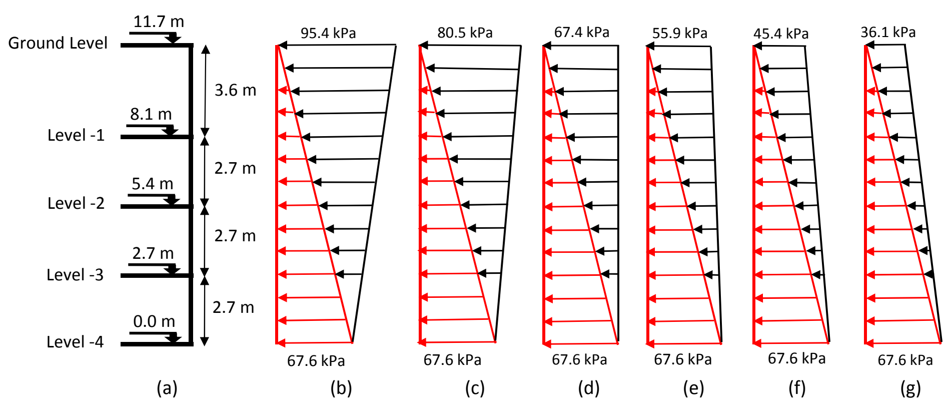

Figure 3.2: (a) Floor heights in the 4-level basement wall and the calculated lateral earth pressure distributions from the second load combination using the modified M-O method with (b) 100% PGA, (c) 90% PGA, (d) 80% PGA, (e) 70% PGA, (f) 60% PGA, and (g) 50% PGA, where PGA=0.46g, based on the NBCC (2010) for Vancouver.

Figure 3.2 presents the distribution of the lateral earth pressure along the height of the basement walls designed for different fractions of the NBCC (2010) PGA, based on the second load combination. This figure shows the linear triangular distribution of the static active component of pressure, $p_A(z)$, with the highest pressure at the base of the wall. The value of PGA/g is used as the pseudo-static horizontal seismic coefficient (k_h) in the calculation of the dynamic increments, $\Delta p_{AE}(z)$ distributed in an inverted triangular with the highest pressure at the top of the wall, following the modified M-O method described in Section 2.4. The basement wall is designed for the conditions of horizontal backfill without any surcharge load or water pressure.

The design moment considered at each depth of the wall is the maximum of the calculated moments from the aforementioned load combinations (1) and (2) defined previously . This design moment must be less than or equal to the factored moment resistance, M_r (See Appendix A). The wall is designed to the Canadian Concrete Design Code (CAN/CSA-A23.3-04, 2004) by SEABC structural engineers (DeVall, 2011). The nominal moment capacity of the wall, approximated as $M_n(z) = 1.3\, M_r(z)$, is used in the computational model for evaluating the response of the walls to a suite of ground motions. Note that the member over-strength factor of 1.3, calculated as $1/0.85 \times 1.1$ following NBCC (2010), is used to estimate the "nominal" bending strength of the wall. This assumes the bending strength for lightly reinforced wall sections is governed by the yield strength of the steel. The factor of $1/0.85$ removes the resistance factor from the yield strength, and the factor of 1.1 approximates the over strength of the steel.

Consistent with the six scenarios of lateral earth pressures shown in Figure 3.2, six levels of yielding moment are calculated for the walls based on different fractions of the code-mandated PGA. The calculated moment from the first and the second load combinations are compared and the maximum value at each depth is chosen. The values of the nominal moment capacity, $M_n(z)$, along the height of the walls designed for different fractions of PGA are illustrated in Figure 3.3.

The moment capacity of all six walls end up to be different only from the height of 7.2 m to 11.7 m from the base of the wall, where the second load case governs the design moment. The moment capacity of these six walls appear to be the same from height of 0.0 to 3.6 m from the base, where the static load case governs

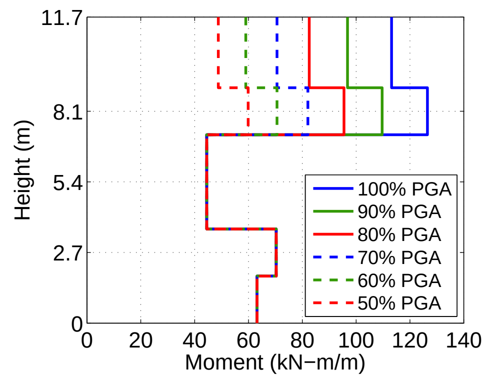

Figure 3.3: Moment capacity distribution along the height of the 4-level basement walls designed for various fractions of the code PGA.

the design moment, and from height of 3.6 m to 7.2 m from the base, where the concrete code minimum reinforcement requirement governs the moment capacity. The responses of these basement walls to the actual expected code demand have then been evaluated using a series of nonlinear dynamic computational analyses, as will be described in the next chapter.

The factored shear resistance based on the unreinforced concrete section alone and using the Canadian Concrete Design Standard (CAN/CSA-A23.3-04, 2004) is calculated as 134.6 kN/m by DeVall (2011). The material resistance factor (ϕ_c) is 0.65 and this gives a nominal resistance of $V_n(z) = 134.6/0.65 = 207\ kN/m$. An intermediate shear value that reflects a common code elastic response cut-off of $R_d.R_o = 1.3$ force level is $134.6 \times 1.3 = 175\ kN/m$ (note that it also corresponds to the flexural over-strength factor of 1.3). However, this value is for information only as there currently is no code provision for using $R_d.R_o = 1.3$ force level cut-off for retaining walls.

The walls in this study have been kept relatively thin (thickness $= 250\ mm$) and based on current design practice require shear ”stirrup/tie” reinforcement in portions of the wall height when the shear in the wall due to either the static or earthquake load case generate shears greater than the factored shear capacity of the concrete section alone. Details of the basement wall designs prepared by DeVall (2011) are presented in Appendix A. Note that for even designs less than PGA, the walls are designed for full PGA for shear.

3.3 Description of the computational model

A series of two-dimensional nonlinear dynamic analyses have been conducted using the finite difference computer program FLAC 2D (Itasca, 2012) to assess the seismic performance of the basement walls.

FLAC (Fast Lagrangian Analysis of Continua) is an explicit finite difference program for conducting the soil–structure interaction analysis under static and seismic loading. FLAC has been used widely as a design tool by geotechnical, civil, and mining engineers for modeling geomechanical problems. This program simulates the behavior of structures built of different materials that may undergo plastic flow when their yield limits are reached. FLAC provides a range of constitutive models from linearly elastic models to highly nonlinear plastic models. In addition, it allows user-defined models to be incorporated. The null model is commonly used in simulating excavations or construction, where the finite difference zones are assigned no mechanical properties for a portion of the analysis. Also this program has interface element feature, which facilitates the simulation of the interaction between the backfill soil and the concrete basement wall.

A finite difference model of the typical basement wall is developed consisting of two-dimensional plane-strain quadrilateral elements to model the soil medium, structural elements to model structural components, and interface elements to simulate frictional contact between the structure and the surrounding soil. Details of the computational model, including the model building procedure, boundary conditions, applied ground motions, and soil properties used in these analyses, are described in this section.

3.3.1 Modeling the construction sequence

It is important to model the construction sequence of the basement wall as closely as possible in order to provide a reasonable representation of the initial, static shear stresses in the structure. So in order to ensure the proper initial stress distribution on the basement structure, the actual construction sequence is modeled in stages to simulate the actual sequence of excavation. The basement wall model is numerically constructed in FLAC similar to the way an actual wall would be constructed. As each stage is excavated, the excavation support is installed and later on removed. Under this condition the soil pressures applied to the wall are representative of the actual pressures. FLAC model can incorporate interaction of the soil and the structure using interface elements and provides direct information on the ground movements outside of and inside the excavation.

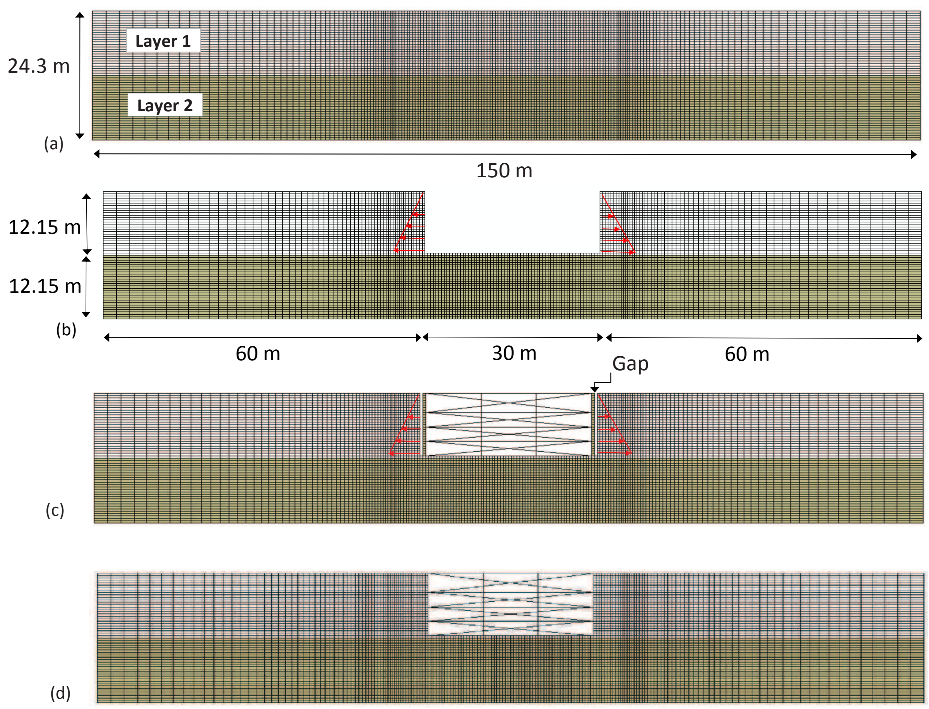

Figure 3.4: Different stages of the computational model building procedure.

The analysis is started by carrying out a set of initial stage analyses to simulate initial geostatic stresses followed by the construction of the basement wall and the backfill soil. First, a 24.3 m deep and 150 m wide layer of soil is created. Figure 3.4(a) shows the mesh adopted to carry out the analyses. The model consists of two soil layers that will be discussed further in this Chapter. The horizontal and vertical stresses are initialized based on self-weight of the soil and a coefficient of at rest earth pressure K_0 from Jaky's equation (Jaky, 1948). A first approximation of the stresses in soil-wall system are estimated using an elastic analysis and the model is brought to equilibrium under gravity forces. Then these stresses are corrected by re-analyzing the system using Mohr–Coulomb model. This procedure is adopted to speed up the analyses.

In the next stage, a part of the upper soil layer is excavated in lifts to a depth of 11.7 m and a width of 30.0 m. As each lift is excavated, lateral pressures (shoring) equal to the corresponding active pressure are applied to retain the soil (Figure 3.4(b)). This is because deep building basement walls are constructed in open excavations are generally shored, which cause the retained soils to be in a yielded (active) conditions already (Lew et al., 2010b). Then the basement wall is constructed, leaving a gap between the soil and the structure, and the static analysis is repeated to establish the equilibrium static stress condition (Figure 3.4(c)). Finally, the gap between the basement wall and the backfill soil is filled, and the shoring pressures are removed in stages, allowing the load from the soil to transfer to the basement wall (Figure 3.4(d)). Note that following the current state of practice in British Columbia, in the present study the building above the ground level is not considered and inertial loading of the surface structures on basement wall pressures are not taken into an account.

The following sections outline the procedures used to determine the various model parameters.

3.3.2 Input ground motions characterization

In performance-based seismic design of structures, it is critical to develop a criteria for selecting an appropriate number of acceleration time histories in which the mean acceleration response spectrum of the selected ground motions provides a good match to the target spectrum over the period range of interest. In practice a suite of input motions is used to capture the motion-to-motion variability present in earthquake ground motions as each ground motion has its unique detailed characteristics, such as frequency content and duration that influence the induced dynamic response differently.

There are two main methods of scaling/matching the input ground motion to insure that the input motion match the code specified intensity of the seismic hazard which is typically specified by the Uniform Hazard Spectrum (UHS). The first method is to linearly scaled the ground motions, which each accelerogram is multiplied by a scalar coefficient to become more compatible with the target spectrum. In this method the average spectrum of the scaled motions matches the UHS over the period range of interest. This approach has an advantage of preserving the frequency content and characteristics of each ground motion record and ensures that the variability between earthquake ground motions is reflected in the analyses.

The second approach is spectral matching where each input motion by itself is matched to the UHS in the period range of interest. Spectrum-compatible ground motions greatly reduce the dispersion in the elastic response spectra of the input ground motion and enhance the variability of the output of nonlinear response history analyses. Spectral matching is popular in engineering practice because it reduces the variance of the structural responses due to motion-to-motion variability and provides a platform to estimate the mean value of the engineering demand parameter with fewer number of analyses (Seifried and Baker, 2014).

In this chapter the spectral matching method is used to modify earthquake time histories to become compatible with the NBCC (2010) UHS for Vancouver. As it is generally considered desirable to maintain the measure of variability between the ground motions, other than spectral matching, different intensity-based linear scaling methods are discussed in Chapter 6 to capture motion-to-motion variability. The results of these analyses are compared with the corresponding average value and scatter of the demand concluded from spectrally-matched motions.

Selection of ground motion records:

Regarding to the number of ground motions, following the recommendation of NEHRP (2011), ASCE/SEI 7-05 (2005) and ASCE/SEI 7-10 (2010) for selecting and scaling earthquake ground motions in response-history analyses, by selecting seven or more ground motions an arithmetic mean of the peak response can be used for performance checking. However this rule does not have any technical basis and is strongly depends on the goodness of the fit of the scaled motion to the target spectrum (NEHRP, 2011). Increased number of time histories result in a closer average match to the target and higher confidence in determining the mean response and its variability to the design-level motions. The appropriate number of motions, which is dependent on the application, is still a topic of needed research (Buratti et al., 2010; Hancock et al., 2008; Heo et al., 2010; Kalkan and Chopra, 2010; Michaud and Léger, 2014; NEHRP, 2011; Reyes and Kalkan, 2011).

In this study a suit of seven crustal ground motions, each consists of two horizontal components (total of 14 ground motion records), are selected. The records are selected to cover the inherent uncertainties associated with earthquake motions such as amplitude, frequency content and duration of ground excitation.

The main considerations in selecting ground motion records are earthquake magnitude, site-to-source distance and local site condition. Appropriate ranges of magnitudes and distances to earthquake sources, which contribute most strongly to the hazard at the site in question, are determined based on the de-aggregation of the current seismic hazard. Based on the results of de-aggregation of the UHS for Vancouver (Pina et al., 2010), searching criteria for the crustal ground motions is set as the magnitude range of 6.5 to 7.5, with the closest distance of 10-30 km of the causative fault plane from the earthquake sites. The reference soil classification, site class C, proposed by the National Building Code of Canada (NBCC, 2010) is selected as the site condition at the point of application of ground motions. According to the NBCC (2010), site class C is defined by a time-averaged shear wave velocity in the upper 30 m (V_{s30}) between 360 m/s and 760 m/s, which is considered as a dense soil or soft rock.

The spectral shape of the ground motion in comparison with the target spectrum over the period range of interest is a parameter that plays an important role in the selection process of ground motion records. Selecting the motions whose spectral shapes are similar to the target spectrum minimizes the need for spectral modification.

Based on aforementioned selection criteria, time histories are selected from the Pacific Earthquake Engineering Research Center (PEER) ground motion database (Chiou et al., 2008; PEER, accessed on January 2013). In order to take into an account the spectral shape of the ground motions, the candidate records are chosen based on the best linearly scaled motions to the UHS of Vancouver in the period range of 0.02-1.7 sec. The Mean Squared Error (MSE) of the difference between the spectral acceleration of the record and the target spectrum is chosen as a criterion for selecting the best linear-scaled records. In addition, in order to eliminate the potential bias towards one specific event, no more than two out of seven records are selected from a single seismic event. Table 3.1 listed the selected seven crustal ground motions. For each record, the PEER-NGA database provides two horizontal components of acceleration time histories, which have been rotated to Fault-Normal (FN) and Fault-Parallel (FP) directions. The use of rotated time histories does not imply that they are only for use in time history analyses in FN and FP directions, whereas they can be used in any other direction (Wang et al., 2013). Both components of the selected records are decided to be used which leads to a total of 14 crustal ground motions (G1–G14).

Table 3.1: List of the selected crustal ground motions.

No.	Event Name	Year	Station	Magnitude	V_{s30} (m/s)	Direction
G1 G2	Friuli- Italy	1976	Tolmezzo	6.5	424.8	FN FP
G3 G4	Tabas- Iran	1978	Dayhook	7.35	659.6	FN FP
G5 G6	New Zealand	1987	Matahina Dam	6.6	424.8	FN FP
G7 G8	Loma Prieta	1989	Coyote Lake Dam (SW Abut)	6.93	597.1	FN FP
G9 G10			San Jose - Santa Teresa Hills		671.8	FN FP
G11 G12	Northridge	1994	LA - UCLA Grounds	6.69	398.4	FN FP
G13 G14	Hector Mine	1999	Hector	7.13	684.9	FN FP

Spectral matching the selected ground motion records:

The computer program, SeismoMatch (Seismosoft, 2009*a*) has been used to spectrally match the ground motions to the target UHS in the period range of 0.02–1.7 sec. Grant and Diaferia (2013) investigated the period range for spectral matching and concluded that matching up to three times the fundamental period is beneficial in reducing dispersion in the results.

SeismoMatch is an application uses the wavelet algorithm proposed by Abrahamson N.A. (1992) and Hancock et al. (2006) to adjust earthquake ground motions and obtain a response spectrum with a close match to the target spectrum in a period range of interest. The basic characteristic of the original record with respect to the amplitude and frequency content of the record over the time history duration is preserved and a developed design time histories have a spectra similar to the a design spectrum (NEHRP, 2011).

The spectrally matched ground motions are baseline corrected with a linear function and filtered with a bandpass Butterworth filter with cut-off frequencies of 0.1 Hz and 25 Hz, using the computer program SeismoSignal (Seismosoft, 2009*b*).

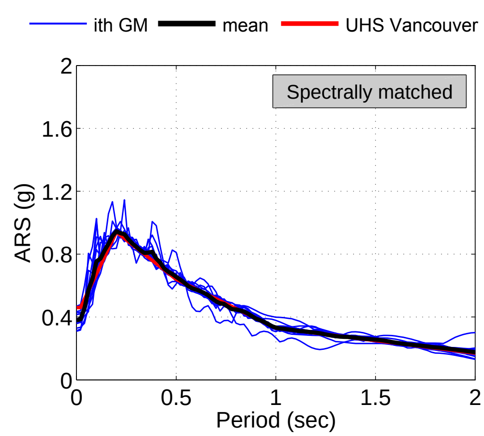

Figure 3.5: The 5% damped acceleration response spectra of the selected 14 crustal input ground motions, all spectrally matched to the target NBCC (2010) UHS of Vancouver in the period range of 0.02-1.7 sec.

The 5% damped acceleration response spectra of suite of ground motions G1–G14 in comparison with the target NBCC (2010) UHS for Vancouver is presented in Figure 3.5. Also the acceleration time histories of the spectrally matched ground motions corresponding to the 2% in 50 year hazard level specified in the NBCC (2010) are presented in Figure 3.6.

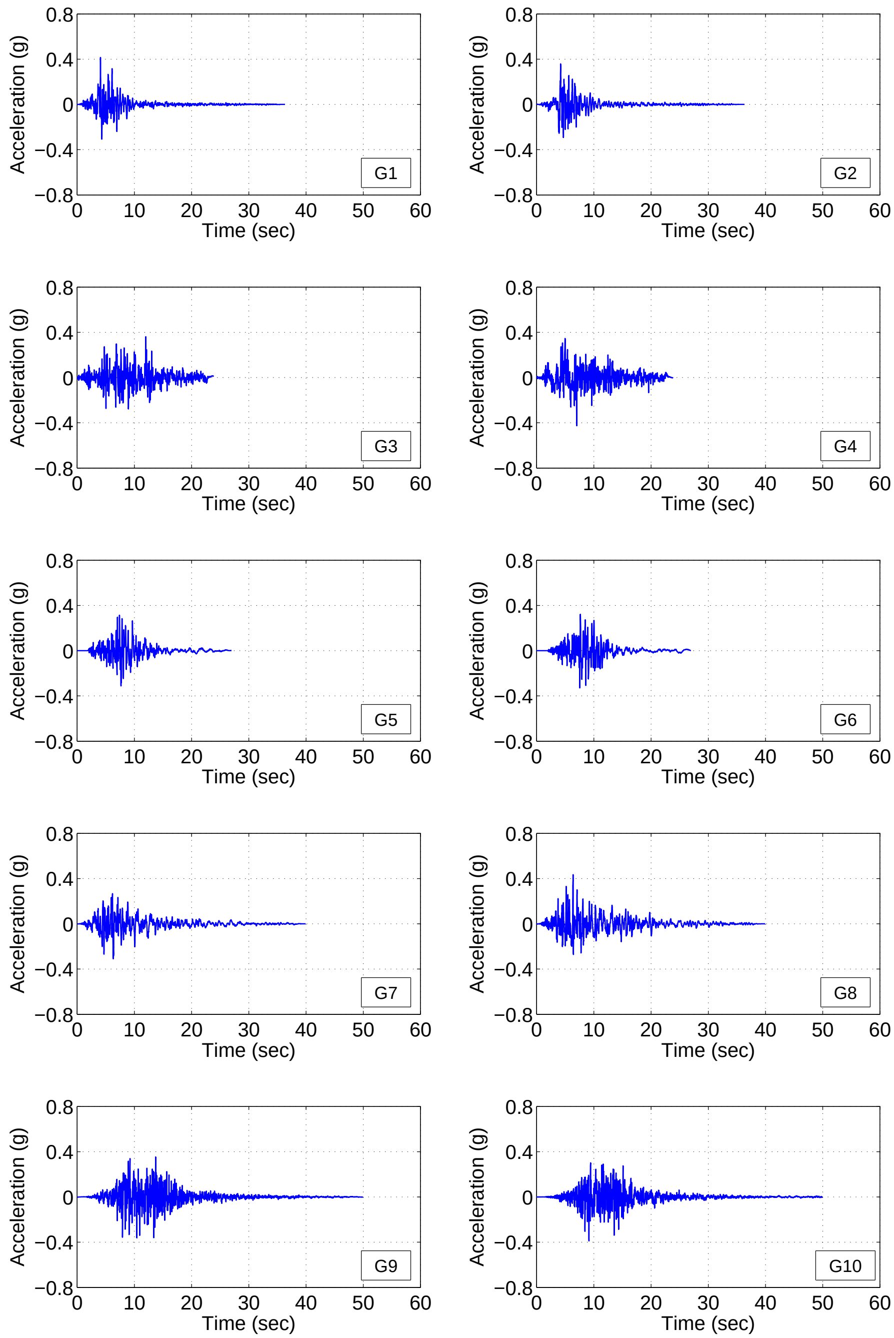

Figure 3.6: Continued.

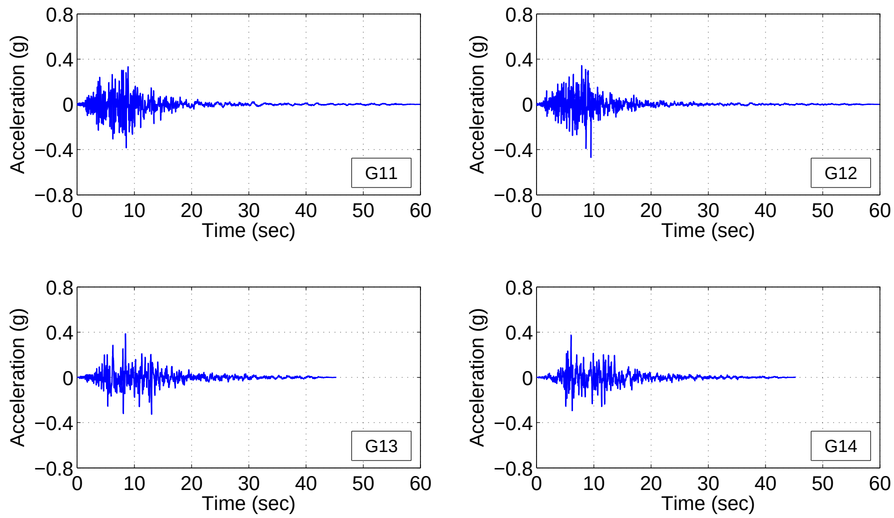

Figure 3.6: Acceleration time histories of the selected 14 crustal ground motions spectrally matched to the NBCC (2010) UHS of Vancouver.

3.3.3 Structural elements

Structural elements of the model including basement walls, interior walls, concrete floor slabs, foundation and braces are modeled using beam elements in FLAC (Itasca, 2012). Beam elements are two-dimensional elements with three degrees of freedom (x–translation, y–translation and rotation) at each end node. The beam is assumed to behave as a linearly elastic material with no failure limit. However if desired, a plastic moment may also be specified to model inelastic behavior of the structure (FLAC User's guide).

The flexural behavior of the basement walls is simulated by elastic-perfectly plastic beam elements with uniform properties of $E = 2.74 \times 10^7$ kPa, $A = 0.25$ m^2/m, and $I_{cr} = 0.00104$ m^4/m, and with varying yield moments along the height of the walls, as obtained for different designed walls in the previous section and presented in Figure 3.3.

Based on recommendation of the NBCC (2010) Commentary J, the effects of cracked sections must be taken into consideration in determining the stiffness and strength of reinforced concrete elements. For this purpose the moment of inertia of the cracked concrete section (I_{cr}) is used for the basement walls. The Los Angeles Tall Buildings Structural Design Council (LATBSDC, 2014) recommended to use $I_{cr} = 0.8I_g$ for the reinforced concrete basement walls under earthquakes events having 2% probability of being exceeded in 50 years (2475 year return period). An additional analyses conduced on cracked section with $I_{cr} = 0.5I_g$ show that the seismic response of the basement wall is not significantly sensitive to the choice of reduction factors applied to the stiffness of the uncracked cross section.

The basement wall nodes are created at the same geometric location as the soil nodes along the height of the wall and the interface elements maintain the nodal connectivity between the soil and the wall. The basement walls are braced by concrete floor slabs, which are pinned at the wall and take no moment. The actual model is for a below grade structure that is basically a box of walls with internal floor diaphragms that span horizontally to the end walls by acting as horizontal beams as they support the retaining wall being loaded by the soil and earthquake actions. This is a complicated model and the effects of the supporting floor slabs and walls are reduced to a series of stiffnesses supporting the retaining wall being analysed. A sensitivity analysis using various stiffnesses was performed in the initial stages to study the effects. The results were not very sensitive to the various assumptions and the one giving the most conservative results were used to proceed with the rest of the work.

3.3.4 Representative soil properties

Soil medium beneath and around the basement wall in this soil-structure model is simulated by using finite difference mesh composed of quadrilateral elements. These two-dimensional plane-strain soil elements behave in accordance with a prescribed constitutive model in response to applied loads and boundary conditions.

The elastic-perfectly plastic Mohr–Coulomb model with non-associated flow rule is adopted as the soil constitutive model for the sake of simplicity and its popularity among local practitioners. This model has been employed by many researchers to simulate nonlinear behavior of the soil domain under seismic loading.

A typical and simplified stratigraphy of an underlying soil layers are recommended by practitioners in Vancouver. In consultation with the geotechnical engineers and the members of the SEABC Task Force (DeVall et al., 2010, 2014), the soil properties listed in Table 3.2 are proposed for the two soil layers in Figure 3.4, representing the site condition relevant for high-rise construction, especially in downtown Vancouver.

Table 3.2: Soil layer material properties.

Soil layer	Density (kg/m^3)	V_{s1} (m/s)	Poisson's ratio	Cohesion (kPa)	Friction angle (°)	Dilation angle (°)
1	1950	200	0.28	0	33	0
2	1950	400	0.28	20	40	0

The shear wave velocity (V_s) is known to be a function of an effective overburden stress σ_0' and based on the suggestion of Robertson et al. (1992), can be presented in the form of a normalized shear wave velocity:

$$V_{s1} = V_s \left(p_{at}/\sigma_0'\right)^{0.25} \tag{3.1}$$

where p_{at} is the reference atmospheric pressure. Normalized shear wave velocities (V_{s1}) of 200 and 400 m/s are assigned to soil layers 1 and 2, respectively. These values result in a shear wave velocity profile, which varies along the depth of the model due to the change of confining pressure (Figure 3.7). The small strain shear wave velocity is directly related to the small strain shear modulus via $G_{\max} = \rho V_s^2$, where ρ is the mass density of the soil medium.

In order to more appropriately simulate the nonlinear response of soil in the linear elastic range of the Mohr–Coulomb model in a nonlinear analyses, it is necessary to incorporate shear modulus reduction and additional material damping to account for stiffness reduction and cyclic energy dissipation during the elastic range of the response. This approximate method is recommended by FLAC User's Guideline (Itasca, 2012) when Mohr–Coulomb material model is employed for representing the soil response in the full soil-structure system. Similar approach was adopted by other researches (Argyroudis et al., 2013; Gazetas et al., 2005; Gil et al., 2001; Hashash et al., 2001) for the analysis of buried structures. It is worth mentioning that the equivalent linear methods are more reliable only for low-strain levels. For higher strain levels the effect of nonlinearity is captured through the Mohr–Coulomb yield criterion used for modeling stress–strain response of the soil medium in the 2D model. To this aim a site response analyses are conducted in the free-field to determine depth-varying parameters such as shear modulus and damping ratio of soil at different soil layers through-out the model in an absence of the wall structure.

The state of practice for site response analysis is to use the computer program SHAKE (EduPro Civil Systems Inc., 2003; Schnabel et al., 1972), in which an equivalent linear approach is utilized to obtain reasonable estimates of ground nonlinear response. SHAKE is a widely used one-dimensional linear-elastic wave propagation code for site response analysis in the frequency domain using transfer functions. In this code the vertical shear waves propagate through a semi-infinite horizontally-layered soil deposit overlying a uniform half-space. The method incorporates soil nonlinearity through the use of strain-compatible soil properties for each soil layer. This code is based on the multiple reflection theory and within each layer, the wave equation can be expressed as the sum of an upward-propagating motion and a downward-propagating motion following the general approach of Kramer (1996). The equivalent linear method has the advantage of short computational time and few input parameters.

A series of equivalent linear analyses are conducted on the two-layered soil profile subjected to the selected spectrally matched earthquake ground motions (G1–G14). Each soil layer is divided into number of sublayers with almost the same height. A constant density of 1950 kg/m^3 is assigned to all sublayers throughout the model. The assigned shear wave velocity to each sublayer is reported in Figure 3.7. The dynamic characteristics of the sublayers are assumed to be governed by the shear modulus degradation and damping ratio curves as a function of shear strain. Following the recommendation of Task Force Report (2007) for geotechnical design in Greater Vancouver region, the upper-bound modulus reduction curve and the lower-bound damping curve of Seed et al. (1986) are selected for representing the cyclic response of the sandy soil in the equivalent linear analyses.

The profiles of the shear modulus reduction and damping ratios through-out the free-field soil column are presented in Figure 3.8. Average values of damping ratios

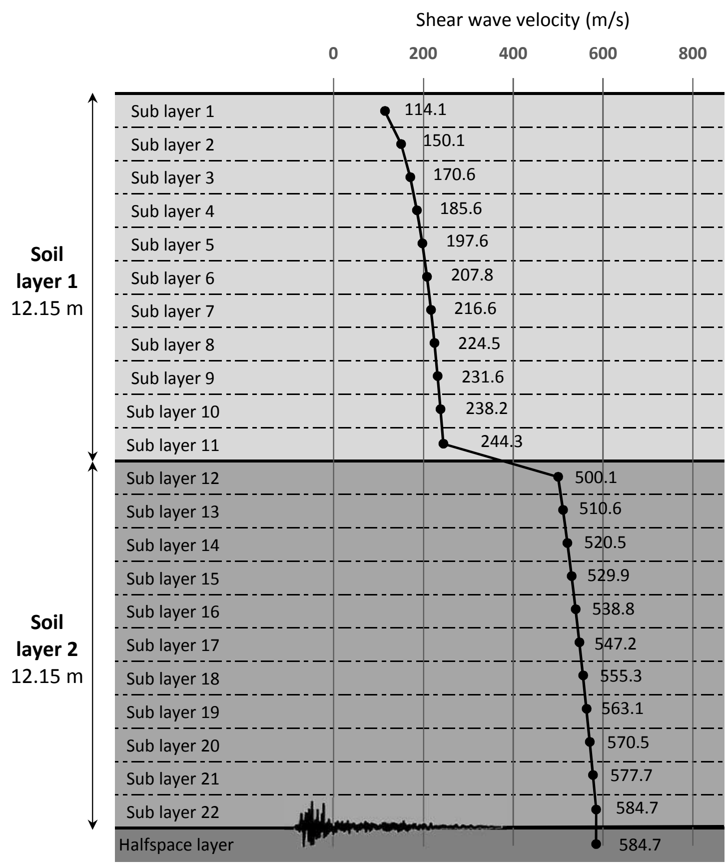

Figure 3.7: Schematic sketch of the SHAKE model reporting on the number of sublayers, the assigned shear wave velocities at each sublayer and the depth at which the ground motions are applied.

and shear modulus reduction factors are estimated for each layer and incorporated into the FLAC model. The results of the equivalent linear analyses of the free-field soil column presented in Figure 3.8(a) suggest an equivalent $G/G_{\max}$ of 0.41 and 0.81 for the first and the second soil layers, respectively. These average equivalent modulus reduction values are used for modifying the $G_{\max}$ to G, at different depths of the FLAC model. Similarly, Figure 3.8(b) suggests the equivalent damping

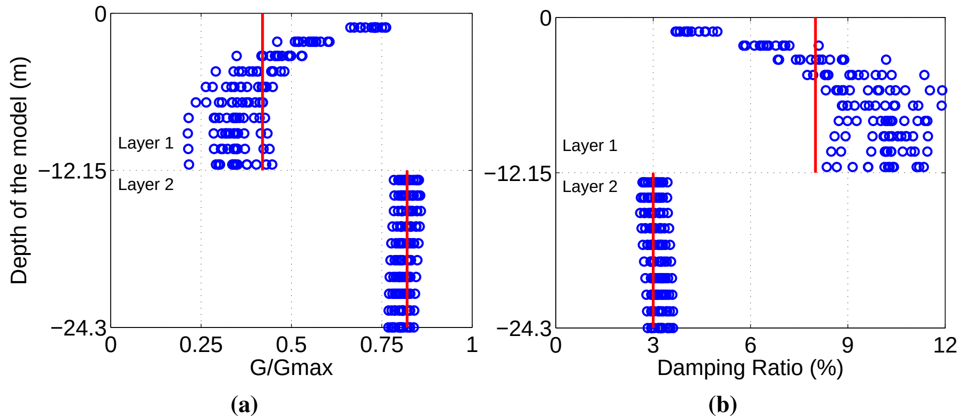

Figure 3.8: Resulting (a) $G/G_{\max}$ and (b) damping ratios along the depth of the model from the equivalent linear analyses of the free-field column of soil subjected to G1–G14. The red solid lines show the average values of $G/G_{\max}$ and damping ratio in the first and the second soil layers used in the subsequent nonlinear analyses in FLAC.

ratios of 8% and 3% for the first and the second soil layers, respectively. These damping ratios are added to the nonlinear analyses of the soil-structure system in the form of Rayleigh damping. The only draw back of using high values of damping ratio is that it causes the reduction in time step of the explicit solution and consequently increases calculation time.

Although Rayleigh damping is frequency-dependent, it is commonly used to provide frequency-independent damping over a restricted range of frequencies. Therefore, selection of an appropriate range of frequencies is essential to obtain proper results. Velocity response spectrum of any input record has a flat region that spans about a 3:1 frequency range. Thus, by applying constant Rayleigh damping over a span of roughly 3:1 (or one-third) of the frequency range, the damping can be considered frequency independent. This flat region in velocity response contains most of the dynamic energy in the spectrum and is centered at the dominant frequency. The idea in dynamic analyses is to adjust a center frequency of the Rayleigh damping, f_{min}, so that its 3:1 range coincides with the range of predominant frequencies in the problem, in order to provide the right amount of damping at the important frequencies (FLAC User's Guide).

The center frequency of Rayleigh damping is set to the dominant frequency of the input records, 1 Hz, which is basically calculated using velocity response spectrum of the selected input records in logarithmic space. As is shown in Figure 3.9, the velocity spectrums of all motions have an almost flat region of 3:1 over a frequency range of 0.5 Hz to 1.5 Hz.

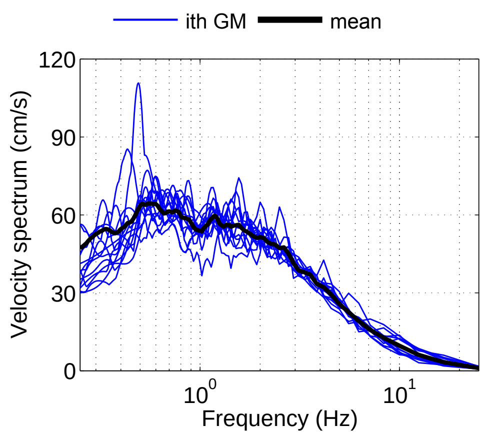

Figure 3.9: Velocity response spectrum versus frequency of the selected 14 crustal ground motions (G1–G14).

The small strain natural period of the basement wall-soil system in the FLAC model is estimated to be approximately 0.4 sec, as determined by the peak of the transfer function from the base of the model to the top of the backfill. The predominant period of the system can also be calculated by applying a constant shear stress at the base of the model for a short time and then allow the whole system vibrate under the damped free vibration condition till the initial displacement decays with time. Comparing the results of these two studies confirm that natural period of the soil–basement wall system is about 0.4 second. At higher strains, it is expected that the natural period of the system to be higher due to yielding.

3.3.5 Mesh refinement of the soil domain

Proper dimensioning of the finite difference zones is required to avoid numerical distortion of propagating ground motions and preparing an acceptable wave transmission through-out the model. Based on the work of Kuhlemeyer and Lysmer (1973), the FLAC User's guide recommends to restrict the length of the element (Δl) to one-tenth or one-eight of the shortest wavelength ($\lambda = V_s/f_{max}$) associated with the fundamental frequency of the input motion and velocity of propagation in the soil media, i.e.,

$$\Delta l \leq \frac{V_s}{10.f_{max}} \tag{3.2}$$

From this equation, the finite difference zone with the lowest V_s and a given Δl limits the highest frequency that can pass through the zones without numerical distortion. After conducting number of trial dynamic analyses on the model with different levels of mesh refinement, a relatively fine mesh size with the length of 0.45 m is selected to be used at both sides of the basement wall structure. The element size increases gradually toward the left-side and right-side boundaries as is shown in Figure 3.4. Using Equation 3.2 and $\Delta l = 0.45\ m$ as a finest mesh size used in the simulation, one can concluded that the assigned mesh size can adequately propagate shear waves having frequencies up to 40 Hz. This value is well above the 25 Hz cut-off frequency used in the preparation of ground motions in Section 3.3.2 and well above the estimated fundamental frequency of the basement wall–soil system.

Figure 3.10 shows the cumulative power spectral densities of the ground motions G1–G14 and presents information about input energy and frequency content of each record. As is shown in this figure, more than 99% of the earthquakes power are concentrated within frequency range of 0.1 to 25 Hz, which were set as the corners of bandpass filtering process described in Section 3.3.2. Thus, it can be concluded that filtering frequencies greater than 25 Hz and lower than 0.1 Hz in order to avoid any numerical distortion due to wave propagation process, does not affect the original characteristics of the input ground motions.

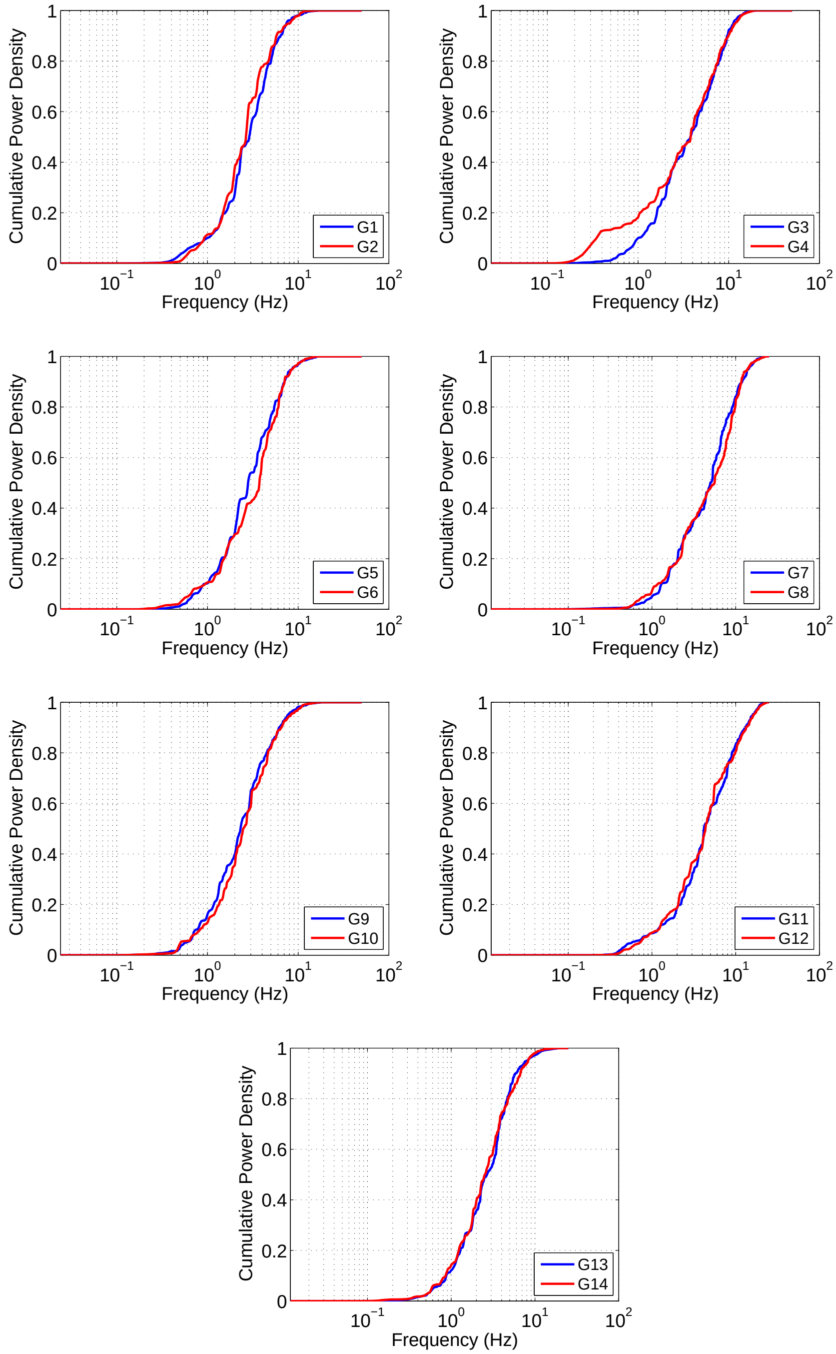

Figure 3.10: Cumulative power densities of the unfiltered selected 14 crustal ground motions spectrally matched to the NBCC (2010) UHS for Vancouver.

3.3.6 Modeling soil–wall interaction using an interface elements

Simulating the interaction between the backfill soil and the concrete basement wall plays an important role in modeling the soil–structure interaction. To simulate sliding and loss of contact at the soil–wall interfaces, nulled zones with zero thickness containing interface elements are employed in FLAC. Without an interface element the structure and the soil are tied together and no relative displacement (slipping/-gapping) is allowed between them. By using an interface element, node pairs are created at the interface of the structure and the soil. From a node pair, one node belongs to the structure and the other node belongs to the soil. The interaction between these two nodes consists of two elastic-perfectly plastic shear and normal springs, which allow modeling of opening (separation) and slippage between the soil and the wall in normal and shear directions, respectively.

A simple elastic-perfectly plastic response consisting of constant values for both shear and normal stiffnesses (k_s and k_n) is used for modeling the interface contact in FLAC. The shear response of the interface element is controlled by Coulomb shear strength criterion, which limits the shear force to the maximum shear strength defined as a function of cohesion and friction angle of the interface element, i.e.,

$$F_{s\ max} = cA + \tan\phi F_n \tag{3.3}$$

where $F_{s\ max}$ is the maximum shear strength, c and ϕ are the cohesion and friction angle of the interface and F_n is the normal force. Equation 3.3 assumes absence of pore water pressure.

The yield relationship in the normal direction is controlled by the (positive) normal tensile strength (σ_t):

$$F_{n\ max} = \sigma_t \tag{3.4}$$

At every time step in FLAC calculation, the normal compression/tension force (F_n) and shear force (F_s) of interface nodes are compared to the normal tensile strength (σ_t) and maximum shear strength ($F_{s\ max}$), respectively, which leads to the following three cases:

- If $F_n < \sigma_t$ and $F_s < F_{s\ max}$, the interface node remains in the elastic range. In this case the interfaces are declared glued and no slippage or opening is allowed.

- If $F_n < \sigma_t$ and $F_s > F_{s\ max}$, the interface node falls into Coulomb sliding state and the shear force is corrected as $F_s = F_{s\ max}$. The interface may dilate at the onset of slip and causes an increase in effective normal force on the target face after the shear-strength is reached. In this case the normal force will be corrected as:

$$F_n = F_n + \frac{(|F_S|_0 - F_{s\ max})}{L\ k_s} \tan\psi\ k_n \tag{3.5}$$

  where $|F_S|_0$ is the magnitude of shear force before the correction and ψ is the dilation angle of the interface.

- If $F_n > \sigma_t$, the bond breaks for the segment and the segment behaves thereafter as un-bonded and the separation and slip are allowed.

In these analyses, a friction angle of $\delta = 10°$ equal to one-third of the angle of internal friction of backfill soil (ϕ) and a dilation and tensile strength of zero are assigned to the interface element.

The values of the interface stiffnesses (k_n and k_s) in comparison with the surrounding soil should be high enough in order to minimize the contribution of interface elements to the accumulated displacements (Comodromos and Pitilakis, 2005). In addition, k_n should be greater than or equal to k_s, otherwise penetration will occur between the soil and the wall faces, which does not correspond to actual condition. To satisfy the above requirement, the FLAC guideline proposes values for k_n and k_s in the order of ten times the equivalent stiffness of the stiffest neighbouring zone:

$$k_n = k_s = 10\ max[\frac{K + 4/3G}{\Delta z_{min}}] \tag{3.6}$$

In this equation, Δz_{min} is the smallest width of the adjoining zones on both sides of the interface and K and G are the bulk and shear modulus of the neighbouring zone, respectively. The $max[\ ]$ notation indicates that the maximum value over all zones adjacent to the interface is to be used. The FLAC manual warns against using arbitrarily large values for stiffnesses, as is commonly done in finite element analyses, which leads to a very small time step and therefore long computational times. Using Equation 3.6, a value of 9×10^6 kPa/m is assigned for k_n and k_s in these analyses.

3.3.7 Boundary conditions

Simulation of dynamic soil–structure interaction problem requires appropriate conditions to be enforced at the computational model boundaries. Boundary conditions of the 2D finite difference mesh comprise:

- The lateral boundaries of the model should be placed at a location which the presence of the structure does not have any influence on the free-field conditions at the lateral boundaries of the mesh. Studies of Rayhani et al. (2008) based on computational modeling and centrifuge testing showed that in dynamic analysis, the horizontal distance of the lateral boundaries should be at least five times the width of the structure. As illustrated in Figure 3.4, horizontal distance of the lateral boundaries of the model is assumed to be 150 m, which is five times the 30 m width of the structure and is far enough to avoid boundary effects. A series of an additional sensitivity analyses conducted on the continuum model with various soil domain dimensions confirmed that the proposed dimensions are appropriate for the analyses and a free-field condition at the lateral boundaries are properly captured.

- A free-field boundaries are applied to the lateral boundaries which account for the existence of the free-field condition in an absence of the structure (Kramer, 1996). Free-field boundaries consists of a one-dimensional column of unit width, simulating the behavior of the extended media. These boundaries are placed at distances far enough to minimize wave reflection back to the model and simulate the free-field condition on both sides.

- The velocity of the base nodes of the soil continuum model are fixed and prevented from changing in the horizontal and vertical directions. The lateral boundary nodes are fixed in a vertical direction, while they can move freely in the horizontal direction.

- Lateral boundary conditions are imposed to slave the displacement degrees of freedom of the nodes across the soil continuum. Each grid point on the left-side boundary (e.g., $i = 1, j = n$) is attached to its corresponding grid point at the same height on the right-side boundary (e.g., $i = k, j = n$). This ensures that the lateral boundaries of the mesh move simultaneously.

- Since the mesh cannot extended infinitely, there is a need for some sort of absorbing boundaries in order to simulate the radiation of energy at the base of the model. This is achieved by using a compliant boundary condition along the base of the FLAC mesh, which means no large dynamic impedance contrast is meant to be simulated at the base of the model. A quiet (absorbing) boundary (Lysmer and Kuhlemeyer, 1969), consisting of two sets of dashpots attached independently to the mesh in the normal and shear directions, are applied along the base of the model to minimize the effect of the reflected waves. The viscous dashpots of the quiet boundary absorb downward propagating waves so that they are not reflected back into the model.

  For the compliant-base boundary, the input motion is the upward-propagating motion, which is half of the outcrop target motion (Mejia and Dawson, 2006). At a quiet boundary, an acceleration time history cannot be input directly because the boundary must be able to move freely to absorb incoming waves. To this end first the acceleration-time history is integrated to obtain the velocity time history, and then the following equation is used to convert the velocity time history to shear stress time history that can be applied at the base of the model:

$$\tau_s = 2\rho V_b v_{su} \tag{3.7}$$

  In this equation ρ and V_b are the density and shear wave velocity of the base material, and v_{su} is the particle velocity of the upward propagating motion. A factor of two is added to the calculation of the shear stress time history because half of the stress is absorbed by the viscous dashpots of the quiet base (Mejia and Dawson, 2006). Figure 3.11 illustrates the shear stress time histories of the selected 14 crustal ground motions (G1–G14), which are

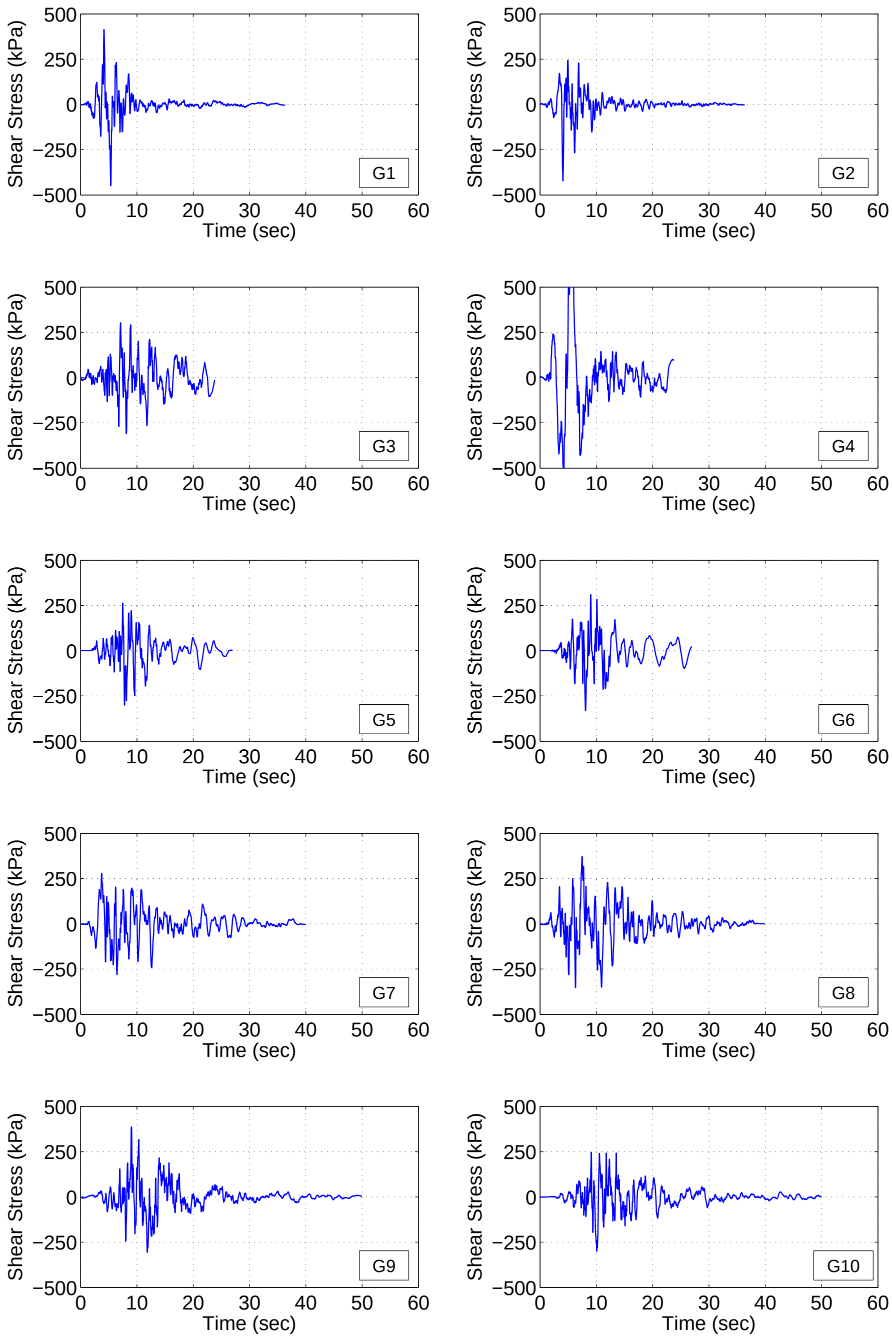

Figure 3.11: Continued.

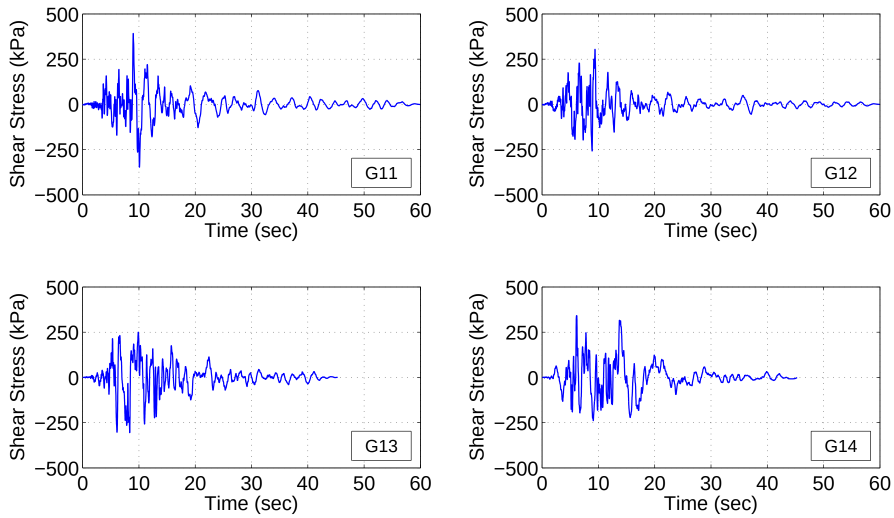

Figure 3.11: Shear stress time histories of the selected 14 crustal ground motions applied at the base of the FLAC model.

applied at the compliant-base of the FLAC model as an input motion.

- The comprehensive study of Roesset and Ettouney (1977) on the effect of different types of boundary condition on structural response shows that applying quiet (viscous) boundaries at lateral boundaries can significantly reduce the reflection of the waves produced by lateral boundaries back to the model. The sensitivity analyses in this study showed that due to a sufficient horizontal distance of the lateral boundaries, the presence of viscous dashpots at lateral boundaries do not have any effect on dynamic response of the structure under study. Therefore, no viscous dashpots are assigned at the lateral boundaries of the soil model.

Chapter 4

Seismic performance of a typical 4-level basement wall

The most important thing is to keep the most important thing the most important thing.
— From the book ”Foundation design”, by Donald P. Coduto (1994)

4.1 Introduction

The seismic performance of the 4-level basement wall designed for six different fractions of the NBCC (2010) PGA as discussed in Chapter 3, are numerically analyzed. Each wall is subjected to 14 crustal ground motions spectrally matched to represent the seismic hazard level enforced by the NBCC (2010) in Vancouver.

The seismic response of the basement walls are obtained from the nonlinear dynamic analyses and presented in the form of the time histories and envelopes of the lateral earth pressures along the height of the walls, lateral earth forces on the walls, envelopes of the bending moments, shear forces, lateral deformations and drift ratios in Sections 4.2 to 4.4. The results indicate that flexibility of the wall has significant effect on the distribution of the seismic lateral earth pressures on the wall and consequently its seismic performance. Based on the results of the analyses, recommendations for an appropriate fraction of NBCC (2010) PGA to be used in the M-O analysis to have a satisfactory performance, in terms of the resulting drift ratio along the height of the wall are made. In addition, number of sensitivity analyses on different input parameters are conducted, and the results are presented and discussed in Section 4.5.

Sections 4.2 to 4.4 presents the seismic response of the left-side walls, while the response of the right-side walls are found to be very similar to the left-side walls.

4.2 Lateral earth forces and pressures on the wall

Distribution and magnitude of the seismically induced lateral earth pressure on a basement walls are important issues to address since they directly affect the applied total forces on the wall and consequently influence the magnitude of the imposed shear and moment forces in structural elements. Figure 4.1 shows the distribution of the lateral pressure at different heights of the basement wall designed for 100% of the code PGA subjected to earthquake ground motion G1. As shown in this figure each element of the wall undergoes a different regime of lateral pressure, which varies by time and height of the wall.

During an earthquake event, the stress distribution is nonlinear and changes as a function of wall deflection. Figure 4.2 shows the time histories of lateral earth pressure at different levels along the height of the 4-level basement wall designed for 100% PGA subjected to earthquake G1. At all elevations of the wall, the initial static lateral pressures before the earthquake is lower than the residual static lateral pressures after the earthquake. In addition, during the seismic loading the lateral pressure at each level increases gradually from its initial value to the higher final value. The trend of this increase is slightly different at various locations. In particular, more seismic lateral pressure is absorbed at floor levels with larger lateral support from the structure, than at the mid-height of the floor levels where the wall is not directly supported by the slabs.

The resultant lateral earth force at a specific time can be calculated by integrating the induced lateral earth pressures along the height of the wall at that time. Figure 4.3 shows the time histories of resultant lateral earth force on the wall designed for 100% of the code PGA subjected to 14 ground motions (G1-G14). As

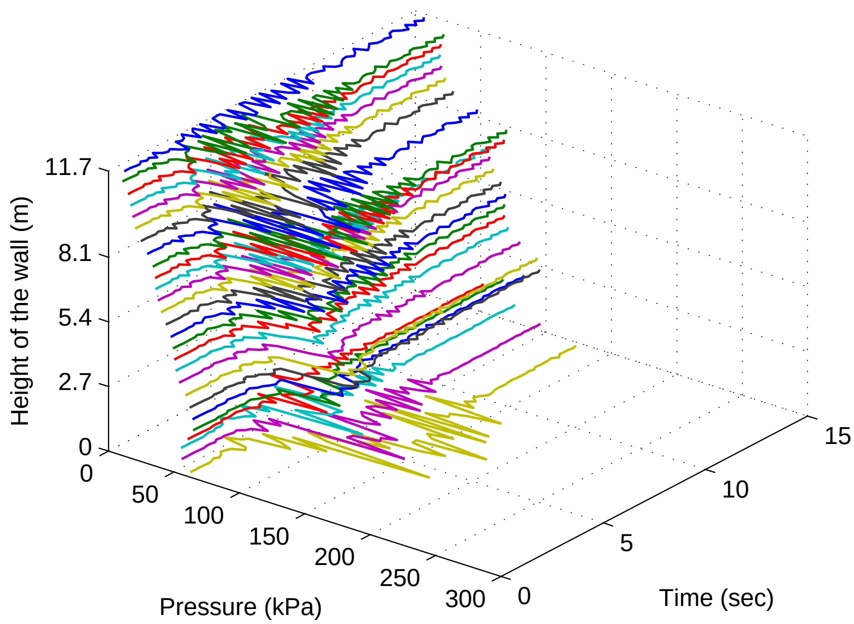

Figure 4.1: Lateral earth pressure distribution along the height of the basement wall designed for 100% code PGA subjected to ground motion G1 (only the first 15 sec response is illustrated).

shown in this figure the lateral earth force starts from the static active thrust, oscillates at different levels during the application of the ground motion, and finally stabilizes at a higher level than was initially, indicating an increase in the residual static earth force at the end of shaking. The M-O method for the same level of PGA ($= 0.46g$) gives an almost similar peak resultant lateral earth force (P_{AE}), as plotted by the dot-dashed line.

Figure 4.4 illustrates the time histories of the corresponding height of application of the resultant lateral earth force measured from the base of the wall normalized with respect to the height of the wall, H. The height of the resultant lateral earth force starts from about $0.33H$ prior to shaking, i.e., the level suggested by Coulomb's theory for static lateral earth pressure distribution. Then it oscillates at different levels during the application of the ground motion. As illustrated in this figure, the M-O method using the same level of PGA results in a similar height

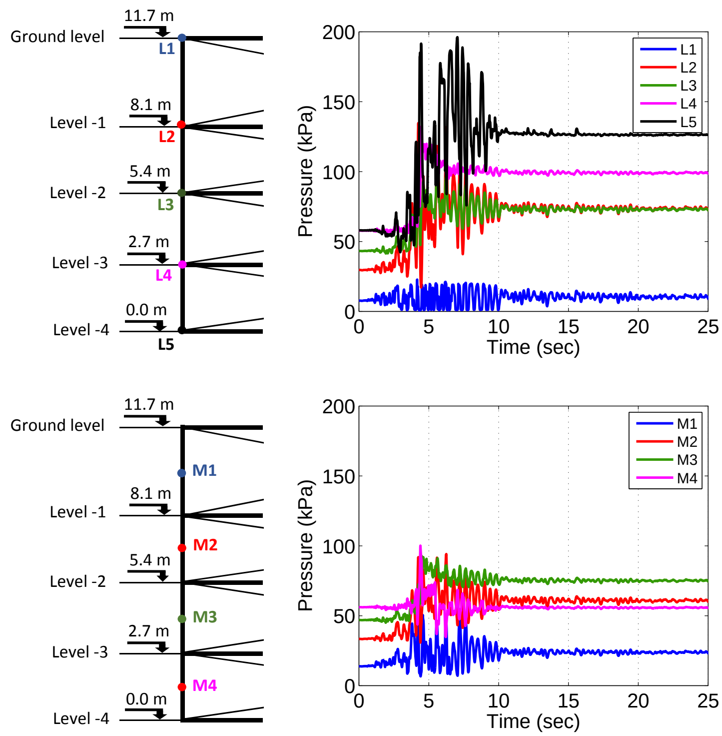

Figure 4.2: The lateral earth pressure time histories at floor levels and mid-height of the floor slab levels along the 4-level basement wall designed for 100% PGA subjected to ground motion G1.

of application of the resultant lateral earth force at the instance of peak resultant lateral earth force.

Figures 4.5 and 4.6 show the dynamic analysis results for ground motions G1–G14 in terms of the maximum resultant lateral earth forces and their corresponding normalized heights of application from the base of the wall designed for 100% of the code PGA. These figures also present the maximum resultant forces and their corresponding normalized heights of application from the M-O method using 100% PGA for comparison. As illustrated in Figure 4.5, the maximum resultant forces from dynamic analyses are in an approximate range of $\pm 10\%$ of the calculated maximum resultant force using the M-O method with 100% PGA. Figure 4.6 shows that the corresponding heights of application of the maximum resultant forces on all the walls subjected to 14 ground motions are consistently around mid-height of the wall.

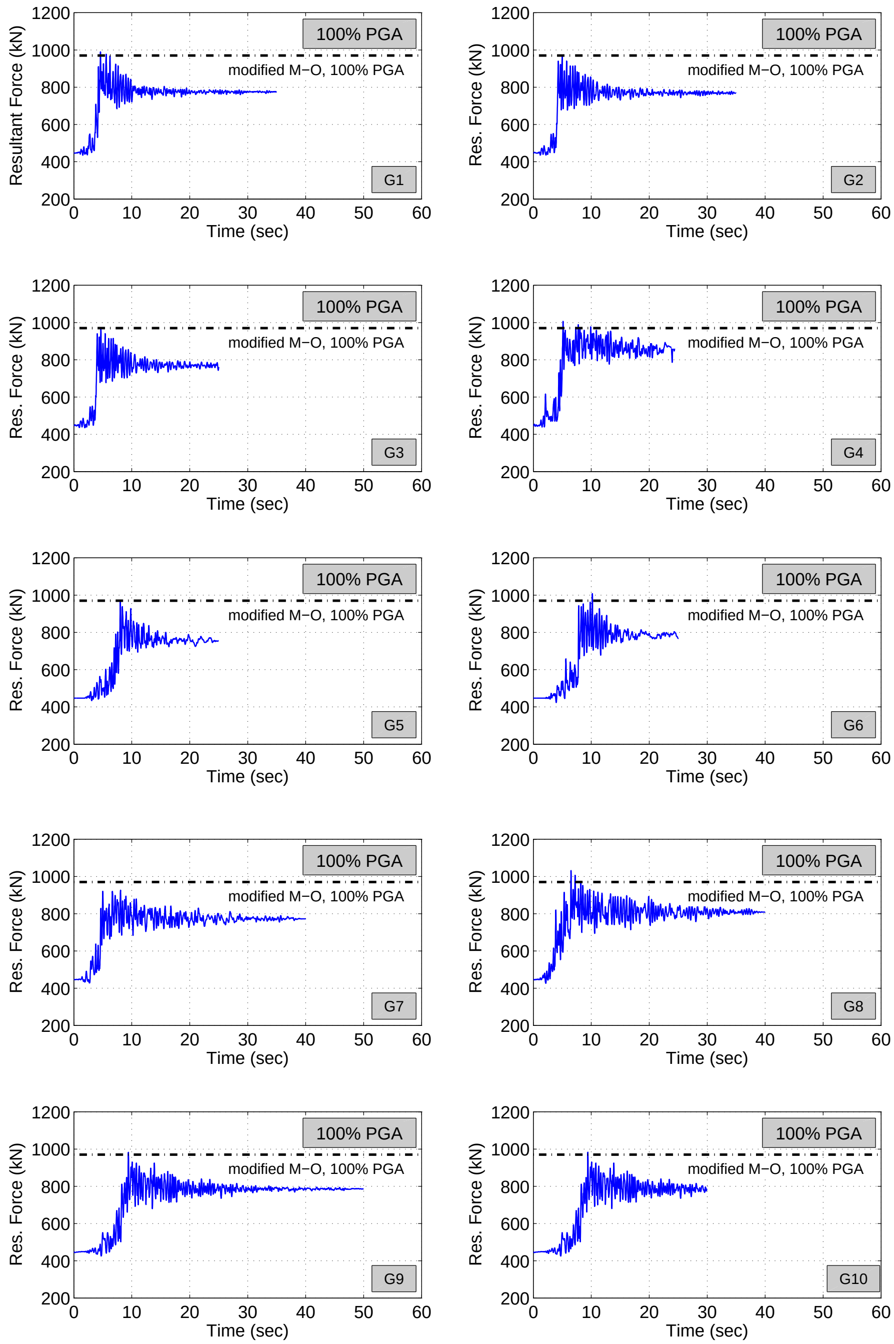

Figure 4.3: Continued.

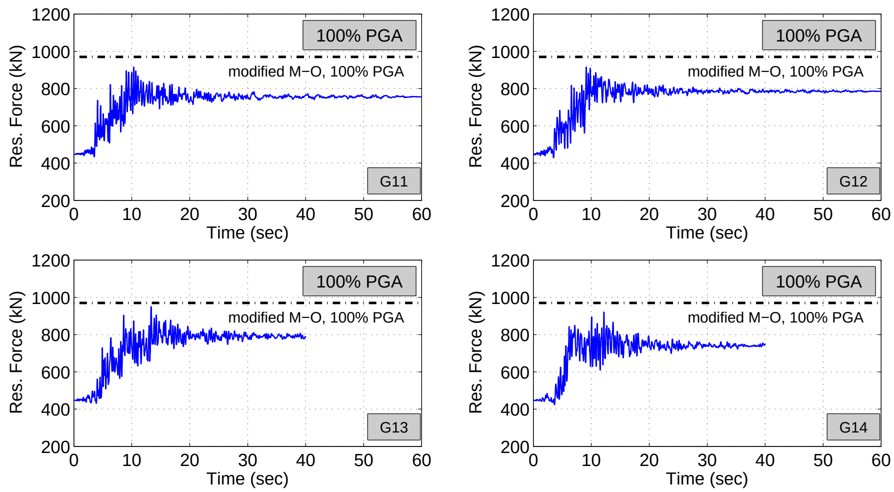

Figure 4.3: Time histories of the resultant lateral earth force of the wall designed for 100% PGA subjected to 14 ground motions, compared with the corresponding P_{AE} calculated from the modified M-O method.

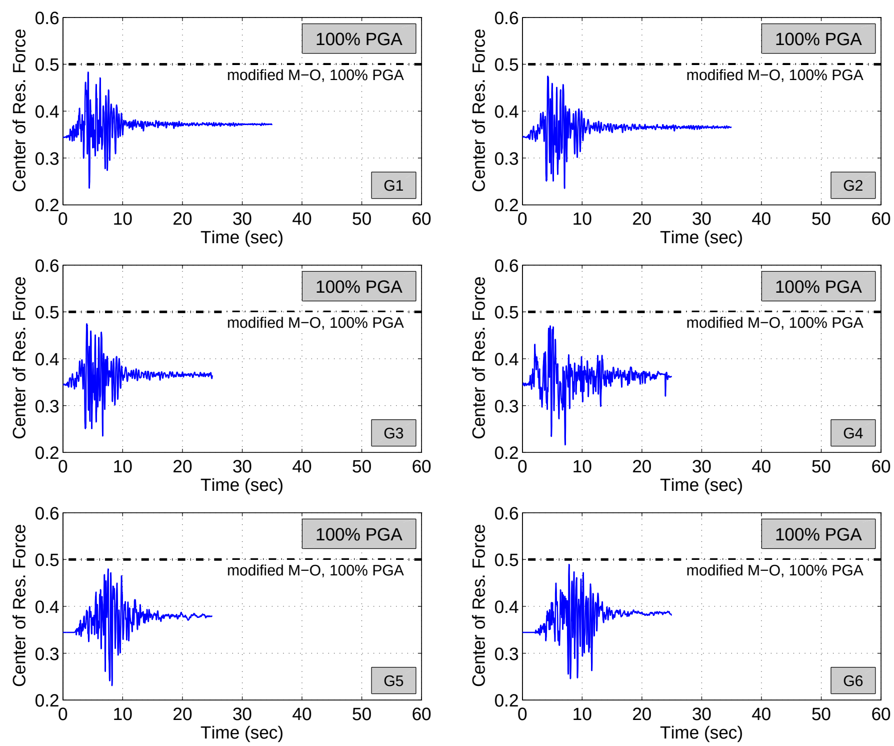

Figure 4.4: Continued.

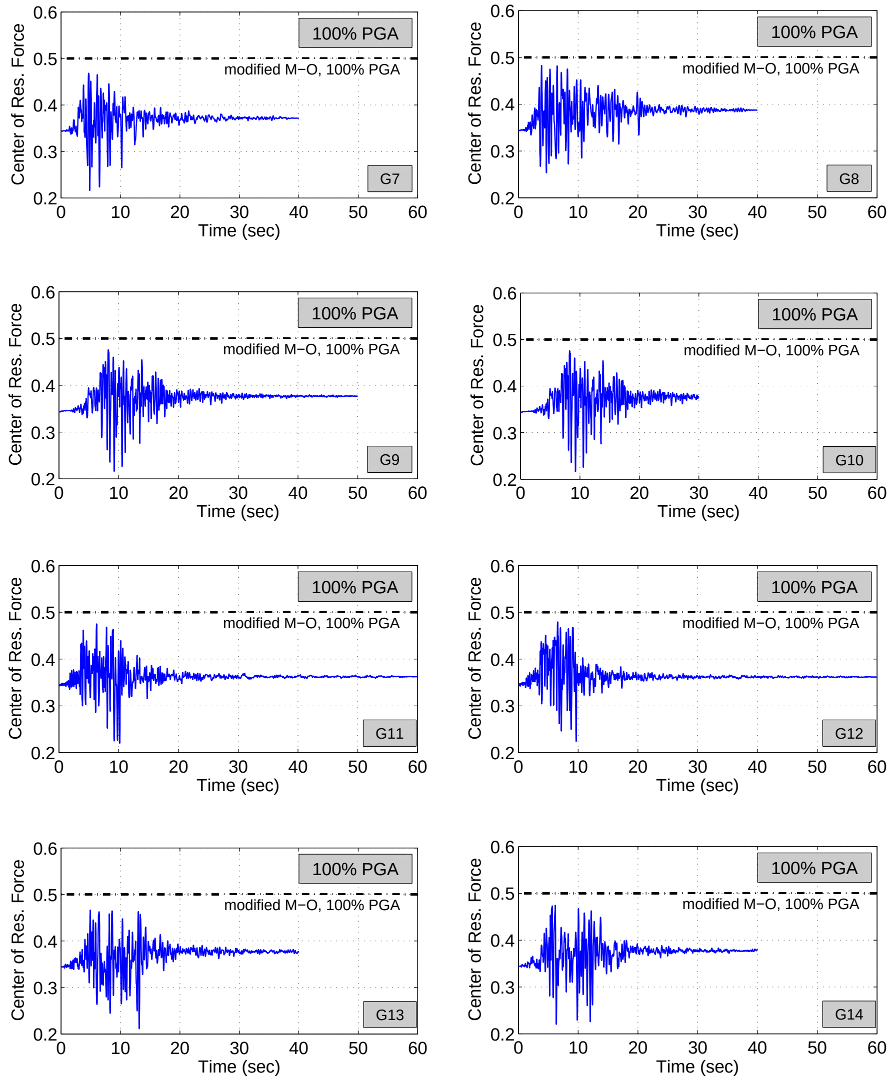

Figure 4.4: Time histories of the normalized height of application of the lateral earth force from the base of the wall designed for 100% PGA subjected to 14 ground motions, compared with the corresponding P_{AE} calculated from the modified M-O method.

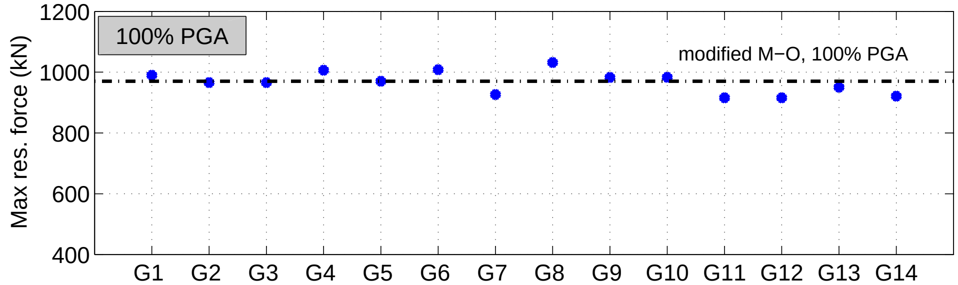

Figure 4.5: Maximum resultant lateral earth forces on the walls designed for 100% PGA subjected to 14 ground motions, compared with the corresponding P_{AE} values calculated from the modified M-O method using the same fraction of PGA.

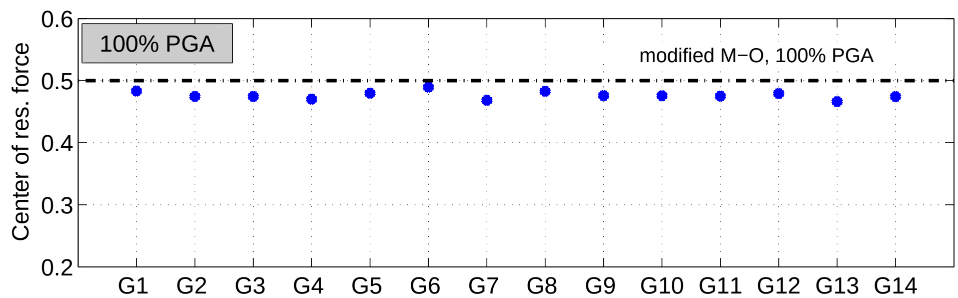

Figure 4.6: The normalized heights of application of the maximum resultant lateral earth forces from the base of the wall designed for 100% PGA subjected to 14 ground motions, compared with the corresponding normalized heights of application of P_{AE} from base of the wall calculated from the modified M-O method using the same fraction of PGA.

Figure 4.7 shows the distribution of the maximum lateral earth pressures along the height of the wall at different times during ground motion excitation. The maximum value of the lateral earth pressure that each element located at specific height of the wall is experienced during the ground motion shaking in this study is

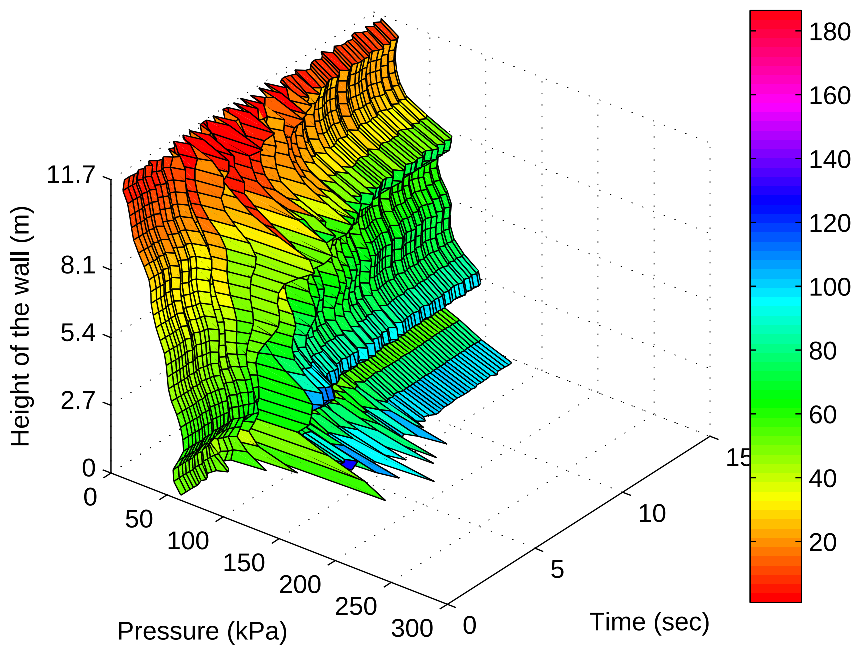

Figure 4.7: Distribution of the maximum envelope of the lateral earth pressure along the height of the basement wall designed for 100% code PGA subjected to earthquake ground motion G1 (only the first 15 sec response is illustrated).

referred to as the "maximum envelope" of earth pressure. Similarly the minimum lateral earth pressure along the height of the wall during excitation is referred to as the "minimum envelope". The distribution of the pressure at the end of excitation is known as the "residual".

Figure 4.8 shows the average of the maximum envelopes, average of the minimum envelopes, and the residual lateral earth pressures along the height of the basement walls designed for different factions of code PGA and subjected to ground motions G1–G14. The instantaneous distributions of earth pressure at different times during the shaking event fall between the maximum and the minimum envelopes. Three particular cases of these instantaneous distributions of earth pressure are: (1) the residual pressures at the end of shaking as is shown in Figure 4.8, (2) the static lateral pressure at the beginning of the dynamic analysis as illustrated in Figure 4.9 and (3) the pressures at the instance of occurrence of the maximum resultant lateral earth force shown in Figure 4.10.

Figure 4.9 shows the averages of pressure distribution at the beginning of dynamic analysis of the walls designed for different fractions of code PGA subjected to ground motions G1–G14. In this figure the averages of pressure distribution is compared with the suggested distribution of lateral pressures from Coulomb's static theory (black dashed line). It can be concluded from this figure that the computational analyses results at $t = 0$ *sec* adequately match those obtained from the Coulomb's theory for static lateral earth pressure distribution and distributed approximately linearly with depth prior to earthquake and the computational model simulates the static condition properly.

The averages of pressure distribution patterns at the instance of occurrence of maximum resultant lateral force for ground motions G1–G14 are shown in Figure 4.10. The corresponding linear distributions of the total active lateral pressure (p_{AE}) used in seismic design of the walls, calculated from the modified M-O method using the same fraction of PGA (Figure 3.2), are also plotted for comparison. In case of the weaker walls designed for 50% to 60% of the code PGA, the dynamic pressure distributions at the instance of maximum resultant force are different from the pressure distributions calculated from the modified M-O method used in the design of the walls. In these walls the distributed pressures on the walls at the instance of occurrence of the maximum resultant lateral earth force are more concentrated at the floor levels than between the floor levels. The flexibility and yielding of these weaker walls at different locations along their height result in a very different displacement pattern compare to the stronger ones (90% and 100% PGA).

Figure 4.10 shows that when the wall is designed for any fraction less that 100% PGA based on the modified M–O procedure but still subjected to ground motions corresponding to the full current seismic demand, the design pressure underestimates the average of the actual soil pressure acting on the wall. The performance of the basement walls depend on what happens between floor levels and the dynamic pressures on the more flexible walls do not violate the performance

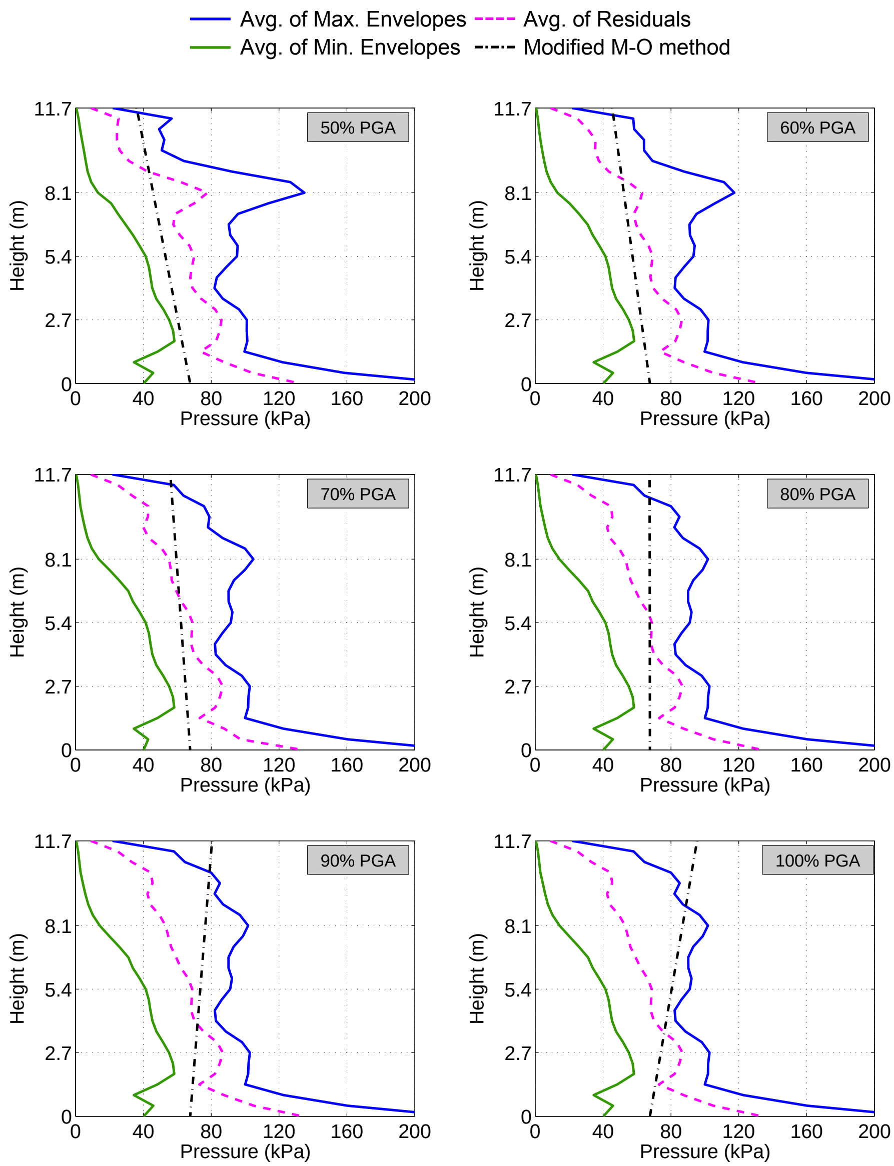

Figure 4.8: Average of maximum envelopes, average of minimum envelopes, and residual lateral earth pressures for ground motions G1–G14, along the height of the walls designed for different fractions of the code PGA, compared with the corresponding p_{AE} calculated from the M-O method for the same fraction of PGA used for design of each wall.

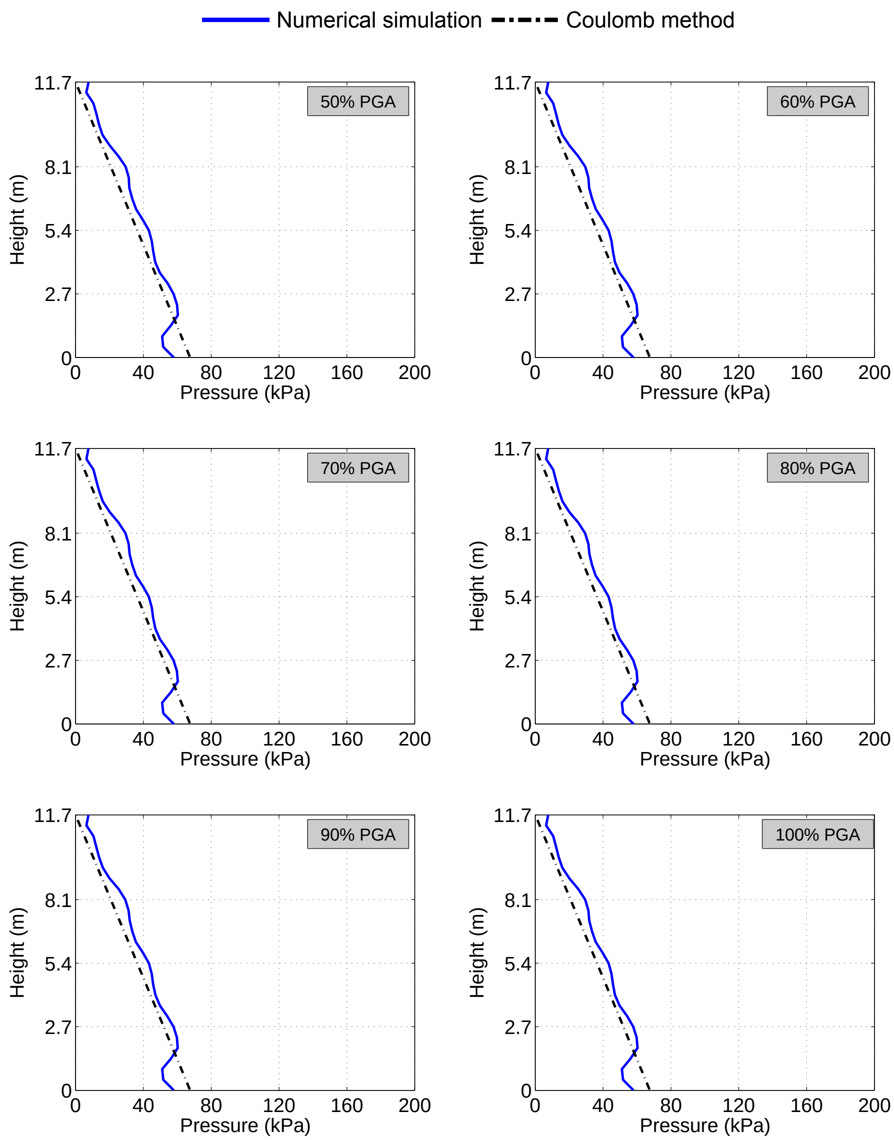

Figure 4.9: Average of static pressures prior to the dynamic analysis for ground motions G1–G14, along the height of the walls designed for different fractions of the code PGA, compared with the corresponding p_A calculated from the Coulomb static theory.

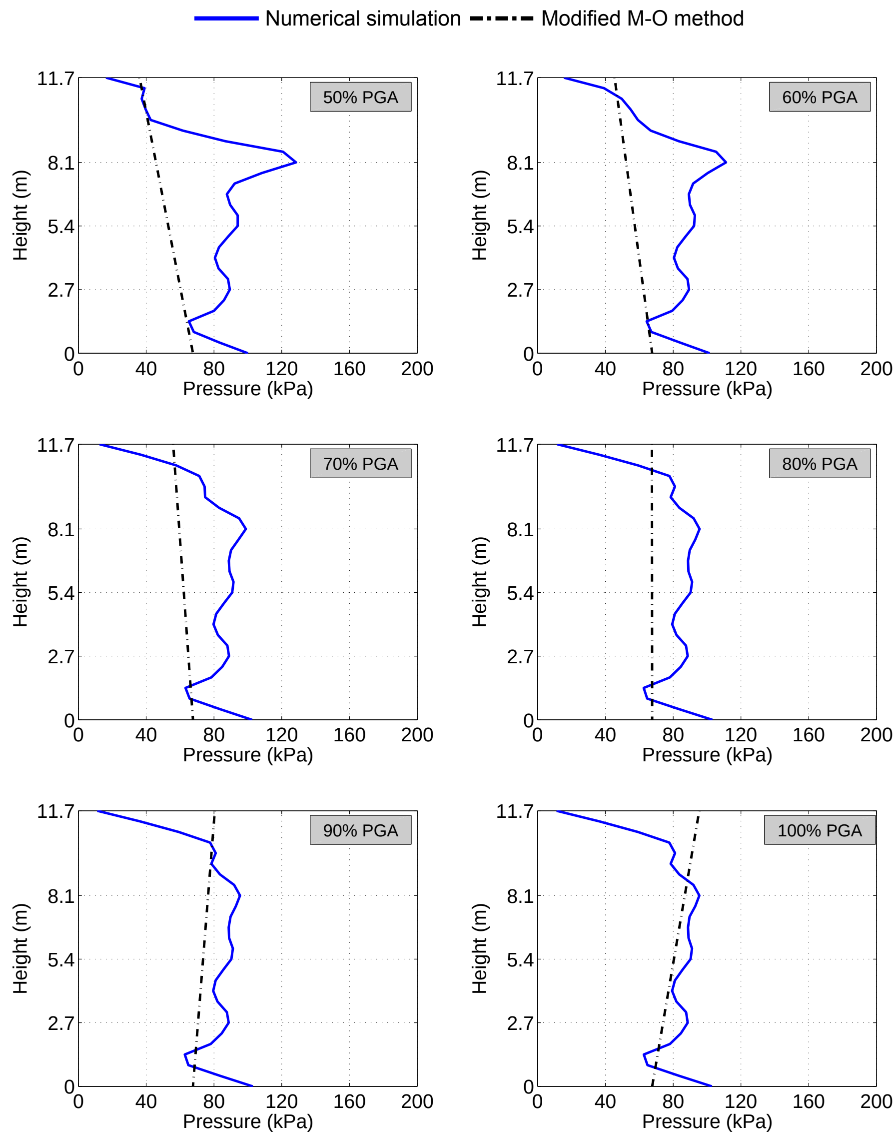

Figure 4.10: Average of pressure patterns at the instance of occurrence of maximum resultant lateral earth force for ground motions G1–G14, along the height of the walls designed for different fractions of the code PGA, compared with the corresponding p_{AE} calculated from the M-O method for the same fraction of PGA used for design of each wall.

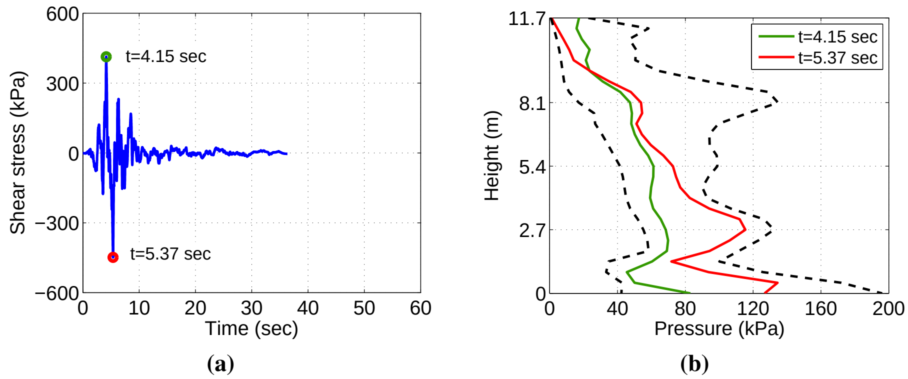

Figure 4.11: (a) Shear stress time history corresponding to earthquake ground input motion G1 and (b) the lateral earth pressure distributions at the instances of the maximum shear stress along the height of the basement wall designed for 50% PGA; black-dashed lines represent the average of the maximum and minimum envelopes of the lateral earth pressures for ground motions G1–G14.

criteria, which is related to the mid-level deflections between floors as will be presented and discussed later on. The results also show that near the base of the walls the pressures are generally higher than the corresponding modified M–O pressures, and that might be attributed the higher lateral restraint at the base and the fact that the foundation of the wall is embedded in the second stiffer layer, which significantly affects the displacement pattern on the wall.

There might be a hypothesis that the maximum pressure on the wall occurs at the time of the maximum shear stress applied at the base of the model. Figure 4.11 illustrates the earth pressure distribution along the height of the wall subjected to ground motion G1 at $t = 4.15$ *sec* and $t = 5.37$ *sec*, which the shear stress time history reaches its maximum values at different directions. It can be concluded from this figure that the maximum shear base and the maximum pressure on the wall do not happen simultaneously. Besides, the size and the shape of the earth pressure distribution change over time, which is in contrast with hypothetical condition of the Mononobe-Okabe method that assumes the earth pressure distribution does not change with time.

4.3 Bending moments and shear forces on the wall

Figures 4.12 and 4.13 show the average of the maximum and minimum bending moment and shear force envelopes, and the residual bending moments and shear forces, for ground motions G1–G14. In both of these figures the results are shown for the wall designed for six different fractions of the code PGA. The corresponding profiles of nominal moment capacity $M_n(z)$ and shear capacity $V_n(z)$ for each wall as discussed and calculated in Section 3.2 are illustrated in these figures for comparison.

Yielding occurs where the seismic moment or shear envelopes reach the moment or shear capacities, respectively. Figure 4.12 shows that the strong walls, designed for 100% down to 80% of the code PGA, almost remain elastic at all basement wall levels. They barely yield in moment at the mid-height of the basement level -4 and at the floor of basement levels -3 and -2 (basement level No. is in accordance with Figures 3.1 and 3.2). However, the walls designed for lower percentages of PGA (70% to 50%) show more significant signs of yielding in moment at different elevations. The weakest wall, designed for 50% PGA, shows significant yielding at the mid-height of the basement level -1. It also shows signs of yielding at the mid-height of the basement level -4 and at the floor of basement levels -1, -2, and -3.

The shear envelopes in Figure 4.13 show that in all cases the shear demand is considerably less than the shear capacity along the height of the wall.

4.4 Displacements and drift ratios on the wall

Given that the weaker walls yield in moment in various elevations along their height, from the engineering performance-based design standpoint it is very important to monitor the resulting deformations and drift ratios of the walls, which can be considered as representative parameters for assessing the performance of a structure.

The deformations are calculated as displacements of the wall at each elevation relative to the base of the wall. To the best knowledge of the author, except for a recommendation by the ASCE Task Committee on Design of Blast-Resistant Buildings in Petrochemical Facilities (ASCE-TCBRD, 2010), there is no other sig-

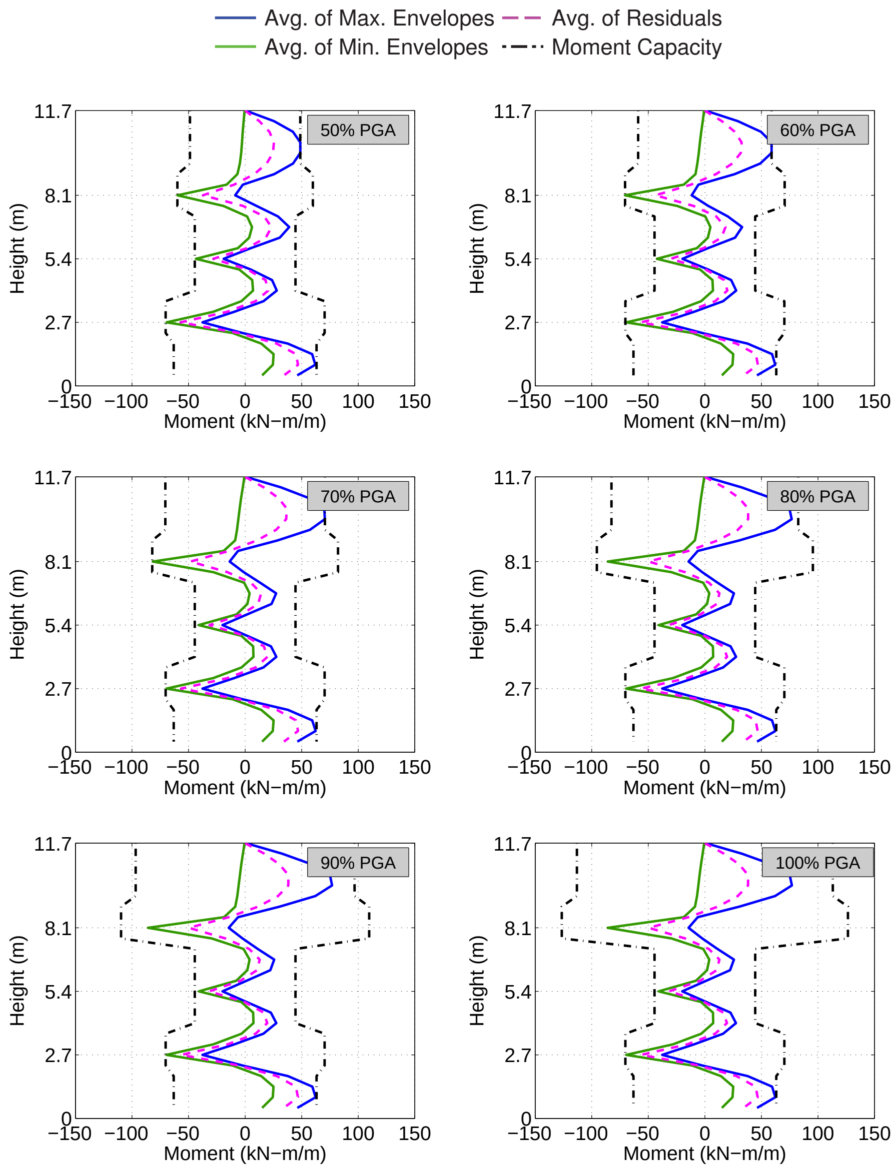

Figure 4.12: Average of maximum envelopes, average of minimum envelopes, and residual bending moments for ground motions G1–G14, along the height of the walls designed for different fractions of the code PGA, compared with the corresponding nominal moment capacity, $M_n(z)$, of each wall.

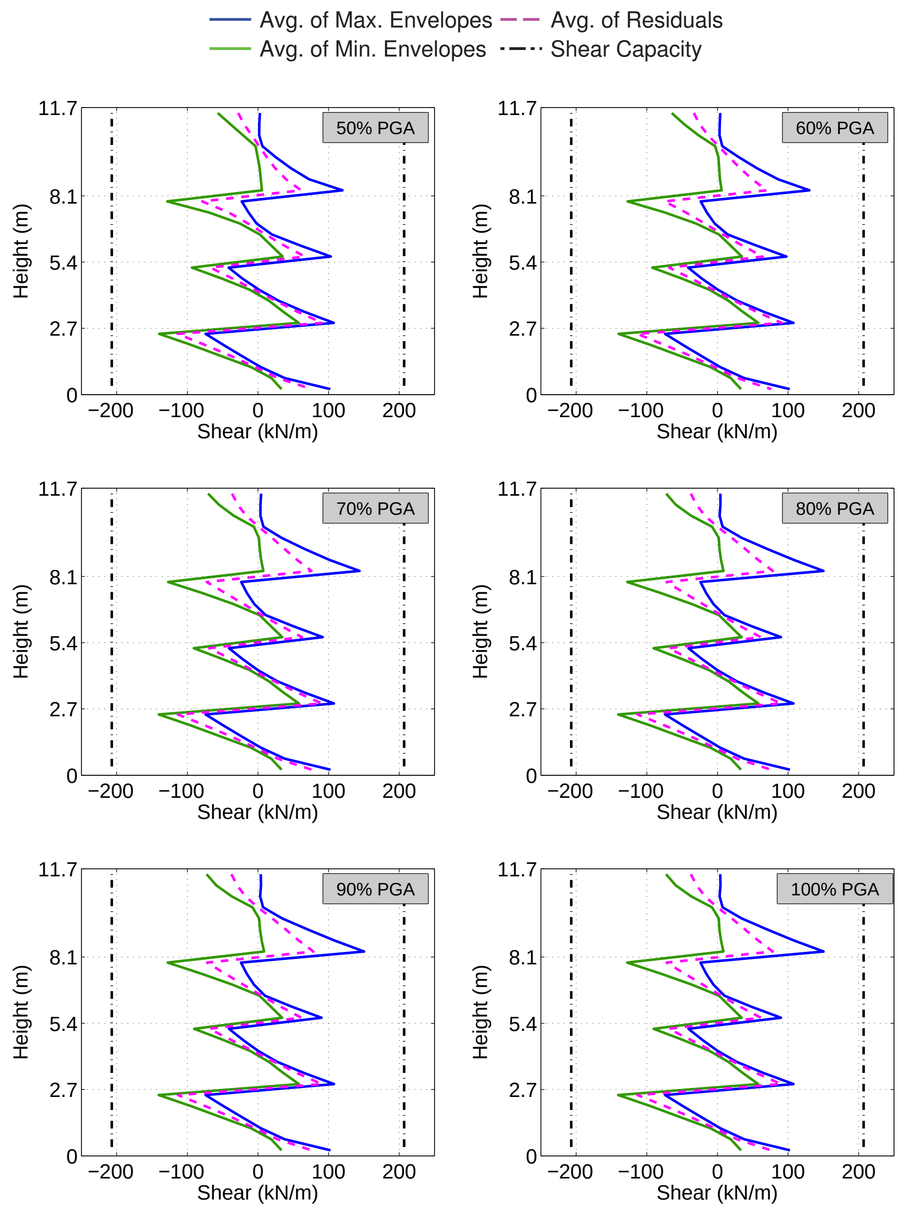

Figure 4.13: Average of maximum envelopes, average of minimum envelopes, and residual shear forces for ground motions G1–G14, along the height of the walls designed for different fractions of the code PGA, compared with the corresponding nominal shear capacity, $V_n(z)$, of each wall.

nificant report presented in the literature on the acceptable drift ratios for constrained walls with distributed lateral loading.

The ASCE-TCBRD (2010) introduced hinge rotation at support of beams, slabs, and panels as a measure of member response that indicates the degree of instability present in critical areas of the member. In the search for an appropriate performance level, and in the absence of any other reported criteria, the recommendations of the ASCE task committee is adopted as the performance standard for the walls. To this end, and consistent with the concept of hinge rotation at support, the drift ratio of a basement wall at the middle of each storey is calculated as the difference between the displacement of the wall at that level and the average displacements of the wall at the top and bottom of the storey divided by half of the storey height, as illustrated in Figure 4.14. In this figure, h is the floor height, $u_{\text{floor,top}}$ and $u_{\text{floor,bottom}}$ are the wall deformations at the floor levels, and u_{wall} is the wall deformation at the mid-height of the storey.

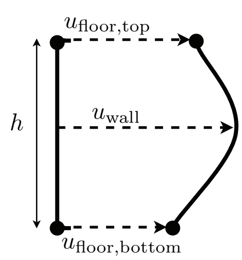

$$\text{Drift ratio} = \frac{2u_{\text{wall}} - (u_{\text{floor,top}} + u_{\text{floor,bottom}})}{h}$$

Figure 4.14: Definition of drift ratio for each level of the basement wall.

The ASCE committee specified two performance categories that may apply to basement walls: low and medium response categories. The Low Response Category is defined as: “Localized component damage. Building can be used, however repairs are required to restore integrity of structural envelope. Total cost of repairs is moderate”. The Medium Response Category is defined as: “Widespread component damage. Building should not be occupied until repaired. Total cost of repairs is significant.” The response limits associated with these two response states for “reinforced concrete wall panels (with no shear reinforcement)” are 1° hinge rotation at support (hence 1.7% drift ratio) and 2° hinge rotation at support (hence 3.5% drift ratio). The Low Response Category defined above is used as the performance criterion in the present study. Separate calculations were also conducted using standard procedure for calculating curvature demand in reinforced concrete (Park and Pauly, 1975) by SEABC structural Engineers (Appendix A). The results suggested that even a slightly greater drift ratio could be adopted as the performance criterion safely (DeVall and Adebar, 2011).

Profiles of wall deformations (displacements relative to the base of the wall) and the associated drift ratios are shown in Figures 4.15 and 4.16, respectively. These figures show the average of maximum envelopes, average of minimum envelopes, and the residual lateral deformations and drift ratios for ground motions G1–G14, along the height of the 4-level basement wall designed for different fractions of the code PGA. The relative displacements are larger between the floors and are smaller at each floor level. According to the adopted performance criterion for drift ratio, only the response of the top level of the basement wall in the present problem needs careful consideration. Figure 4.16 shows that for the walls designed for 60% and 50% of the code PGA, the average of maximum envelopes of drift ratios in the top basement level for ground motions G1–G14 are about 0.5% and 1.1%, respectively, which fall into the low response category ($< 1.7\%$). At other levels of the basement wall the drift ratios are insignificant. These results suggest that the performance of the wall designed for even 50% of the code PGA for Vancouver seems adequate.

All the results presented so far were based on information regarding to the left-side walls. The right-side walls undergo almost the same performance as the left-side walls. The average of the maximum envelopes of drift ratios along the height of the both right-side and the left-side walls designed for different fractions of the code PGA, are presented in the left-hand-side column of Figure 4.17. In these plots the solid line corresponds to the average of the maximum drift ratio along the height of the both right-side and left-side walls subjected to 14 crustal ground motions (G1–G14) spectrally matched to the NBCC (2010) hazard level. By assuming normally distributed drift ratios, average $\pm 1\sigma$ represents the first standard deviation with a 68% chance that the mean falls within the range of standard error.

Right-hand-side column of Figures 4.17 illustrates a detailed information regarding to the distribution of the maximum drift ratios along the height of the wall

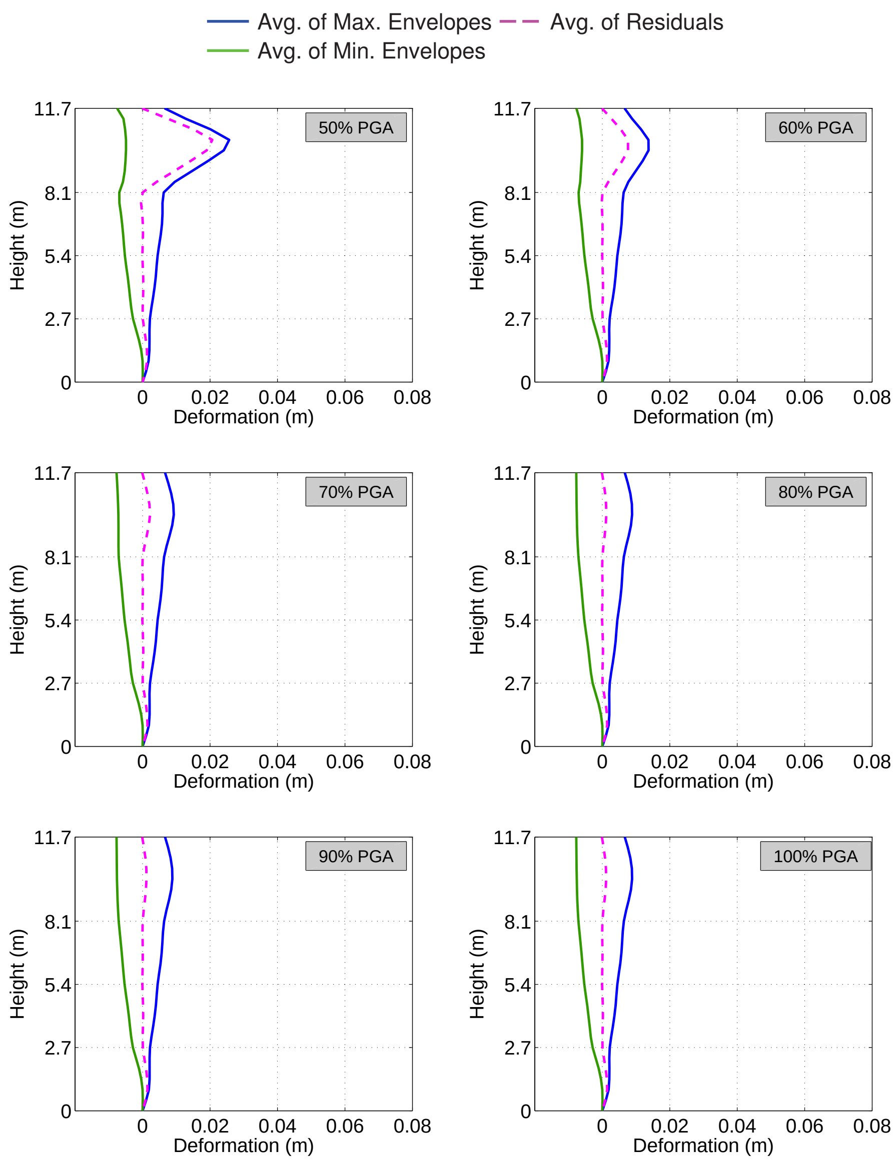

Figure 4.15: Average of maximum envelopes, average of minimum envelopes, and residual lateral deformations (displacements relative to the base of the basement wall) for ground motions G1–G14, along the height of the walls designed for different fractions of the code PGA.

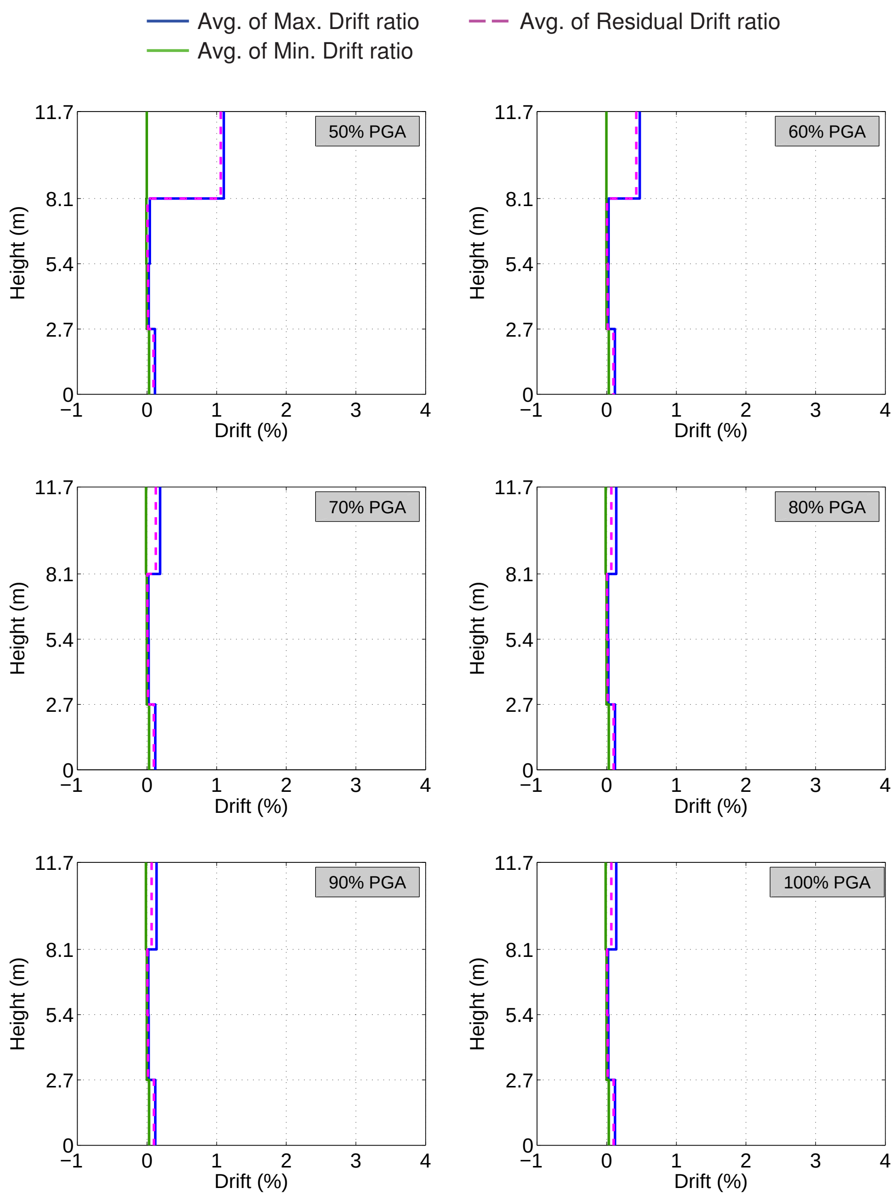

Figure 4.16: Average of maximum envelopes, average of minimum envelopes, and residual drift ratios for ground motions G1–G14, along the height of the walls designed for different fractions of the code PGA.

in the form of exceedance probability. Each point in these plots corresponds to the maximum drift ratio of the right-side and the left-side walls subjected to one ground motion. Exceedance probability presented in the y-axis is the probability of an event being greater than or equal to a given value; e.g., in the case of the wall designed for 50% PGA, there is a 40% chance that the maximum drift ratio exceeds 1.2%. In these figures the value of the center of the distribution is the drift ratio at which the curve crosses the 50% line from the vertical axis and represents an average value of the response.

4.5 Sensitivity analyses

A series of sensitivity analyses are conducted to identify sensitive or important input parameters and study their effects on the seismic performance of the basement wall. The nonlinear dynamic response of the wall in the present soil-structure system can be assessed in many ways. As it is not possible to cover all aspects of the seismic performance results, it is decided to only focus on the maximum drift ratio of the wall, which has the greatest significance for engineering design and can be evaluated based on an adopted performance criterion.

The results presented in this section cover the sensitivity analyses on the employed shear wave velocity, friction and dilation angles of the backfill soil, the modulus reduction factor ($G/G_{\max}$), the Rayleigh damping ratio (D) for the top soil layer, applied shoring pressure during excavation process and also the properties of the interface element between soil and the basement wall. In all these analyses, the wall is designed for 50% of the code PGA and is subjected to the selected 14 crustal ground motions spectrally matched to NBCC (2010) UHS for Vancouver (G1–G14). Based on these sensitivity analyses, the parameters which have more effect on the seismic performance of the basement walls are determined and discussed in more detail in Chapter 5.

4.5.1 Soil–wall interface element

Wall response is found to be sensitive to the interface friction angle, as shown in Figure 4.18. In all the analyses presented so far, an interface friction angle of $\delta = 10^\circ$ ($\simeq \phi/3$) based on a judgment of local consultants is used. Two additional

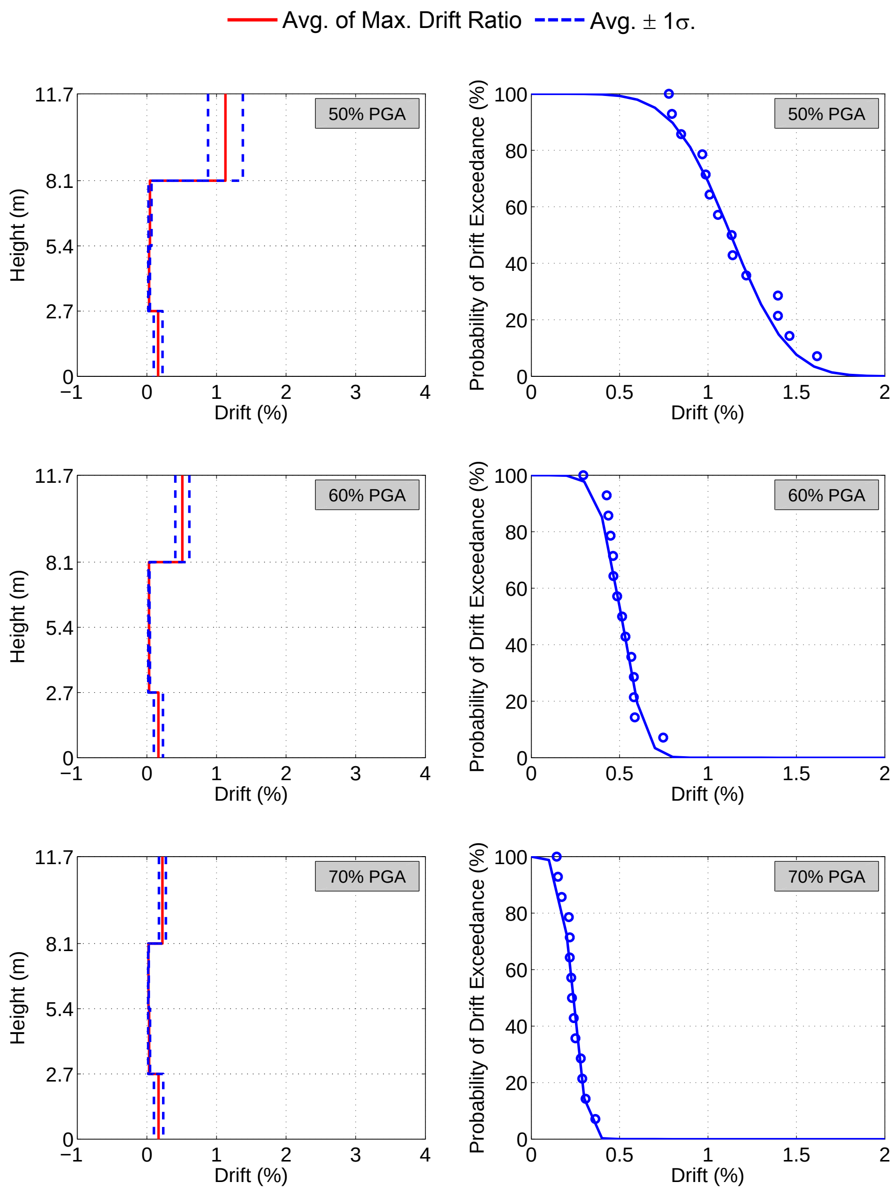

Figure 4.17: Continued.

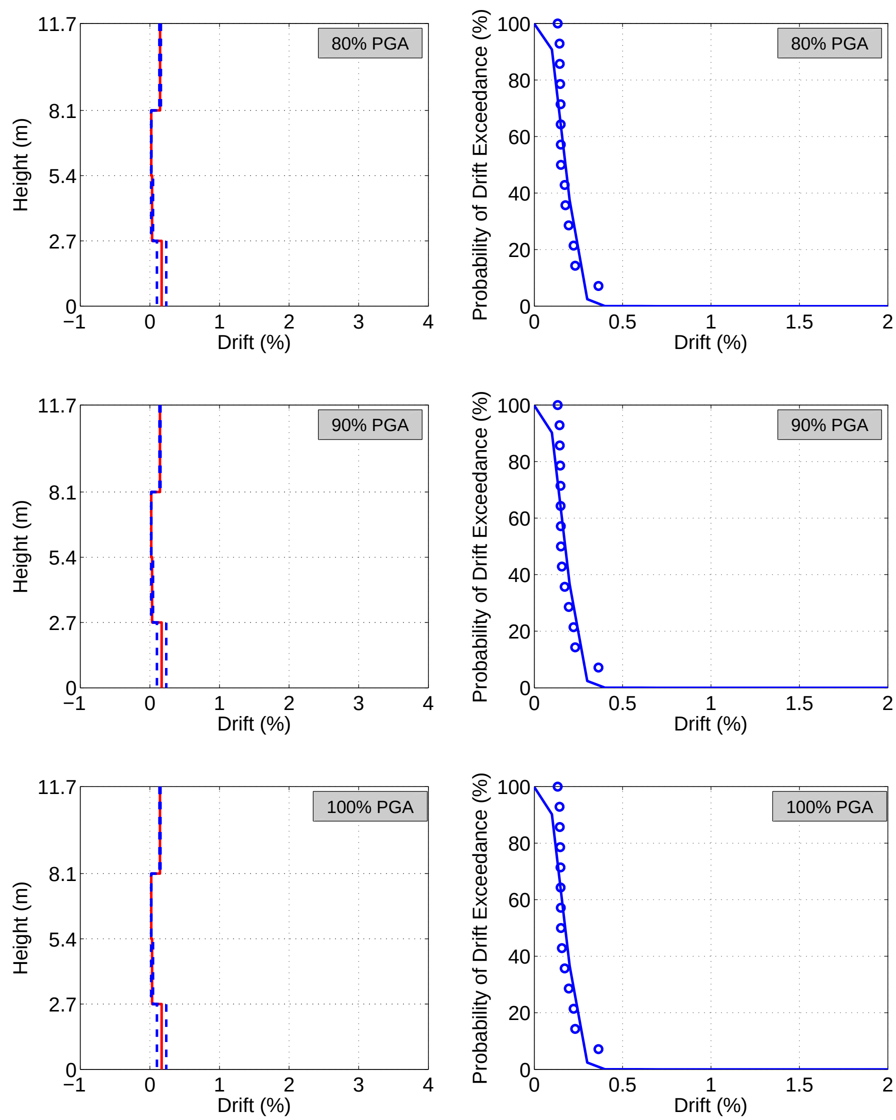

Figure 4.17: (Left-hand-side column) Average of maximum envelopes of drift ratios and the corresponding average ± one standard deviation along the height of the wall;(right-hand-side column) distribution of the maximum drift ratios in the form of exceedance probability of the walls designed for different fractions of the code PGA, subjected to ground motions G1–G14 spectrally matched to NBCC (2010) UHS for Vancouver.

sets of analyses are conducted, with $\delta = 5^\circ$ and 15°, to check the sensitivity of wall response to interface friction angle. As expected higher values of interface friction angle lead to smaller wall drift ratios. An additional analyses are conducted to check the importance of allowing soil–wall slippage and separation. To this aim a series of analyses are conducted in which opposite nodes are not allowed to separate from each other and consequently no slippage or opening is allowed along the interface element. The results of these simulation show that considering interface slippage and separation is crucial for realistic evaluation of wall performance.

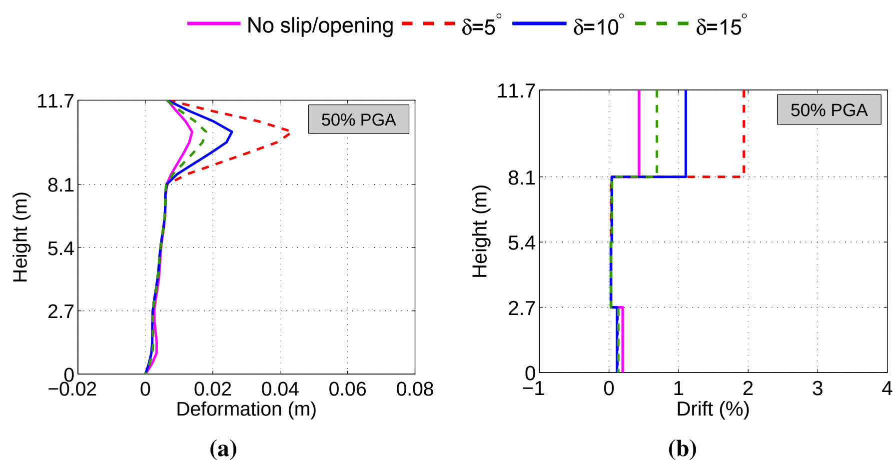

Figure 4.18: Average of maximum envelopes of (a) lateral deformations and (b) drift ratios along the height of the wall designed for 50% the code PGA, subjected to ground motions G1–G14 showing the sensitivity of response to variation of the friction angle of the soil–wall interface element, including the case where no slippage and/or opening is allowed.

Sensitivity analyses show that the drift ratios are not sensitive to elastic normal and shear stiffnesses of the interface element (k_n and k_s), even if these values are increased or decreased by ten times as illustrated in Figure 4.19. This is consistent with the conclusion of Day and Potts (1998).

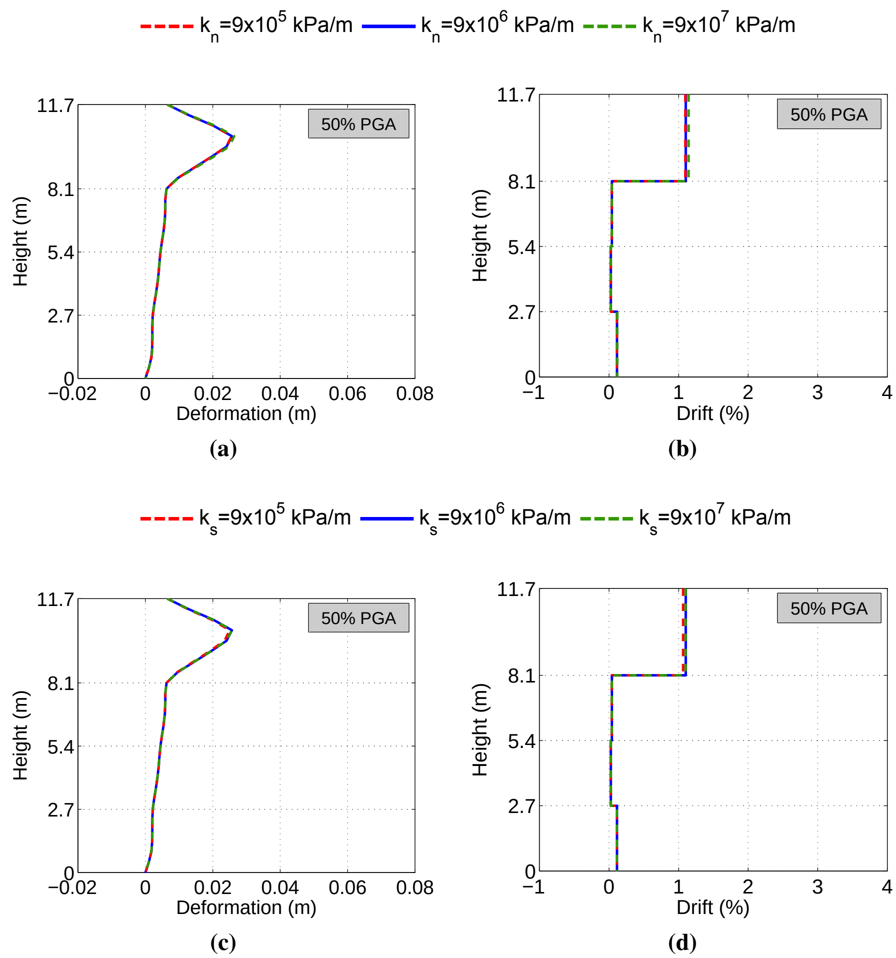

Figure 4.19: Average of maximum envelopes of (a,c) lateral deformations and (b,d) drift ratios along the height of the wall designed for 50% the code PGA subjected to ground motions G1–G14, showing the lack of sensitivity of response to variation of the normal and shear stiffnesses of the soil–wall interface element.

4.5.2 Dilation angle of the backfill soil

The angle of dilation controls an amount of plastic volume change over plastic shear strain. The soil in the current study is modeled using the non-associative flow rule by adopting a dilation angle of $\psi = 0^\circ$ in the Mohr–Coulomb model, which corresponds to the volume preserving deformation in shear. For soils the dilatancy angle is known to be significantly smaller than the friction angle.

In this section the importance of the soil dilation angle and its influence on the seismic performance of the basement walls are examined. The importance of dilation angle is determined by examining two additional dilation angles of $\psi = 5^\circ$ and $\psi = 10^\circ$.

A series of sensitivity analyses are conducted on the 4-level basement wall designed for 50% PGA and subjected to ground motions G1–G14. The result of these analyses presented in Figure 4.20 show the lack of sensitivity of the wall displacements and drift ratios to the change in the dilation angle of the top soil layer between zero and 10°.

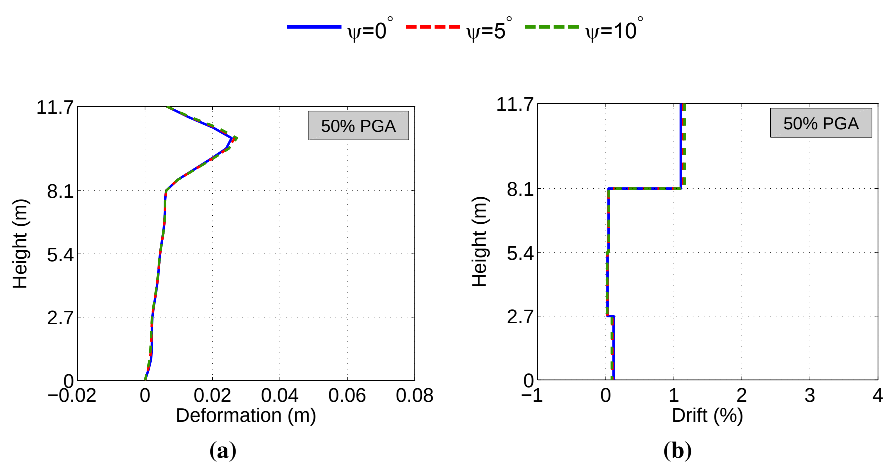

Figure 4.20: Average of maximum envelopes of (a) lateral deformations and (b) drift ratios along the height of the wall designed for 50% the code PGA subjected to ground motions G1–G14, showing the lack of sensitivity of the response to variation of top soil dilation angle.

4.5.3 Friction angle of the backfill soil

This section evaluate the effect of slightly change (± 5°) in the friction angle of the backfill soil, which was assumed as 33° in the benchmark analyses. The results of this study presented in Figure 4.21 confirm that there is not a considerable effect on the performance of the structure if the wall is embedded in a backfill soil with slightly higher or lower friction angles of 28° and 38°.

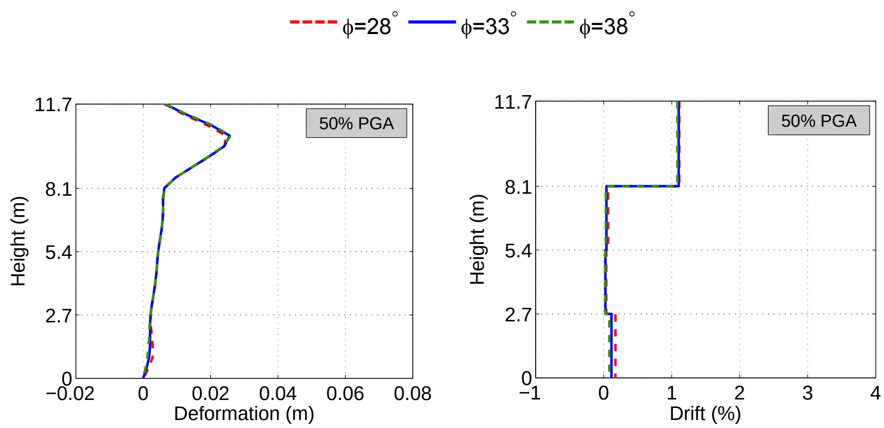

(a) (b)

Figure 4.21: Average of maximum envelopes of (a) lateral deformations and (b) drift ratios along the height of the wall designed for 50% the code PGA subjected to ground motions G1–G14, showing the lack of sensitivity of the response to variation of top soil friction angle.

4.5.4 Shear wave velocity of the backfill soil

The normalized shear wave velocity (V_{s1}) of the top soil layer was assumed to be 200 m/s in the benchmark analyses. The value of $V_{s1} = 200\ m/s$ was recommended by the geotechnical engineers in practice for Vancouver. In order to study the effect of the top soil layer stiffness, the performance of the basement wall embedded in two other soil profiles with the normalized shear wave velocities of 150 m/s and 250 m/s at their top soil layer are studied. The resulting two different profiles of the shear wave velocity in the first soil layer as well as the shear wave velocity profile of the second layer corresponding to $V_{s1} = 400$ m/s are presented in Figure 4.22. Following the procedure described in Section 3.3.4 for calculating the equivalent modulus reduction and damping ratios from the SHAKE analyses, Table 4.1 presents the calculated G/G_{max} and damping ratios correspond to two new soil profiles. It is worth to mention that the values of interface stiffnesses which are the function of the stiffness of the stiffest neighbouring zones (See Equation 3.6) along the interface elements are also modified accordingly in these analyses.

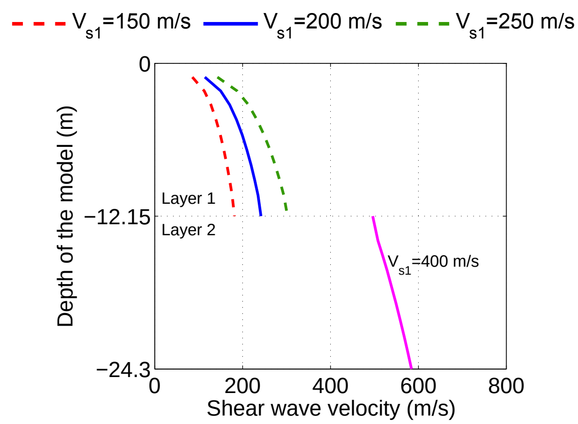

Figure 4.22: Different scenarios of the shear wave velocity profiles of the soil along the depth of the model.

Table 4.1: Soil modulus reduction and damping ratios obtained from SHAKE analyses for different normalized shear wave velocities of top soil layer.

V_{s1} (m/s)	Modulus reduction, $G/G_{\max}$		Damping ratio, D (%)	
Layer 1	Layer 1	Layer 2	Layer 1	Layer 2
150	0.25	0.84	11.5	2.5
200*	0.41	0.81	8.0	3.0
250	0.60	0.79	6.0	3.3

* Calcultaed from Figure 3.8 and used for the benchmark analyses.

Simulations are conducted based on the corresponding elastic shear modulus and the Rayleigh damping ratios applied to two levels of V_{s1} at the top soil layer for the wall designed for 50% of the code PGA excited by ground motions G1–G14. The resultant average of the maximum envelopes of lateral deformations and drift ratios for each value of V_{s1} are presented in Figure 4.23. The results of the benchmark analyses with $V_{s1} = 200\ m/s$ are also added for comparison. This figure suggests considerable sensitivity of the results to the shear wave velocity of the top soil layer, based on the adopted method of analysis. As illustrated in this figure, increasing the shear wave velocity in the top soil layer decreases the drift ratio of the wall. The sensitivity analysis shows that a $V_{s1} = 150$ m/s, which might be a bit low for the high-rise construction sites in Vancouver, results in a maximum drift ratio of about 2.5% in the basement wall. This is still in the lower range of the medium response category, as defined by ASCE-TCBRD (2010).

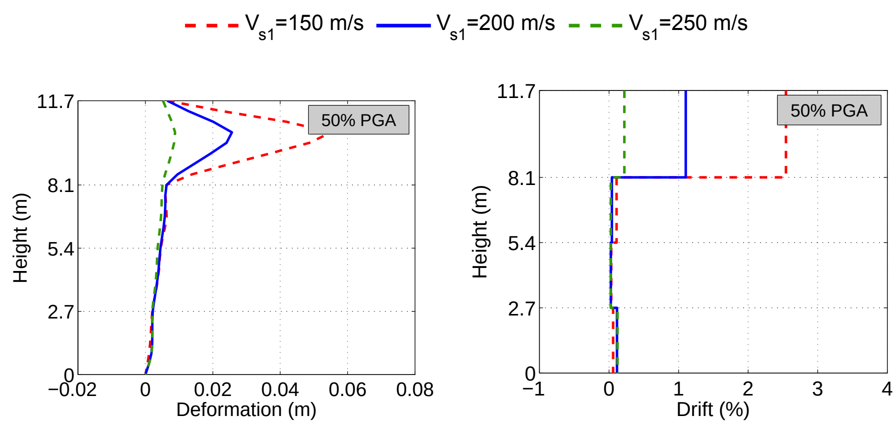

(a) **(b)**

Figure 4.23: Average of maximum envelopes of (a) lateral deformations and (b) drift ratios along the height of the wall designed for 50% the code PGA subjected to ground motions G1–G14, showing the sensitivity of response to variation in the normalized shear wave velocity of the top soil layer.

Due to the considerable amount of sensitivity of the resultant maximum drift ratio of the basement wall to the shear wave velocity profile of the site, an extensive study on the effect of underlying soil stiffness is conducted in Chapter 5.

4.5.5 Modulus reduction and Rayleigh damping

In the benchmark analyses presented in Sections 4.2 to 4.4, the top soil layer was modeled using an average value of $G/G_{\max} = 0.41$ and $D = 8\%$. Additional analyses are conducted on two additional modulus ratios, $G/G_{\max} = 0.3$ and 0.5 both with $D = 8\%$, and with two additional levels of damping $D = 6\%$ and 10% both with $G/G_{\max} = 0.41$, on the weakest wall designed for 50% of the code PGA and subjected to 14 ground motions (G1–G14).

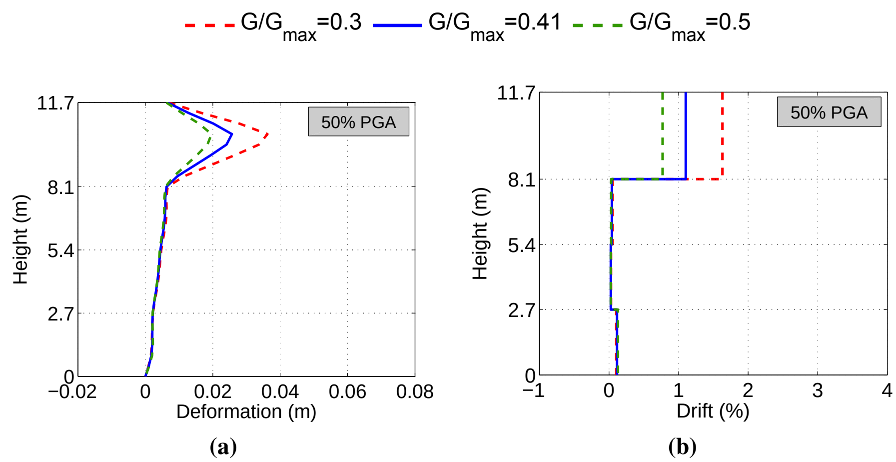

Figure 4.24: Average of maximum envelopes of (a) lateral deformations and (b) drift ratios along the height of the wall designed for 50% the code PGA subjected to ground motions G1–G14, showing the sensitivity of the response to variation in the modulus reduction of the top soil layer.

Figures 4.24 and 4.25 show the sensitivity of the maximum envelope of lateral deformations and drift ratios to variations of the modulus reduction and damping ratios of the first soil layer, respectively. These results suggest that lower values of $G/G_{\max}$ and damping result in higher wall drift ratios.

The fact that the results produced using Mohr–Coulomb model with an additional modulus reduction factor and Rayleigh damping are sensitive to the selection of G/G_{max} and damping values suggests that the seismic performance of the basement walls may be dependent on the nature of the stress–strain response of the soil material and using more representative constitutive model could be helpful. The influence of more advanced nonlinear constitutive model with hysteresis damping on seismic performance of the embedded basement walls is examined in Chapter 5.

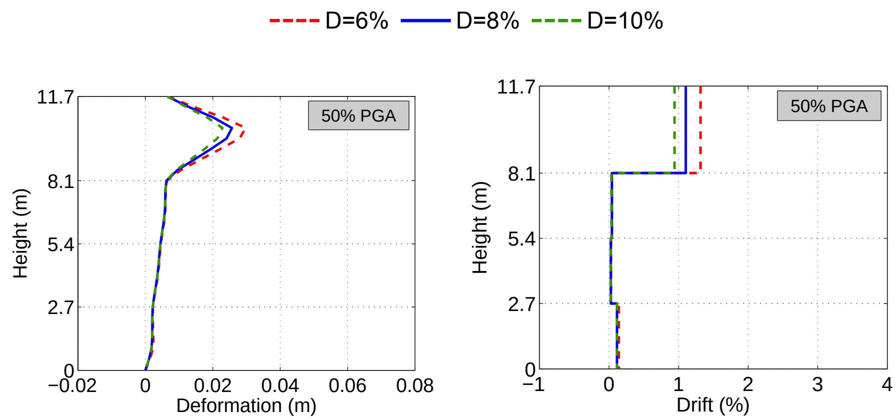

(a) **(b)**

Figure 4.25: Average of maximum envelopes of (a) lateral deformations and (b) drift ratios along the height of the wall designed for 50% the code PGA subjected to ground motions G1–G14, showing the sensitivity of the response to variation in the damping ratio of the top soil layer.

4.5.6 Shoring pressure during excavation stage

In most cases deep building basement walls are constructed in open excavations that are generally shored, which cause the retained soils to be in a yielded (active) conditions already. For this reason in all the results presented so far it was assumed that during excavation stage of analysis the wall is free to move outward and the soil mass moves sufficiently to mobilize its shear strength. Therefore, in modeling the construction sequence of the basement walls in benchmark analyses, the active earth pressure coefficient (K_A) has been used to calculate the applied shoring pressure to restrain the soil during excavation.

In some cases where surface settlements adjacent to the excavation are of concern, a shoring system providing restraint equivalent to at-rest earth pressure (K_o) rather the active earth pressure (K_A) could be appropriate. For this purpose an additional analyses are conducted using at rest shoring pressures, which causes the wall to experience no lateral movement during the excavation stage of analyses. This typically occurs when the wall is restrained from movement, such as along a basement wall that is restrained at the bottom by a slab and at the top by a floor framing system prior to placing soil backfill against the wall. Geotechnical practitioners have traditionally calculated the at-rest earth pressure coefficient, K_o against non-yielding walls using Jaky (1944) equation:

$$K_o = 1 - Sin(\phi) \tag{4.1}$$

Where K_o is the at-rest earth pressure coefficient and ϕ is the angle of internal friction of the soil. Result of the analyses presented in Figure 4.26 suggests that the displacement and drift response of the wall in the present problem are not sensitive to the applied shoring pressures during the excavation stage of analysis, being set to either the active or the at-rest pressures.

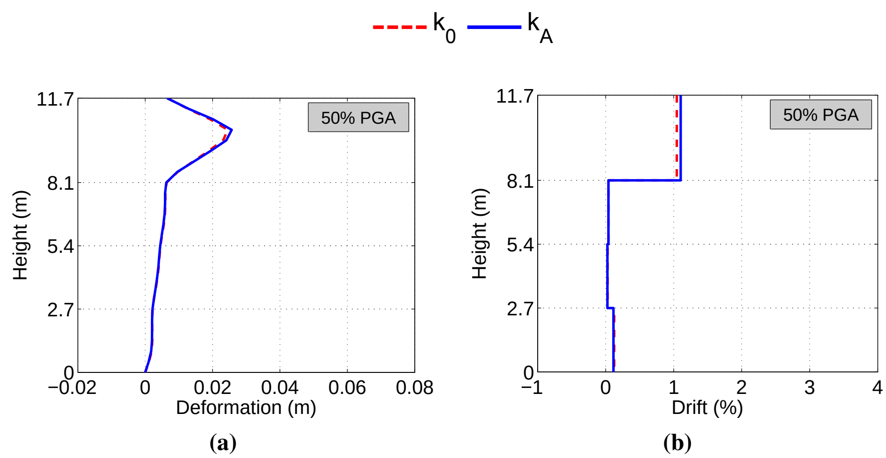

Figure 4.26: Average of maximum envelopes of (a) lateral deformations and (b) drift ratios along the height of the wall designed for 50% the code PGA subjected to ground motions G1–G14, showing that the results are not sensitive to the initial shoring pressure during excavation stage.

Chapter 5

Additional studies on soil properties and wall geometries

No amount of experimentation can ever prove me right; a single experiment can prove me wrong.— Albert Einstein (1879–1955)

5.1 Introduction

The importance of Soil–Structure Interaction (SSI) in dynamic analysis has been well known and well established during the past decades and several literatures covered the computational and analytical approaches to solve these problems. The dynamic response of structures supported on soft soil deposits are completely different than the response of a similarly excited, identical structures supported on stiff ground due to their different dynamic characteristics.

In this Chapter the effects of dynamic soil–structure interaction on seismic performance of the basement walls and the resultant lateral structural response are studied in order to provide guidance on the selection of an appropriate fraction of the NBCC (2010) PGA to be used in the M-O analysis. The maximum resultant drift ratio of the basement wall is selected as a parameter for evaluating the seismic performance of the basement walls due to its greatest significance for engineering design. The seismic performance of the basement walls are re-evaluated using more representative constitutive model instead of the simple elastic–perfectly plastic Mohr–Coulomb model. Two additional wall geometries including (1) a 4-level basement wall with a higher 5.0 m top storey (instead of the 3.6 m height which was used in benchmark analyses in Chapters 3 and 4) with a total height of 13.1 m and (2) a 6-level basement wall with a total height of 17.1 m are selected. Each wall is founded on various NBCC (2010) site class D soil profiles. The nonlinear dynamic response of the basement walls have been compared and discussed and further evidences for evaluating the recommended fraction of the code mandated PGA used in the M–O method in order to achieve an acceptable seismic performance of basement walls are presented.

5.2 Nonlinear stress-strain characteristics of soil

It is now standard practice in seismic engineering to take into consideration the nonlinear behavior of soils undergoing time-varying deformations caused by earthquake ground motions. Among different soil models that could be used in the first set of analyses, the linear elastic–perfectly plastic Mohr–Coulomb model was chosen because it is simple and has been widely used locally by practitioners. The aforementioned procedure conducted in SHAKE for estimating a modulus reduction factor ($G/G_{\max}$) and damping ratio (D) used in the elastic range of Mohr–Coulomb model in FLAC analysis is normally followed by the prominent geotechnical analyst in Vancouver.

In this procedure as outlined in Section 3.3.4, the upper-bound modulus reduction curve and the lower-bound damping curve of Seed et al. (1986) were used to develop the strain–compatible shear modulus reduction and Rayleigh damping values, which were used in the elastic portion of the Mohr–Coulomb model. For this purpose the equivalent linear analyses of the free-field soil column were conducted in SHAKE to calculate the equivalent G/G_{max} and damping ratio for each soil layers. These average equivalent modulus reduction values were used for modifying the G_{max} to G, at different depths of the model in the elastic range of the elastic-plastic Mohr–Coulomb model. Similarly, the equivalent damping ratios for each layer were added to the nonlinear analyses of the soil-structure system in the form of Rayleigh damping.

This approach is an attempt to approximate the actual stress–strain response of the soil material, following the current state of practice, and is crude, especially when there are significant nonlinearity effects. In this section the seismic performance of the basement walls using the more representative advanced nonlinear constitutive model, UBCHYST (Naesgaard, 2011), are examined.

5.2.1 Description of the UBCHYST soil model

The behavior of soil material under seismic loading is nonlinear and depends on several factors such as intensity of loading, duration of loading, soil type, and insitu soil condition. Soil constitutive models have been used to characterize the nonlinear hysteretic soil behavior by linking the strain and stress increments. Constitutive models are used to simplify the description of the material response while still being representative of the real behavior of the soil. In most of these models the equivalent secant shear modulus and viscous damping are the parameters which have been used for characterization. Secant shear modulus normalized by maximum shear modulus decreases by increasing the cyclic shear strain, whereas the amount of damping, which is a measure of the energy dissipation in one loading cycle, increases with increasing magnitude of shear strain.

The relatively simple total stress model, UBCHYST, was developed at the University of British Columbia (UBC) for dynamic analyses of soil subjected to earthquake loading. This model was implemented in the two-dimensional finite difference program FLAC (Itasca, 2012) as a FISH source by Naesgaard and Byrne (Naesgaard, 2011). Later on, in order to speed up the computations time, the FISH source code was converted to C^{++} and compiled as a DLL file by a group of researchers at UC–Berkeley (Geraili Mikola, 2012). In the current study the DLL file is used for conducting the nonlinear simulations in FLAC, which is provided by the Itasca website (User Defined constitutive Models (UDM) for the Itasca codes, 2015).

The UBCHYST model is intended to be used with undrained strength parameters in low permeability clayey and silty soils, or in highly permeable granular soils, where excess pore water could dissipate as generated (Naesgaard, 2011). This model simulates non-linear cyclic behavior including shear modulus degra-

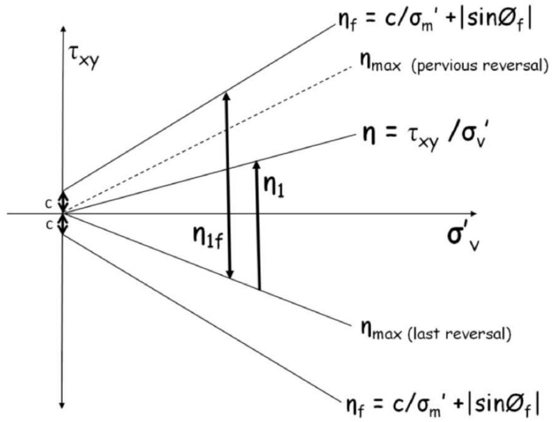

Figure 5.1: UBCHYST model (Naesgaard, 2011).

dation with shear strain and strain-dependent damping ratio. The tangent shear modulus (G_t) is a function of the peak shear modulus, G_{max}, times reduction factors, which are a function of the developed stress ratio and the change in stress ratio to reach failure as are shown in Figure 5.1 and Equation 5.1. In this equation the tangent shear modulus varies through-out the loading cycle to give hysteretic stress–strain loops of varying amplitude and area (damping) through-out the earthquake excitation.

$$G_t = G_{max} \times (1 - (\frac{\eta_1}{\eta_{1f}})^{n_1} \times R_f)^n \times mod1 \times mod2 \tag{5.1}$$

where,

η = stress ratio (τ_{xy}/σ_v'),

η_1 = change in stress ratio η since last reversal $(\eta - \eta_{max})$,

η_{max} = maximum stress ratio (η) at last reversal,

η_{1f} = change in stress ratio to reach failure envelope in direction of loading $(\eta_f - \eta_{max})$,

η_f = $sin(\phi_f) + cohesion \times cos(\phi_f)/\sigma_v'$,

τ_{xy} = developed shear stress in horizontal plane,

σ_v' = vertical effective stress,

ϕ_f = peak friction angle,

n_1, R_f and n = calibration parameters,
$mod1$ = a reduction factor for first-time or virgin loading which typically has a value between 0.6 to 0.8,
$mod2$ = optional function to account for "permanent" modulus reduction with large strain which is defined as $(1-(\frac{\eta_1}{\eta_{1f}})^{rm}) \times dfac \geq 0.2$.

In this model the stress reversals occur when the absolute value of the developed stress ratio (η) is less than the previous value and a cross-over occurs if τ_{xy} changes sign. A stress reversal causes η_1 to be reset to 0 and η_{1f} to be re-calculated.

The UBCHYST model has been combined with the Mohr–Coulomb failure criteria and incorporated into FLAC as a user defined constitutive model. In this model the magnitude of the stress ratio is limited by a Mohr–Coulomb failure envelope in high shear strains as such the shear strength of the soil materials estimated by UBCHYST model is consistent with estimates using Mohr–Coulomb model as is shown in Figure 5.2. This figure shows typical responses of the Mohr–Coulomb and UBCHYST models in a cycles of simple shear test.

The Mohr–Coulomb model captures hysteretic load-unload behavior if plasticity occurs. The advantage of UBCHYST model over a simpler Mohr–Coulomb model is the nonlinear hysteretic loops developed by varying the tangent shear modulus during loading and unloading. This model replicates the behavior of real soil and reduces the necessity of defining G/G_{max} and Rayleigh damping as with the simple Mohr–Coulomb model.

5.2.2 Calibration of UBCHYST input parameters

Number of empirical relations (i.e., shear modulus reduction and damping ratio variation with cyclic shear strain) have been published by several researches for a wide range of soils in order to estimate seismic site response in soil deposits. Different soil parameters such as strain amplitude, mean effective confining pressure, soil type, plasticity, and void ratio influence the dynamic properties of the soil. For cohesionless soils, which is the focus of this study, the variation of dynamic curves with change in soil properties is small and therefore, it is assumed that modulus degradation and damping curves fall within a narrow range for most cohesionless

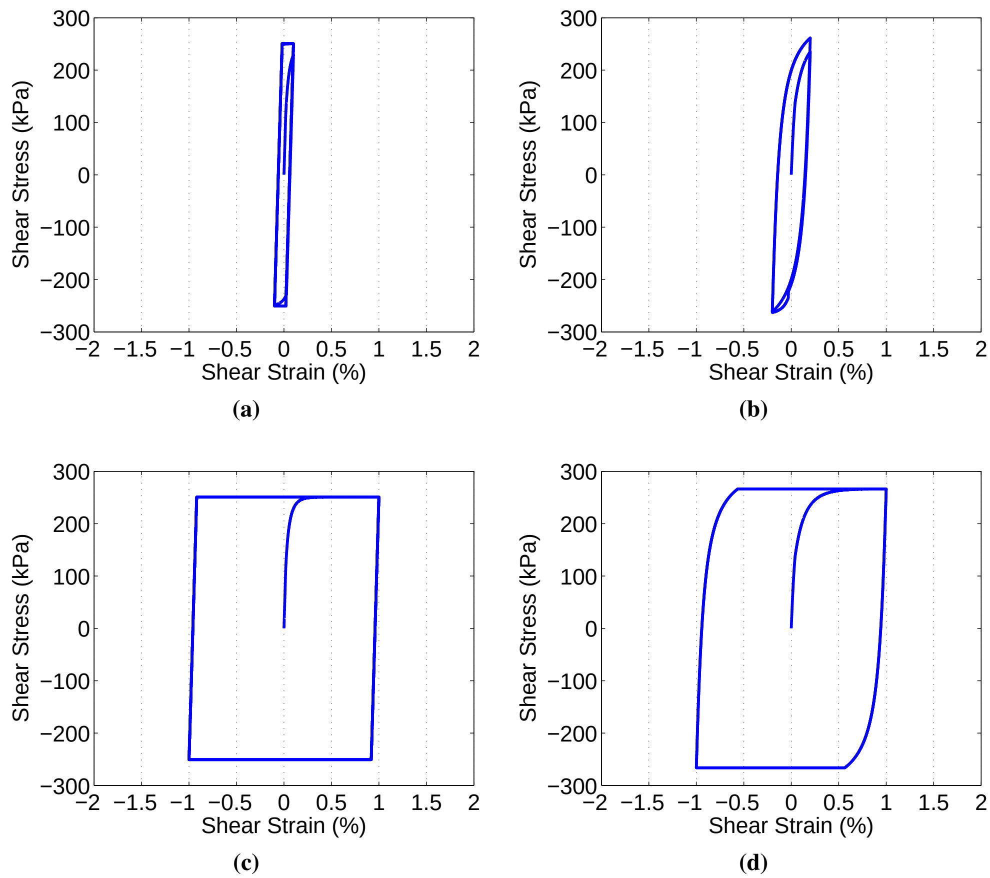

Figure 5.2: Typical schematic stress–strain response of (a,c) Mohr–Coulomb and (b,d) UBCHYST soil materials in a cyclic direct shear test in a case of 0.2% and 1% maximum shear strains.

soils (Hashash and Park, 2001; Seed and Idriss, 1970).

The UBCHYST model was calibrated against modulus degradation and damping curves published by Darendeli (2001). Figure 5.3 shows Darendeli (2001) normalized shear modulus and material damping curves corresponding to the cohesionless sandy soils (PI=0) at different confining pressures (0.25 atm, 1 atm, 4 atm, and 16 atm). In this figure both shear modulus and material damping vary with shear strain amplitude. The shape of the shear modulus reduction curve im-

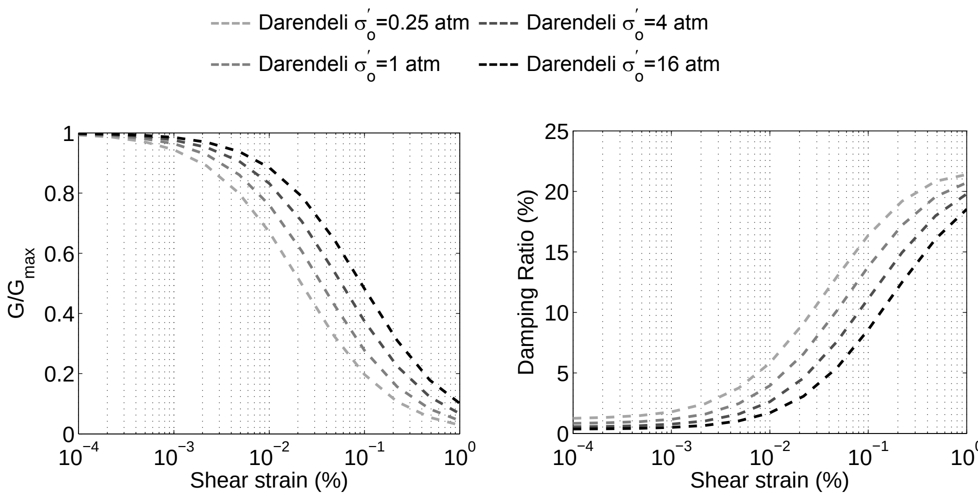

Figure 5.3: Normalized modulus reduction and material damping curves recommended by Darendeli (2001) for different confining pressures for cohesionless sandy soils with PI=0.

parts valuable information regarding to the behavior of a soil, while the damping curve provides a complimentary plot of the rate of damping increases with shear strain.

Darendeli (2001) concluded that shear modulus and damping values are stress-dependent and lead to changes in shear modulus reduction and the material damping curves. This effect had been also recognized by other researchers (Hardin and Drnevich, 1972; Hardin et al., 1994; Ishibashi and Zhang, 1993; Iwasaki et al., 1978; Kokusho, 1980; Laird and Stokoe, 1993). Figure 5.3 shows that increasing the confining pressure results in a lower shear modulus degradation and damping ratio at a given cyclic shear strain.

In calibration process, an initial estimate of each parameter is made at each soil layer based on a sensitivity analysis that has been computed. An element cyclic simple shear test (CSS) using UBCHYST constitutive model is conducted in FLAC at different depth of the model over a range of strain levels, in order to generate shear modulus and material damping curves corresponding to that specific confining pressure.

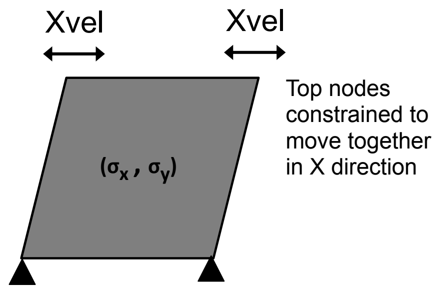

Figure 5.4: Element cyclic simple shear (CSS) test in FLAC.

As illustrated in Figure 5.4, an element cyclic simple shear test is simulated in FLAC by applying a constant x-velocity at the top nodes of an element while the base nodes are fixed in both x and y directions. The total displacement resulting from applied x-velocity is limited by shear strain value. The top nodes are allowed to deform laterally until the developed shear strain at the top nodes become equal to the specified maximum value. Then, the x-velocity is reversed until the absolute value of shear strain is achieved in the opposite direction. This generates the familiar hysteresis loop associated with cyclic simple shear laboratory tests.

The nonlinear shear stress versus shear strain response of soil under cyclic loading results in a hysteresis loop as illustrated in Figure 5.5(a). The tips of the hysteresis loops at different cyclic shear strain amplitudes create a locus of points forming the backbone curve. The hysteresis loop at different levels of shear strain can be characterized by its inclination and its breadth. The inclination of hysteresis loop depends on the soil stiffness, which is characterized by the secant shear modulus as illustrated in Figure 5.5(a) at three different shear strain levels (G_1, G_2 and G_3). The breadth of the hysteresis loop is related to the area inside the loop which is a measure of energy dissipation in one cycle of oscillation and is described by the damping ratio (D_1, D_2 and D_3) in Equation 5.2:

$$D = \frac{W_D}{4\pi W_s} = \frac{1}{2\pi}\frac{A_{loop}}{G\gamma_{max}^2} \tag{5.2}$$

In this equation W_D is the dissipated energy, W_s is the maximum strain energy

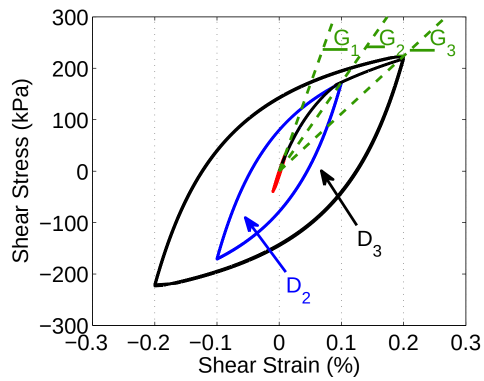

(a)

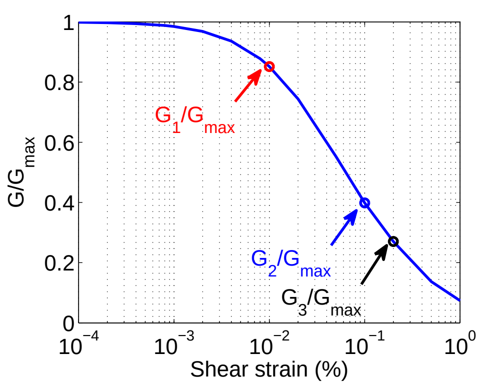

(b)

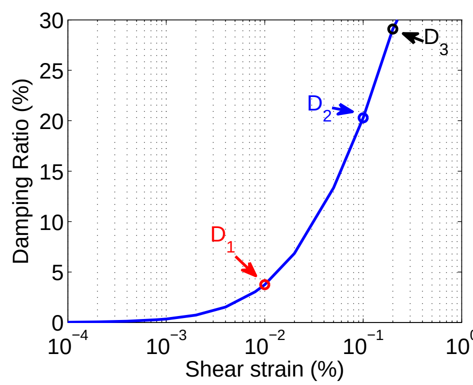

(c)

Figure 5.5: (a) The typical nonlinear shear stress versus shear strain response of soil under cyclic loading for three different levels of shear strain, (b,c) shear modulus reduction and damping curves that characterize the nonlinear response of soil.

and A_{loop} is the area of the hysteresis loop.

To relate a nonlinear stress–strain model to a measured modulus reduction and damping curves, the nonlinear behavior of the soil in the form of hysteresis loops at different strain levels are converted into the equivalent G/G_{max} and damping curves. The slope of the backbone curve at the origin corresponds to the maximum tangent shear modulus (G_{max}) but at greater cyclic shear strain amplitudes the modulus ratio (G/G_{max}) will drop to values less than one. The variation of shear modulus ratio with shear strain, which is represented by a modulus reduction curve provides the same information as the backbone curve. As shown in Figures 5.5(b,c) by increasing the shear strain, the modulus reduction (G/G_{max}) decreases and damping (D) increases.

The values of normalized shear modulus and material damping are plotted versus shear strain for 15 strain levels, ranging from 0.0001% to 1% shear strain. The nonlinear fitting parameters of UBCHYST soil model are selected such that the resultant equivalent modulus reduction and damping curves from the nonlinear model match the Darendeli (2001) laboratory test curves at different confining pressures (Geraili Mikola, 2012; Jones, 2013).

Input parameters for the UBCHYST model include the maximum shear modulus (G_{max}), bulk modulus (K), Mohr–Coulomb failure criteria parameters such as cohesion, friction angle, dilation angle and tensile strength and also a set of calibration parameters, which control the shape and the size of the stress–strain loops. The list of the parameters used in UBCHYST model are presented in Table 5.1.

Figures 5.6 and 5.7 show a comparison of modulus reduction and damping curves from the empirical model of Darendeli (2001) with those from the UBCHYST model at different depths of the first and the second layers. As illustrated in these figures, the model overestimates the damping response at medium to large ($> 0.1\%$) shear strains. This issue is common with nonlinear models and the reason for this overestimation of damping factor appears to be due to the shape of the modified stress–strain curve at large strains and has been pointed out before by many researchers (Callisto et al., 2013; Cundall, 2006; Geraili Mikola, 2012; Jones, 2013; Kottke, 2010; Mánica et al., 2014; Naesgaard, 2011).

The UBCHYST model provides almost no energy dissipation at very low cyclic strain levels, which may be unrealistic. In this study a small amount of Rayleigh

Table 5.1: Soil parameters of the UBCHYST constitutive model used in FLAC analyses.

Parameter description	Parameters	Layer 1	Layer 2
Unit weight (kN/m^3)	γ	19.5	19.5
Cohesion (kPa)	c	0	20
Peak friction angle (deg)	ϕ	33	40
Dilation angle (deg)	ψ	0	0
Small strain shear modulus (MPa)	G_{max}	17-143	580-885
Poisson's ratio	ν	0.28	0.28
Stress rate factor	R_f	0.98	0.85
Stress rate exponent	n	3.3	2.0
Stress rate exponent	n_1	1.0	1.5
First cycle factor	$mod1$	0.75	0.75
Large strain exponent	rm	0.5	0.5
Large strain factor	$dfac$	0	0

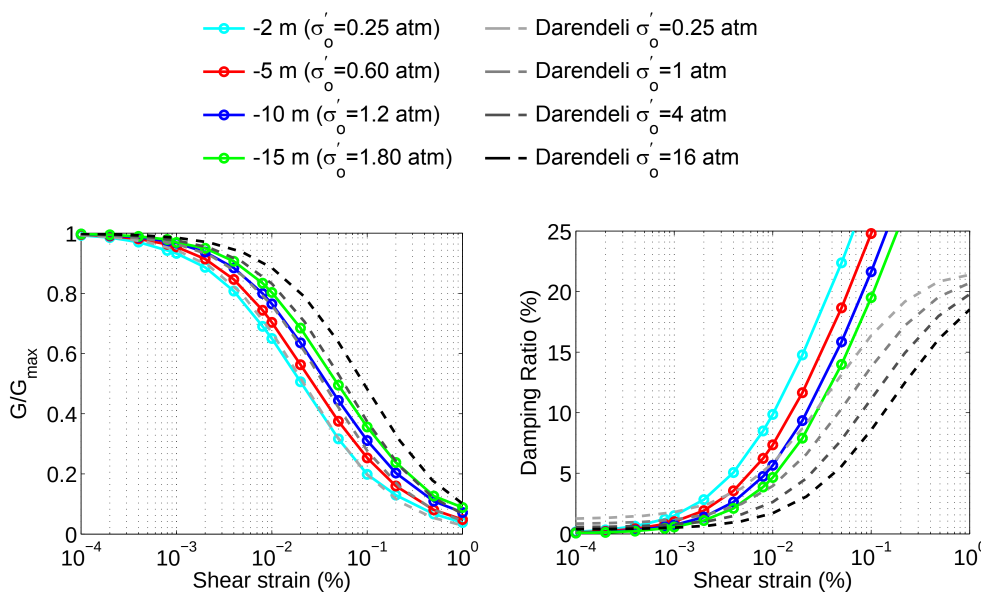

Figure 5.6: Variation of shear modulus and damping ratio with cyclic shear strain amplitude at different depths of the first soil layer estimated by FLAC using UBCHYST model.

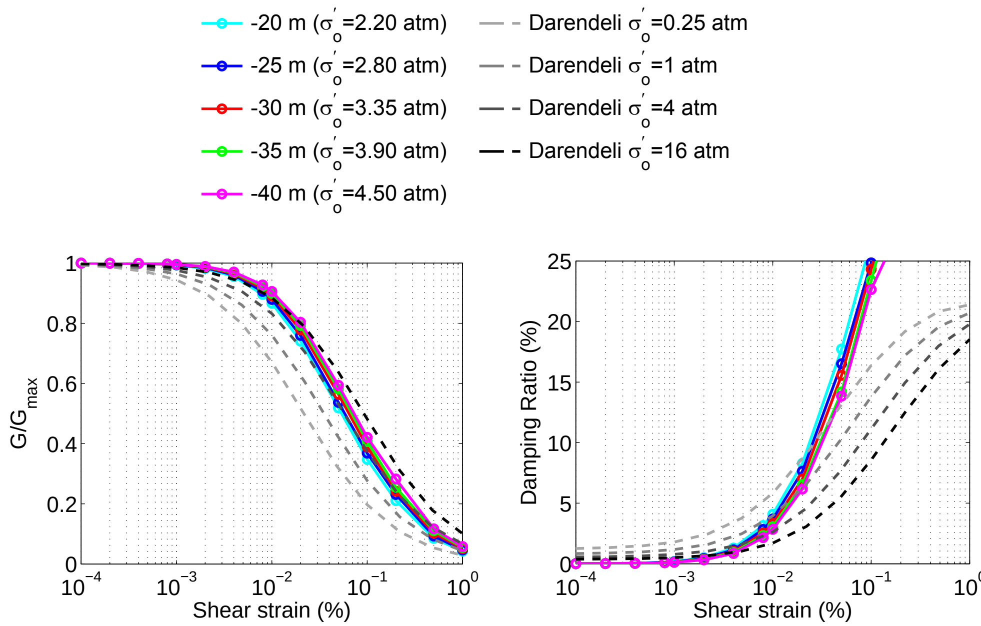

Figure 5.7: Variation of shear modulus and damping ratio with cyclic shear strain amplitude at different depths of the second soil layer estimated by FLAC using UBCHYST model.

damping (e.g., 0.5%) is used to provide damping in the analysis at very small strains and avoid low-level oscillation, where the hysteretic damping from the nonlinear soil models is nearly zero.

5.2.3 Simulation results

A series of dynamic computational analyses are conducted to study the effect of using more representative constitutive model in seismic response of the basement walls, in order to more appropriately simulate nonlinear stress–strain response of the soil medium.

Figure 5.8 shows the maximum drift ratios along the height of the 4-level basement walls, designed for different fractions of code PGA and subjected to 14 crustal earthquake ground motions (G1–G14) spectrally matched to the hazard level in Vancouver. In these analysis the UBCHYST soil model is used instead of the

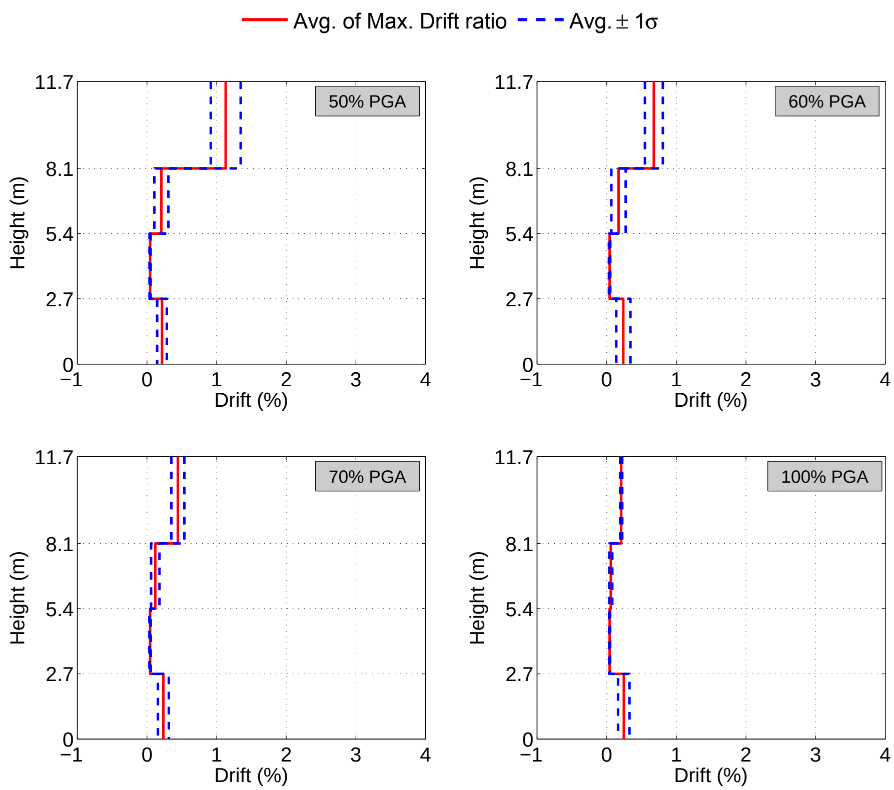

Figure 5.8: Average of maximum envelopes of drift ratios $\pm$ one standard deviation along the height of the 4-level basement wall, designed for four different fractions of the code PGA subjected to 14 spectrally matched crustal ground motions (G1–G14), using UBCHYST constitutive model.

simple Mohr–Coulomb model for simulating the stress–strain response of the soil media. The red solid lines in these plots represent an average of the maximum drift ratio of the both right-side and left-side walls subjected to 14 seismic events. Assuming normally distributed drift ratios, average $\pm$ one standard deviation (σ) shown by blue dashed lines represent the first standard deviation with a 68% chance that the average value of response falls within the range of standard error.

The exceedance probability of drift ratios for the basement walls designed for different fractions of code PGA are presented in Figure 5.9. This figure illustrates a detailed information about the distribution of the resultant maximum drift ratio of the walls designed for different fractions of code PGA subjected to 14 crustal ground motions in the form of exceedance probability. Each point represents the maximum value of the resultant drift along the height of the left-side and the right-side walls subjected to one out of 14 ground motions. As mentioned in Chapter 4, the acceptance criterion for the basement walls is a drift ratio not larger than 1.7% at any point along the height of the wall. Results shown in Figure 5.9 suggest that even in the case of the weakest wall (designed for 50% PGA) none of the 14 scenarios results in a drift ratio higher than acceptance criterion.

The result of the analyses using more sophisticated and more representative constitutive model confirms the conclusion made based on using simple Mohr–Coulomb model (Figure 4.17) that the performance of the basement walls designed for 50% to 60% of the code PGA for Vancouver and founded on relatively dense sandy soil seem adequate. Also it can be concluded that for a hazard level of 2% in 50 years in Vancouver, design to the associated PGA$=0.46\,g$ may not be warranted and leads to an over-conservative performance.

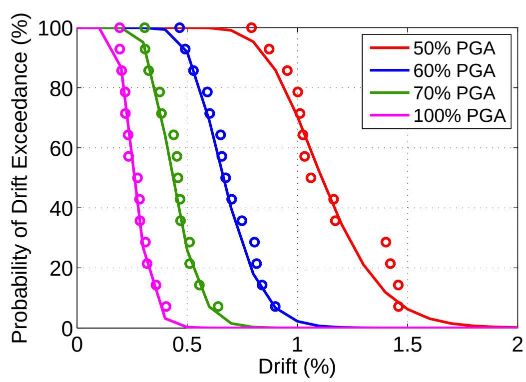

Figure 5.9: Exceedance probability of drift ratio for 4-level basement walls designed for different fractions of the code PGA subjected to 14 spectrally matched crustal ground motions (G1–G14), using UBCHYST constitutive model.

5.3 Local site condition

During an earthquake event, local amplification of strong ground motion by shallow soft soil layers can have a large impact on the intensity of ground shaking around the structure and consequently dynamic behavior of the soil–wall system. The site conditions in terms of geometrical and geological structures of the softer surface deposits affect the waves from the underlying stiff soil during wave transmission to the surface, so a structure supported on soft ground can have a completely different behavior from the same structure supported on stiff soil or rock subjected to an identical earthquake motion. Therefore, neither the structure nor its underlying soil can act independently. This phenomenon is referred to as Soil–Structure Interaction (SSI) effect.

Site amplification in some cases causes a bedrock outcrop motion to be amplified about five times (Finn and Wightman, 2003) and can have devastating effects on structures with periods close to the site period. Damage patterns in some earthquakes, such as the Mexico City, Mexico (1985), and Loma Prieta, California (1989) confirm the significant effect of site amplification on earthquake-induced damages (Anderson et al., 1986; Holzer, 1994). The study by Holzer et al. (1999) of ground failure observations during the Northridge, California earthquake (1994) showed that the local subsurface conditions affect the overall dynamic response of the ground and may also help to explain localized variations in recorded ground motions. Therefore, site condition and soil profile play important roles in establishing seismic performance of basement walls and deserve an extra attention.

As described in the geotechnical earthquake engineering literature (Das, 1992; Kramer, 1996; Towhata, 2008), local site conditions can affect a number of important characteristics of strong ground motions, such as an amplitude and a frequency content of a record. Ground motion amplification is mainly controlled by few parameters such as:

- the ratio of the predominant period of the applied motions to the fundamental period of the system,
- the relative stiffness between different soil layers characterized by the impedance ratio, α. The impedance of a soil layer is the mass density multiplied by the

shear-wave velocity of the material. Therefore, the impedance ratio is defined as $\alpha = \rho_t V_{st}/\rho_b V_{sb}$, where ρ is the mass density, V_s is the shear wave velocity and t and b refer to the top surface layer and bottom underlying layer, respectively, and

- the strain amplitude level reached during a seismic event, which has a direct impact on the amount of modulus reduction and damping ratio.

The local site condition has been addressed in the seismic provisions of most building codes (NBCC, 2005, 2010; NEHRP, 2003, 2009), and the average shear wave velocity of the top 30 m is recommended for site characterization. Recent editions of the National Building Code of Canada (NBCC, 2005, 2010) quantified the amplification potential of site conditions by the use of foundation factors. As site classification is critical for seismic hazard assessment of underground structures, the NBCC (2005, 2010) categorizes site conditions into five major soil types, site class A (hard rock) to site class E (soft soil), based on time-averaged shear wave velocity in the upper 30 m of a site ($\overline{V}_{s30}$). This classification scheme follows that developed by the National Earthquake Hazards Reduction Program provisions in the United States (NEHRP, 2000, 2003, 2009). Its application to the NBCC is described by Finn and Wightman (2003).

A time-averaged shear wave velocity is calculated as the time for a shear wave to travel from a depth of 30 m to the ground surface. As shown in Equation 5.3, the time-averaged $\overline{V}_{s30}$ is calculated as 30 m divided by the sum of the travel times for shear waves to travel through each layer. The travel time for each layer is calculated as the layer thickness (h_i) divided by the shear wave velocity associated with each layer, ($V_{s,i}$):

$$\overline{V}_{s30} = \frac{30}{\sum_i h_i/V_{s,i}} \tag{5.3}$$

In the benchmark analyses presented in Chapter 4, the chosen soil profile was suggested by a group of geotechnical engineers as representative of the site condition relevant for high-rise construction in downtown Vancouver. In this section the 4-level basement wall is founded on different soil profiles, with variation of the ground shear wave velocities differentiating the cases. Seismic performance of the basement wall in terms of drift ratio is evaluated. The selected soil profiles are intended to capture a range of practical scenarios, which address the effect of the soil profiles with various stiffnesses and amplification factors as a result. This section is an attempt to account for two influential factors affecting seismic site response:

- Depth to a stiff soil layer with a significant impedance contrast.
- Stiffness of the soil layers underneath the structure and their corresponding impedance contrast. A time-averaged shear wave velocity is adopted as a measure of the overall site stiffness.

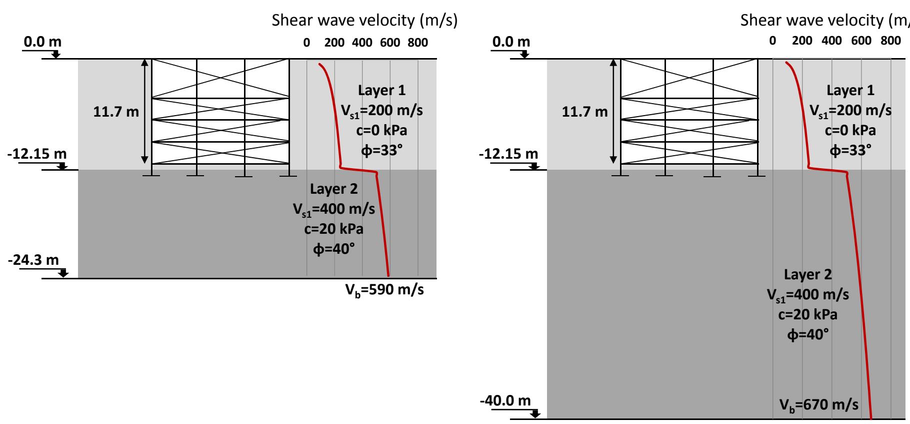

Figure 5.10: Schematic of the 4-level basement wall model with different model depths (dimensions are not to scale).

To simulate the top 30 m of the soil profile, the original depth of the model in the benchmark analyses (24.3 m) is extended to 40.0 m, as illustrated in Figure 5.10. A series of sensitivity analyses are conducted on the effect of the depth of the model on the seismic performance of the embedded basement wall. By increasing the depth of the model from 24.3 to 40.0 m, the shear wave velocity at the base of the model (V_b), which has been used for calculation of shear stress time histories (see Equation 3.7), increases from 590 to 670 m/s. Therefore, the applied shear stress time histories at the base of the 40.0 m model are about 13% stronger than those of a model with 24.3 m depth. The results of these tests, shown in Figure

5.11, suggest that depth of the model does not a have significant effect on the seismic performance of the embedded structures. Hereafter, the depth of 40.0 m will be used in all the analyses.

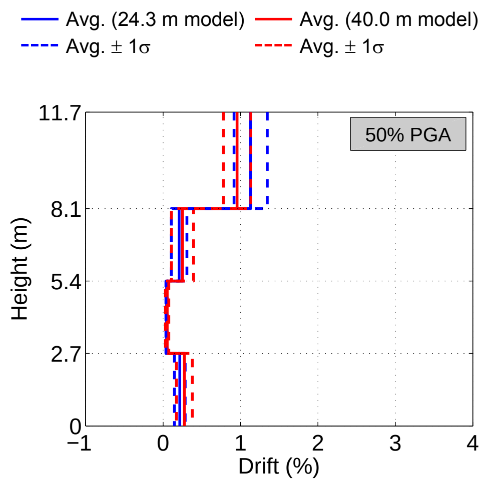

Figure 5.11: Average of maximum envelopes of drift ratios $\pm$ one standard deviation along the height of the 4-level basement wall, designed for 50% of the code PGA embedded in 24.3 and 40.0 m soil deposits, subjected to 14 spectrally matched crustal ground motions.

5.3.1 General subsurface conditions in Vancouver

The soil condition in parts of Vancouver can be represented using a number of main stratigraphic sections (Atukorala et al., 2008; Hunter and Christian, 2001; Hunter et al., 1999; Monahan, 2005). In the order of increasing depth, these are:

Deltaic sediments: These sediments consist of silts, fine sands and silty clay. Despite the different sand–silt–clay ratios of the sediments, the average shear wave velocity of these materials can be characterized by the empirical curve fitted to the data $V_s = 71.22 + 35.26\, Z^{\,0.4632} \pm 2\sigma\ m/s$ as a function of the depth, as proposed by Hunter and Christian (2001).

Glaciomarine and glacial deposits: Underlying the marine sediments is a thick layer of till-like sediments deposited during glacial and interglacial periods.

These deposits occur at or near the surface in much of the city of Vancouver (Monahan, 2005). While the shear wave velocity of 400 to 1100 m/s is proposed by Hunter and Christian (2001) with a poorly defined depth dependency for these materials, Atukorala et al. (2008) reported a depth–dependent maximum shear modulus as $169(\acute{\sigma}_m/Pa)^{0.5}$ (MPa).

Bedrock: Britton et al. (1995) developed a map of bedrock surface beneath the Fraser River Delta consists of sandstone, shales and coal beds (i.e., sedimentary rocks). The geotechnical investigation conducted in downtown Vancouver and presented by Atukorala et al. (2008) found that bedrock exists at depths ranging from 10 to 45 m below ground surface, is in various states of significantly weathered to slightly weathered, and is generally classified as very weak to weak. The average shear wave velocity at the bedrock boundary of 1200 to 1500 m/s is proposed by Atukorala et al. (2008) and Hunter and Christian (2001).

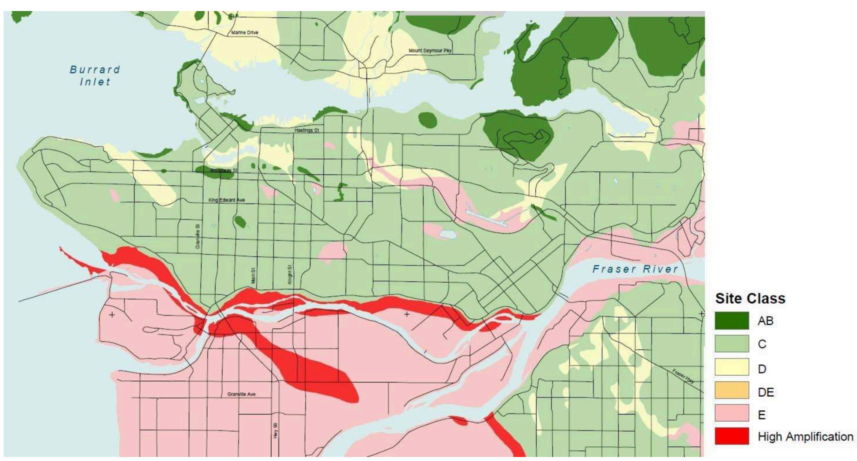

Figure 5.12: Soil type map for the Greater Regional District of Vancouver (Monahan, 2005).

Figure 5.12 shows the soil hazard map for the Greater Regional District of Vancouver for assessing the earthquake hazard due to lateral ground shaking presented by Monahan (2005). This map reflects surface geological conditions in the form of the NBCC site classes. As previously mentioned, the shear wave velocity–depth function of the top 30 m of the soil profile can be used to determine the soil classification of the site under study.

The City of Vancouver is mainly constructed on the NBCC site class C and D soil deposits (Monahan, 2005; White et al., 2008). As in general, the intensity of ground shaking increases from site class C ($360\ m/s < \overline{V}_{s30} < 760\ m/s$) to the softer site class D ($180\ m/s < \overline{V}_{s30} < 360\ m/s$), it is conservative to study a seismic response of the basement walls founded on site class D soil profiles. In order to investigate the effect of geometrical and geological structure of underlying soil deposits on wave transmission to the surface, a series of analyses are carried out on the various NBCC (2010) site class D soil deposits in the following sections.

5.3.2 Depth to the significant impedance contrast

In this section as illustrated in Figure 5.13 two soil profiles, Case I and Case II, are considered. Case I is the benchmark soil geometry that has been studied so far in Chapters 3 and 4. It has a 12.15 m thickness of the first layer and by considering a 11.7 m height for the 4-level basement wall results in the foundations being embedded in the second stiff soil layer. Case II as illustrated in Figure 5.13(b) is another variation derived from Case I soil profile with an overall lower soil stiffness in order to highlight the influence of the depth to the second stiff soil layer. In Case II, the first soil layer is 17.1 m deep, which results in the foundation of the basement wall to be embedded in this layer. Both soil profiles have the same soil properties as described in Table 5.1. Their only difference is the depth to the second layer, which leads to different shear wave velocity profiles along the height of the model. Both soil profiles can be categorized in the NBCC (2010) site class D based on their average shear wave velocities in the top 30 m ($\overline{V}_{s30,I} = 310\ m/s$ and $\overline{V}_{s30,II} = 282\ m/s$).

A series of dynamic nonlinear soil–structure interaction analyses are conducted to explore the effect of the first soil layer thickness on the seismic performance of the basement walls designed for different fractions of NBCC (2010) PGA (50% PGA, 60% PGA, 70% PGA, and 100% PGA). Figure 5.14 shows the finite difference grid and soil layer geometries together with the layouts of the basement wall structures founded on Case I and Case II soil deposits. Details of the boundary con-

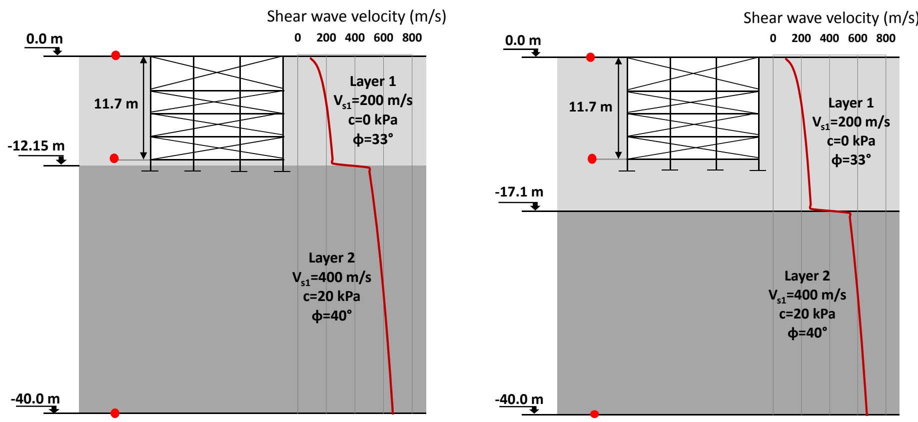

(a) Case I **(b)** Case II

Figure 5.13: Schematic of the 4-level basement walls supported on (a) Case I and (b) Case II soil profiles (dimensions are not to scale).

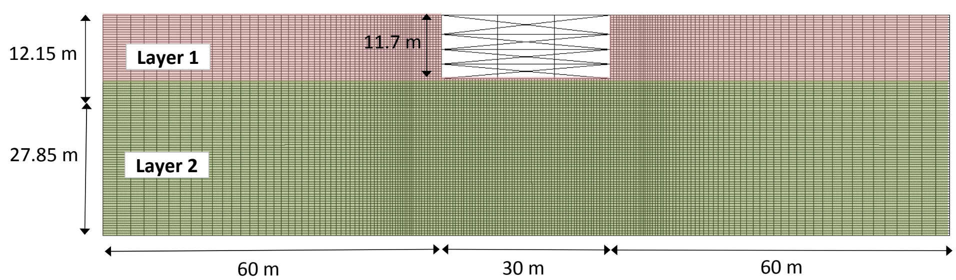

(a) Case I

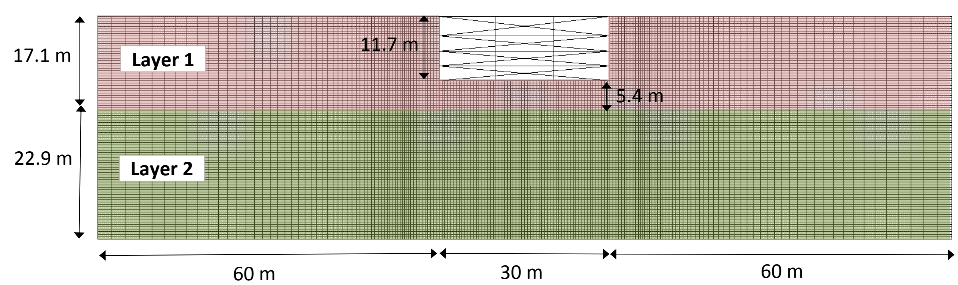

(b) Case II

Figure 5.14: FLAC models of the 4-level basement walls with a total height of 11.7 m founded on Case I and Case II soil profiles.

ditions, construction simulation, and structural and interface elements are similar to those described in Chapter 3. The analyses are conducted using the UBCHYST constitutive model. These soil–basement wall systems are subjected to a suite of 14 crustal ground motions (G1–G14) spectrally matched to the NBCC (2010) UHS of Vancouver, as outlined in Chapter 3.

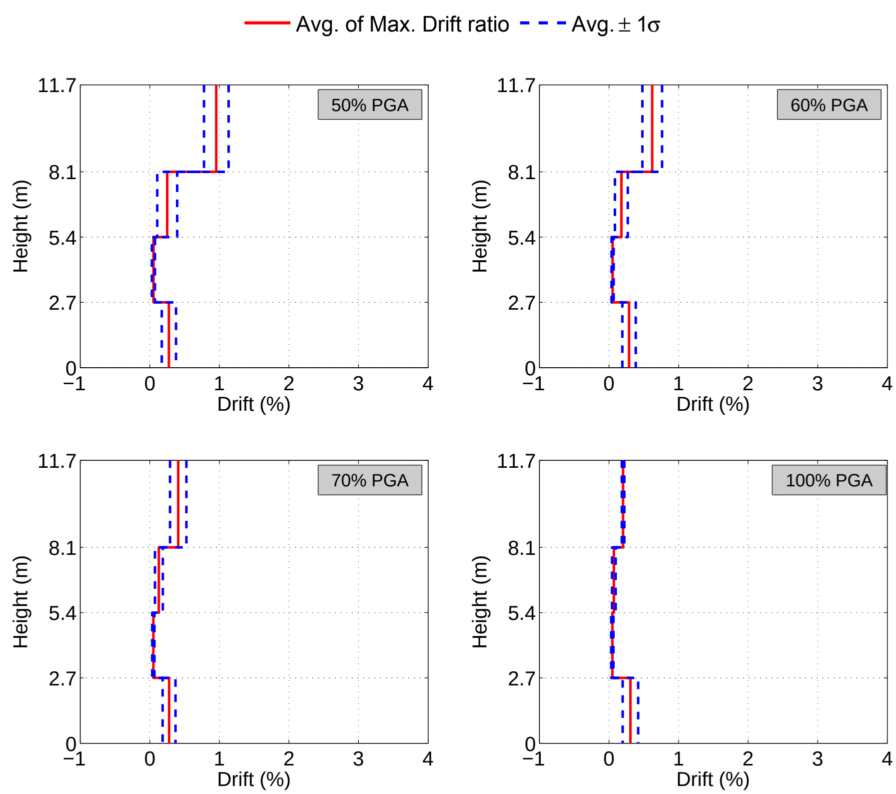

Figure 5.15: Average of maximum envelopes of drift ratios $\pm$ one standard deviation along the height of the 4-level basement wall embedded in Case I soil profile, designed for four different fractions of the code PGA subjected to 14 spectrally matched crustal ground motions.

Results of the computational study are presented in the form of the envelope of the maximum drift ratios along the height of the walls. Figures 5.15 and 5.16 confirm that all the basement walls founded on the Case I soil profile have a critical behavior just at the top basement level (similar to the conclusion drawn in chapter 4), whereas if the same walls are embedded in the Case II soil profile, the performance of the bottom basement levels also become critical. In both soil profiles the drifts at the bottom level vary with different earthquakes but they do not vary much with changing the percentage of PGA used in the design. This is attributed to the fact that the assigned moment capacity in the design of the walls is the same at lower levels. In these levels of the walls the static Coulomb pressure (with the factor of 1.5) governs the moment capacity (see Figure 3.3).

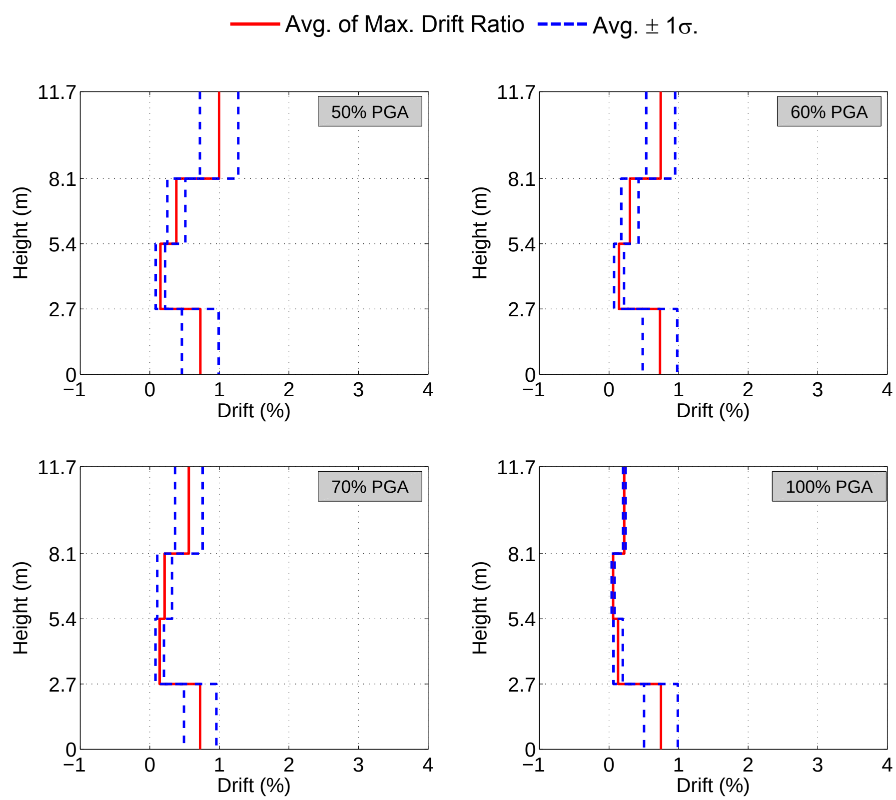

Figure 5.16: Average of the maximum envelopes of drift ratios $\pm$ one standard deviation along the height of the 4-level basement wall embedded in Case II soil profile, designed for four different fractions of the code PGA subjected to 14 spectrally matched crustal ground motions.

The probabilities of drift ratio exceedance of the basement walls founded on the Case I and Case II soil profiles are presented in Figure 5.17. As shown in this figure, the probability curves of the walls designed for different fractions of the code PGA founded on the Case II soil profile are closer to each other compared to the similar curves corresponding to the soil Case I. The walls designed for 70% and 100% PGA founded on the Case II soil profile have almost the same probabilities of drift exceedance rates. This attributed to the fact that in the Case II soil profile, as shown in Figure 5.16, the performance of the lowest basement levels designed for

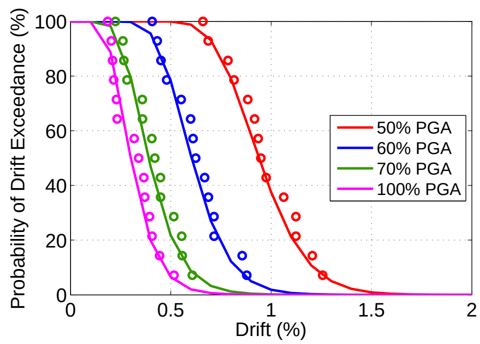

(a) Case I

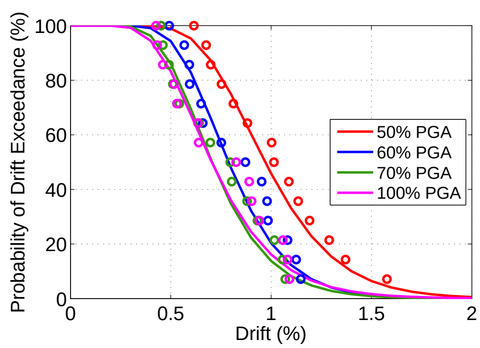

(b) Case II

Figure 5.17: Exceedance probability of drift ratio of the 4-level basement wall designed for different fractions of code PGA founded on (a) Case I and (b) Case II soil profiles and subjected to 14 crustal ground motions spectrally-matched to the UHS of Vancouver.

70% and 100% PGA dominant the response, and the top basement levels basically undergo very small drift ratios compared to the bottom levels. Whereas, in the Case I soil profile, the bottom basement level experiences very small drift ratio with an average value of 0.2% and the top level results in a considerably higher drift and consequently dominates the response.

Thus, it can be concluded from Figures 5.15 to 5.17 that the performance of the 4-level basement wall designed for a specific fraction of PGA (e.g., 50%) is highly sensitive to the stiffness and strength of a soil layer that the foundation of the basement wall is embedded in. In addition, the resultant drift ratios along the height of the basement walls vary dramatically with the percentage of PGA used for their design, which provide valuable information for determining what percentage of PGA is a reasonable engineering value to be used for seismic design of the basement walls. The results presented in these figures confirm that a basement wall designed for 50% to 60% PGA would result in a satisfactory performance in term of resultant drift ratio, even if the foundation of the wall is founded on a softer sandy soil with lower shear wave velocity.

The reason for different patterns of resultant drift ratios along the height of the basement walls founded on two different soil profiles is attributed to the local soil condition and dynamic soil–structure interaction effects. For this purpose it is of interest to calculate the spectral acceleration at the surface of the soil deposits or at the foundation level of the walls in an absence of the basement wall structure, which in this study is referred to as the free-field condition. Presence of the structure can significantly affect the motion at the base of the structure and results in its deviation from the free-field condition. Therefore, nonlinear site response analyses on the free-field column of the Case I and Case II soil profiles are conducted in FLAC using UBCHYST constitutive model with the properties presented in Table 5.1. Each soil column is subjected to a suite of 14 crustal ground motions (G1–G14) spectrally matched to the NBCC (2010) UHS of Vancouver, as described in Chapter 3.

The influence of the soft soil layer at the foundation of the wall in the Case II soil profile results in increasing the fundamental period of the system as well as the amplification level and leads to higher drift ratios at the bottom basement level under seismic loading. To evaluate the amplification ratio at different locations along the height of the model, the 5% damped spectral acceleration at various locations through-out the model is normalized with respect to the 5% damped spectral acceleration of the applied motion at the base of the model. Figure 5.18 illustrates the amplification ratios at the foundation level of the wall as well as the ground surface with respect to the base of the model for both Cases I and II. The location of the surface level, foundation level, and base of model are indicated in Figure 5.13 by red circles. As expected, the Case II soil profile, which has a lower average shear wave velocity ($\overline{V}_{s30,II} = 282\ m/s$) compared to Case I ($\overline{V}_{s30,I} = 310\ m/s$), results in a softer site with longer fundamental period and larger amplification ratio.

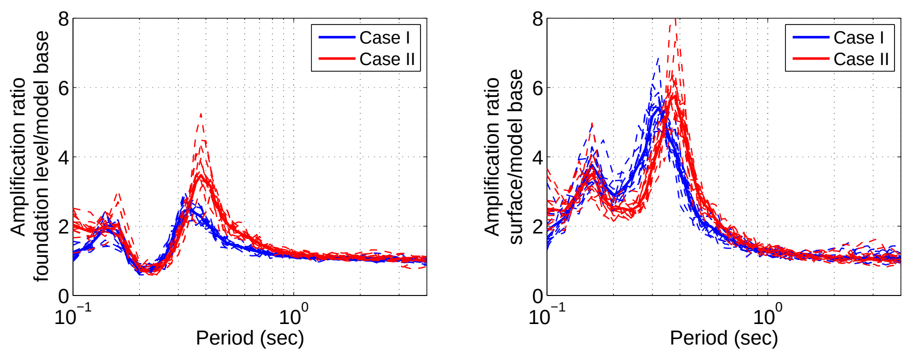

(a) **(b)**

Figure 5.18: Results of the nonlinear site response analyses conducted in FLAC in the form of amplification ratio at the (a) foundation level and (b) ground surface with respect to the base of the free-field column of soil subjected to 14 ground motions (G1–G14), the solid red and blue lines show the mean value of the response for each case.

Figure 5.19 shows the amplification ratio along the depth of the model at the fundamental period of the Case I and Case II soil profiles. Each ground motion amplifies as it propagates vertically through–out the model but with different rates. As expected, the rate of amplification of ground motions in the stiffer second layer is lower than that in the softer first layer. By comparing the results of the nonlinear site response analyses presented in Figures 5.18 and 5.19, one can conclude that the mean values of amplification ratios at ground surface in both Cases I and II soil profiles are almost the same, whereas there is a significant difference between

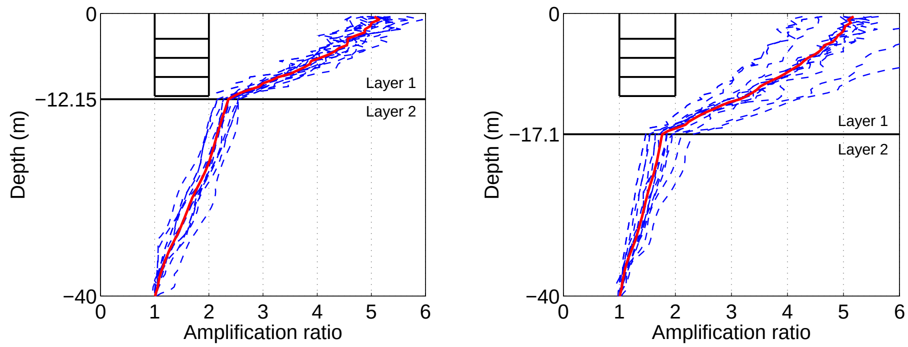

(a) Case I **(b)** Case II

Figure 5.19: Results of the nonlinear site response analyses conducted in FLAC in the form of amplification ratio at the fundamental period of the systems along the depth of the free-field column of soil subjected to 14 ground motions (G1–G14), the solid red lines show the mean value of the response. The sketch of the location of the 4-level basement wall with respect to the soil geometry is added for comparison.

the amplification ratios at the foundation level. This fact justifies the difference between the performances of the bottom level of the basement walls founded on Cases I and II soil profiles and demonstrates the importance of the underlying foundation soil stiffness on the seismic performance of the basement walls.

5.3.3 Shear wave velocity and impedance contrast of the soil deposits

The analyses presented in Section 4.5.4 suggested considerable sensitivity of the resultant drift ratio of the basement wall to the shear wave velocity of the top soil layer, using a simple Mohr–Coulomb model. In order to investigate the effect of the local site conditions on the dynamic response of the 4-level basement wall using a more representative UBCHYST model, ten soil profiles are selected and their corresponding free-field two-dimensional models are developed in FLAC (Itasca, 2012) following the same procedure outlined in the previous section.

The same soil domain geometry as the Case II soil profile is used for the subsequent case studies, which are delineated by different material stiffnesses of the first and the second soil layers. The goal of this study is to highlight the potential influence of the underlying soil stiffness on the earthquake motion amplification and consequently the drift ratio of the wall elements at different locations along the height of the basement wall. The descriptions of the proposed ten soil profiles in terms of shear wave velocity of the first and the second soil layers are summarized in Table 5.2, and their corresponding geometries are shown in Figure 5.20. Different combinations of shear wave velocities for the first and the second soil layers are considered, which leads to two uniform (U) and eight non-uniform (N) soil profiles. All these sites are classified as the NBCC (2010) site class D soil materials with an average shear wave velocity in the upper 30 m (V_{s30}) between 180 and 360 m/s, as reported in Table 5.2.

In Table 5.2 ”Nx-y” represent a non-uniform soil profile with normalized shear wave velocities of $V_{s1} = x\ m/s$ and $V_{s1} = y\ m/s$ at the first and the second soil layers, respectively, while in all cases a significant impedance contrast lies at 17.1 m depth. For instance, normalized shear wave velocities of $V_{s1} = 150\ m/s$ and $V_{s1} = 250\ m/s$ are assigned to the model N150-250. This site has an average shear wave velocity of $\overline{V}_{s30} = 203\ m/s$ in the upper 30 m of the soil deposit and based

Table 5.2: Shear wave velocities of the first and the second soil layers corresponding to ten proposed soil profiles. The numbers in the parenthesis represent the average shear wave velocities of the top 30 m of the soil (V_{s30}) used for NBCC (2010) site classification.

		Second Layer V_{s1}		
		250 m/s	300 m/s	400 m/s
First layer V_{s1}	150 m/s	N[a]150-250 ($V_{s30} = 203\ m/s$)	N150-300 ($V_{s30} = 211\ m/s$)	N150-400 ($V_{s30} = 223\ m/s$)
	200 m/s	N200-250 ($V_{s30} = 250\ m/s$)	N200-300 ($V_{s30} = 263\ m/s$)	N200-400 ($V_{s30} = 282\ m/s$)
	250 m/s	U[b]250 ($V_{s30} = 291\ m/s$)	N250-300 ($V_{s30} = 309\ m/s$)	N250-400 ($V_{s30} = 335\ m/s$)
	300 m/s	-	U300 ($V_{s30} = 349\ m/s$)	-

[a]N=Non-uniform soil profile
[b]U=Uniform soil profile

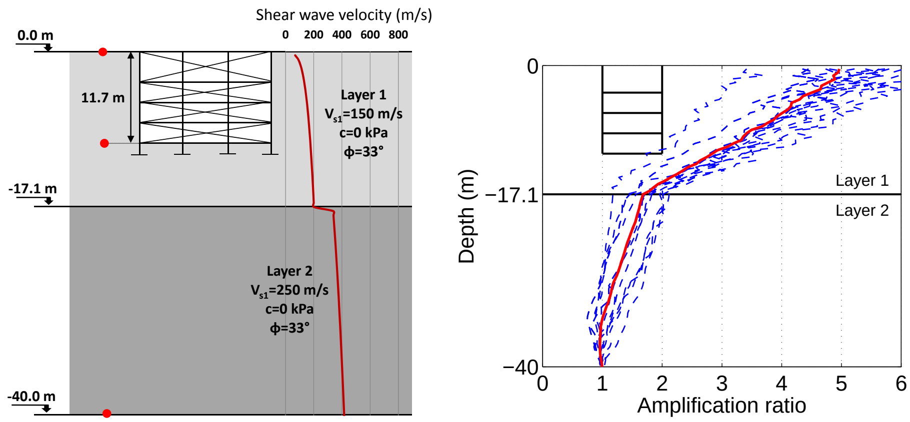

N150-250

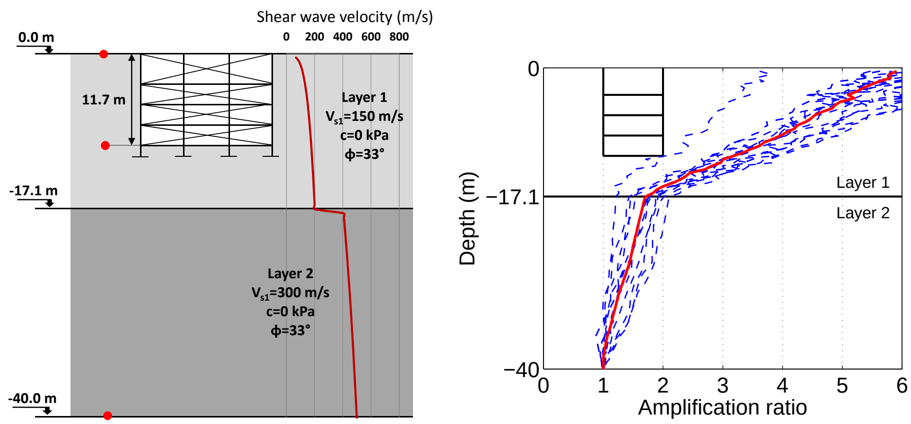

N150-300

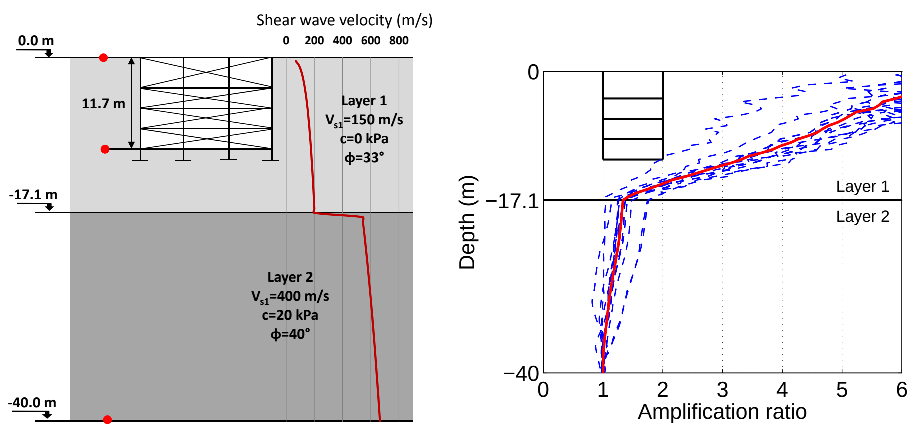

N150-400

Figure 5.20: Continued.

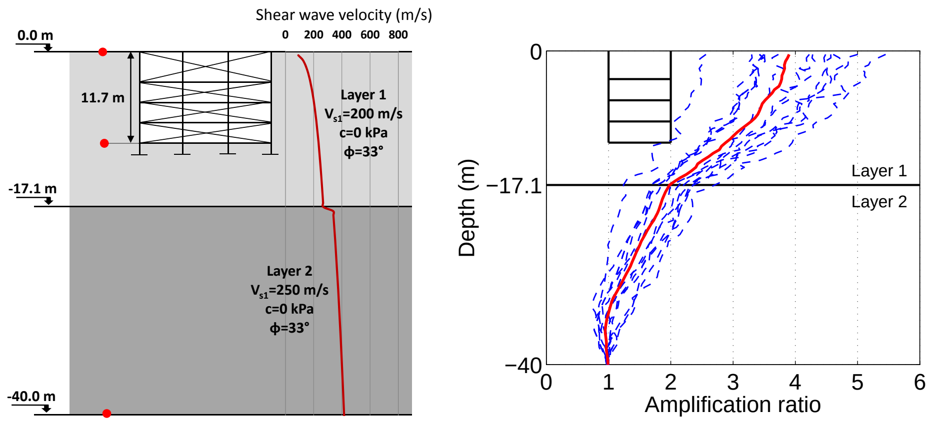

N200-250

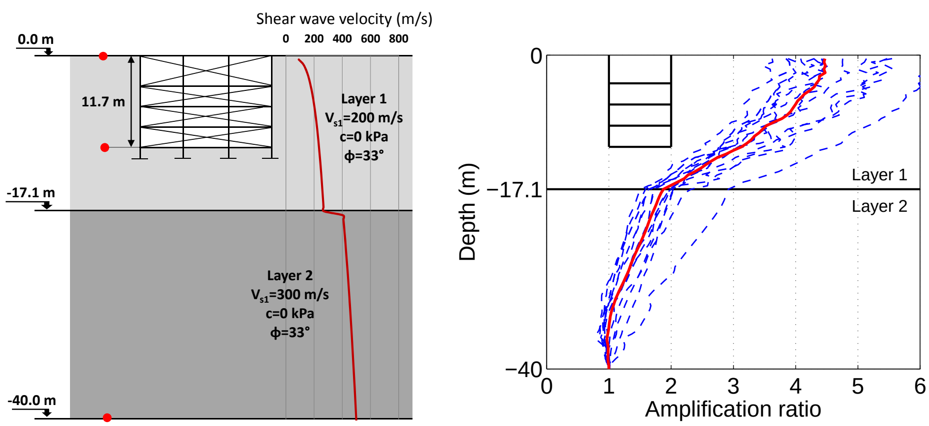

N200-300

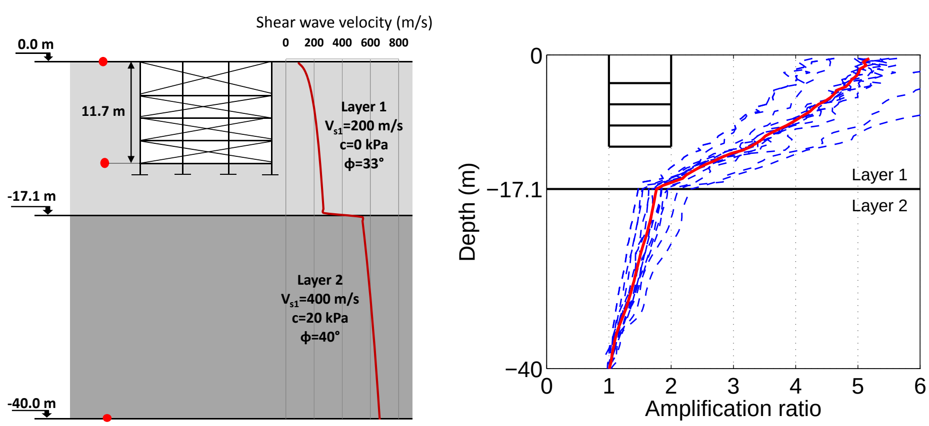

N200-400

Figure 5.20: Continued.

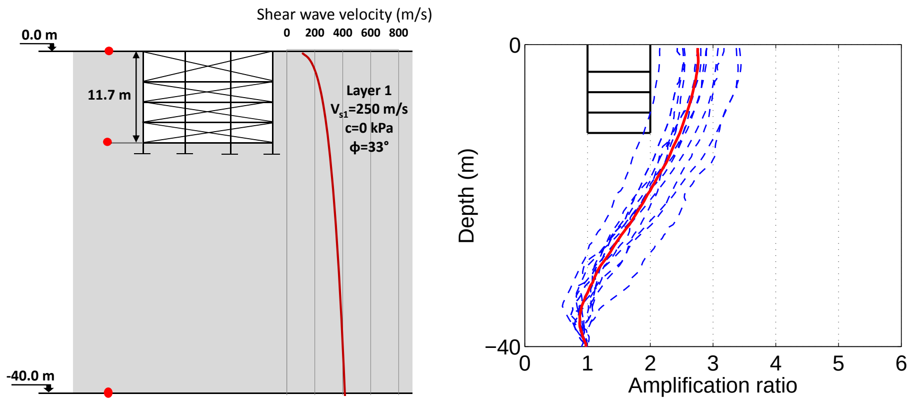

U250

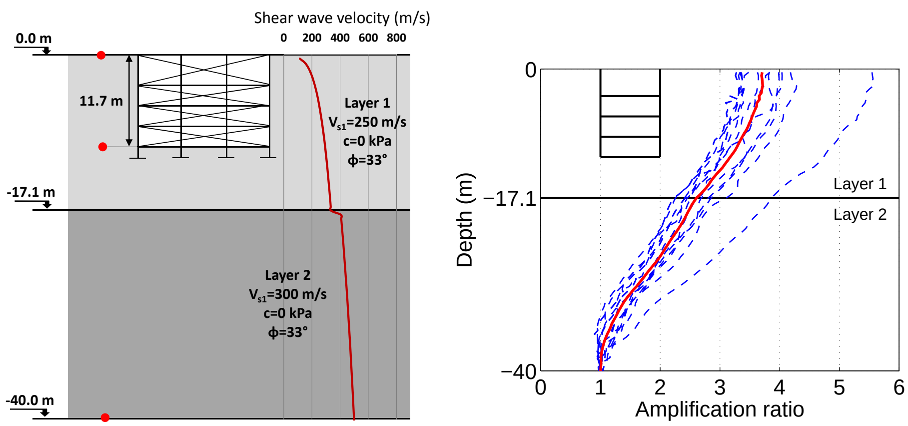

N250-300

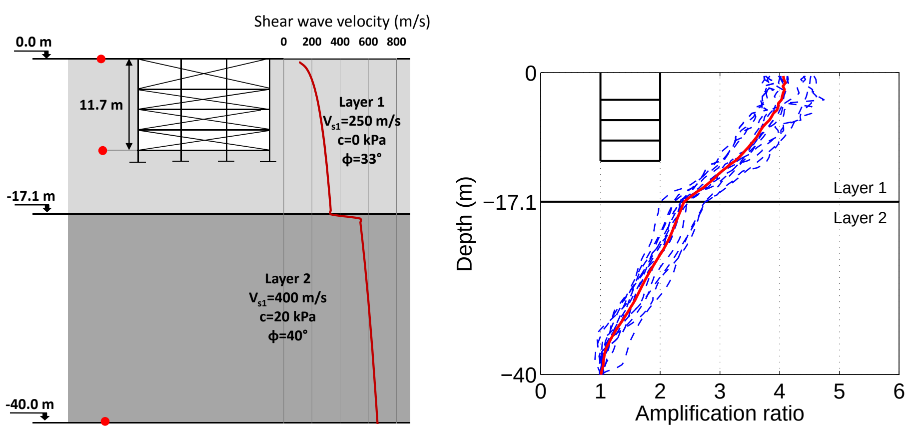

N250-400

Figure 5.20: Continued.

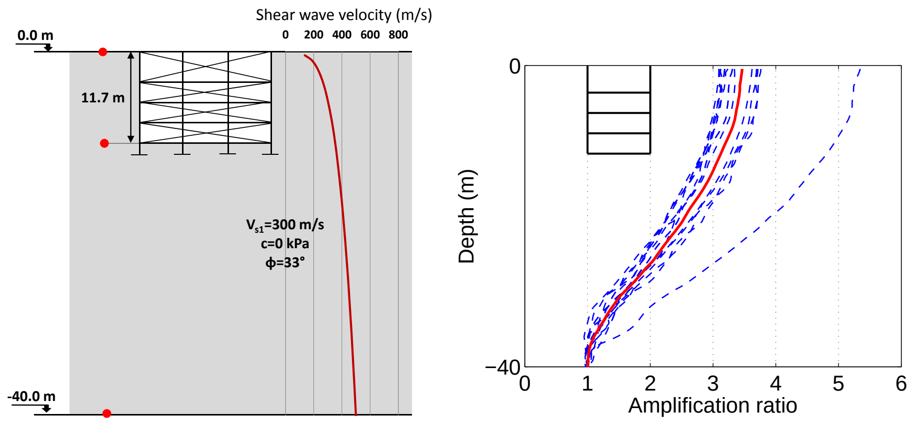

U300

Figure 5.20: Left-hand-side column: schematic of the 4-level basement walls supported on 11 different soil profiles (dimensions are not to scale); Right-hand-side column: results of the nonlinear site response analyses conducted in FLAC in the form of amplification ratio at the fundamental period of the systems along the depth of the far-field column of soil subjected to 14 crustal ground motions (G1–G14) spectrally-matched to the UHS of Vancouver. The solid red lines show the mean value of the response. The sketch of the location of the 4-level basement wall with respect to the soil geometry is added for comparison.

on the NBCC (2010) is categorized in site class D. Likewise, model N200-400 has normalized shear wave velocities of $V_{s1} = 200\ m/s$ and $V_{s1} = 400\ m/s$ at its first and second soil layers, respectively, which corresponds to the soil properties used in the benchmark scenario and has been used so far in this study. The N200-400 soil profile is equal to the Case II soil profile presented in Section 5.3.2. Two uniform soil profiles, U250 and U300, have uniform parabolic distributions of shear wave velocities corresponding to $V_{s1} = 250\ m/s$ and $V_{s1} = 300\ m/s$, respectively throughout the depth of the model. The list of the parameters corresponding to each shear wave velocity used in UBCHYST model is presented in Table 5.3. In the case of $V_{s1} = 200\ m/s$ and $V_{s1} = 400\ m/s$, the same selected parameters are used as described in Table 5.1 .

Figures 5.21 and 5.22 show the modulus reduction and damping curves at different depths of the first and the second soil layers computed by FLAC following

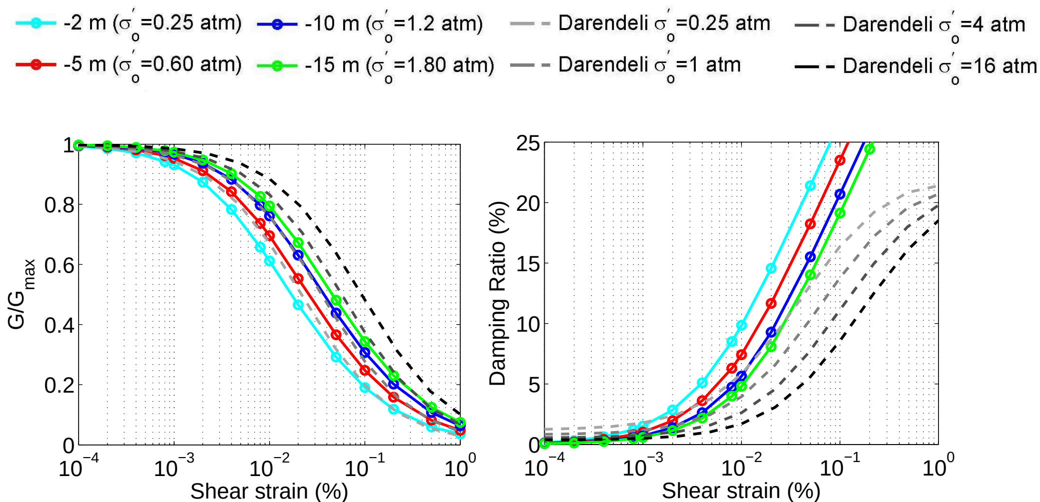

(a) $V_{s1} = 150\ m/s$

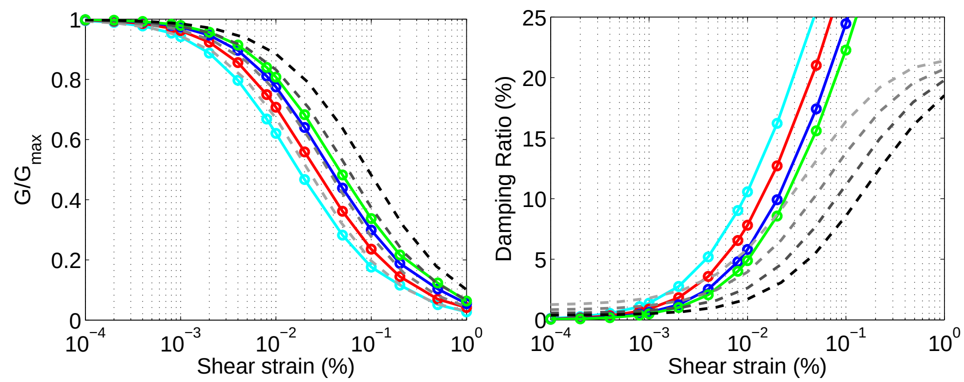

(b) $V_{s1} = 250\ m/s$

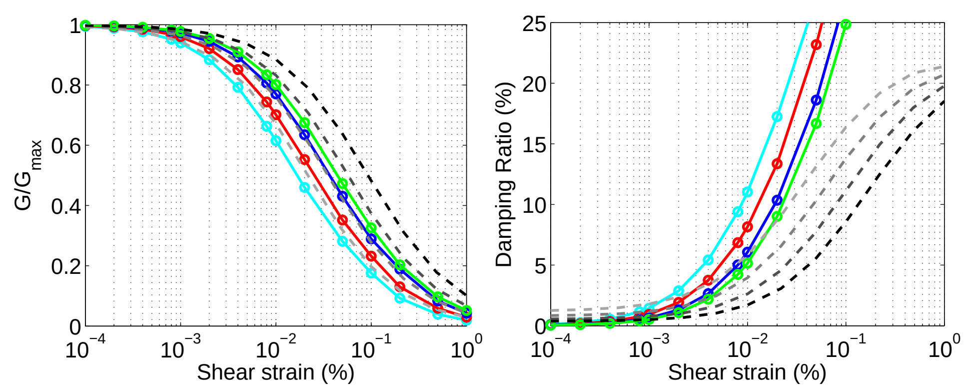

(c) $V_{s1} = 300\ m/s$

Figure 5.21: Modulus reduction and damping curves at different depths of the first soil layers with normalized shear wave velocities of (a) $V_{s1} = 150\ m/s$, (b) $V_{s1} = 250\ m/s$ and (c) $V_{s1} = 300\ m/s$ estimated by FLAC using UBCHYST model.

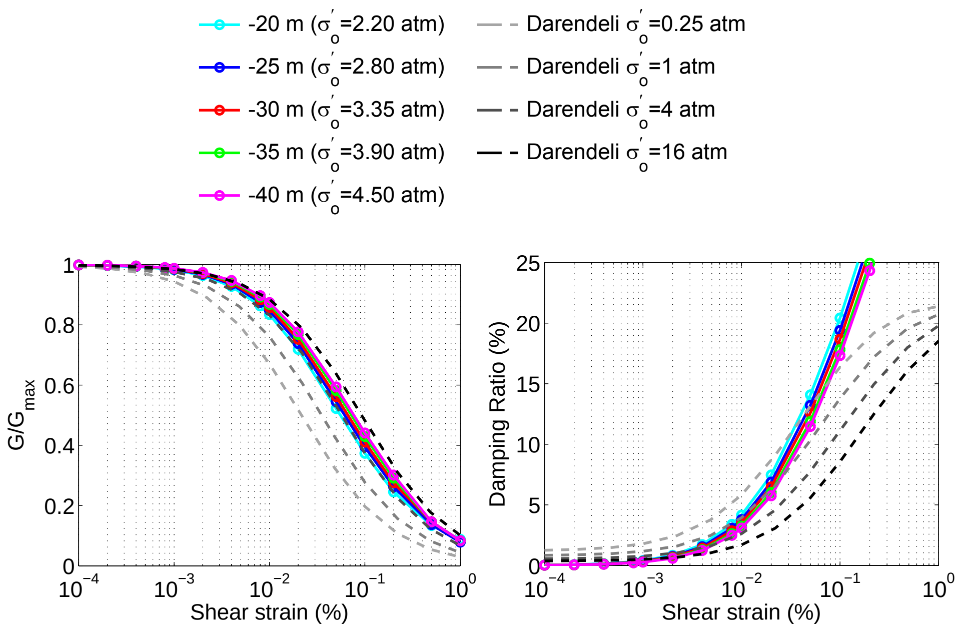

(a) $V_{s1} = 250\ m/s$

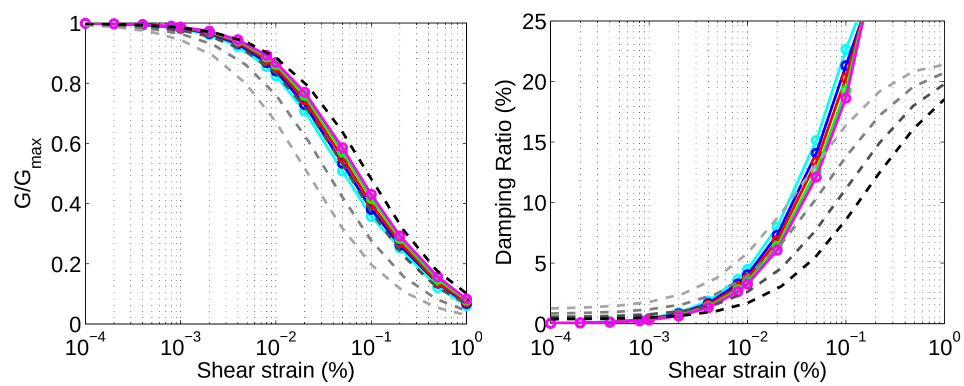

(b) $V_{s1} = 300\ m/s$

Figure 5.22: Modulus reduction and damping curves at different depths of the second soil layers with normalized shear wave velocities of (a) $V_{s1} = 250\ m/s$ and (b) $V_{s1} = 300\ m/s$ estimated by FLAC using UBCHYST model.

Table 5.3: Soil parameters of the UBCHYST constitutive model used in FLAC analyses.

Parameter description	Parameters	V_{s1} (m/s)		
		150	250	300
Unit weight (kN/m^3)	γ	19.5	19.5	19.5
Cohesion (kPa)	c	0	0	0
Peak friction angle (deg)	ϕ	33	33	33
Dilation angle (deg)	ψ	0	0	0
Small strain shear modulus (MPa)	G_{max}	10-124	25-345	38-500
Poisson's ratio	ν	0.28	0.28	0.28
Stress rate factor	R_f	0.98	0.98	0.98
Stress rate exponent	n	6.0	2.5	1.8
Stress rate exponent	n_1	1.0	1.1	1.1
First cycle factor	$mod1$	0.75	0.75	0.75
Large strain exponent	rm	0.5	0.5	0.5
Large strain factor	$dfac$	0	0	0

the procedure outlined in Section 5.2.2 using UBCHYST model parameters listed in Table 5.3. The Darendeli (2001) curves for different confining pressures are also added for comparison. Generally there is a good agreement between the resultant modulus reduction and damping curves calculated by FLAC using UBCHYST soil model and the curves of Darendeli (2001), except that the UBCHYST damping curves are higher at strains greater than approximately 0.1%, as discussed previously.

The nonlinear site response analyses of ten free-field soil columns are evaluated using FLAC (Itasca, 2012). Plots of the amplification ratios at the fundamental period of each site versus depth of the model are presented in the right-hand-side column of Figure 5.20. Even though all these soil profiles are categorized as NBCC (2010) site class D materials and their V_{s30} are almost in the same range, there is a significant difference in the level of shaking experienced at the foundation level as well as at the surface among these cases. It can be concluded from this figure that the stiffness of the soil profile in term of shear wave velocity of each soil layer and the level of impedance contrast between soil layers are two main parameters that affect the nonlinear site response of a site in question.

The presence of a relatively soft soil layer either underneath the basement wall foundation or far below the foundation level substantially affects the amplification of the ground acceleration and consequently the seismic response of the embedded basement wall in terms of the resultant drift ratio. Figure 5.23 shows the amplification ratio of the 5% damped acceleration response spectra at the foundation level and at the surface with respect to the base of the model for four different cases (N150-300, N200-300, N250-300, and U300). All these cases, as highlighted in Table 5.2, have the same shear wave velocity at their second soil layer ($V_{s1} = 300\ m/s$), and are differentiated by the shear wave velocity of their first soil layer, which varies between $V_{s1} = 150\ m/s$ to $V_{s1} = 300\ m/s$. This figure confirms that for the range of stiffnesses shown, a change in the stiffness of the top soil layer can significantly affect the overall site response in terms of spectral accelerations and consequently impact the seismic performance of the basement wall if the foundation of the structure is embedded in top soil layer.

Moreover, in order to investigate the effect of the second layer stiffness on nonlinear site response of the free-field soil column and accordingly the seismic performance of the embedded basement wall, three different cases shown in the highlighted row in Table 5.2 (N200-250, N200-300, and N200-400) are investigated. As shown in Figure 5.24, the stiffness of an underlying second soil layer also has a significant effect on the nonlinear seismic response of the site in the form of amplification level and frequency content of the ground motion at the surface and the foundation level of the basement wall structure.

It is evident from Figures 5.23 and 5.24 that increasing the shear wave velocities of either the first or the second soil layers increases the overall stiffness of the system and as a result decreases the fundamental period of the soil column. As shown in Figure 5.23, increasing the shear wave velocity of the first layer, results in a site with higher overall stiffness and drops the amplification ratio at the surface significantly. In contrast as illustrated in Figure 5.24, a stiffer site results in a higher amplification ratio. This phenomenon can be justified by the impedance contrast between soil layers, which plays an important role in the nonlinear seismic response of the site. For the aforementioned reasons there is no doubt that V_{s30} by itself is not a good indicator of the overall stiffness of the site and the impedance contrast among soil layers should also be considered as a key parameter.

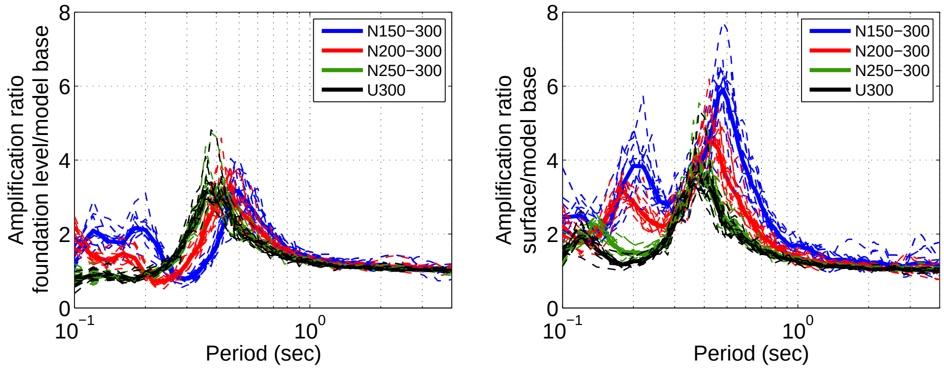

(a) (b)

Figure 5.23: Effect of the shear wave velocity of the first soil layer and the corresponding impedance contrast among different soil layers on amplification ratio at the (a) foundation level and (b) ground surface with respect to the base of the model. Each model is subjected to 14 crustal ground motions (G1–G14) spectrally-matched to the UHS of Vancouver. The mean values of the response are presented in solid lines.

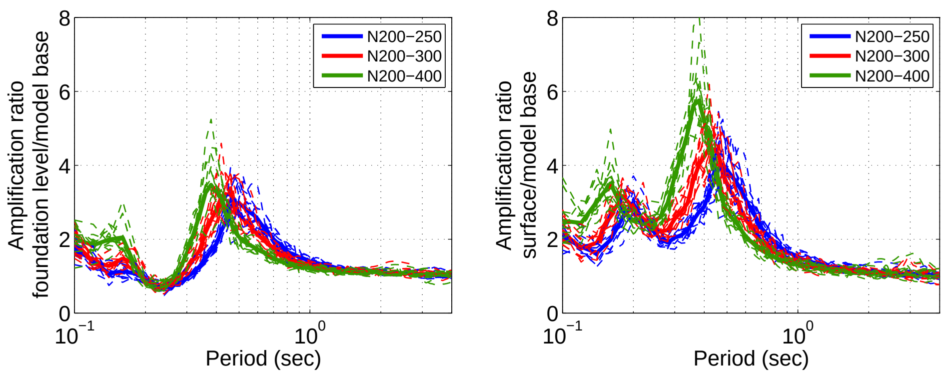

(a) (b)

Figure 5.24: Effect of the shear wave velocity of the second soil layer and the corresponding impedance contrast among different soil layers on amplification ratio at the (a) foundation level and (b) ground surface with respect to the base of the model. Each model is subjected to 14 crustal ground motions (G1–G14) spectrally-matched to the UHS of Vancouver. The mean values of the response are presented in solid lines.

A series of nonlinear two-dimensional finite difference analyses using FLAC (Itasca, 2012) are conducted to model the seismic behavior of the 4-level basement wall designed for 50% and 60% of the NBCC (2010) PGA and founded on ten site class D soil profiles presented in Table 5.2. Each wall is subjected to 14 crustal ground motions (G1-G14) spectrally matched to NBCC (2010) UHS of Vancouver, as described in Chapter 3. The finite difference grid, the soil layer geometries, boundary conditions, construction simulation, and structural and interface elements are the same as the Case II model described in Section 5.3.2. The soil properties of the first and second layers in conjunction with the UBCHYST constitutive model used to model the soil media are reported in Tables 5.1 and 5.3. The values of interface stiffnesses (k_n and k_s), which are the function of the stiffness of the stiffest neighbouring zones (See Equation 3.6) along the interface elements, are also modified based on the stiffness of the soil zones around the structure.

Similar to previous sections the average of the maximum envelopes of the resultant drift ratio along the height of the basement wall (both right-side and left-side walls) is selected as a parameter to be evaluated in this section. For almost all the simulations, the basic shape (distribution) of the drift ratio of the wall along the height of the wall does not change significantly, and the magnitude of the results are the only parameter that varies. The average of the maximum envelopes of drift ratios along the height of the wall designed for 50% and 60% PGA founded on differenet soil profiles highlighted in Table 5.2 are plotted in Figure 5.25.

Figure 5.25 suggests considerable sensitivity of the results to the normalized shear wave velocities of the first and the second soil layers. By comparing the seismic performance of the walls in the form of drift ratio with the results of the nonlinear site response analyses of the corresponding sites presented in Figures 5.23 and 5.24, one can conclude that the level of amplification of the ground motion at the foundation and surface levels has a direct impact on the resultant drift ratios at the bottom and top basement levels. The uniform soil layer (U300), which causes a minimum amplification ratio among all the other cases, results in a very negligible amount of drift ratio along the height of the wall, whereas soil profile N150-300 amplifies the ground motions the most and consequently, the wall founded on this soil profile experiences the largest amount of drift ratio at the top and bottom basement levels.

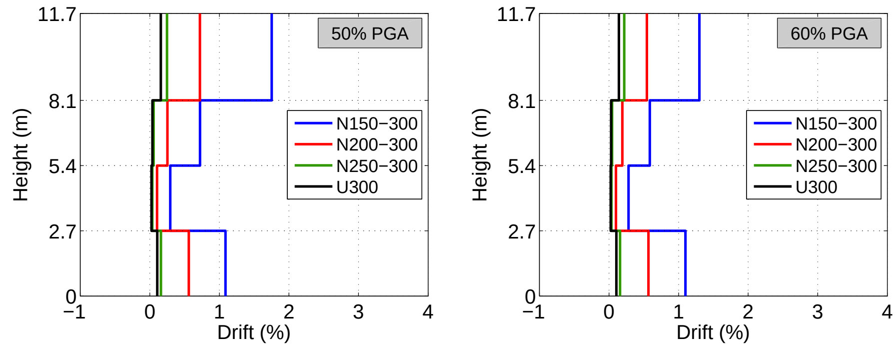

(a)

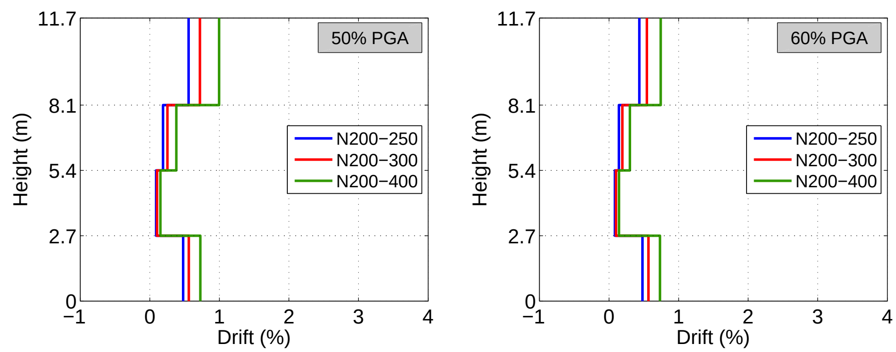

(b)

Figure 5.25: Average of the maximum envelopes of drift ratios along the height of the walls designed for 50% and 60% of the code PGA subjected to 14 crustal ground motions spectrally-matched to UHS of Vancouver (G1–G14) and founded on different soil profiles, showing the sensitivity of response to variation in the normalized shear wave velocities of (a) the first and (b) the second soil layers.

Figure 5.26 provides detailed information regarding to the distribution of the maximum drift ratios of the walls presented in Figure 5.25. Each blue circle on this figure corresponds to the maximum value of the drift ratio along the height of the right-side and left-side walls subjected to one out of 14 ground motion. The average resultant maximum drift ratios along the height of the walls are shown by red solid circles that are comparable with the mean value of the response presented

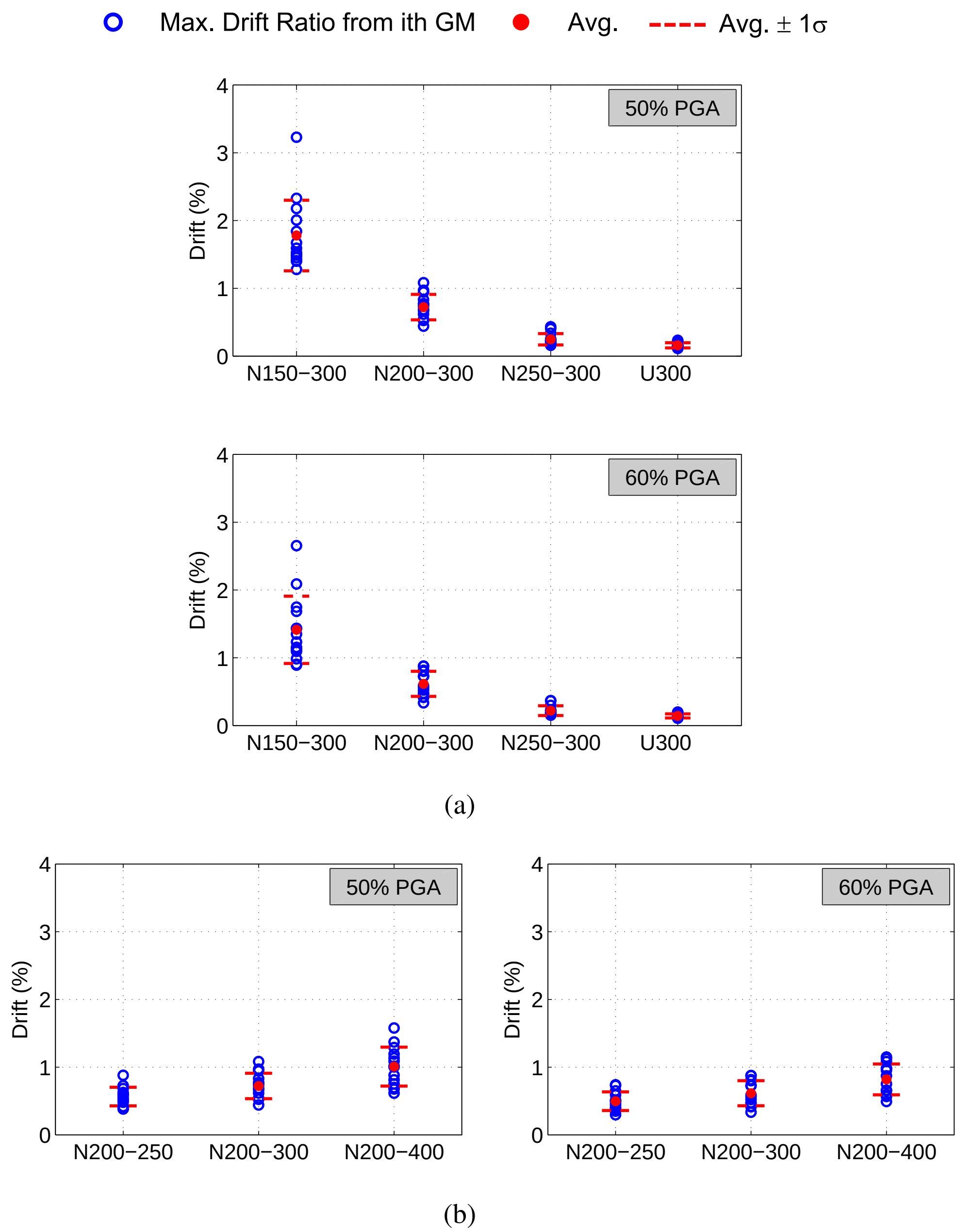

Figure 5.26: Sensitivity of the resultant maximum drift ratios and the corresponding average ± one standard deviation of the 4-level basement wall designed for 50% and 60% PGA to variation of the normalized shear wave velocities of (a) the first and (b) the second soil layers. The walls are subjected to 14 crustal ground motion spectrally-matched to the UHS of Vancouver.

in Figure 5.25. For instance, as illustrated in Figure 5.25, an average of the resultant maximum drift ratio of the basement wall founded on N150-300 soil profile and subjected to ground motions G1–G14 has a maximum value of 1.77% at the top basement level, which is consistent with an average value plotted by the red circle in Figure 5.26.

In addition, Figure 5.26 quantifies the amount of variation and dispersion of the maximum drift ratios resulting from the basement wall founded on certain soil profile excited by 14 spectrally-matched ground motions. The standard deviation measures the spread of the data about an average value. A lower standard deviation indicates that the maximum resultant drift ratios tend to be very close to an average value from 14 ground motions, while a high standard deviation shows that the maximum drift ratios spread out over a wider range of values. In this figure, if one assumes normally distributed drift ratios, the red dashted-lines represent an average$\pm$ one standard deviation with a 68% chance that the mean falls within a range of standard error.

According to the adopted performance criterion for drift ratio (ASCE-TCBRD, 2010), Figure 5.26 shows that except for the case of N150-300, the resultant average $\pm$ one standard deviation of all basement walls designed for even 50% and 60% PGA falls within an acceptance range ($< 1.7\%$) when subjected to the current seismic hazard level in Vancouver, with a 2% chance of being exceeded in 50 years. It is worth mentioning that there are some concerns about using $V_{s1} = 150\ m/s$ as the normalized shear wave velocity of the first soil layer because according to practitioners (DeVall et al., 2010, 2014) it might be a bit low for high-rise construction in Vancouver. Even in the case of constructing the 4-level basement wall on the N150-300 soil profile, the analyses show that the resultant maximum drift ratio falls within a range of $1.77\% \pm 0.52\%$ and $1.41\% \pm 0.49\%$ for the basement walls designed for 50% and 60% code PGA, respectively. These are in the lower range of the medium response category ($< 3.5\%$) defined by ASCE-TCBRD (2010).

Figure 5.27 is an extended version of Figure 5.26, which summarizes the maximum values of drift ratios along the height of the walls designed for 50% and 60% PGA and founded on ten soil profiles outlined in this section. In these three-dimensional figures, horizontal axes represent the normalized shear wave velocities of the first and the second soil layers, as described in Table 5.2. The vertical

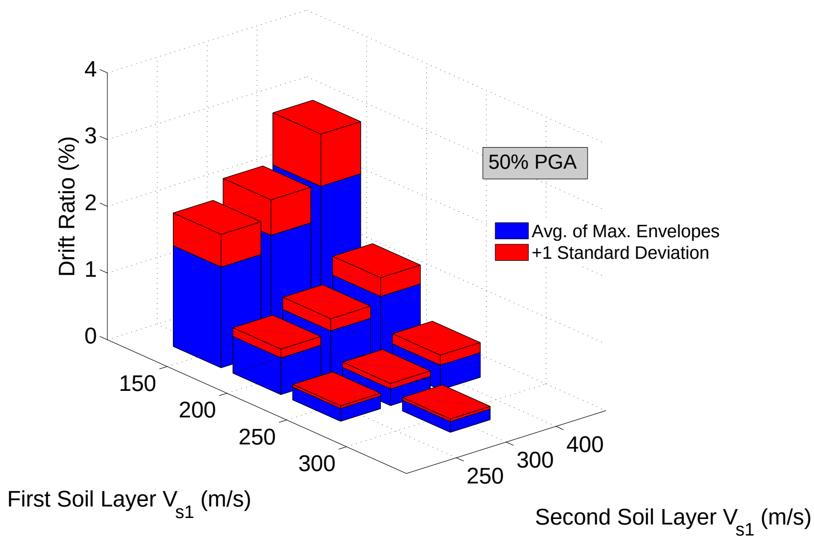

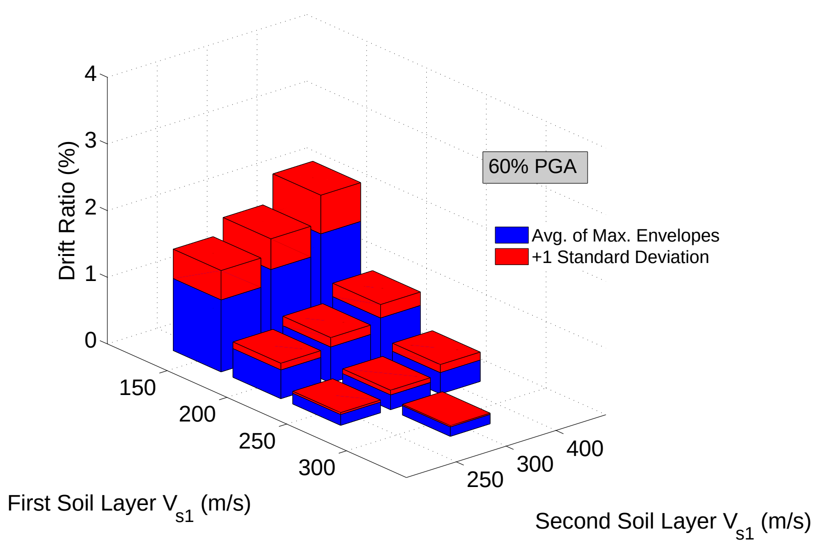

Figure 5.27: Average of the maximum drift ratios and the corresponding one standard deviation of the 4-level basement wall designed for different fractions of the code PGA and founded on ten different soil profiles. Each wall is subjected to 14 crustal ground motions (G1–G14) spectrally-matched to the UHS of Vancouver.

axis presents the mean of the maximum drift ratios along the height of the 4-level basement walls and the corresponding mean + one standard deviation. It can be concluded from this figure that decreasing the shear wave velocity of the first soil layer increases the resultant drift ratio along the height of the basement wall. In contrast, decreasing the shear wave velocity of the second soil layer decreases the drift ratio. Moreover, two uniform soil profiles (U250 and U300) result the minimum value of the resultant drift ratios compare to the non-uniform soil profiles. In fact, the mean value of the maximum drift ratio increases proportionally to the increase of the impedance ratio between two soil layers.

According to the performance criterion adopted for drift ratio (1.7%), except for the cases in which $V_{s1} = 150\ m/s$ is assigned for the first soil layer, the wall designed for 50% PGA using modified M-O method, performs adequately under full seismic demand driven from the NBCC (2010). The resultant drift ratios of the wall designed for 60% PGA confirm that the walls founded on a soil profile with a very loose first soil layer ($V_{s1} = 150\ m/s$) and with relatively high impedance contrast with the second soil layer (N150-250 and N150-300) would perform adequately under the demand corresponding to an exceedance rate of 2% in 50 years. It is worth mentioning that the case in which the basement wall is founded on a soft soil with a very high impedance contrast with the second soil layer (N150-400) needs an extra attention. In this case as is illustrated in Figure 5.27, the seismic response would fall in the lower range of the medium response ($< 3.5\%$) category defined by ASCE-TCBRD (2010).

5.4 Effect of basement wall geometry

In an expensive and congested urban area of downtown Vancouver, deep basement walls have been constructed extensively to allow for underground parking and other usages. Deep excavations induce significant changes in both stress and strain of the surrounding soil and, therefore, generate permanent displacements and potentially more severe damages.

This section investigates the effect of the geometric parameters of the basement walls (e.g., total height and top storey height) on the seismic performance of the structure and is considered as an extension of the study on the 11.7 m 4-level basement wall described earlier in Chapter 4. The result of the analyses presented in Chapters 4 and 5 showed that the performance of the top and bottom basement levels are critical. As it is common in design practice to allow higher height to the top basement storey a set of sensitivity analyses are conducted in this section to study the effect of the higher top basement height (e.g. 5.0 m instead of 3.6 m, which has been used so far in this study). In addition to the 4-level basement wall, deeper basement structures with higher number of underground levels and deeper depths are studied in this section.

Therefore, two very common configurations in practice of deep basement walls are designed by SEABC structural engineers (DeVall, 2011) for various fractions of the NBCC (2010) PGA:

- 4-level basement wall with 5.0 m top storey and a total height of 13.1 m, as shown in Figures 5.28 and 5.30,
- 6-level basement wall with a total height of 17.1 m, as illustrated in Figures 5.29 and 5.31.

In order to take into an account the effect of soil stiffness at the foundation level, each wall is founded on Case I and Case II soil profiles outlined in Section 5.3.2.

5.4.1 Seismic design of a 4-level basement wall with higher top storey height and a 6-level basement wall

As discussed previously in Section 3.2, the state of practice for seismic design of basement walls is to use two load combinations prescribed by the National Building Code of Canada (NBCC, 2010): (1) 1.5 times an active lateral pressure, $p_A(z)$, which $p_A(z)$ is not less than 20 kPa compaction/surcharge pressure as illustrated in Figures 5.28 and 5.29, and (2) $p_{AE}(z) = p_A(z) + \Delta p_{AE}(z)$ where $p_{AE}(z)$ is the total active lateral pressure consists of $p_A(z)$, the static lateral active pressure and $\Delta p_{AE}(z)$, the dynamic increment of the lateral earth pressure acting on the wall. Each basement wall is designed for four fractions of the code PGA (=0.46 g) following the state of practice in British Columbia using the modified M-O method as illustrated in Figures 5.30 and 5.31.

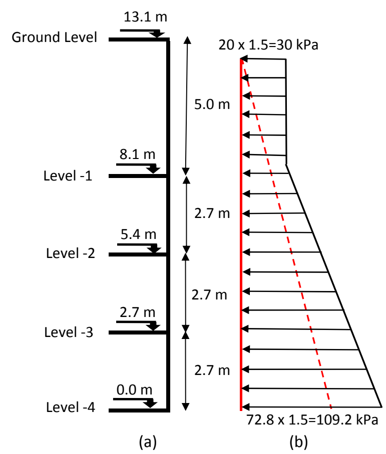

Figure 5.28: (a) Floor heights in the 4-level basement wall with 5 m top storey and (b) the calculated lateral earth pressure distributions from the first load combination.

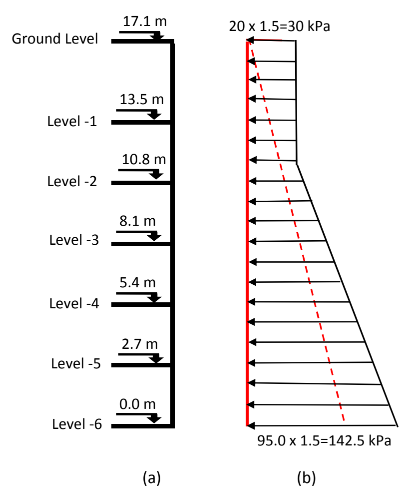

Figure 5.29: (a) Floor heights in the 6-level basement wall and (b) the calculated lateral earth pressure distributions from the first load combination.

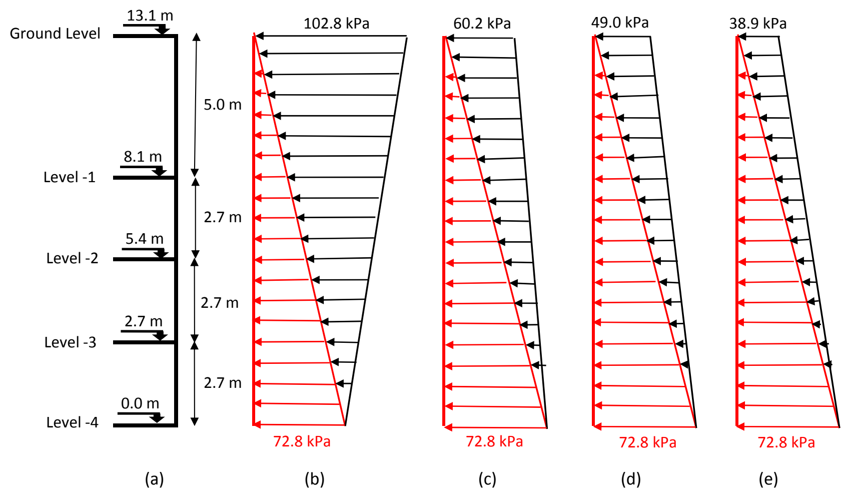

Figure 5.30: (a) Floor heights in the 4-level basement wall with 5 m top storey and the calculated lateral earth pressure distributions from the second load combination using the M-O method with (b) 100% PGA, (c) 70% PGA, (d) 60% PGA, and (e) 50% PGA, where PGA=0.46g.

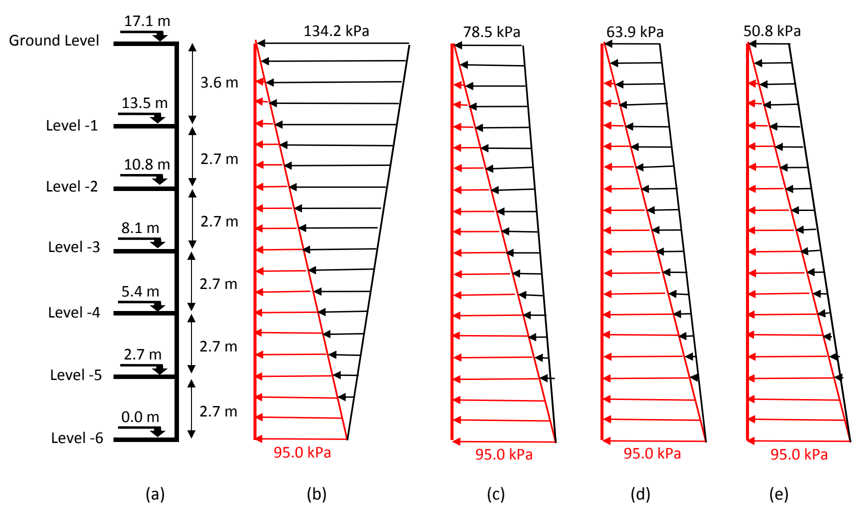

Figure 5.31: (a) Floor heights in the 6-level basement wall and the calculated lateral earth pressure distributions from the second load combination using the M-O method with (b) 100% PGA, (c) 70% PGA, (d) 60% PGA, and (e) 50% PGA, where PGA=0.46g.

For each wall consistent with four scenarios of lateral earth pressure corresponding to four different fractions of PGA (50%, 60%, 70% and 100%), four levels of yielding moments are calculated and presented in Figure 5.32. Details about the calculation of moment capacities at different elevations along the height of the walls are discussed in Appendix A.

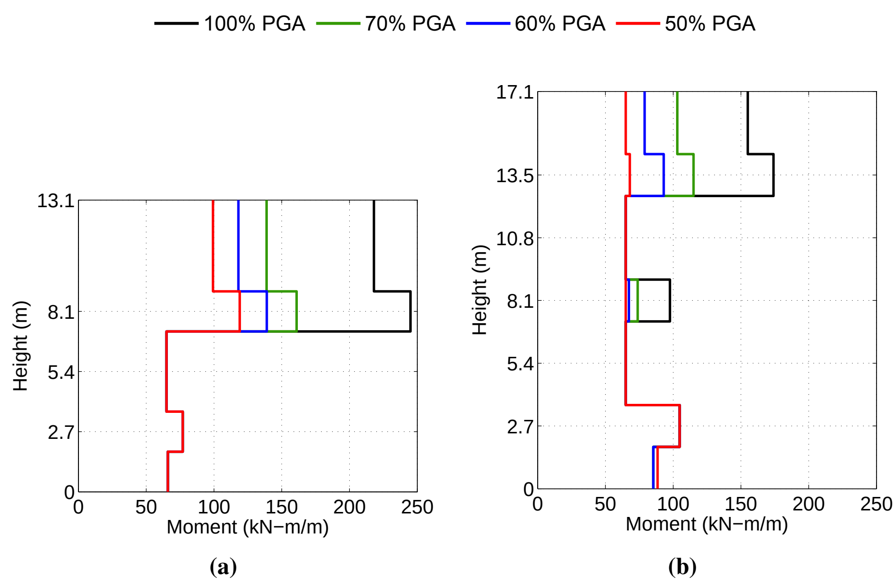

Figure 5.32: Moment capacity distribution along height of (a) the 4-level basement wall with 5.0 m top storey and (b) the 6-level basement wall designed for different fractions of the NBCC (2010) PGA for Vancouver (= 0.46 g).

5.4.2 Simulation results

A series of nonlinear two-dimensional finite difference analyses using FLAC 2D are conducted to model the seismic behavior of the 4-level and 6-level basement walls designed for various fractions of the NBCC (2010) PGA for Vancouver. The description of the boundary conditions, construction simulation, and structural and interface elements can be found in Chapter 3. Each basement wall is founded on two different soil profiles, Cases I and II, as described in Section 5.3.2. Figures 5.33 and 5.34 show the finite difference grids and the soil geometries together with

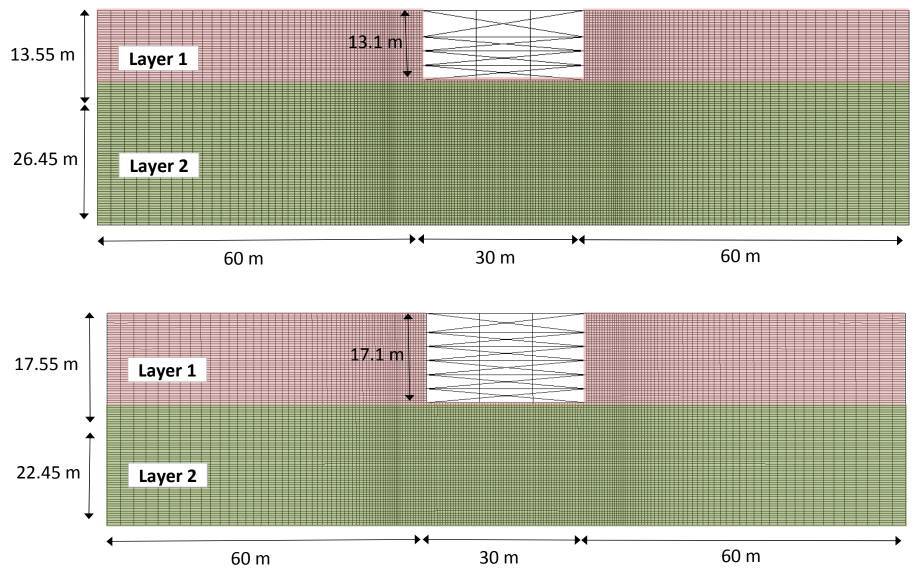

Figure 5.33: (a) 4-level basement wall with 5.0 m top storey and total height of 13.1 m and (b) 6-level basement walls with a total height of 17.1 m founded on Case I soil profile.

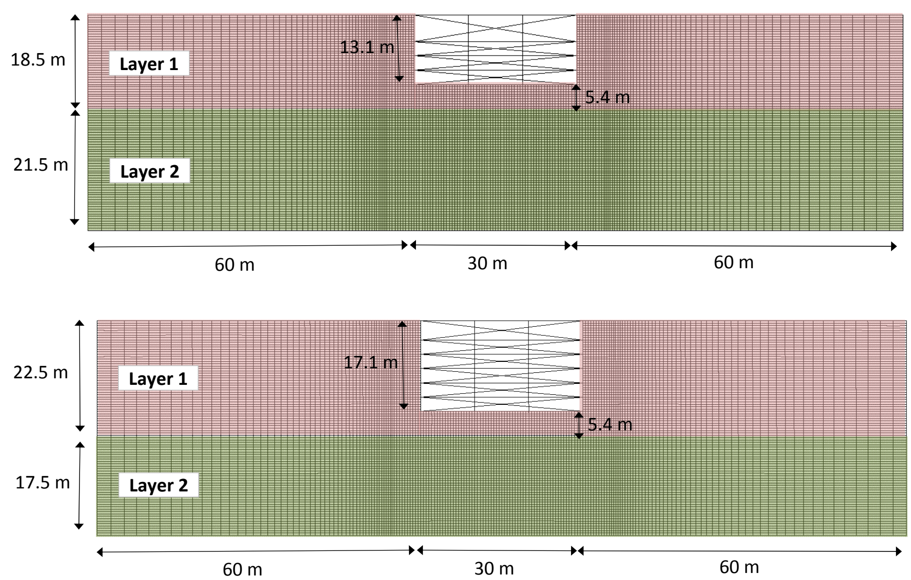

Figure 5.34: (a) 4-level basement wall with 5.0 m top storey and total height of 13.1 m and (b) 6-level basement walls with a total height of 17.1 m founded on Case II soil profile.

a layout of the 4-level and 6-level basement walls founded on Case I and Case II soil profiles. In each case the depth from the foundation level of the basement wall to the second stiff soil layer is constant. The soil properties of the first and the second soil layers in Cases I and II soil profiles are as reported in Table 5.1 and are modeled using the UBCHYST constitutive model.

The average of the maximum envelopes of drift ratios along the height of the walls designed for different fractions of the code PGA subjected to 14 crustal ground motion records spectrally-matched to the UHS of Vancouver (G1–G14) and embedded in Case I and II soil profiles are presented in Figures 5.35 to 5.38. In these plots an average value corresponds to the average of the maximum envelopes of drift ratio along the height of the both right-side and left-side walls subjected to 14 ground motions. If normally distributed drift ratios are assumed, average$\pm 1\sigma$ represents the one standard deviation with a 68% chance that the mean falls within the range of standard error.

From these figures one can conclude that the walls embedded in Case II soil profile result in slightly higher drift ratios compared with the ones founded on Case I site. For instance, the 13.1 m 4-level basement wall designed for 50% PGA founded on Case I soil profile results in an average of the maximum drift ratio of 0.80%$\pm$0.15%, whereas the same wall embedded in the Case II soil profile undergoes the maximum drift ratios in a range of 0.88%$\pm$0.25%. The results of this study confirm that the response of both the top and bottom levels of either 4-level and 6-level basement walls are critical and need careful consideration. According to the adopted performance criterion for drift ratio (1.7%), the maximum resultant drift ratios along the height of the 4-level and 6-level basement walls (with total hight of 13.1 m and 17.1 m) designed for 50% to 60% code PGA, founded on sandy soil materials and subjected to the full seismic hazard level in Vancouver with a 2% chance of being exceeded in 50 years, fall into the acceptance criterion.

Figures 5.39 and 5.40 illustrate a probability of the maximum drift ratio exceedance. As discussed previously, exceedance probability is the probability of an event being greater than or equal to a given value. These figures describe detailed information regarding the distribution of the maximum resultant drift ratio of the basement walls subjected to 14 ground motions spectrally matched to the NBCC (2010) seismic hazard in Vancouver.

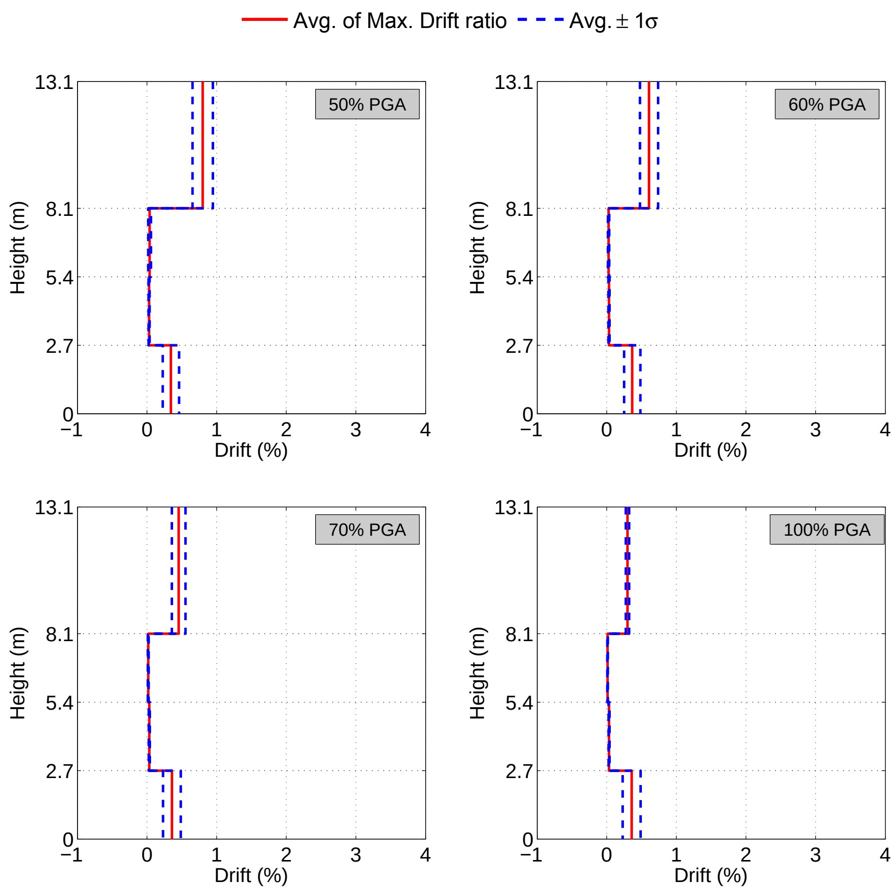

Figure 5.35: Average of the maximum envelopes of drift ratios and ± one standard deviation along the height of the 13.1 m 4-level basement walls designed for different fractions of the code PGA, founded on Case I soil profile subjected to 14 crustal ground motions (G1–G14) spectrally-matched to the UHS of Vancouver.

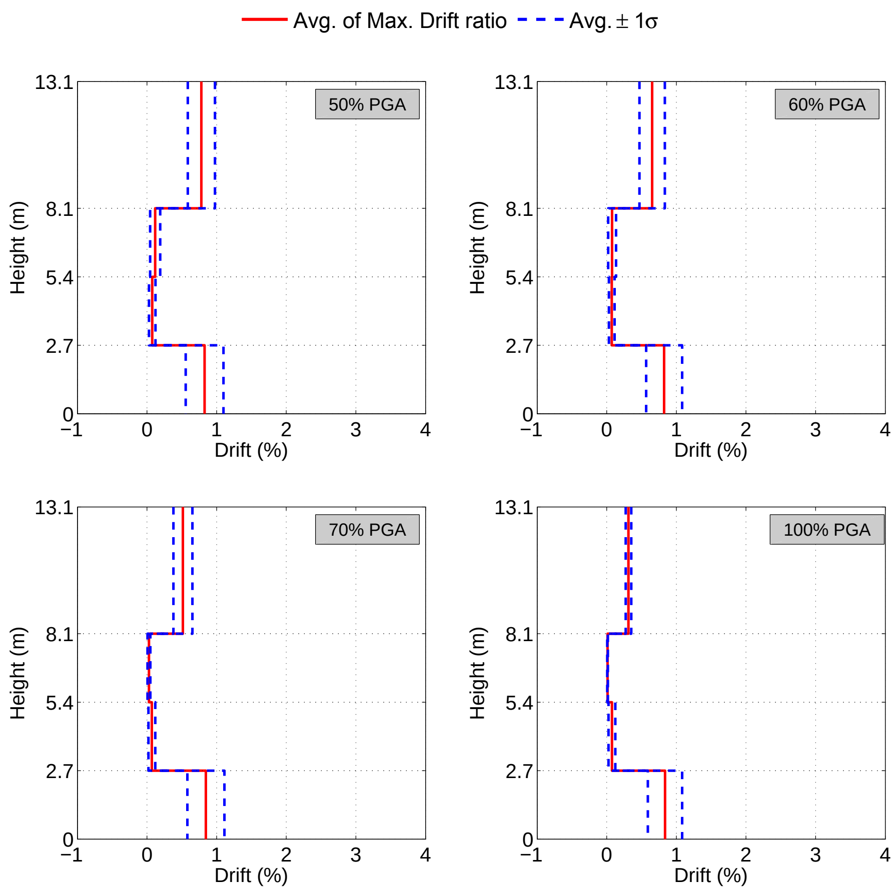

Figure 5.36: Average of the maximum envelopes of drift ratios and ± one standard deviation along the height of the 13.1 m 4-level basement walls designed for different fractions of the code PGA, founded on Case II soil profile subjected to 14 crustal ground motions (G1–G14) spectrally-matched to the UHS of Vancouver.

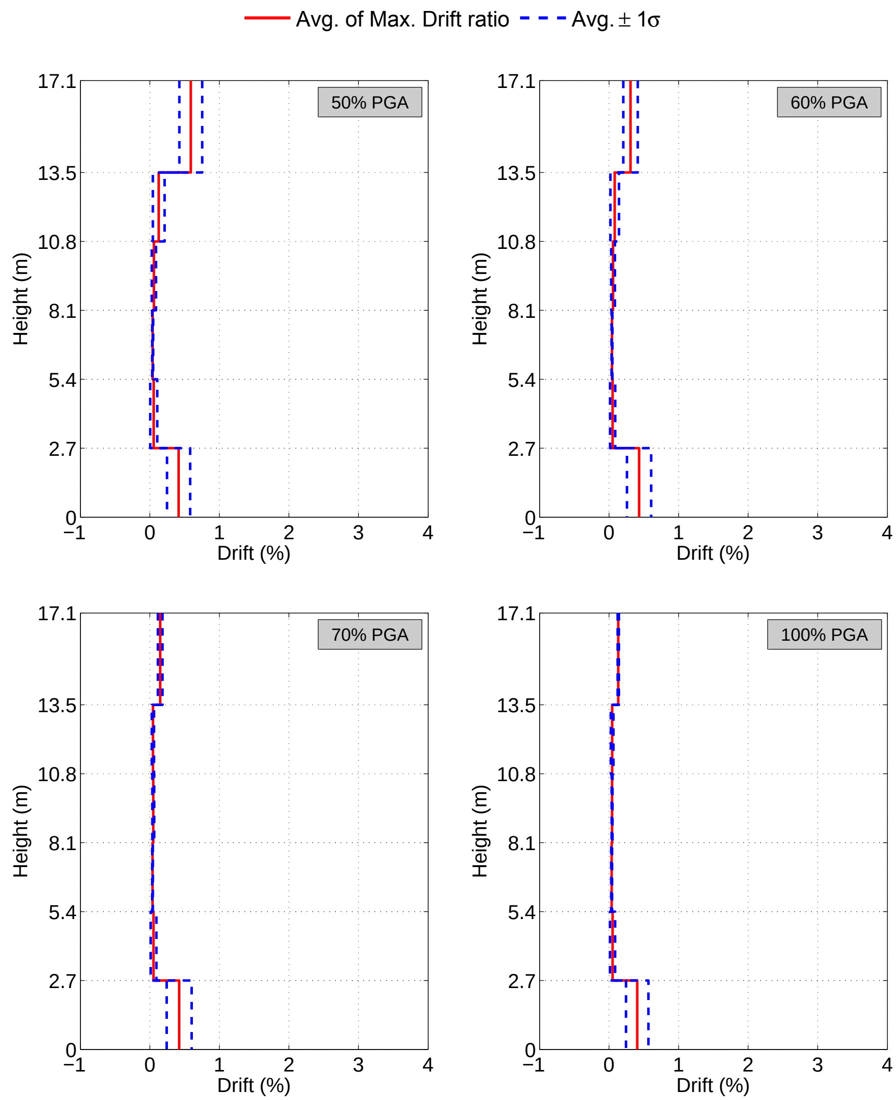

Figure 5.37: Average of the maximum envelopes of drift ratios and ± one standard deviation along the height of the 17.1 m 6-level basement walls designed for different fractions of the code PGA, founded on Case I soil profile subjected to 14 crustal ground motions (G1–G14) spectrally-matched to the UHS of Vancouver.

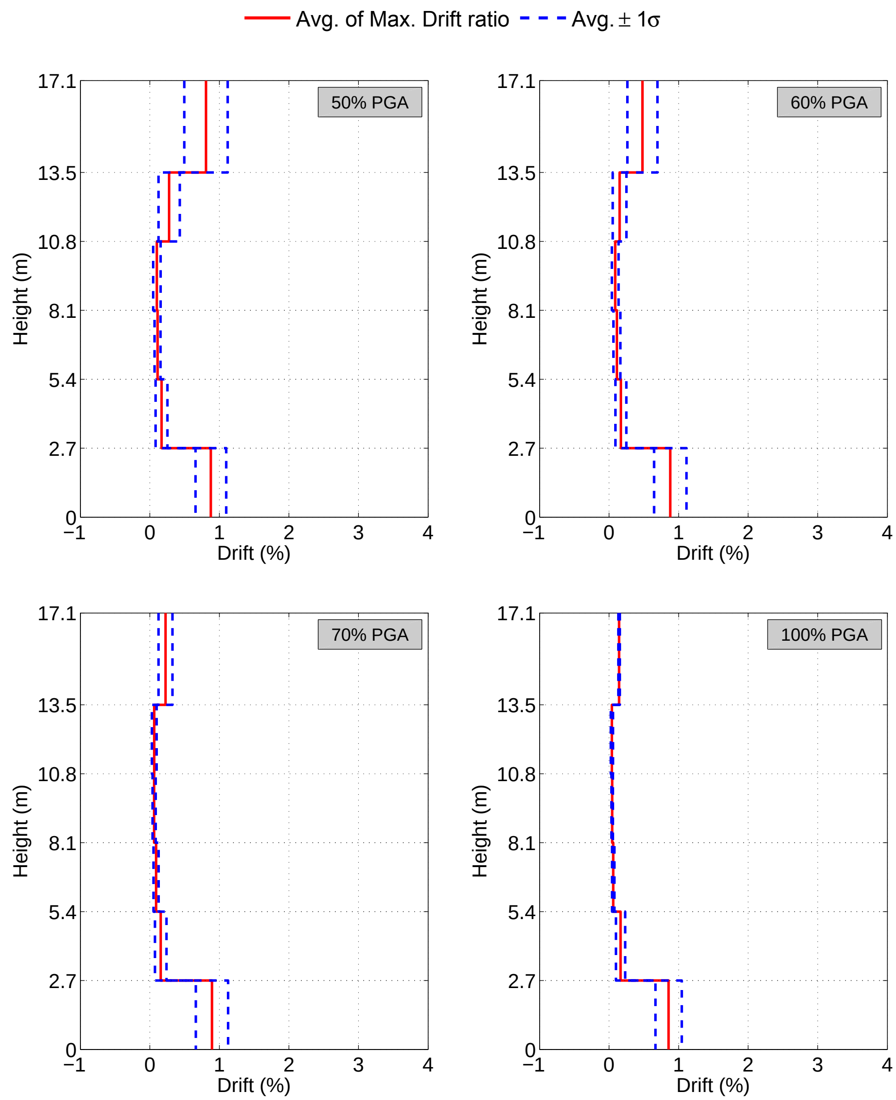

Figure 5.38: Average of the maximum envelopes of drift ratios and ± one standard deviation along the height of the 17.1 m 6-level basement walls designed for different fractions of the code PGA, founded on Case II soil profile subjected to 14 crustal ground motions (G1–G14) spectrally-matched to the UHS of Vancouver.

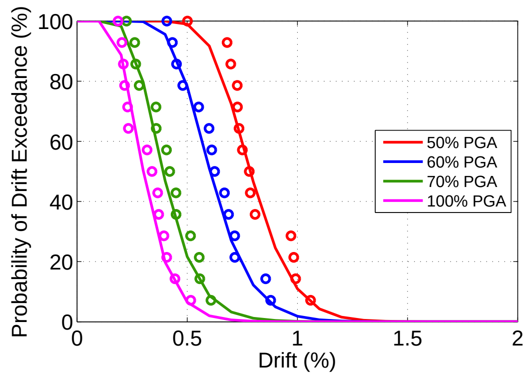

(a) Case I

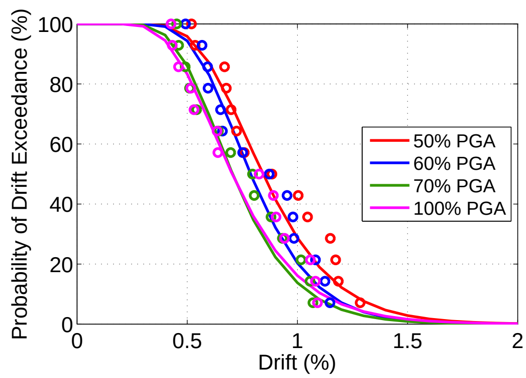

(b) Case II

Figure 5.39: Probability of drift ratio exceedance of the 13.1 m 4-level basement walls designed for 50%, 60%, 70% and 100% of the code PGA, founded on Case I and II soil profiles subjected to 14 crustal ground motions (G1–G14) spectrally-matched to the UHS of Vancouver.

Figure 5.41 summarizes and compares the resultant maximum drift ratios of the 11.7 m, 13.1 m and 17.1 m basement walls founded on both Case I and Case II soil profiles according to the adopted performance criterion for drift ratio in this study ($< 1.7\%$). It can be concluded that the behavior of the basement walls designed for 50% to 60% PGA, founded on relatively dense or loose sandy materials are satisfactory when subjected to the current seismic hazard level in Vancouver with a 2% chance of being exceeded in 50 years. Within a significant range of

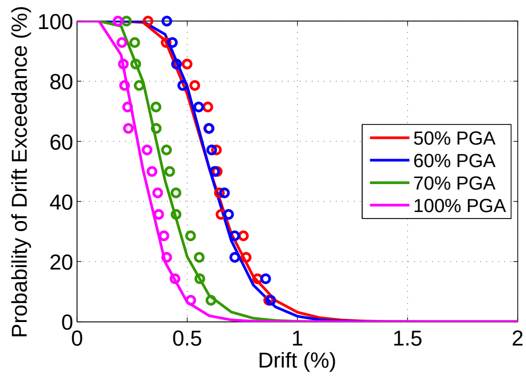

(a) Case I

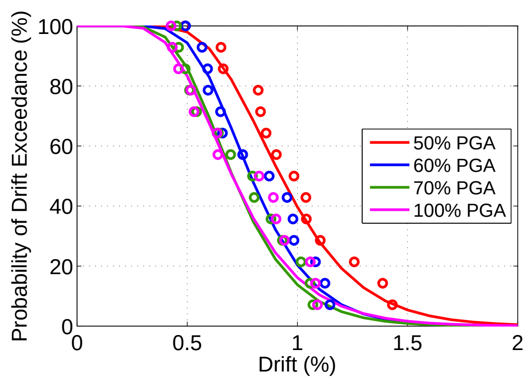

(b) Case II

Figure 5.40: Probability of the maximum drift ratio exceedance of the 17.1 m 6-level basement walls designed for different fractions of the code PGA, founded on Case I and II soil profiles subjected to 14 crustal ground motions (G1–G14) spectrally-matched to the UHS of Vancouver.

variations, the conclusion still stands that the basement walls can be safely designed with 50–60% NBCC (2010) PGA using the modified M-O method. The present design procedure in Vancouver using 100% PGA leads to very expensive and overly-conservative structures and the findings of this research can have considerable impact on cost effectiveness of the design of the basement walls.

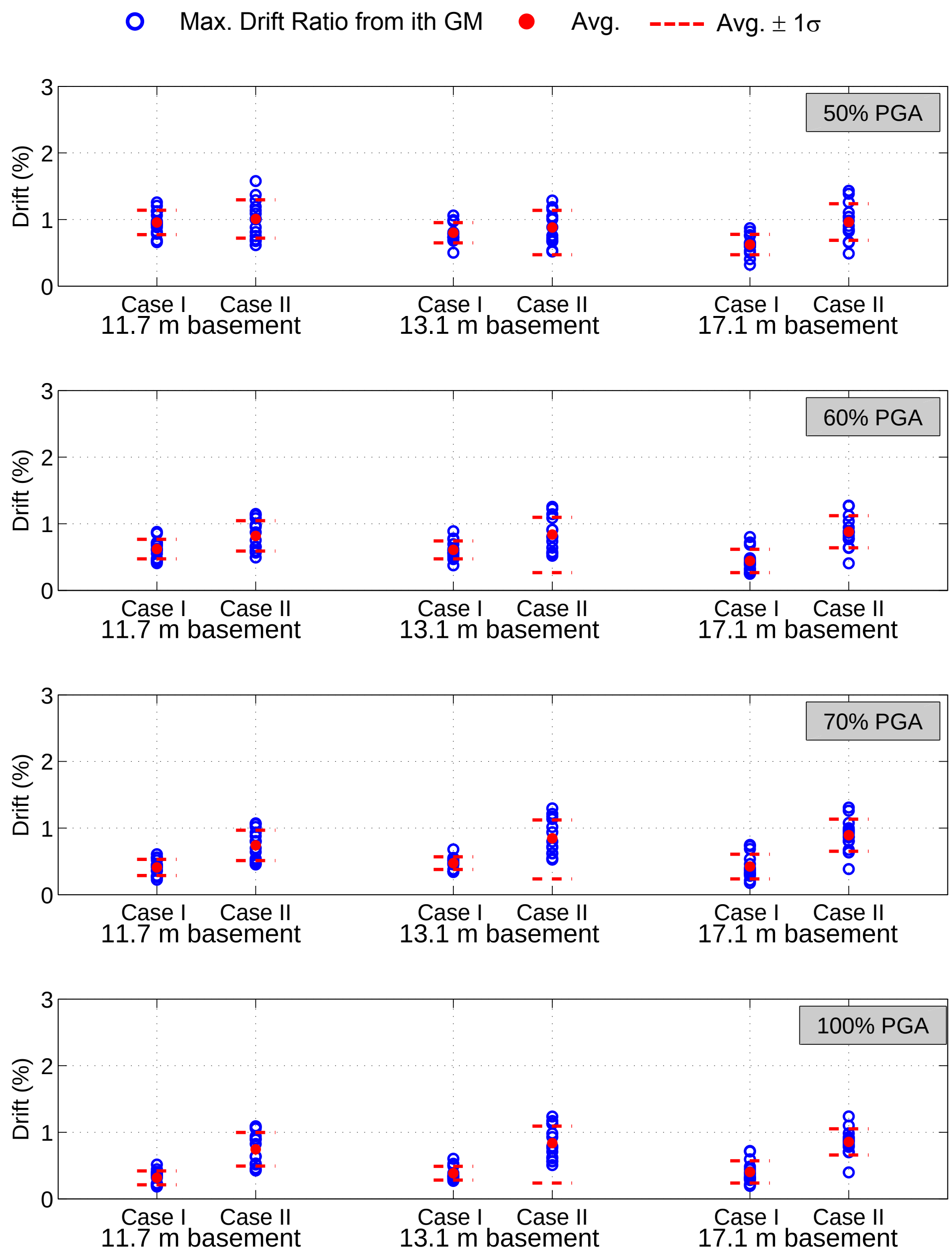

Figure 5.41: The resultant maximum drift ratios and the corresponding average and average $\pm$ one standard deviation of the 4-level and 6-level basement walls designed for different fractions of the NBCC (2010) code PGA, founded on Case I and Case II soil profiles and subjected to 14 crustal ground motions spectrally-matched to the UHS of Vancouver.

Chapter 6

Selection and modification of time histories for Vancouver

Make things as simple as possible, but not simpler.
— Albert Einstein (1879–1955)

6.1 Introduction

The goal of ground motion selection and scaling is to develop a suite of acceleration time histories representative of the seismic demand anticipated for the analysis of a structure at a specific site. The absence of recordings at the site forces practitioners to modify the existing time histories to match the target spectrum at the site. Selected ground motions are scaled to match the Uniform Hazard Spectrum (UHS) for the site within a period range of interest.

The objective of scaling the ground motions is to get reliable estimate of the mean response of a structure and an adequate assessment of its variation about the mean (Baker and Allin Cornell, 2006; Hancock et al., 2006; Shome et al., 1998). For this purpose, an appropriate number of ground motions are selected and their corresponding structural responses are estimated by subjecting the soil–structure system to acceleration time histories that are compatible with the scenario in question.

As discussed previously in Chapter 3, a spectrally matched ground motions, due to the nature of the method, result in lower variance of the structural response and consequently provide a robust value of the mean response with lower number of motions. The mean value of the structural response is used for design basis, however estimating the probability of collapse requires the estimation of the potential variability of a basement wall response. Therefore, the intensity-based linear scaling methods, which preserve the motion-to-motion variability are preferred over spectral matching techniques, which modify the frequency content and phasing of the record to match its response spectrum to the target spectrum (Kalkan and Chopra, 2010).

So far the conclusion drawn on the seismic performance of the basement walls designed for different fractions of the NBCC (2010) PGA was on the basis of one type of ground motions: crustal earthquakes. Besides, in order to expedite extensive parametric analyses, the mean value of the structural response established by spectrally matched ground motion records to the target spectrum were reported. In this Chapter the seismic performance of the designed basement walls will be re-evaluated by subjecting them to motions from other dominant types of earthquake sources in British Columbia.

The seismicity of the south-western British Columbia and the dominant types of earthquake sources in the area are discussed in Section 6.2. Various options for scaling and matching earthquake records to be representative of the seismic hazard (NBCC, 2010) are studied in Section 6.3. Comprehensive procedures for selection and modification of strong ground motions for the seismic assessment of basement walls in Vancouver are presented in Section 6.4. The the maximum resultant drift ratio of the basement wall designed for different fractions of NBCC (2010) PGA using modified M-O method, subjected to linearly scaled ground motions are presented in Section 6.5. Based on these results an appropriate fraction of the code PGA for design of the basement walls using the modified M-O method is evaluated.

6.2 Seismicity of south-western British Columbia

Each year, seismologists with the Geological Survey of Canada (Natural Resources Canada, 2012) record and locate more than 1000 earthquakes in Pacific Coast, which is the most seismically active regions of Canada. Ten moderate to large (M6–7) earthquakes have occurred within 250 km of Vancouver and Victoria during the last 130 years (Clague, 2002; Rogers, 1998).

Four tectonic plates meet and interact in south-western British Columbia and three different types of plate movements take place, resulting in significant earthquake activities. Plates move towards each other at converging, apart at diverging and past each other at transform (strike-slip) boundaries as illustrated in Figure 6.1.

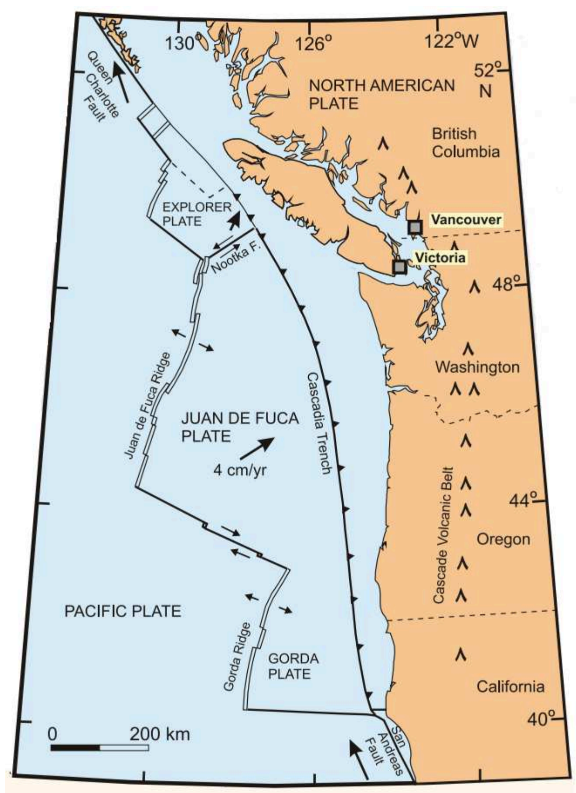

Figure 6.1: Tectonic plates in west coast of Canada and the United States (Natural Resources Canada, 2012)

The tectonic setting of south-western British Columbia is mainly influenced by the subduction of the oceanic Juan de Fuca plate beneath the North America continental plate as shown in Figure 6.2. This region is called the Cascadia subduction zone, which is located about 50 km beneath Vancouver and extends along the coast from northern California to central Vancouver Island. Another small plate, the Explorer, is also sliding underneath the North American plate, and at the same time the Juan de Fuca plate is sliding along the Nootka fault. In the north, there is a major strike-slip fault boundary between the Pacific plate moving northwest and the North American plate moving southeast relative to one another, called the Queen Charlotte fault. This fault was the site, in 1949, of the largest earthquake recorded in Canada (M8.1).

Given these facts, the seismicity of the west coast of British Columbia has significant hazard contributions from shallow crustal earthquakes in the North America plate, deeper subcrustal earthquakes in the subducting Juan de Fuca plate, and very large (M8+) Cascadia subduction earthquakes at the interface of the two plates extended beneath Vancouver (Finn et al., 2000; Levson et al., 2003; Onur, 2001; Pina, 2010). The crustal and subcrustal ground motions have the major contribu-

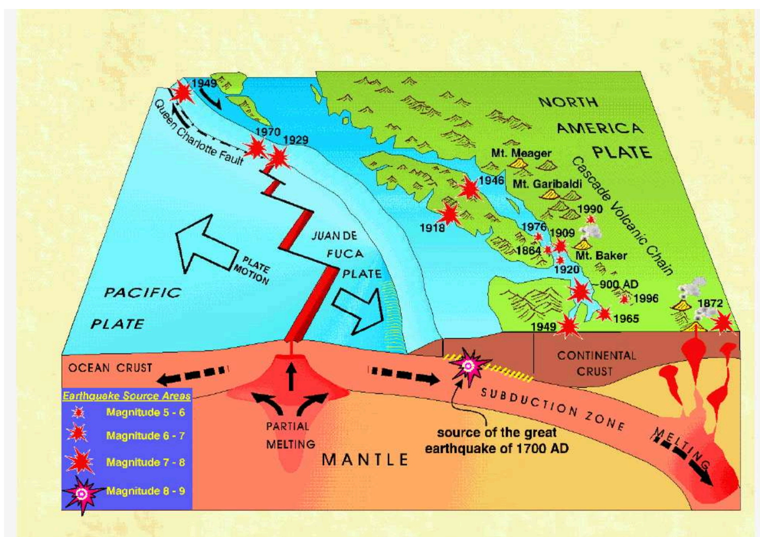

Figure 6.2: Tectonic setting of south-western British Columbia showing the oceanic Juan de Fuca plate is subducting beneath the continental crust of North America plate along the Cascadia subduction zone (Natural Resources Canada, 2012)

tions to hazard at small periods, whereas at long periods, the potential for great megathrust earthquakes on the Cascadia subduction zone is the main concern. A major earthquake associated with either one of these sources could have devastating effects in Vancouver.

The hazard contributions from each scenario is reflected in a calculation of the Uniform Hazard Spectrum (UHS), which is referred as a target response spectrum in the National Building Code of Canada (NBCC, 1995, 2005, 2010). The UHS envelopes the maximum response of a single-degree-of-freedom oscillator with 5% damping and provides the design response spectrum corresponding to different periods.

The probability level used in 1995 edition of the National Building Code of Canada (NBCC, 1995) was 0.0021 per year and had a 10% chance of exceedence in 50 years (a 475-year return period earthquake), whereas the recent versions of the code (NBCC, 2005, 2010) provide the 2% chance of exceedence in 50 years equivalent to an annual probability of 0.000404 (a 2475-year return period earthquake). In computation of the 2% in 50 years robust probabilistic hazard values for Vancouver, the hazard due to shallow crustal and deeper subcrustal earthquakes and also a great earthquake along the Cascadia subduction zone are included. According to NBCC (2010), for the western Canadian cities the crustal and subcrustal data has been treated probabilistically and subduction data deterministically (Adams and Halchuk, 2003).

The corresponding hazard values for different cities (e.g., Vancouver) are reported in the NBCC (2010). The proposed design UHS also depends on the location of the site and its local soil condition (Finn and Wightman, 2003). Based on the NBCC (2010), soil condition is classified into different categories according to the time-averaged shear wave velocity in the top 30 m of the soil deposit (V_{s30}). The site conditions range from class A: hard rock ($V_{s30} > 1500\ m/s$), Class B: rock ($760\ m/s < V_{s30} < 1500\ m/s$), class C: very dense soil and soft rock ($360\ m/s < V_{s30} < 760\ m/s$), class D: stiff soil ($180\ m/s < V_{s30} < 360\ m/s$), and Class E: soft soil ($V_{s30} < 180\ m/s$).

The rate of occurrences of crustal, subcrustal and subduction earthquakes are different and so are their effects on seismic hazard. Therefore, for nonlinear dynamic time history analyses of basement walls, it is necessary to explore ground motions representative of different types of expected earthquake motions, and match each record to the NBCC (2010) target UHS over the period range of interest. There are number of acceptable methods for obtaining UHS-compatible time histories which will be outlined in the next section.

6.3 Ground motion scaling methods

Scaling/matching ground motions plays an important role in engineering performance design and enables determination of the structural response with higher confidence and through fewer number of analyses compare to using unscaled accelerograms. The premise to verify is to modify a time history so that its response spectrum matches within a prescribed tolerance level the target response spectrum (Finn, 2000). Reducing the dispersion in the elastic response spectra of the input ground motion reduces the variability in the output of nonlinear response history analyses.

For conducting nonlinear dynamic analyses of basement walls, several methods of scaling/matching the input ground motions are chosen to modify accelerograms to become representative of the site-specific hazard level (e.g., the uniform hazard spectrum) at the site. Scaling the ground motions is necessary in evaluating the performance of the basement walls in order to expose the structure to the level of ground motion corresponds to the probability of exceedance adopted in the NBCC (2010).

As mentioned previously in Chapter 3, there are two main options for scaling/-matching the ground motions:

(1) adding wavelets in the time domain and modifying the spectral shape of the response spectrum to match the target demand, which is known as spectral matching; and

(2) linear scaling of accelerograms without affecting frequency content or phasing by minimizing the difference between a target spectrum and the spectrum of a scaled ground motion, either at a single period or over a period range.

The spectral matching method was used in Chapter 3 to modify the selected 14 crustal earthquake time histories to become compatible with the NBCC (2010) hazard level in Vancouver. This method is popular in engineering practice, because it reduces the variance of the structural responses and provides a platform to estimate the mean response with fewer numbers of analyses (Carballo and Cornell, 2000; Seifried and Baker, 2014); thereby the computational cost is significantly reduced. A gross rule of thumb is that one spectrum compatible time series is worth three scaled time series in terms of the variability of the mean of the nonlinear response of structures (Al Atik and Abrahamson, 2010; Bazzurro and Luco, 2006). For example, if it takes engineering analyses of 12 scaled time series to get 20% accuracy in the mean structural response, then it takes only analyses of four spectrum compatible time series to get the same accuracy. In addition, the spectral matching technique has an advantage of meeting the target spectrum requirements adequately. In this method, the frequency content and phasing of actual record is manipulated to match a smooth target spectrum (Bolt and Gregor, 1993; Carballo and Cornell, 2000; Hancock et al., 2006; Heo et al., 2010; Lilhanand and Tseng, 1989). The only argument can be made is that the spectral matching process artificially smooth out the natural peaks and troughs of the original record response spectra and may obscure somewhat the potential variability of the response (Atkinson, 2009; Luco and Cornell, 2007).

On the other hand, in linear scaling methods the whole accelerogram time history is multiplied by a scalar coefficient to become more compatible with the target spectrum. In these methods the deviation from the target is measured by various parameters. To keep the records realistic, it is recommended to scale the records with required scaling factors in the range from 0.5 to 2.0 (approximately). Although there will be some occasions later on in this chapter that due to the absence of the recordings with the desired characteristics, higher values of scaling factors are used. An additional ground motion criteria proposed by Pina et al. (2010) is considered in this study in scaling process of ground motions as an average of acceleration response spectrum of a selected suite of ground motion must be above the 90% the target spectrum within the period range of interest.

Five ground motion scaling methods are investigated as follows:

6.3.1 PGA scaling

In this method, the selected record is multiplied by a scalar coefficient in a way that the PGA of the scaled record becomes equal to the PGA of the target spectrum, which based on the NBCC (2010) for Vancouver is 0.46 g. The drawback of this method is the fact that the frequency content and spectral shape of the accelerogram over a range of periods are not taken into consideration. Even though all scaled ground motions have the same PGA, their response spectrum fall in a very wide range through-out the different periods and produce inaccurate estimates with large dispersion of an engineering demand parameter (Miranda, 1993; Nau and Hall, 1984; Shome and Cornell, 1998; Vidic et al., 1994).

6.3.2 Sa(T_1) scaling

Accounting for the vibration properties of the structure led to an improved method of scaling based on an elastic spectral acceleration at the fundamental vibration period of the structure, T_1, which provides improved results for structures whose response are dominated by their first-mode (Shome et al., 1998). The objective of this method is to use a multiplier to scale the records so that the spectral acceleration at a fundamental period of the system, also called as the spectral intensity, $Sa(T_1)$, matches the target spectral acceleration at that period, i.e.,

$$f = \frac{Sa^{target}(T_1)}{Sa^{record}(T_1)} \tag{6.1}$$

This method provides a set of scaled time histories, whose spectral acceleration of all are equal to the target spectrum at the fundamental period of the system. Shome and Cornell (1998) demonstrated that in the cases of SDOF and MDOF structures, the seismic demand estimates are strongly correlated with the linear-elastic spectral response acceleration at the fundamental period of the structure and the scatter in the demand can be significantly reduced.

One of the main concerns in using this methodology in the complex basement wall model is losing accuracy and efficiency at higher modes of vibration and far into the inelastic range due to yielding and nonlinear behavior, which elongates the vibration periods (Kurama and Farrow, 2003; Mehanny and Deierlein, 1999). Moreover, scaling a record just based on one specific period is not a good indicator of the strength and frequency content of the ground motion and the first-mode period does not necessarily dictate the response of the system (Huang et al., 2011).

6.3.3 ASCE scaling

The procedures and criteria in International Building Code (IBC, 2009) and California Building Code (CBC, 2010) for selection and scaling ground motions in nonlinear response history analyses of structures are based on the recommendation of the American Society of Civil Engineering (ASCE/SEI 7-05, 2005; ASCE/SEI 7-10, 2010). It recommends intensity-based scaling of ground motion records such that the average value of the 5% damped response spectra for the suites of scaled motions is not less than the design response spectrum over the period range of $0.2T_1$ to $1.5T_1$, where T_1 is the first mode natural vibration period of the system. The upper limit on the period range of $1.5T_1$ is intended to account for period elongation due to inelastic action, and $0.2T_1$ is intended to capture higher modes of response.

The ASCE scaling procedure does not insure a unique scaling factor for each record. Obviously, various combinations of scaling factors can be defined to insure that the average spectrum of the scaled records remains above the design spectrum. In this study the procedure recommended by Reyes and Kalkan (2011) has been used for scaling the suite of selected records in order to utilize a minimum scaling factor closest to unity for each record.

6.3.4 SIa scaling

In this method, the multiplier is applied to each accelerogram in a way that the area under the response spectrum becomes equal to the integration of spectral acceleration in the period range of interest $0.2T_1$ to $1.5T_1$ (Michaud and Leger, 2014).

6.3.5 MSE scaling

In this method a quantitative measure of the overall fit of the record to a target spectrum is the Mean Squared Error (MSE) of the difference between the spectral accelerations of the record and the target spectrum, computed using the logarithms of the spectral acceleration. For this purpose a period range of interest is subdivided into a large number of points equally-spaced and the target and the record response spectra are interpolated to provide spectral acceleration at each period, respectively. The MSE is then computed using the following equation over the selected period range as:

$$MSE = \frac{\sum w(T_i)\{ln[Sa^{target}(T_i)] - ln[f \times Sa^{record}(T_i)]\}^2}{\sum w(T_i)} \quad (6.2)$$

In this equation, $Sa^{target}(T_i)$ is the spectral acceleration of the target spectrum, $Sa^{record}(T_i)$ is the spectral acceleration of the scaled ground motion, and $w(T_i)$ is a weight function that allows the user to assign relative weights to different periods over the period range of interest. In this study an equal weight is assigned to all periods (i.e., $w(T_i) = 1$). Parameter f is a linear scaling factor applied to the entire response spectrum of the record in order to minimize MSE between the target spectrum and the response spectrum of the record.

The U.S. Army Corps of Engineers (USACE) (2009) recommends a criteria for the fit of an average spectrum of the scaled time histories to the design spectrum in seismic analyses, design, and evaluation of civil works structures. Based on this recommendation the mean spectrum should not be below the design response spectrum by more than 10% at any spectral period over the period range of interest and the average of the ratios of the mean spectrum to the design spectrum over the same period range should not be less than 1.0.

6.4 Selection of ground motion records

Commonly, a suite of input motions is used to capture the inherent motion-to-motion variability of the earthquake ground motions. A suite of earthquake records is required due to the fact that unique characteristics of each input motion influence the induced dynamic response differently. The selection procedure considers the important characteristics of the ground motions (magnitude, distance, site condition and etc.) consistent with the hazard conditions. Selecting records by taking into an account the hazard demand for a given site, increases accuracy in determining the mean value of the structural response by reducing the dispersion of the results.

As stated by Finn (2000), determining appropriate scenario earthquakes for selecting appropriate recorded ground motions for nonlinear analyses is one of the difficulties in design based on spectra. The probabilistic response spectrum represents the aggregated contribution of a range of earthquake magnitudes on different faults and seismic zones at various distances from the site, and also includes the effect of random variability for a given magnitude and distance. Appropriate earthquakes can be determined using a procedure proposed by McGuire (1995), which deaggregates the contributions to the spectrum by magnitude and distance. As outlined previously in Chapter 3, Pina et al. (2010) determined appropriate ranges of magnitudes and (closest) source-to-site distance by de-aggregating the seismic hazard in Vancouver and selected the values that contribute most strongly to the hazard for different earthquake scenarios. In addition, in this study the reference soil classification, site class C, adopted by the NBCC (2010) is selected as a site condition, which is consistent with the site condition at the depth of earthquake motion application in the FLAC model.

In this study, four ground motion ensembles representative of the dominant seismic mechanisms in the Greater Vancouver region are investigated. Differences amongst these ensembles can be observed in terms of spectral shapes and frequency content. Each ensembles affect the structure in a different way and therefore, the value of the engineering demand parameter (e.g. drift ratio) substantially varies amongst these types of earthquakes.

The first and the second ensembles each includes a total of 14 records representative of crustal and subcrustal seismic events, respectively. All these accelerograms are linearly scaled to the proposed NBCC (2010) uniform hazard spectrum using different methods of scaling outlined in Section 6.3.

The third ensemble comprises a total of 14 ground motions representative of the Cascadia subduction events. All these records are scaled to the corresponding hazard values of Cascadia subduction earthquake scenario derived from the deterministic (Cascadia) model for a probability of 2% in 50 years presented in Adams and Halchuk (2003) and are representative of the NBCC (2010) hazard level.

The forth ensemble covers 14 near-fault ground motions. These are assumed to occur within a distance of 20 km from the causative fault and contain distinct pulses either in the acceleration, velocity or displacement time histories. Scaling is also necessary for these records in order to expose the structures to the level of ground motion that corresponds to the probability of exceedance adopted by the NBCC (2010).

The records in the Pacific Earthquake Engineering Research Center (PEER) ground motion database (Chiou et al., 2008) have been processed for instrument correction, bandpass filtering (removal of unwanted noise), and baseline correction, as described in Darragh et al. (2004). However, time histories selected from other databases require to be checked for their need to further data processing before ground motion scaling. Each of the selected ground motions is baseline corrected with a linear function and filtered with a bandpass Butterworth filter with cut-off frequencies of 0.1 Hz and 25 Hz, using the computer program SeismoSignal (Seismosoft, 2009*b*). Once it processed, the 5% damped acceleration response spectrum is obtained and used in linear scaling process of ground motions.

6.4.1 Crustal earthquakes

In south-western British Columbia region most crustal earthquakes occur within approximately 20 to 30 km of the surface. These crustal earthquakes usually have a magnitude less than 7.5 and a typical duration of less than one minute.

Fourteen selected crustal ground motions presented in Table 3.1 in Chapter 3 are linearly scaled in this section. Different methods of linear scaling outlined in Section 6.3 are conducted to modify the time histories to become compatible with the target demand. Each selected record is scaled using a constant factor based on different methods of linear scaling. The scaling factors are reported in Table 6.1.

Figures 6.3 to 6.7 illustrate the acceleration time histories of the 14 selected crustal ground motions, linearly scaled to the NBCC (2010) UHS for Vancouver using different linear scaling techniques.

Figure 6.8 shows the 5% damped acceleration response spectrum of each ground motion linearly scaled to the NBCC (2010) UHS for Vancouver, and their corresponding mean spectrum with respect to the target spectrum. The response spectrum of the spectrally matched ground motions is also included for comparison.

Table 6.1: Scaling factors calculated for the selected crustal ground motions using different linear scaling methods.

No.	Event Name	Station	Direction	PGA scaling	$Sa(T_1)$ scaling	ASCE scaling	SIa scaling	MSE scaling
1	Friuli- Italy	Tolmezzo	FN	1.19	0.90	1.07	0.98	1.0
2			FP	1.40	1.05	0.95	0.97	0.99
3	Tabas- Iran	Dayhook	FN	1.46	1.41	1.40	1.14	1.18
4			FP	1.28	0.62	1.25	0.94	0.97
5	New Zealand	Matahina Dam	FN	1.52	0.93	1.61	1.17	1.19
6			FP	1.79	0.82	1.47	1.27	1.31
7	Loma Prieta	Coyote Lake Dam (SW Abut)	FN	2.88	1.83	1.99	2.06	1.99
8			FP	1.02	0.95	0.94	0.94	0.96
9		Centerville Beach Naval Fac	FN	1.74	1.15	1.86	1.26	1.33
10			FP	1.99	1.70	1.63	1.40	1.42
11	Northridge	LA - UCLA Grounds	FN	1.41	1.72	1.76	1.42	1.47
12			FP	1.06	1.63	1.50	1.04	1.10
13	Hector Mine	Hector	FN	1.27	0.97	0.98	0.90	0.95
14			FP	1.59	1.83	1.49	1.36	1.43

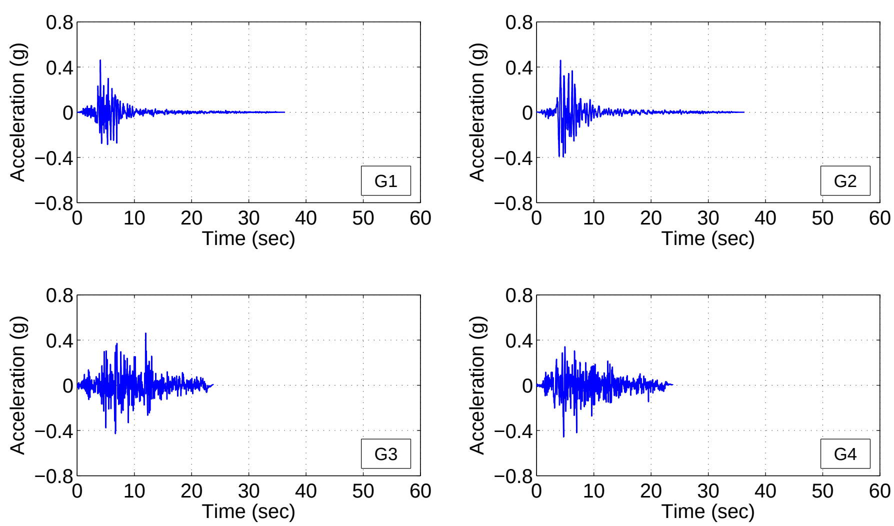

Figure 6.3: Continued.

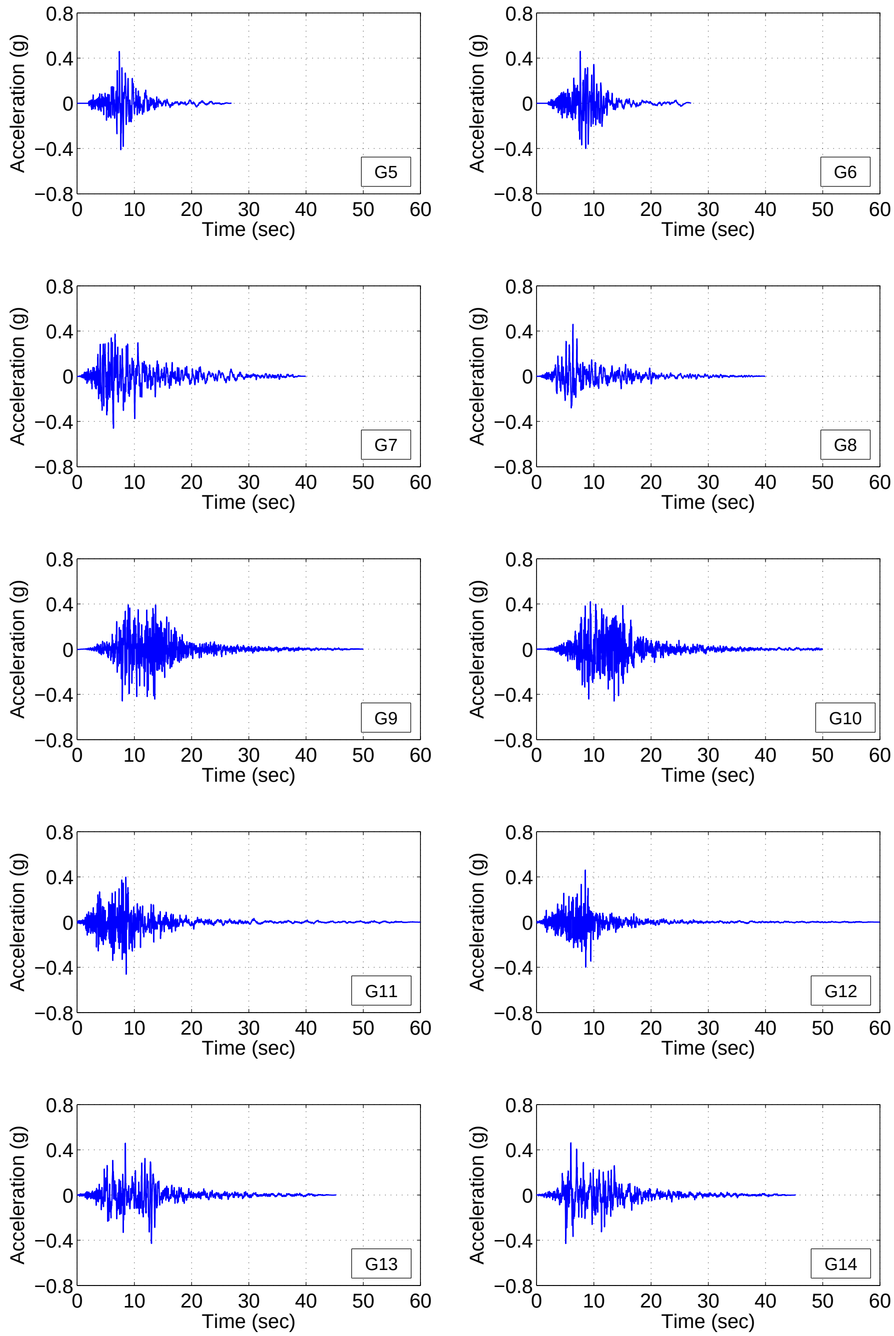

Figure 6.3: Acceleration time histories of the selected 14 crustal ground motions linearly scaled to the NBCC (2010) UHS of Vancouver using PGA scaling method.

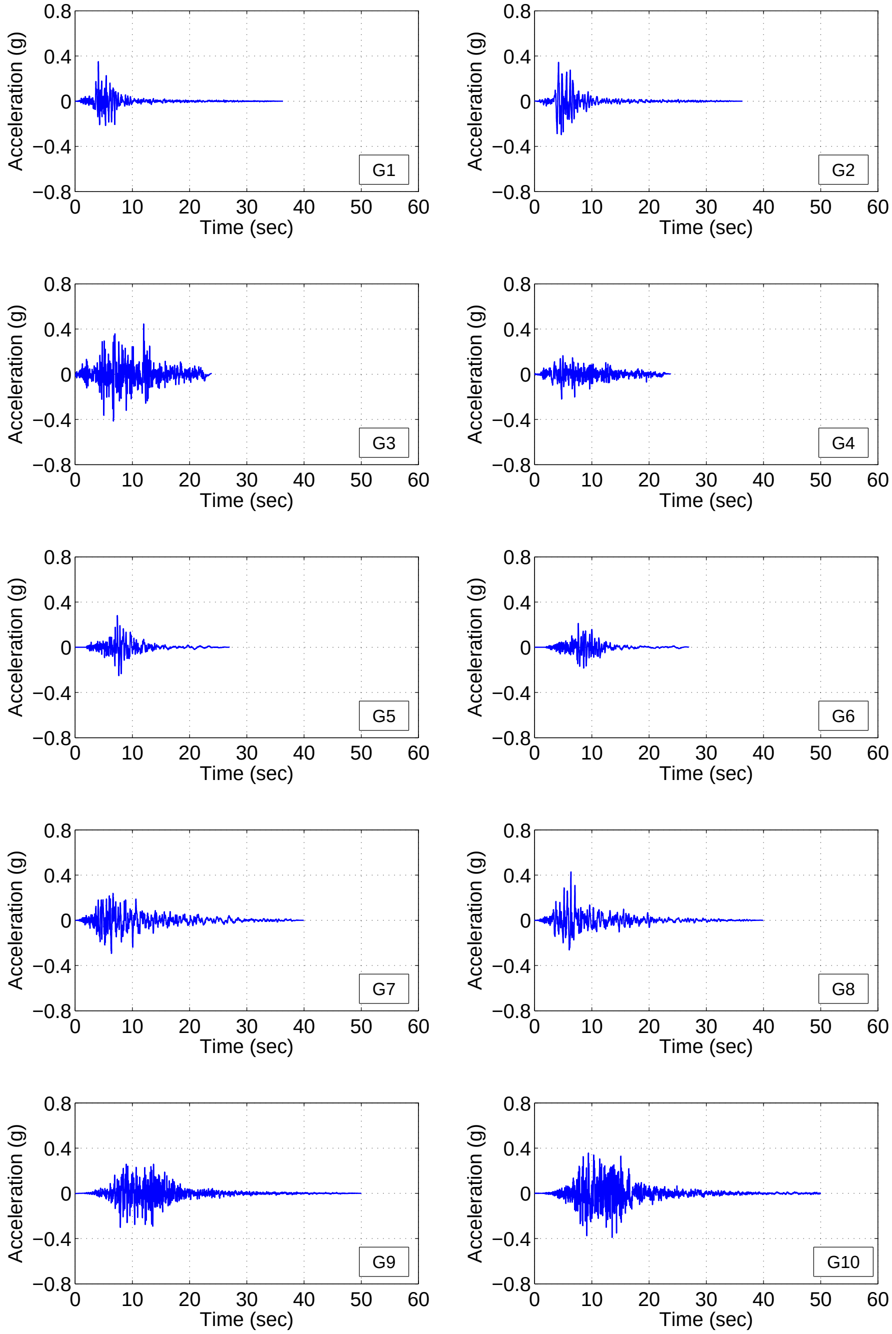

Figure 6.4: Continued.

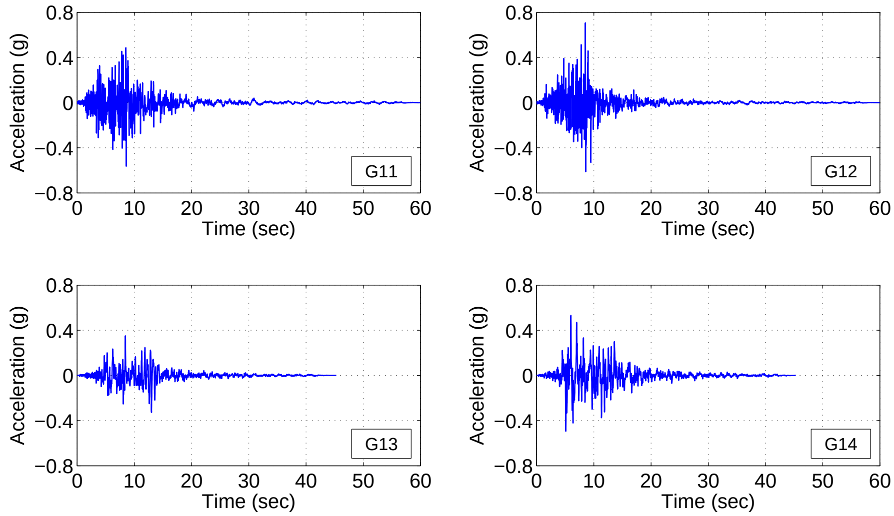

Figure 6.4: Acceleration time histories of the selected 14 crustal ground motions linearly scaled to the NBCC (2010) UHS of Vancouver using $Sa(T_1)$ scaling method.

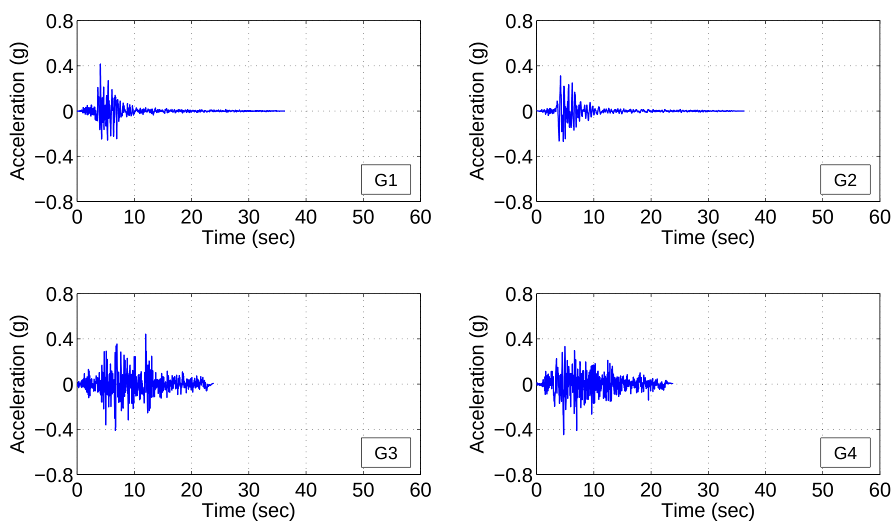

Figure 6.5: Continued.

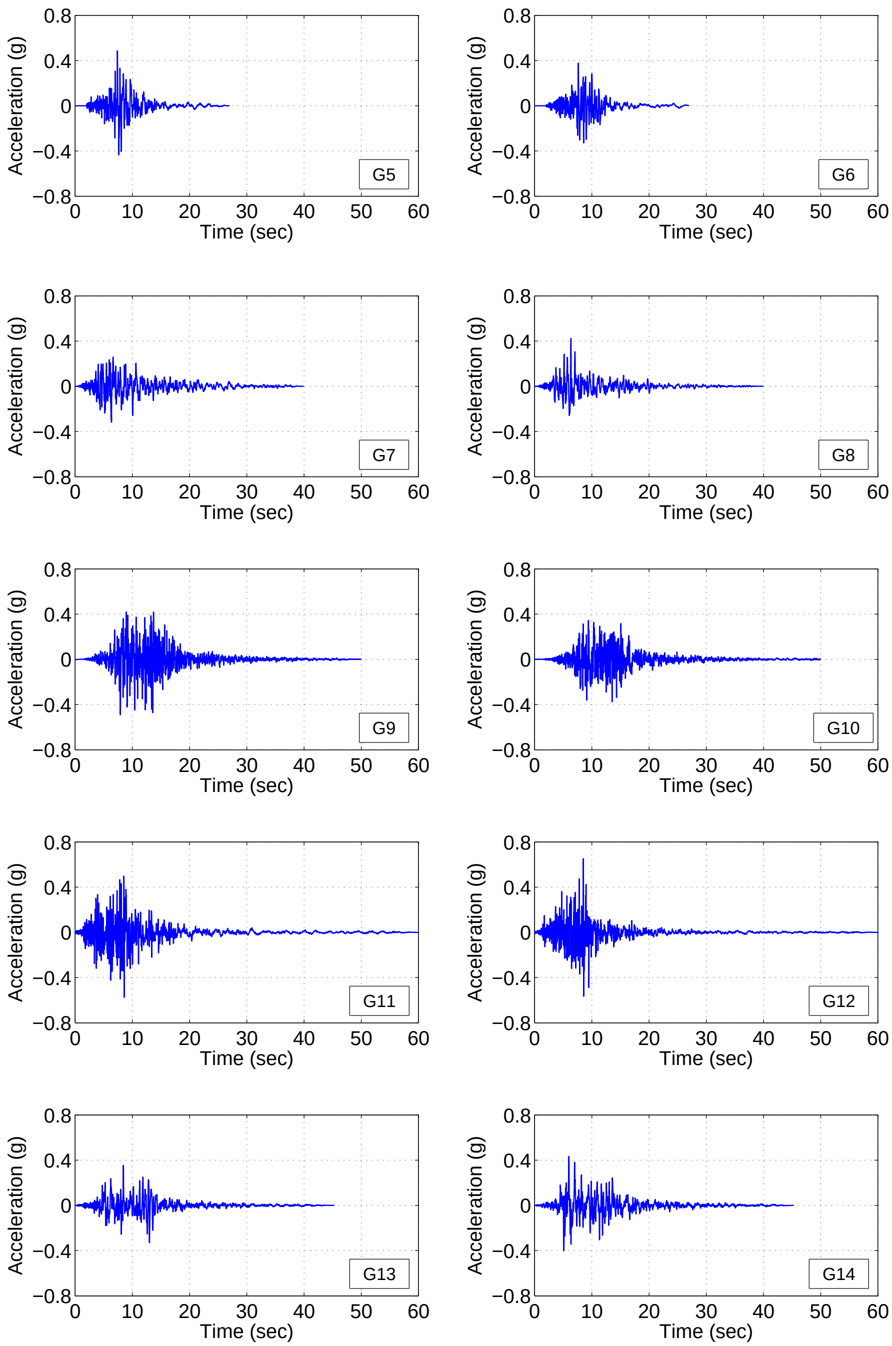

Figure 6.5: Acceleration time histories of the selected 14 crustal ground motions linearly scaled to the NBCC (2010) UHS of Vancouver using ASCE scaling method.

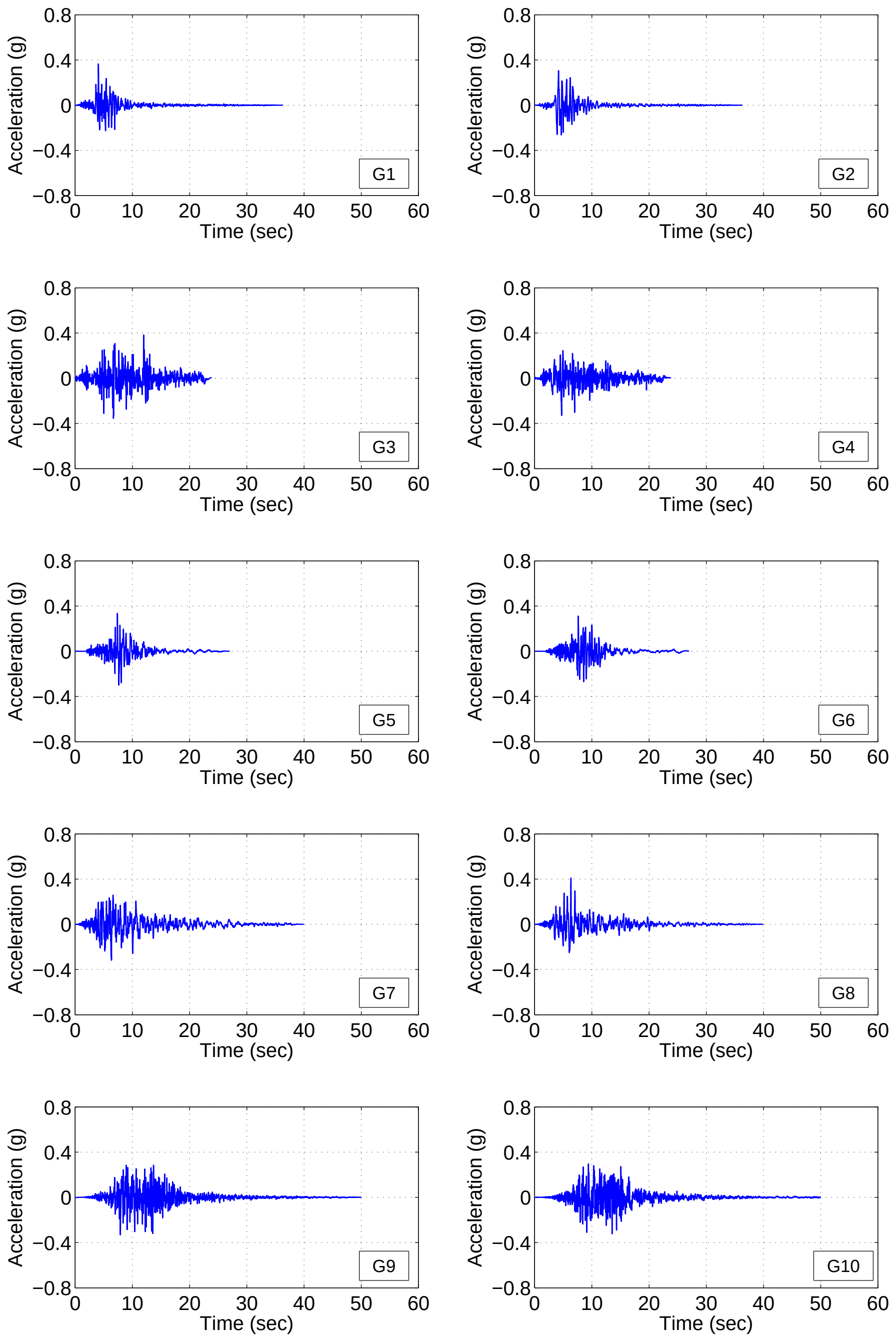

Figure 6.6: Continued.

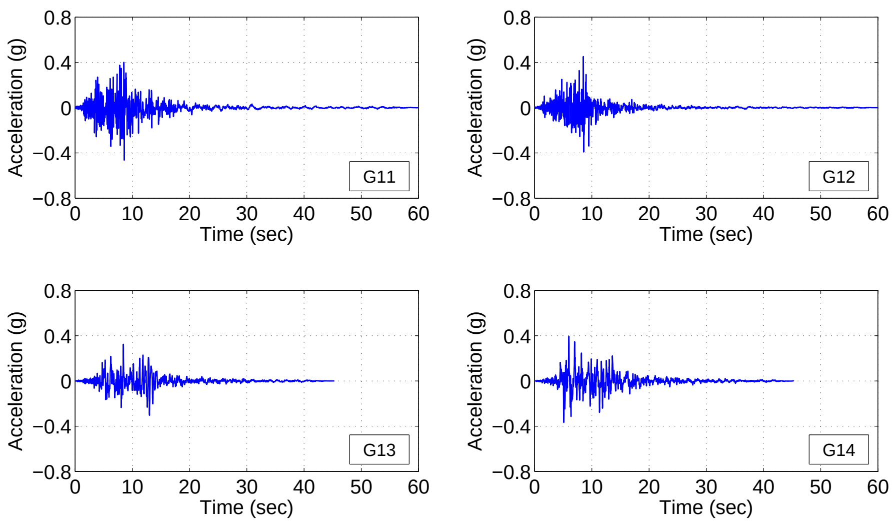

Figure 6.6: Acceleration time histories of the selected 14 crustal ground motions linearly scaled to the NBCC (2010) UHS of Vancouver using SIa scaling method.

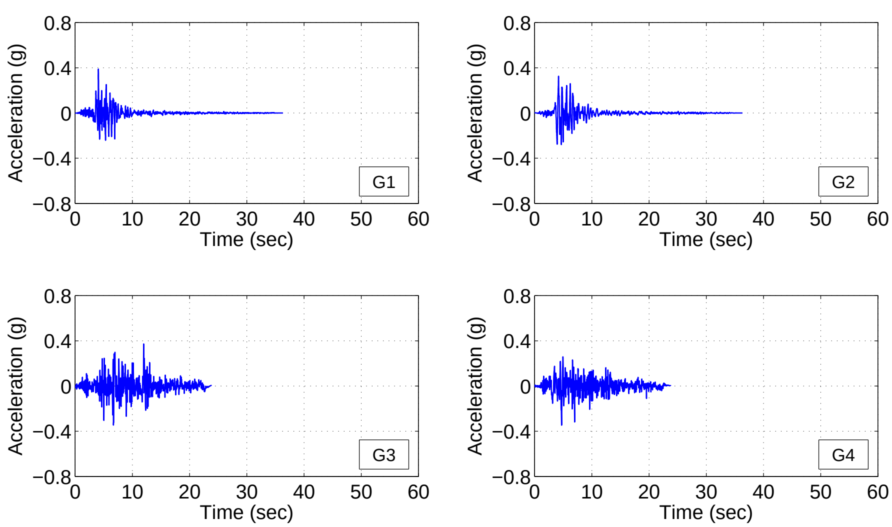

Figure 6.7: Continued.

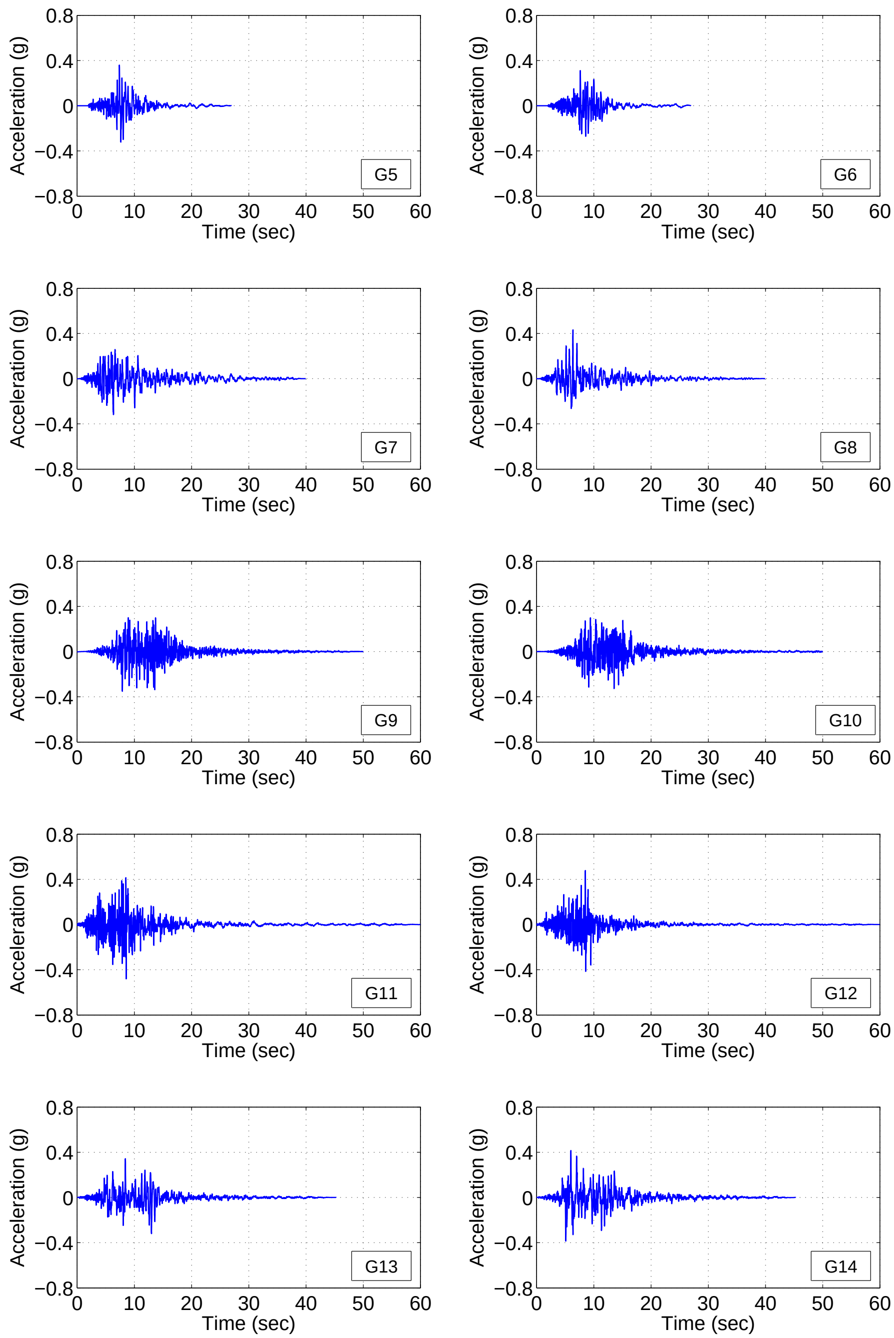

Figure 6.7: Acceleration time histories of the selected 14 crustal ground motions linearly scaled to the NBCC (2010) UHS of Vancouver using MSE scaling method.

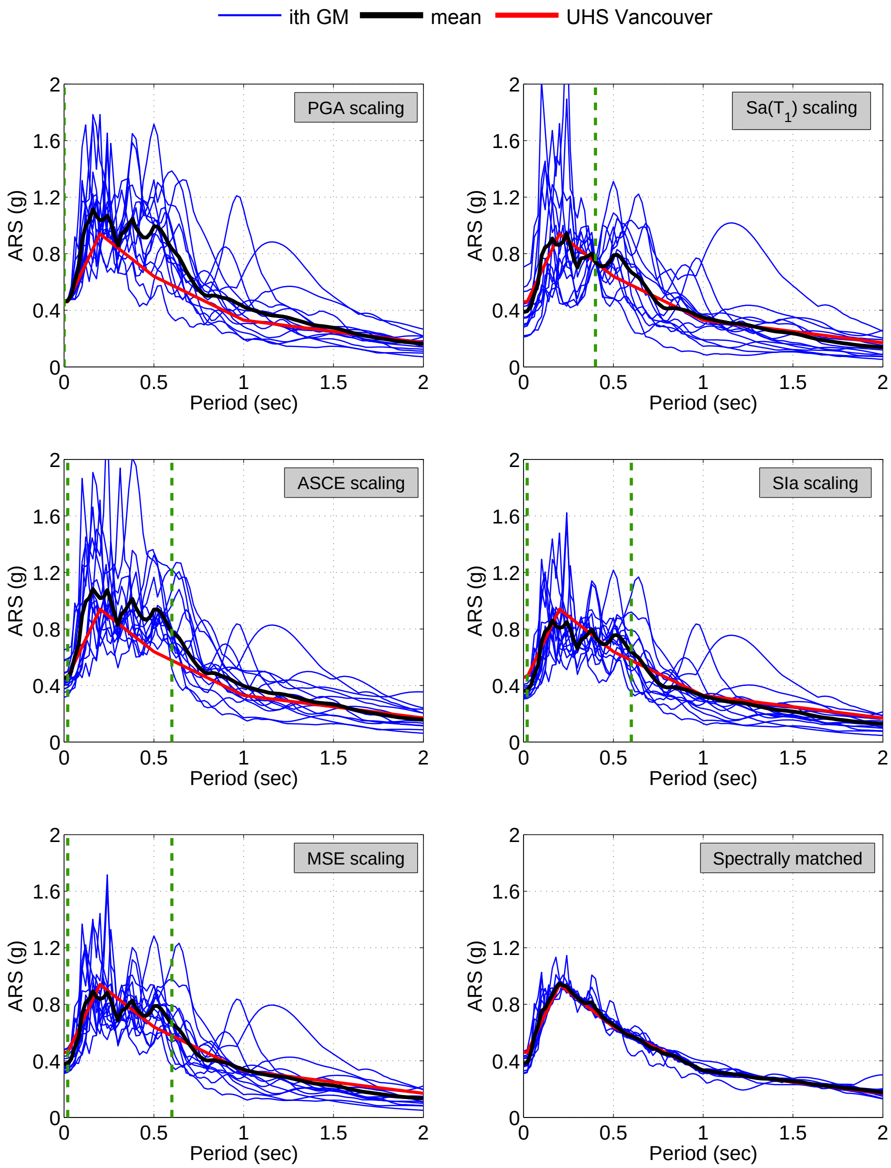

Figure 6.8: The 5% damped acceleration response spectra of the selected 14 crustal ground motions and their corresponding mean response using different methods of scaling/matching with respect to the target NBCC (2010) UHS of Vancouver. Dashed-green lines show the single period or the period range at which the motions are scaled.

6.4.2 Subcrustal earthquakes

Deeper subcrustal earthquakes typically occur between 30 to 45 km depth. Like the crustal earthquakes, these motions usually have a magnitude less than 7.5 with shaking duration of less than a minute.

Searching for the subcrustal records are conducted using S^2GM (accessed on March 2015), which is a web-based tool used to facilitate the selection, scaling, and downloading of ground motion time history records and data. Subcrustal earthquakes are mostly downloaded from the COSMOS database (Archuleta et al., 2006). Japanese earthquakes are directly downloaded from the K-NET (Kinoshita, 1998) and KiK-net (Aoi et al., 2000) databases.

The criteria for selection of the subcrustal ground motions are set as the magnitude range of 6.5 to 7.5, with the closest distance of 30 to150 km of the causative fault plane from the earthquake sites. Also the reference site class C is adopted as the fundamental site condition. Selection of the candidate records are conducted based on the best linearly scaled motions to the UHS of Vancouver in the period range of 0.02 to 0.8 sec, which covers slightly higher range than $0.2T_1$ to $1.5T_1$. Based on aforementioned criteria, the list of the selected 14 subcrustal ground motions are presented in Table 6.2. Both components of E-W and N-S of each ground motion are used in this study.

Table 6.2: List of the selected subcrustal ground motions.

No.	Event Name	Year	Station	Magnitude	V_{s30} (m/s)	Direction	SF
1	Miyagi Oki, Japan	2005	MYG016	7.2	580.0	E-W	2.64
2						N-S	2.78
3			MY6014		706.2	E-W	2.22
4						N-S	2.66
5			FKS010		585.9	E-W	1.56
6						N-S	1.63
7			MYG013		535.5	E-W	1.16
8						N-S	1.63
9			IWT011		565.3	E-W	2.41
10						N-S	1.95
11	Nisqually, WA	2001	Olympia Residence	6.8	-	E-W	2.88
12						N-S	3.09
13	Michoacan, Mexico	1997	Villita Margen Derecha (VILE)	7.3	-	E-W	3.10
14						N-S	3.84

Among five linear scaling methods, the MSE method which is the commonly

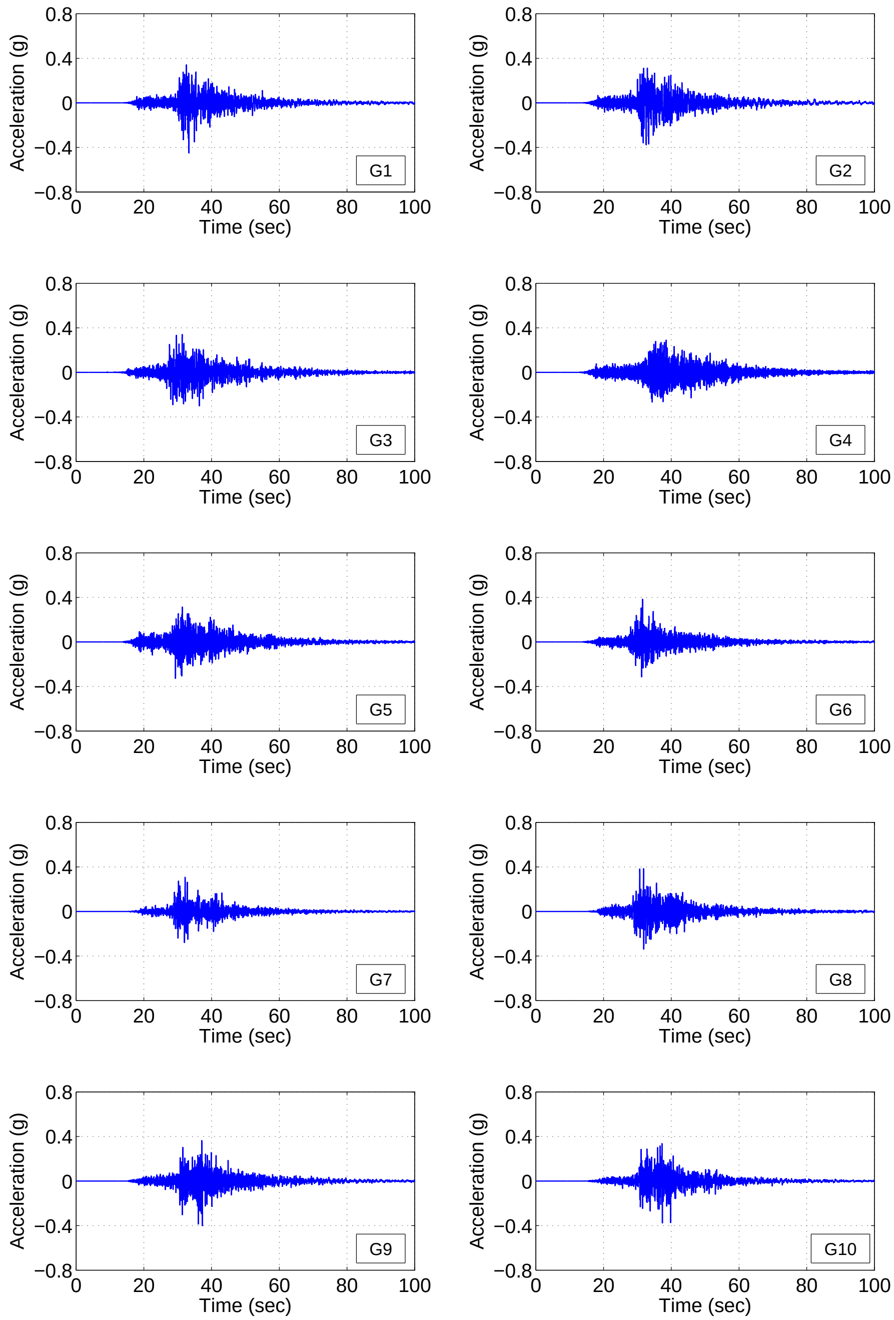

Figure 6.9: Continued.

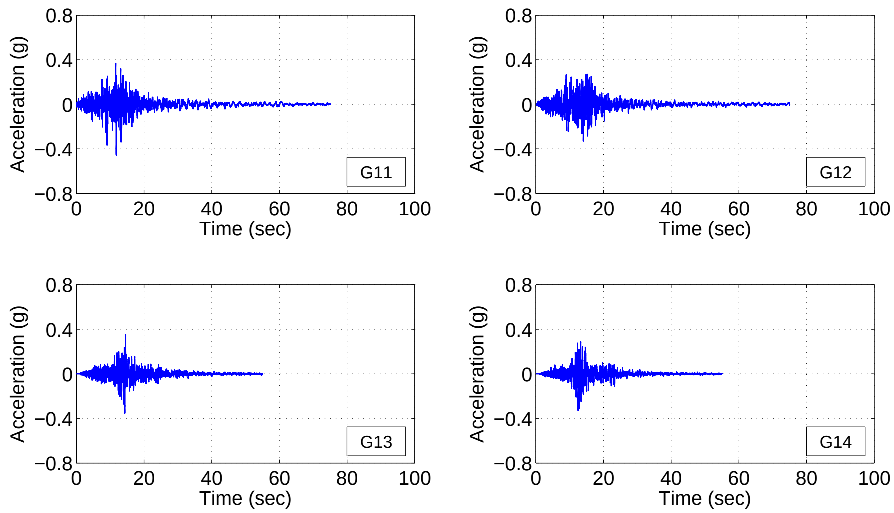

Figure 6.9: Acceleration time histories of the selected 14 subcrustal ground motions linearly scaled to the NBCC (2010) UHS of Vancouver using MSE scaling method.

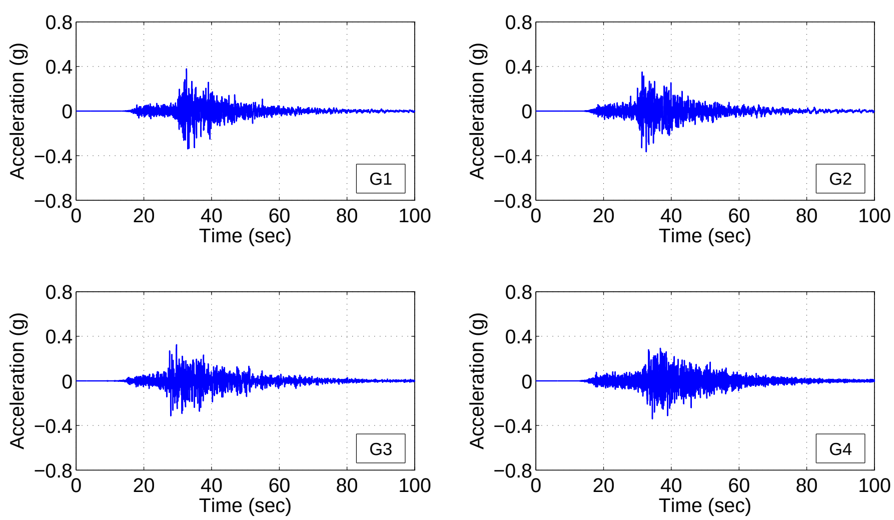

Figure 6.10: Continued.

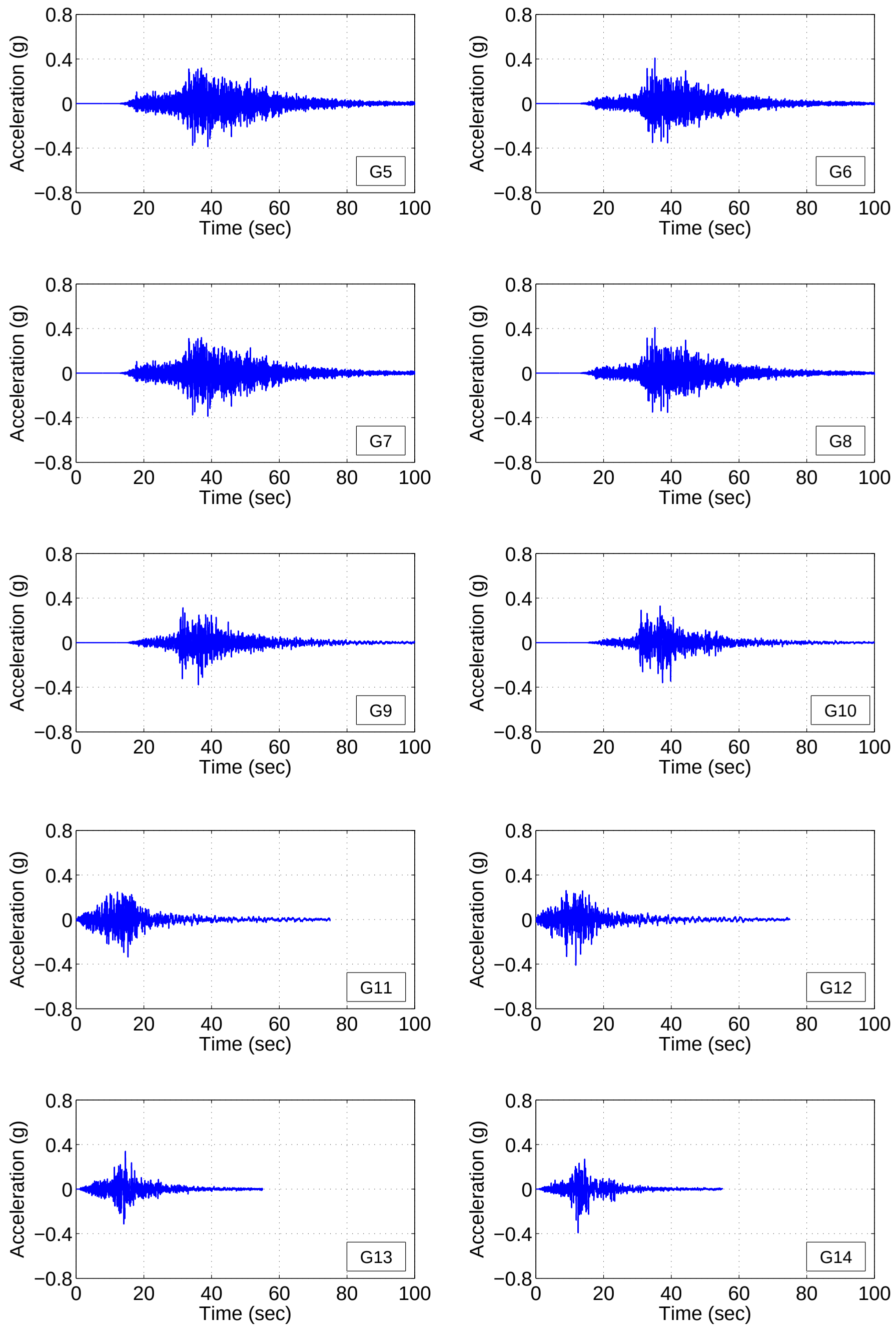

Figure 6.10: Acceleration time histories of the selected 14 subcrustal ground motions spectrally matched to the NBCC (2010) UHS of Vancouver.

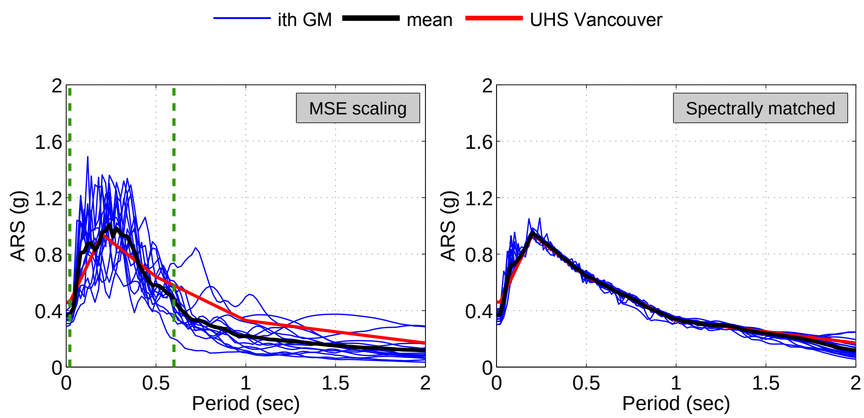

Figure 6.11: The 5% damped acceleration spectra of the selected 14 subcrustal ground motions and the corresponding mean response using MSE linear scaling and spectral matching methods with respect to the target NBCC (2010) UHS of Vancouver. Dashed-green lines show the period range at which the motions are scaled.

used method in practice for scaling the earthquake records and provides a reseanable match to the target UHS (Figure 6.8), is used to linearly scaled the subcrustal ground motions to the UHS of Vancouver. In addition the motions are spectrally matched to the target spectrum in order to evaluate the mean value of the structural response and provide the basis for comparison the seismic performance of the basement walls. The calculated scaling factors from MSE method are reported in Table 6.2.

6.4.3 Subduction earthquakes

The largest earthquakes recorded around the world are subduction interface earthquakes, sometimes called megathrust events. These events are typically greater than M8+ and are associated with shaking in excess of two or three minutes.

Searching criteria for the subduction ground motions is set as the magnitude range of 8.0 to 9.0, with the closest distance of 30 to 150 km of the causative fault from the earthquake sites. Site class C soil is adopted for selecting subduction motion records. Also the spectral shape of the records are compared with the hazard values corresponding to the subduction events presented in NBCC (2010).

Seismic hazard values intended for the NBCC (2010) design data for subduction scenario in Vancouver proposed by Adams and Halchuk (2003) are illustrated in Figure 6.12. These values are determined for firm ground (site class C - average shear wave velocity of 360 to 760 m/s) with the probability of an exceedence of 2% in 50 years. In this figure the solid line corresponds to the hazard values of Cascadia subduction earthquake scenario derived from the deterministic (Cascadia) model for a probability of 2% in 50 years; whereas the dashed line represents the spectral values corresponds to the median spectral ordinates obtained from the probabilistic model for crustal and subcrustal events that has been used so far as the target spectrum in this study.

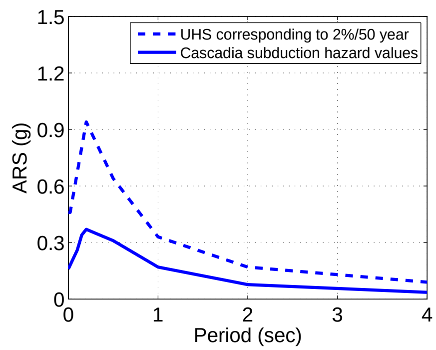

Figure 6.12: The 2% in 50 year robust probabilistic hazard design values from the NBCC (2010) in comparison with the hazard values from deterministic Cascadia subduction earthquake scenario for Vancouver.

Table 6.3 presents the selected Cascadia subduction events and the magnitude and the hypocentral distance of each record. Same as subcrustal ground motions, S^2GM (accessed on March 2015) search engine is used for selecting subduction earthquakes records.

Scaling is also necessary for subduction ground motions in order to expose the structures to the level of ground motion that corresponds to the seismic demand adopted by the NBCC (2010) for Vancouver. All the selected subduction ground motions are linearly scaled to match the proposed design spectra for Cascadia subduction event over the period range of 0.02 to 0.8 sec ($\approx 0.2T_1$ to $1.5T_1$) using the scaling factors presented in Table 6.3.

The 5% damped elastic response spectra of the scaled Cascadia subduction

Table 6.3: List of the selected subduction ground motions.

No.	Event Name	Year	Station	Magnitude	Closest distance (m)	V_{s30} (m/s)	SF
1	Tokachi-Oki, Japan	2003	Noya (HKD107)	8.0	126.4		1.65
2			Obihiro (HKD095)		132.2		1.03
3			Futamata (HKD087)		148.7		0.84
4			Tsurui (HKD083)		163.4		0.97
5	Michoacan, Mexico	1985	Caleta De Campos (CALE)	8.1	38.3		0.91
6			Villita (VILE)		47.8		1.29
7			La Union (UNIO)		83.9		0.75
8			Zihuatanejo (AZIH)		132.6		1.28
9	Hokkaido, Japan	1952	HKD081	8.1	148.4	410	1.82
10			HKD093		123.3	512	1.42
11			HKD094		110.8	381	1.49
12	Tohoku, Japan	2011	FKS015	9.0	95.3	706	0.74
13			TCG015		137.7	464	0.85
14			YMT007		148.9	371	0.83

ground motions with respect to the NBCC (2010) subduction hazard values are shown in Figure 6.13. Unlike crustal and subcrustal earthquake records which have a clear short-period spectral content, in subduction motions the major contributions to hazard is focused on large periods. Acceleration time histories of the linearly scaled subduction ground motion are presented in Figure 6.14.

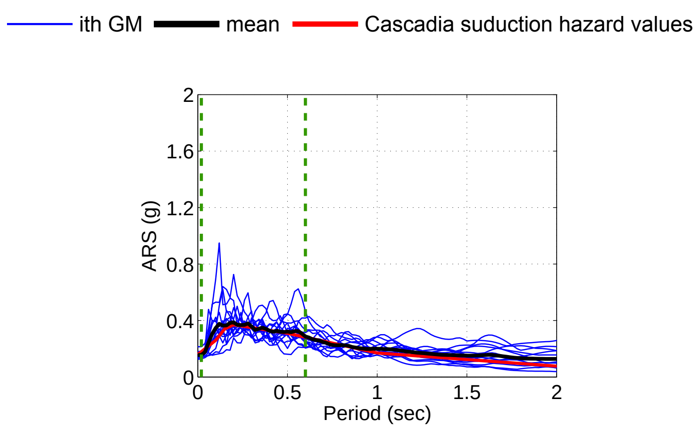

Figure 6.13: The 5% damped acceleration response spectra of 14 subduction records scaled to hazard values for Cascadia subduction earthquake scenario proposed by the NBCC (2010) for Vancouver. Dashed-green lines show the period range at which the motions are scaled.

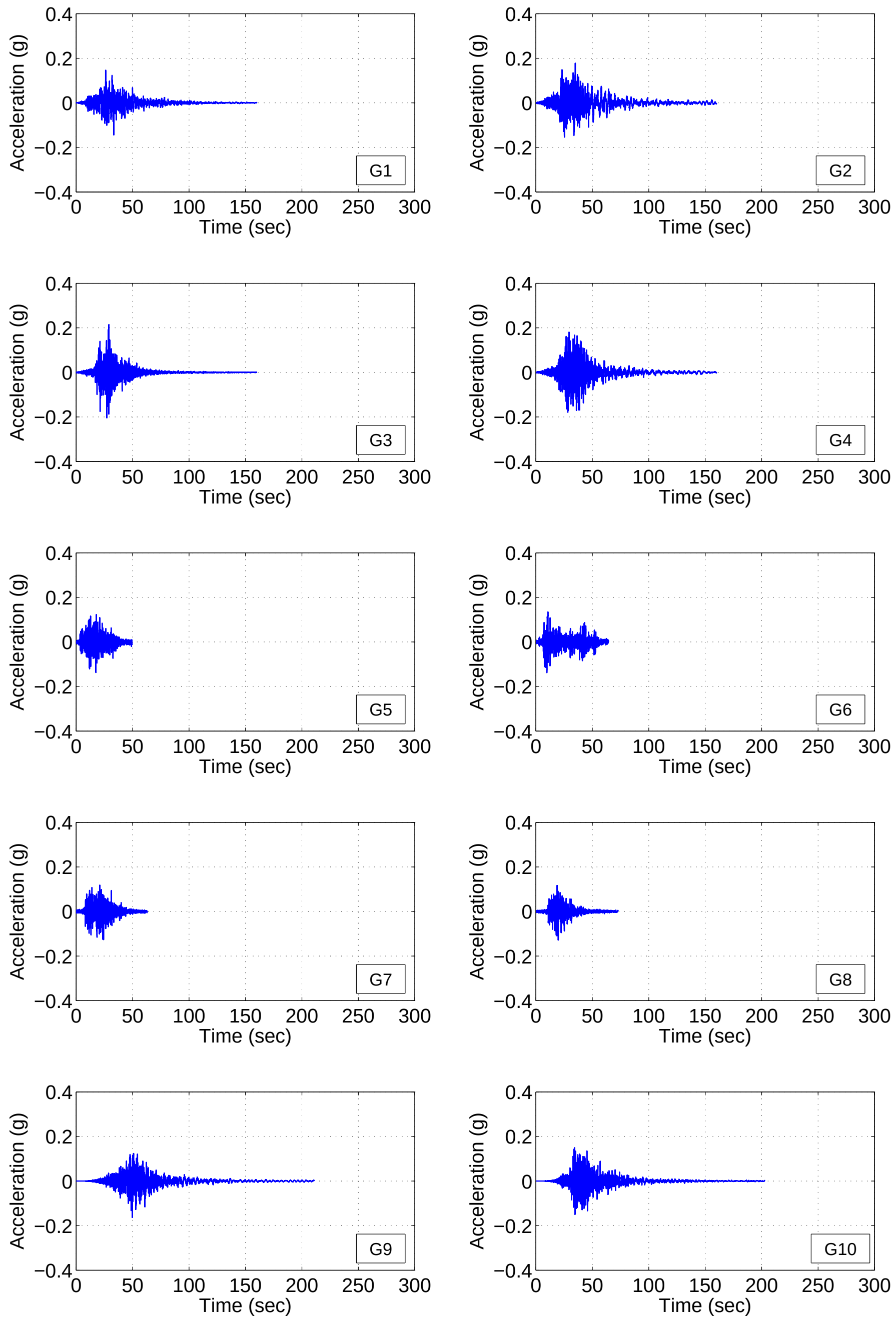

Figure 6.14: Continued.

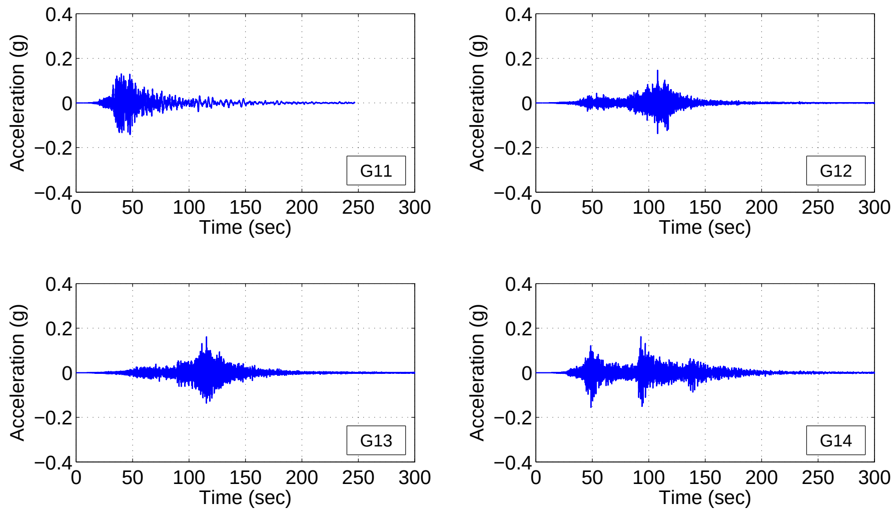

Figure 6.14: Acceleration time histories of the selected Cascadia subduction ground motions.

6.4.4 Near-fault pulse-like earthquakes

As discussed in Section 6.2, there are major faults near British Columbia, which cause earthquakes. It is highly probable that the interaction between tectonic plates generate long-duration pulse-like motions especially in the direction of fault plane rupture. These pulse-like ground motions affect the seismic response of the structures in a different manner than the far-fault ground records and can impose a severe demand on structures to an extent not predicted by typical measures such as response spectra (Alavi and Krawinkler, 2001; Bertero et al., 1978; Bray and Rodriguez-Marek, 2004; Kalkan and Kunnath, 2006; Luco and Cornell, 2007; Makris and Black, 2003).

The response spectrum alone does not adequately characterize near-fault ground motion (Finn, 2000). The pulse-like ground motion is mainly considered to contain a short-duration pulse with high amplitude that occurs early in the velocity time history. One cause of these velocity pulses is the forward directivity effect of the near-fault region. Forward directivity occurs when both the rupture and the direction of slip on the fault are towards the site. This conditions are usually met in strike-slip faulting, where the fault slip direction is oriented horizontally in the direction along the strike of the fault, and rupture propagates horizontally along strike. In addition, the conditions required for forward directivity can be met in dip-slip faulting, including both reverse and normal faults (Somerville et al., 1997). Another near-fault effect is fling step which is mentioned for completeness but is excluded from this study.

Search for the pulse-like ground motions is conducted using PEER-NGA database (Chiou et al., 2008; PEER, accessed on November 2014). In this database pulse-like ground motion records have been identified following the criteria proposed by Baker (2007). The pulse-like ground motions are selected based on moment magnitude of 6.5 to 7.5, occurred within a distance of 20 km from the causative fault and they all belong to the NBCC (2010) site class C. For selection of the near-fault ground motions other than aforementioned criteria, the presence of a short-duration pulse with high amplitude is necessary. It is worth to mention that without a detailed seismological study on individual records, there is no assurance that velocity pulses of the pulse-like records in PEER-NGA database are all due to directivity effect. Although it is likely that other factors may have caused or contributed to the velocity pulses of some records, but it is expected that the pulses are similar to those caused by directivity effect and therefore can be used in modeling the effects of directivity pulses on structures.

Table 6.4 lists the selected 14 near-fault motions. The table provides event name, year, station magnitude, shear wave velocity of the top 30 m of the recorded site, ground motion component and scaling factor. All selected ground motions are linearly scaled to the target UHS of Vancouver in the period range of 0.02–0.8 sec, using MSE linear scaling method. Figure 6.15 illustrates the 5% damped acceleration response spectra of the scaled ground motions with respect to the NBCC (2010) UHS of Vancouver. Acceleration and velocity time histories of the selected near-fault motions are presented in Figures 6.16 and 6.17, respectively.

Table 6.4: List of the selected pulse-like ground motions.

No.	Event Name	Year	Station	Magnitude	V_{s30} (m/s)	Comp.	SF
1 2	Irpinia Italy-01	1980	Sturno (STN)	6.9	382.0	000 270	1.26 1.08
3 4	Loma Prieta	1989	Saratoga - Aloha Ave	6.93	380.9	000 090	1.03 1.17
5 6	Cape Mendocino	1992	Centerville Beach Naval Fac	7.01	459.0	270 360	1.09 0.71
7 8	Northridge-01	1994	Sylmar - Converter Sta East	6.69	370.5	011 281	1.09 0.79
9 10	Bam Iran	2003	Bam	6.6	487.4	L T	0.56 0.67
11 12	Niigata Japan	2004	NIGH11	6.63	375.0	E-W N-S	0.66 0.84
13 14	Chuetsu-oki Japan	2007	Joetsu Kakizakiku Kakizaki	6.8	383.4	E-W N-S	0.92 1.20

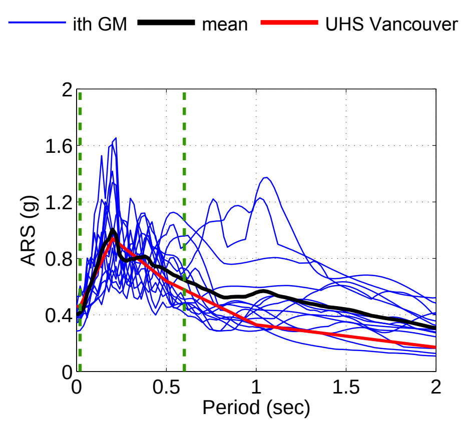

Figure 6.15: The 5% damped acceleration spectra of the selected 14 near-fault pulse-like ground motions and the corresponding mean response using MSE linear scaling method with respect to the target NBCC (2010) UHS of Vancouver.

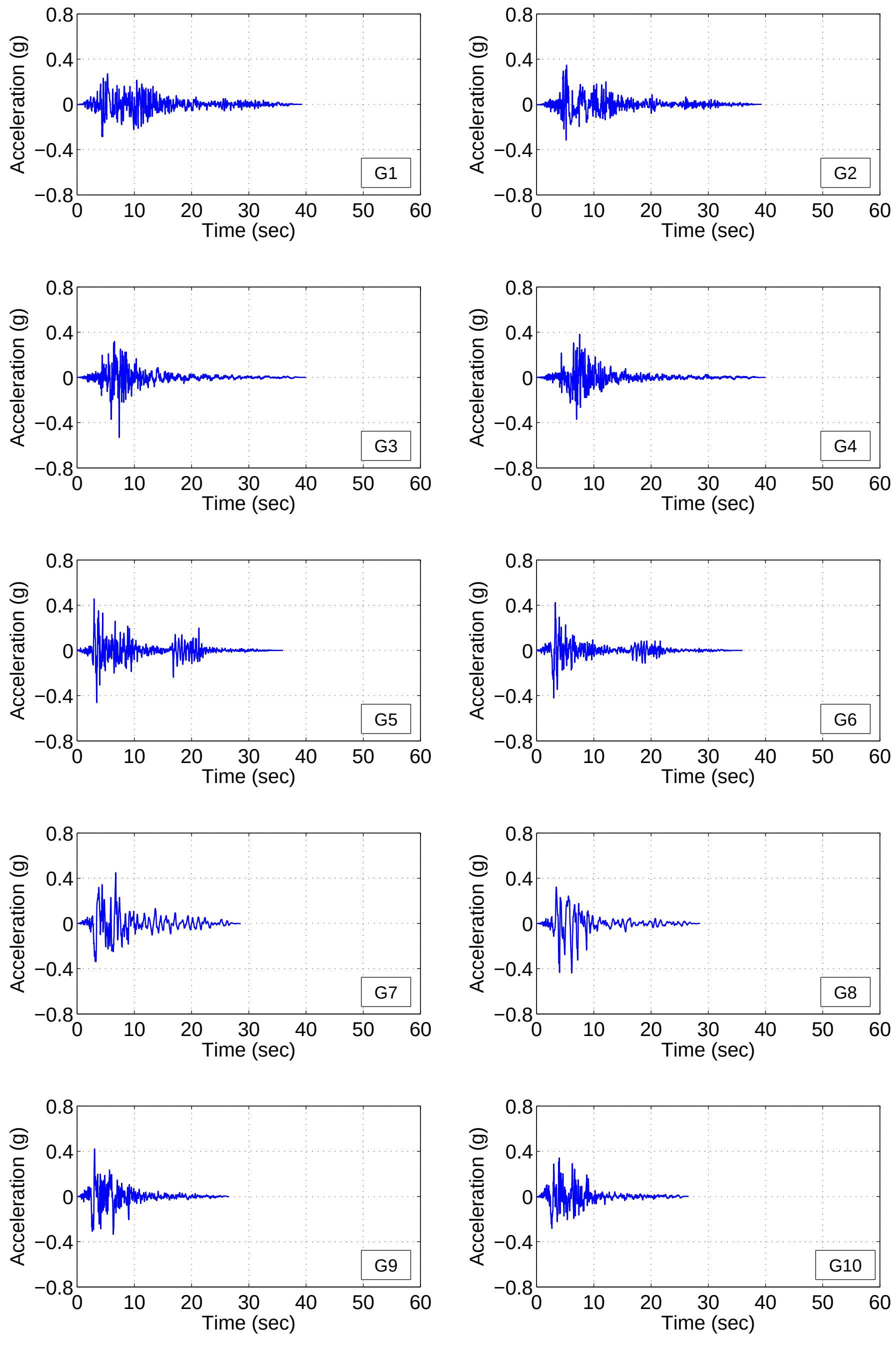

Figure 6.16: Continued.

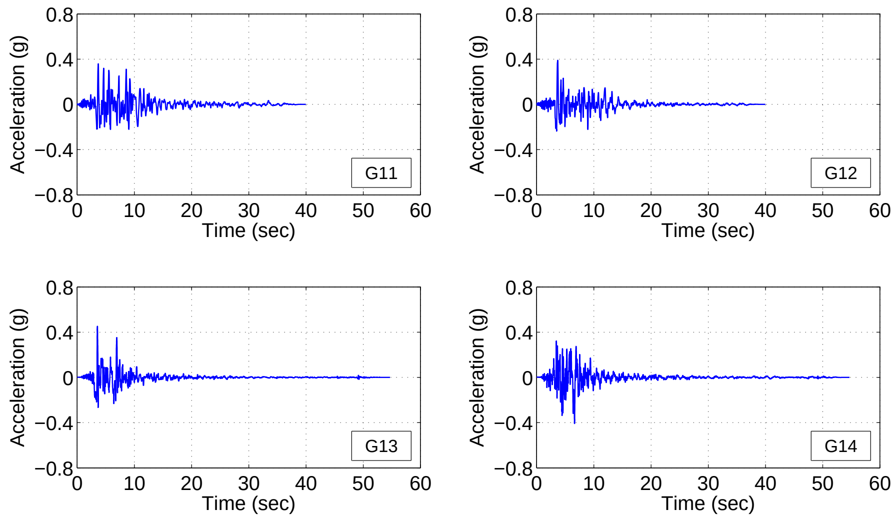

Figure 6.16: Acceleration time histories of the selected 14 near-fault ground motions linearly scaled to the NBCC (2010) UHS of Vancouver using MSE scaling method.

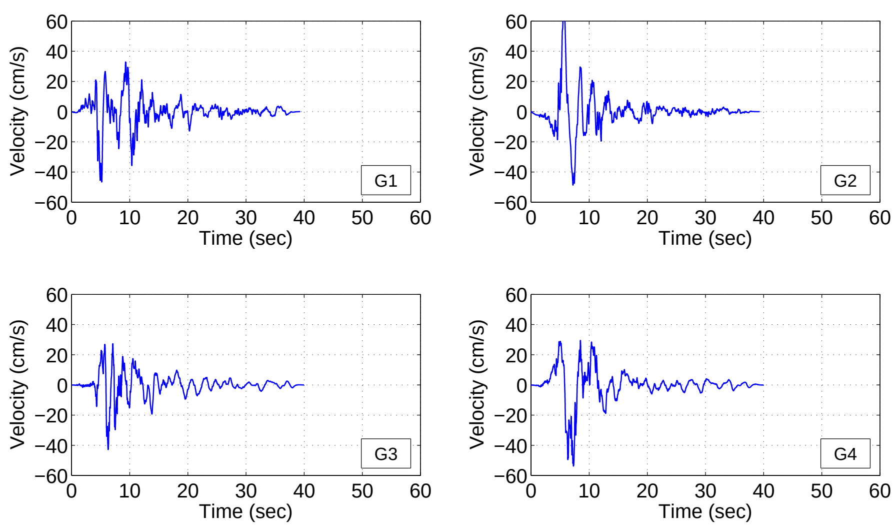

Figure 6.17: Continued.

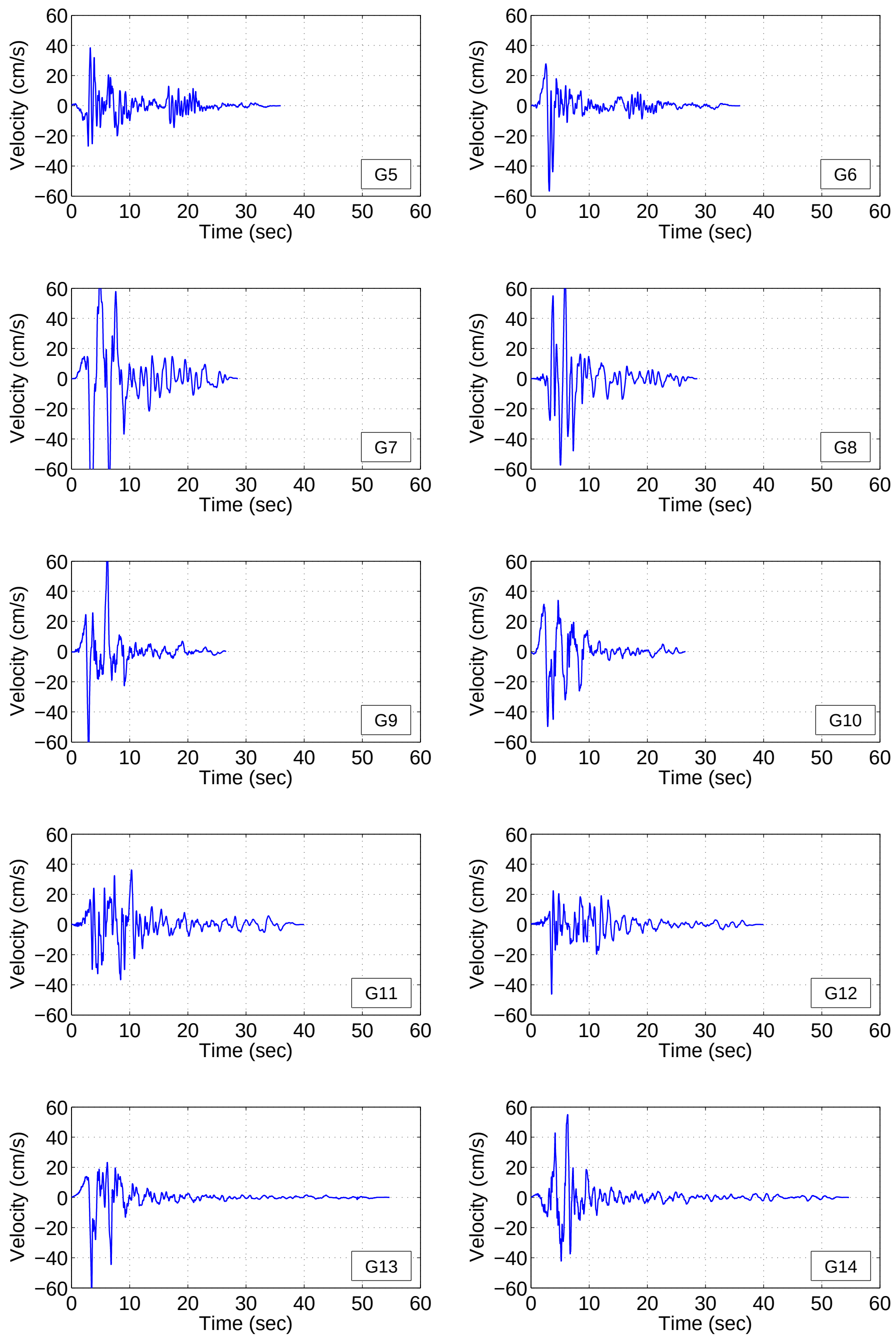

Figure 6.17: Velocity time histories of the selected 14 near-fault ground motions linearly scaled to the NBCC (2010) UHS of Vancouver using MSE scaling method.

6.5 Simulation results

This section presents a distillation of the results of more than 600 nonlinear dynamic analyses performed on basement walls designed for different fractions of the code PGA, subjected to ensembles of dominant seismic mechanisms in south-western BC comprise of shallow crustal, deep subcrustal, interface earthquakes from a Cascadia subduction events and near-fault earthquake motions. Two main methods of spectral matching and linear scaling are used to ensure that the input motions match the NBCC (2010) specified UHS for Vancouver.

All the basement walls presented in this section are founded on Case I soil profile, which result in the foundation of the basement walls be embedded in the second stiff soil layer (Figure 5.13). The normalized shear wave velocities of $V_{s1} = 200\ m/s$ and $V_{s1} = 400\ m/s$ are assigned to the first and the second soil layers, respectively. The UBCHYST soil model with the calibrated set of parameters presented in Table 5.1 are used. The maximum resultant drift ratio along the height of the basement wall is a parameter which is used to compare the nonlinear seismic response of the walls.

Crustal ground motions

The first set of calculations is conducted using the 4-level basement wall with the total height of 11.7 m, designed for different fractions of the code PGA as described in Chapter 3. The main objective of this section is to evaluate the effect of various methods of scaling/matching ground motions on seismic performance of the basement walls. Also the variation of the resultant maximum drift ratios in the form of standard deviation using different scaling/matching techniques is studied.

Figures 6.18 to 6.21 provide comparisons of the envelopes of the maximum drift ratio along the height of the 4-level basement wall designed for different fractions of the NBCC (2010) code PGA, subjected to the suite of 14 crustal ground motions scaled/matched according to the various methods outlined in this thesis. In these plots, the average value corresponds to the mean of the maximum envelopes of the drift ratios resulting from 14 crustal seismic events. Assuming normally distributed drift ratios, average $\pm\ 1\sigma$ represents the first standard deviation with a 68% chance that the mean falls within the range of standard error.

In order to evaluate the performance of the basement walls using different scaling techniques, one must first establish a basis for comparison. The true distribution of drift response corresponding to the suite of crustal records is unknown, so a reference distribution is adopted as a substitute for the true, but ultimately unknowable distribution of drift. It is legitimate to assume that the resultant drift ratio of the system subjected to the spectrally matched ground motions presented in Chapter 4 is an unbiased estimate of the mean response and is defined as a "reference" value (Figures 6.18(f) to 6.21(f)), to provide a basis for comparing the performance of the system subjected to the various scaling methods. As previously mentioned spectral matching reduces spectral variability within a suite of ground motions at a period range of interest and provide an estimation of mean response with a reasonable standard deviation.

Figures 6.18(a,b) to 6.21(a,b) show that scaling the crustal ground motions based on the peak ground acceleration (PGA scaling) and spectral acceleration at the fundamental period of the system (Sa(T_1) scaling), introduce a large scatter in the resultant maximum drift ratio at the top and bottom basement levels. From these figures one can concluded that there is a more pronounced scatter in nonlinear seismic response of basement walls using scaling method based on scalar intensity measures such as PGA and $Sa(T_1)$ than other scaling techniques. These techniques are considered non-efficient and estimation of seismic performance based on them are not accurate. Miranda (1993) and Shome et al. (1998) performed similar studies and observed that using acceleration parameters (such as PGA or $Sa(T_1)$) for scaling ground motions increases the scatter in the nonlinear response of the structures.

As shown in Figures 6.18(a) to 6.21(a), the PGA scaling method leads to designs with significant uncertainty and unknown margins of safety. This is due to the importance of spectral shape of an accelerogram in nonlinear response, as PGA is not a good indicator of the strength and frequency content of the ground motion. Shome and Cornell (1998) and Shome et al. (1998) found that seismic demand estimates are strongly correlated with the linear-elastic spectral response acceleration at the structure fundamental period, T_1 and by using this method the scatter in the demand estimates can be significantly reduced compared with PGA scaling method. Although Sa(T_1) scaling method substantially reduces the scatter in the

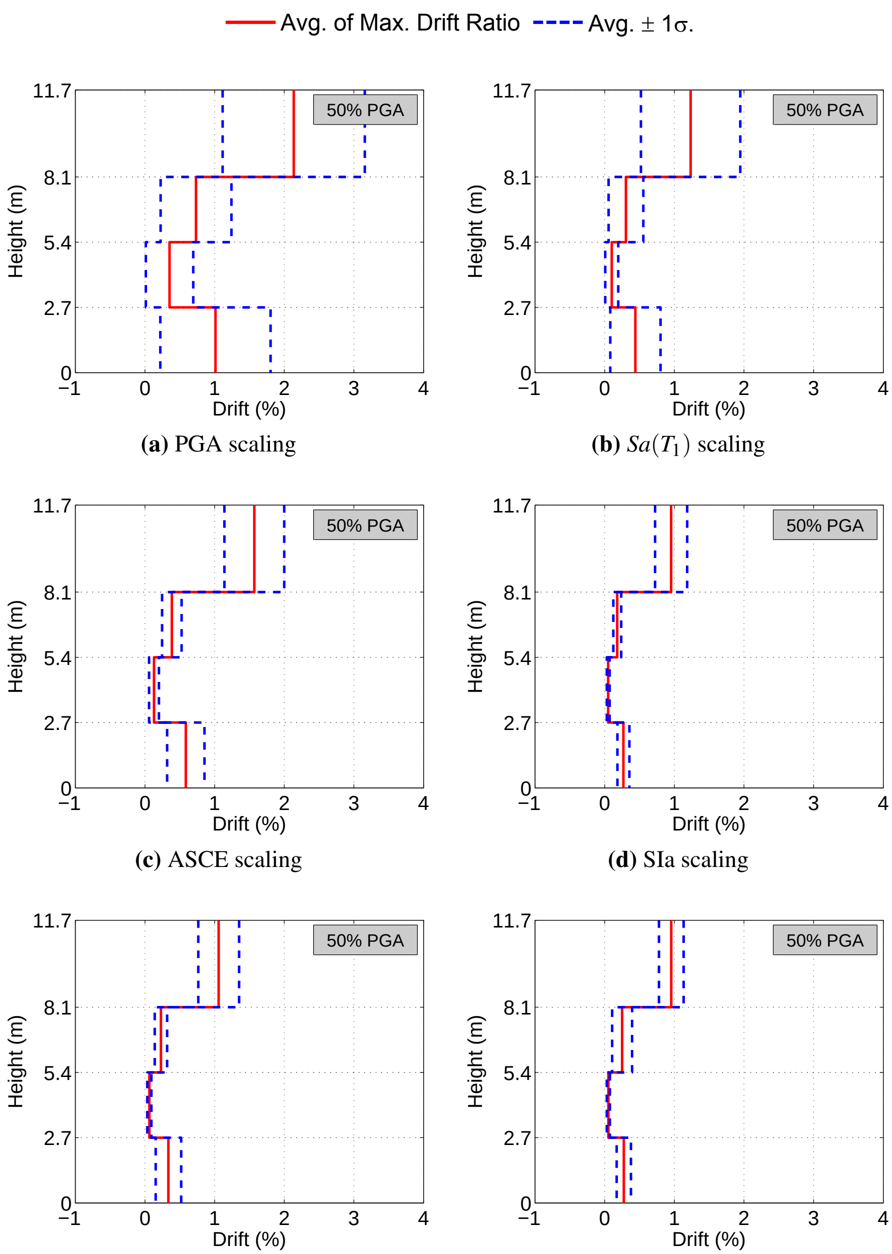

(a) PGA scaling

(b) $Sa(T_1)$ scaling

(c) ASCE scaling

(d) SIa scaling

(e) MSE scaling

(f) Spectral matching

Figure 6.18: Average of the maximum envelopes of drift ratios and the corresponding average ± one standard deviation along the height of the walls designed for 50% of the code PGA subjected to a suite of crustal ground motions scaled/matched using various methods outlined in this study.

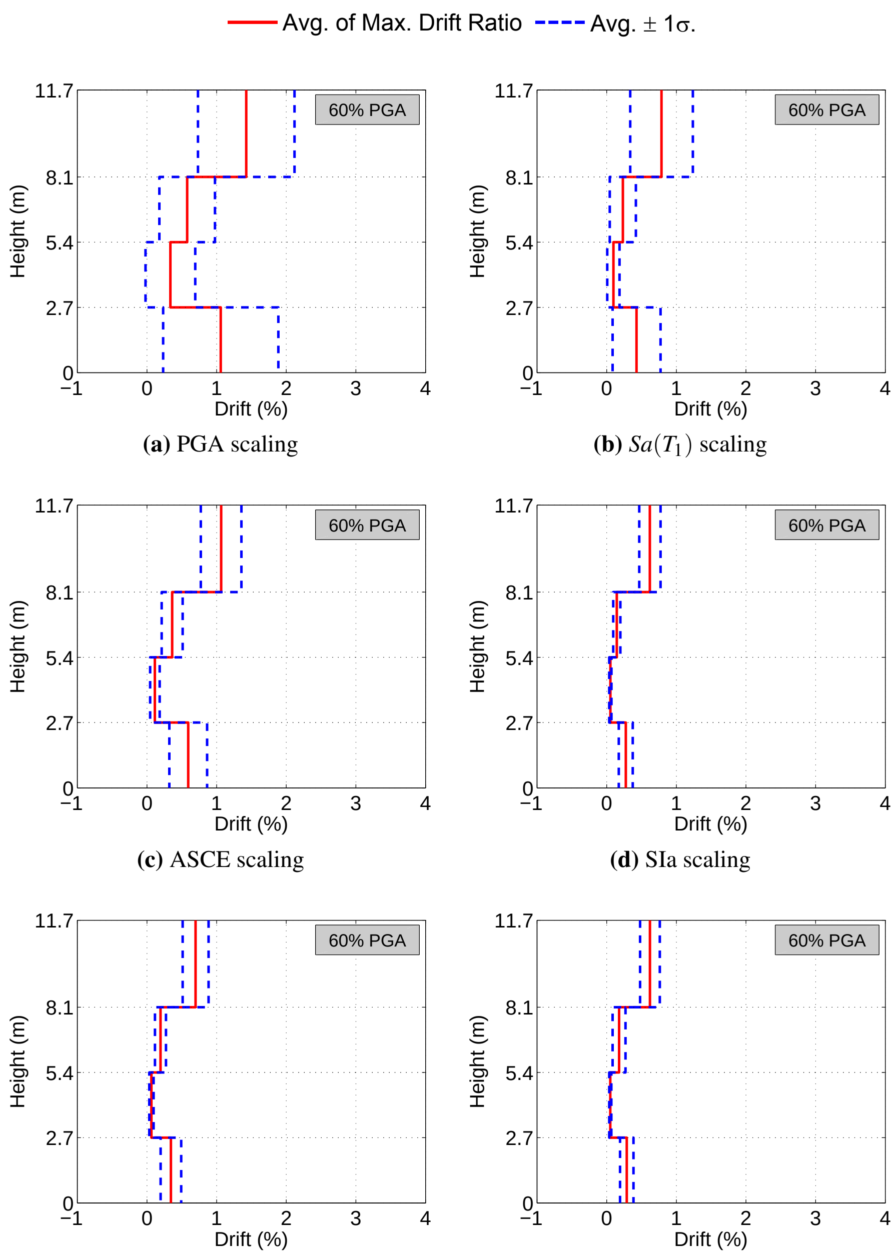

(a) PGA scaling **(b)** $Sa(T_1)$ scaling

(c) ASCE scaling **(d)** SIa scaling

(e) MSE scaling **(f)** Spectral matching

Figure 6.19: Average of the maximum envelopes of drift ratios and the corresponding average ± one standard deviation along the height of the walls designed for 60% of the code PGA subjected to a suite of crustal ground motions scaled/matched using various methods outlined in this study.

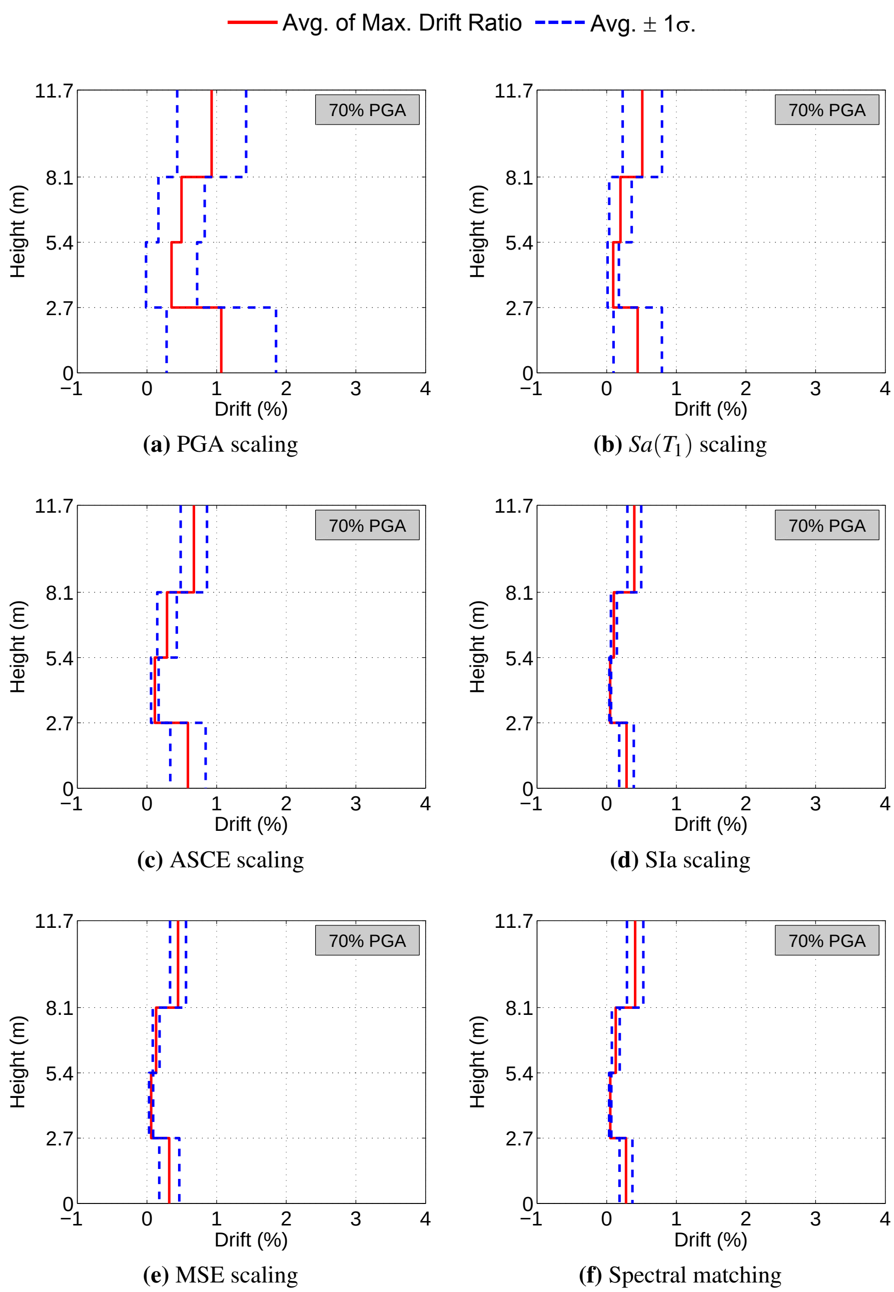

Figure 6.20: Average of the maximum envelopes of drift ratios and the corresponding average ± one standard deviation along the height of the walls designed for 70% of the code PGA subjected to a suite of crustal ground motions scaled/matched using various methods outlined in this study.

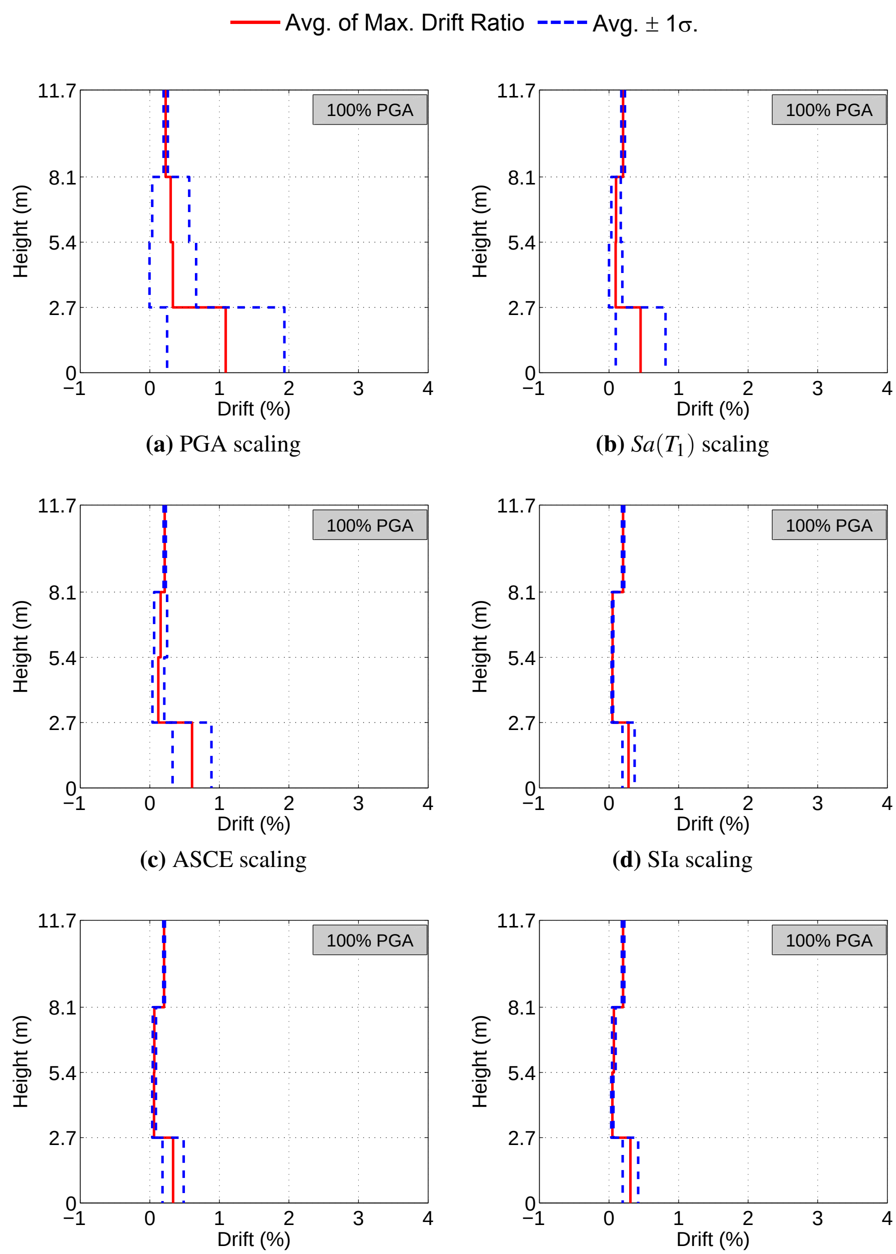

(a) PGA scaling

(b) $Sa(T_1)$ scaling

(c) ASCE scaling

(d) SIa scaling

(e) MSE scaling

(f) Spectral matching

Figure 6.21: Average of the maximum envelopes of drift ratios and the corresponding average ± one standard deviation along the height of the walls designed for 100% of the code PGA subjected to a suite of crustal ground motions scaled/matched using various methods outlined in this study.

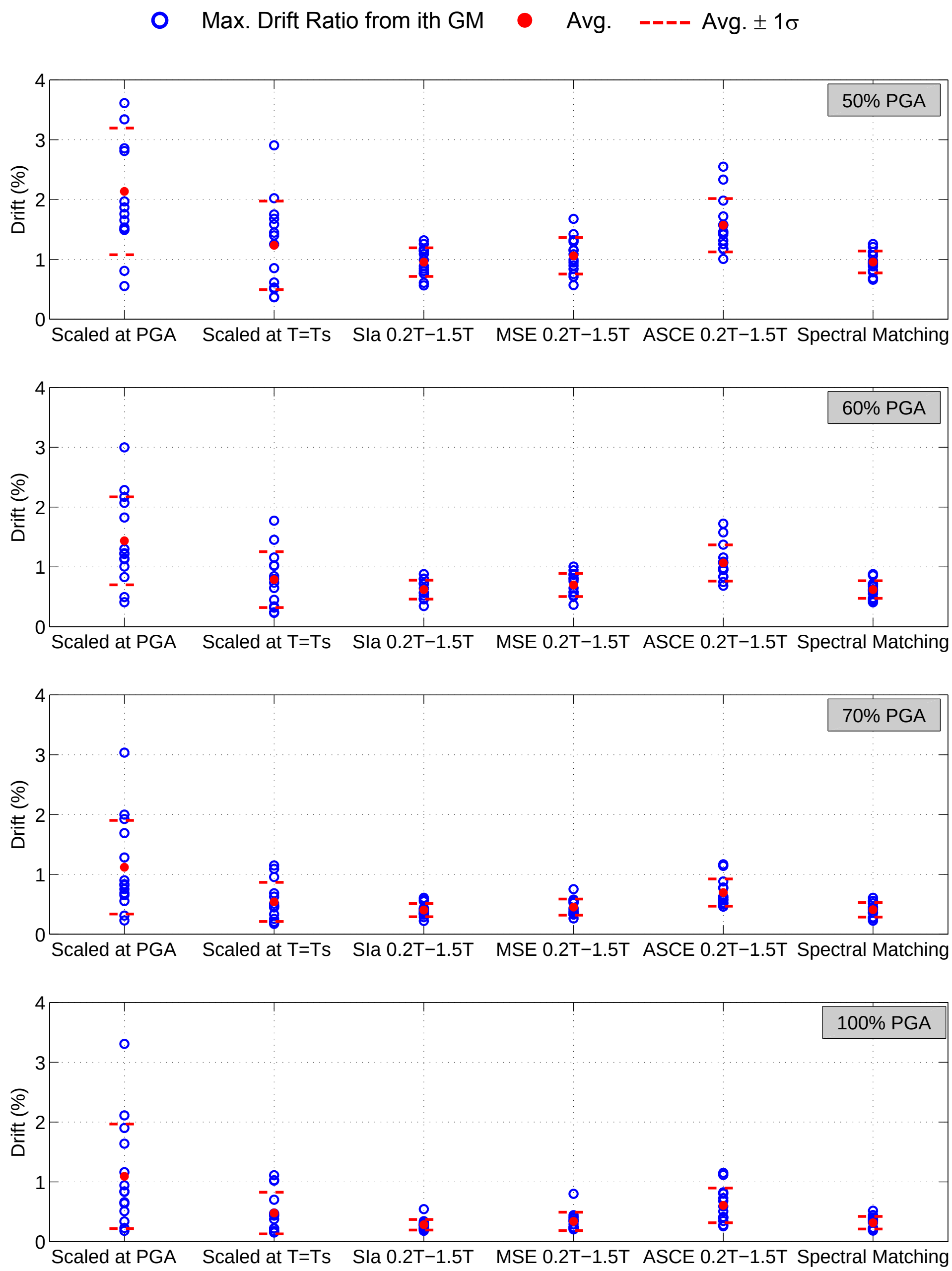

Figure 6.22: The resultant maximum drift ratios and the corresponding mean and mean ± one standard deviation along the height of the wall designed for different fractions of the code PGA subjected to crustal ground motions (G1–G14) scaled/matched using various methods outlined in this study.

demand, but as illustrated in Figures 6.18(b) to 6.21(b) still there is a unacceptable amount of uncertainty and dispersion due to lengthening the apparent period of vibration becuase of yielding compared to other methods of scaling.

Figure 6.22 summarizes the maximum value of drift ratio along the height of the basement walls designed for different fractions of the code PGA, subjected to 14 crustal ground motions all scaled/matched using various methods outlined in this chapter. Within the limitation of the sample size used in this study, discrepancy implies that the use of either linear-scaled records in a period range (SIa, MSE and ASCE methods) or spectrum-compatible records (Spectral matching) introduces a certain degree of bias in the computed structural response. In contrast, the high dispersion calculated as the standard deviation of the resultant maximum drift ratio for a sample size of 14 crustal ground motions scaled to a constant PGA, implies that the demand estimates are subject to significant uncertainty and the results are not suggested to be considered.

As depicted in Figure 6.22, scatter in dynamic response can be reduced by scaling the suites of ground motions over a range of periods instead of a single period, which results in a more reasonable estimate of the mean resultant drift ratio (Martinez-Rueda, 1998; Shome and Cornell, 1998; Shome et al., 1998). This is due to consideration of the spectral shape and frequency content of each ground motion in the scaling factor calculation process. Three different methods of linear scaling over the period range have been evaluated in this study: SIa scaling, MSE scaling, and ASCE scaling methods. Results of the analyses show that using SIa and MSE linear scaling methods lead to a mean drift ratio similar to the reference expected mean value of the response, whereas ASCE scaling generates larger drift ratios. As was illustrated earlier in Figure 6.8 scaling the suites of ground motions based on SIa and MSE scaling methods result in a mean spectrum with an overall good match with respect to the seismic demand in a period range of interest. Consequently, these motions result in a mean drift ratio in agreement with the reference mean value. In contrast, ASCE scaling method generates stronger motions and as a result found to be conservative and generally overestimates the mean value of deformation by 20% in the case of the wall designed for 50% PGA.

The data gathered in this study suggest that although most of the scaling and matching techniques adopted herein are able to adequately capture the expected response of the structure, the level of variability of the response in the form of the standard deviation of the resultant drift ratios are reduced significantly as one moves from:

(1) linear scaling the records to match the target spectrum at PGA or the natural period of the system $Sa(T_1)$, to

(2) linear scaling the records to match the target spectrum over the period range using different methods such as ASCE, MSE and SIa scaling, to

(3) spectrally matching the records in a time domain using the wavelet algorithm proposed by Abrahamson N.A. (1992) and Hancock et al. (2006).

By assuming 1.7% drift ratio as an acceptance criterion, one can concluded that within a significant range of variation, the conclusion still stands that the basement wall founded on dense soil can be safely designed using the M-O method with 50% and 60% PGA and result in a satisfactory performance in a term of drift ratio if subjected to the linear scaled crustal ground motions regardless of the technique used for scaling the records to the target demand.

In addition to the 11.7 m 4-level basement wall, the effect of linearly scaled motions on the walls with deeper depths are also checked. To this aim, a series of analyses are conducted on the 4-level and 6-level basement walls with a total height of 13.1 m and 17.1 m, respectively, subjected to 14 crustal ground motions linearly scaled to UHS of Vancouver. These walls are embedded in Case I soil profiles as shown in Figure 5.33. The results of these analyses in form of the maximum resultant drift ratio are illustrated in Figure 6.23. In this figure MSE scaling method is chosen as a linear scaling method. The resultant drift ratios of the spectrally matched motions, as discussed earlier in Section 5.4, are also plotted for comparison. The results confirm that the maximum resultant drift ratios along the height of the 4-level basement walls with 5.0 m top storey and the 6-level basement walls designed for 50% of the code PGA fall within an acceptable range.

Subcrustal ground motions

Figure 6.24 shows the envelope of the maximum drift ratios along the height of the 4-level basement wall designed for 50% and 60% PGA subjected to a suite of

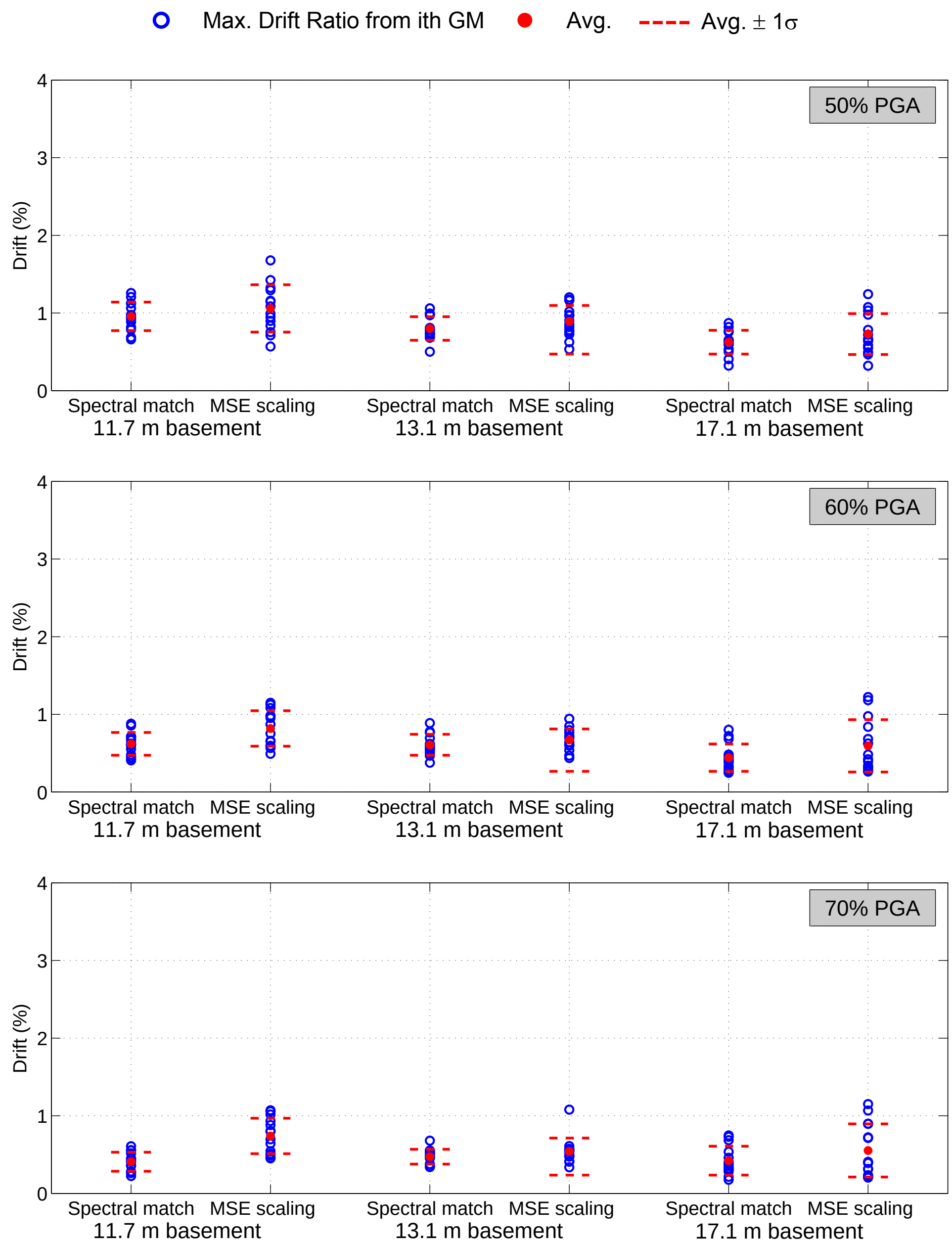

Figure 6.23: The resultant maximum drift ratios and the corresponding mean and mean ± one standard deviation along the height of the 4-level and 6-level basement walls designed for different fractions of the NBCC (2010) code PGA subjected to 14 crustal ground motions scaled/-matched using MSE linear scaling and spectral matching methods.

14 subcrustal ground motions linearly scaled and spectrally matched to the UHS of Vancouver. The resultant drift ratio at the top floor levels of the wall designed for 50% PGA have the maximum values of $1.24\% \pm 0.38\%$ and $1.11\% \pm 0.23\%$ in case the walls subjected to linear scaled and spectrally matched ground motions, respectively which in both cases fall within an acceptable range ($< 1.7\%$).

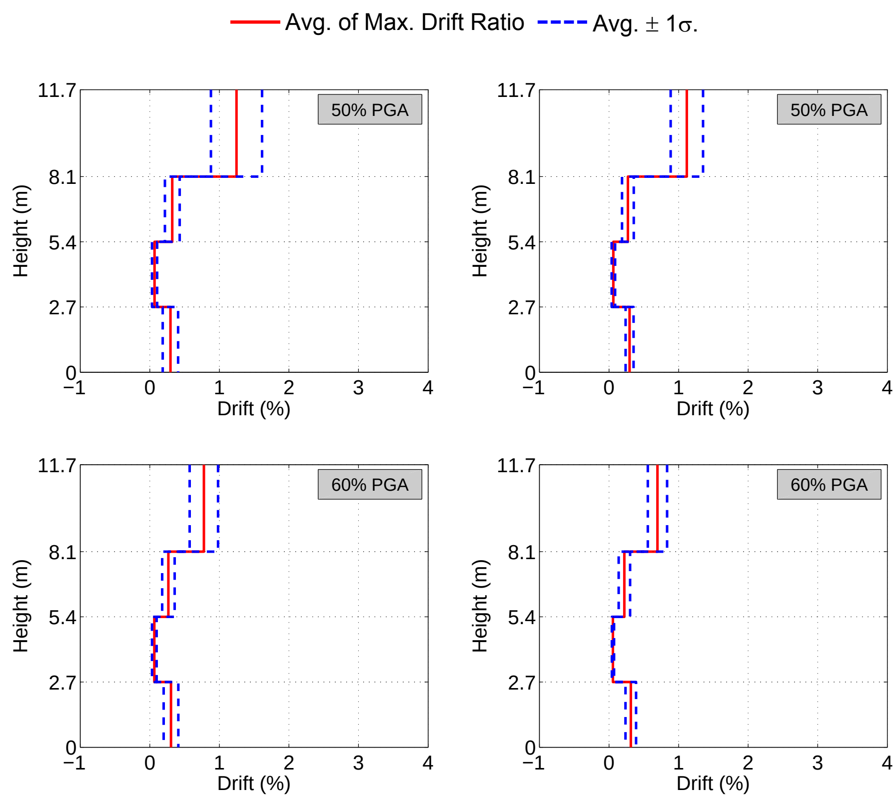

(a) MSE scaling **(b)** Spectral matching

Figure 6.24: Average of the maximum envelopes of drift ratios and the corresponding average ± one standard deviation along the height of the wall designed for 50% and 6% of the code PGA subjected to 14 subcrustal ground motions (a) linearly scaled and (b) spectrally matched to the NBCC (2010) UHS of Vancouver.

Cascadia subduction ground motions

Figure 6.25 shows that the Cascadia subduction motions have no significant effect on the basement walls and result in very low drift ratios ($< 0.2\%$) even on the weakest wall designed for 50% PGA.

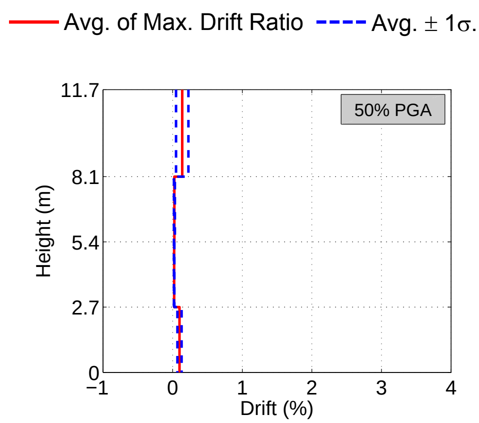

Figure 6.25: Average of the maximum envelopes of drift ratios and the corresponding average $\pm$ one standard deviation along the height of the wall designed for 50% of the code PGA subjected to 14 Cascadia subduction ground motions linearly scaled to the NBCC (2010) subduction hazard values for Vancouver.

Near-fault pulse-like ground motions

Figure 6.26 demonstrate the performance of the 4-level basement walls designed for 50% and 60% of the code PGA, subjected to a suite of 14 near-fault pulse-like ground motions. These motions cause the performance of the bottom basement level become more critical and in some cases dominant, but still in an acceptable range.

The presented results suggest that the basement walls designed for 50% to 60% NBCC (2010) PGA using the modified M-O method and founded on sandy soil would result in satisfactory performance when subjected to ground motions reflecting three dominant seismic mechanism (crustal, subcrustal and Cascadia

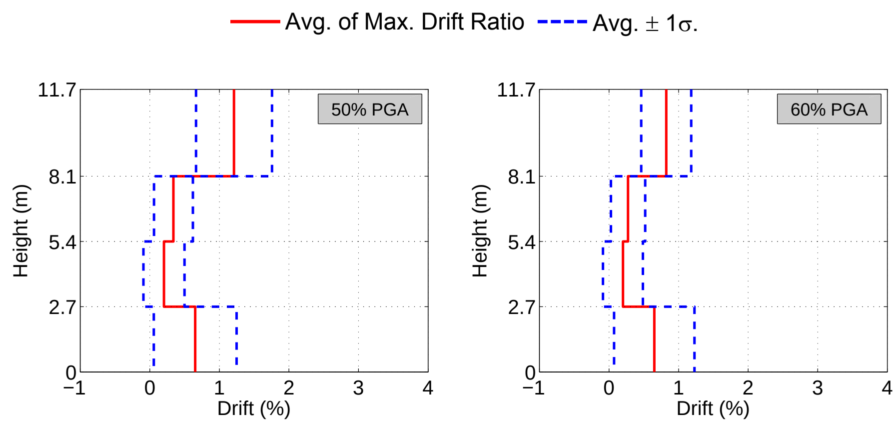

Figure 6.26: Average of the maximum envelopes of drift ratios and the corresponding average $\pm$ one standard deviation along the height of the wall designed for 50% of the code PGA subjected to 14 pulse-like ground motions linearly scaled to the NBCC (2010) UHS of Vancouver.

subduction) and pulse-like near-fault records in Vancouver and matching the code specified intensity of the seismic hazard,which has an exceedance rate of 2% in 50 years.

Chapter 7

Summary and future research

Science never solves a problem without creating ten more.
— George B. Shaw (1856–1950)

7.1 Summary

A comprehensive study of the current seismic design procedure of deep basement walls during earthquake events and the seismic pressures for which they should be designed for is being conducted at the University of British Columbia at the request of the Structural Engineers Association of British Columbia (SEABC).

The current state of practice for seismic design of basement walls in British Columbia is based on the studies of Okabe (1924) and Mononobe and Matsuo (1929) by incorporating the modification suggested by Seed and Whitman (1970) which is referred to as the Mononobe-Okabe (M-O) method. In this method the earthquake thrust acting on the wall is a function of the Peak Ground Acceleration (PGA), which is representative of the seismic demand anticipated for the subject structure at the site in question.

The seismic hazard level in the National Building Code of Canada (NBCC, 2010) for design of buildings has a probability of exceedance of 2% in 50 years and the related PGA hazard of 0.46 g for Vancouver. For designers who have been using the M-O method for estimating the seismic lateral pressures and eventually designing the basement walls, using the full PGA leads to very large seismic forces that make the resulting structures expensive and over-designed. Because there has been no reports of damage to building basement walls as a result of seismic earth pressures in recent United States earthquakes including the San Fernando (1971), Whittier Narrows (1987), Loma Prieta (1989), and Northridge (1994) earthquakes, SEABC became interested in designing the walls under the new code mandated PGA and set up a task force to review the current seismic design procedure of basement walls in British Columbia.

The seismic performance of the typical basement wall designed according to the state of practice in Vancouver was examined. It is important to point out that in this practice the building above the ground level is not considered and inertial loading of the surface structures on basement wall pressures are not taken into an account. In the benchmark analyses, the typical 4-level basement wall structure with a total height of 11.7 m, was designed by SEABC structural engineers for different fractions of the NBCC (2010) PGA for Vancouver.

An enhanced dynamic nonlinear soil–structure interaction analyses were then conducted on computational model of these basement walls to capture the essential features and response characteristics of the basement wall-backfill system under seismic loading and explore the capacity of the walls to absorb demand corresponding to NBCC (2010) with an exceedance rate of 2% in 50 years. For this purpose each wall was subjected to the full demand imposed by a suite of 14 crustal ground motions spectrally matched to the UHS of Vancouver. The soil–structure model employed elastic-plastic beam elements to model all structural components of the model including basement walls. The soil layers consisted of two-dimensional plane-strain quadrilateral elements simulated using the simple Mohr-Coulomb material model. With an insight from equivalent linear analyses, degraded elastic modulus and equivalent damping ratio in the form of Rayleigh damping were employed for closer representation of nonlinear soil system response in seismic loading. Interface elements represented by two elastic-perfectly plastic normal and shear springs between the soil and the structure were utilized to simulate interaction between the concrete basement structure and surrounding soil and facilitate modeling opening (separation) and slippage. In order to avoid reflection of outward propagating waves back into the model, quiet (viscous) boundaries, comprising independent dashpots in the normal and shear directions, were placed at the base of the soil medium. The lateral boundaries of the soil grid were coupled to the free-field boundaries at the sides of the model to simulate the free-field condition, which would exist in the absence of the structure.

The results of the computational benchmark study were presented in the form of typical time histories of the lateral earth pressure, resultant lateral earth force and the corresponding normalized height of application from the base of the wall. Also, envelopes of bending moments, shear forces, lateral deformations, and drift ratios along the height of the walls were presented and discussed. In an absence of any report on the acceptable drift ratios for constrained walls with distributed lateral loading, the ASCE-TCBRD (2010) was selected as the performance standard. The results of the benchmark analyses suggested that the walls designed for 100% PGA were over conservative and the behavior of the basement wall designed for 50% to 60% PGA resulted in satisfactory performance when subjected to the current seismic hazard for Vancouver with an exceedance rate of 2% in 50 years.

A series of sensitivity analyses were conducted to identify the impact of various parameters on the seismic performance of the basement wall. Table 7.1 lists the evaluated parameters, a range of variation and the sensitivity of the resultant drift ratio along the height of the wall to the variation:

Table 7.1: Summary of the sensitivity analyses conducted in this study.

Parameter description	Parameter	Range of sensitivity	Sensitivity	
			high [a]	low [b]
Friction angle of the interface element	δ	$5^\circ - 15^\circ$	✓	
Normal stiffness of the interface element	k_n	$9\times10^5 - 9\times10^7\ kPa/m$		✓
Shear stiffness of the interface element	k_s	$9\times10^5 - 9\times10^7\ kPa/m$		✓
Dilation angle of the backfill soil	ψ	$0^\circ - 10^\circ$		✓
Friction angle of the backfill soil	ϕ	$28^\circ - 38^\circ$		✓
Shear wave velocity of the backfill soil	V_{s1}	$150 - 250\ m/s$	✓	
Modulus reduction in Mohr-Coulomb model	G/G_{max}	$0.3 - 0.5$	✓	
Damping ratio in Mohr-Coulomb model	D	$6\% - 10\%$	✓	
Shoring pressure during excavation	$K_A - K_o$	$0.3 - 0.5$		✓

[a] Greater than 25% change.
[b] Equal or less than 25% change.

The benchmark analyses were conducted on a specific basement depth, founded on dense soil deposit modeled using a simple Mohr-Coulomb model. Because of the radical shift in design practice suggested by these findings, extensive studies were conducted to more fully validate the major conclusion regarding design and analyses presented. In order to have a clear and comprehensible conclusion regarding the effects of the structural height, subsoil stiffness, and ground motion characteristics on seismic response of the basement walls under the influence of SSI, a comprehensive computational investigation has been conducted. A series of analyses were carried out on number of primary soil–structure interaction parameters in order to assess the effect of input parameters' uncertainties on proposed design seismic coefficient of basement walls and the robustness of the results. To this aim the seismic performance of the basement walls designed for different fractions of the NBCC (2010) PGA were re-calculated under alternative assumptions listed in Table 7.2 to determine their impact on the conclusion drawn from the benchmark analyses. The effect was measured by monitoring changes in the resultant maximum drift ratios along the height of the wall as summerized in Figure 7.1.

Table 7.2, Case 2: Adopting more representative constitutive model for simulating nonlinear stress–strain response of the soil medium to obtain realistic estimates of an interaction between the basement wall and the surrounding soil. For this purpose the relatively simple total stress UBCHYST model was used, which replicates the behavior of real soil and reduces the essence of defining modulus reduction and Rayleigh damping with the simple Mohr–Coulomb model. The results of the analyses show that changing soil constitutive model does not have a considerable effect on the seismic performance of the basement wall.

Table 7.2, Cases 3–12: Evaluate the effect of local site condition in terms of geometrical and geological structure of soft soil deposits underneath the basement wall, which cause a huge impact on the intensity and frequency content of ground shaking around the structure. The seismic performance of the basement wall founded on various soil deposits that the variation of the shear wave velocity profiles and the depth to an impendence contrast between soil layers differentiating the cases were evaluated. The importance of the impedance contrast and stiffness of soil layers on characterizing the site response were assessed in terms of amplitude and frequency content and eventually the response of the embedded basement wall was evaluated.

According to the results of the nonlinear site response analyses, it was observed that the presence of a relatively soft soil layer underneath the basement wall structure and the impendence contrast between various soil layers, substantially affect the rate of ground motion amplification at different basement wall levels and consequently the resultant seismic deformation at various basement levels.

Figure 7.1 shows that except for the cases 5 and 6, the resultant average $\pm$ one standard deviation of all basement walls designed for even 50% and 60% PGA falls within an acceptance range ($< 1.7\%$) when subjected to the current seismic hazard level in Vancouver, with a 2% chance of being exceeded in 50 years. Eventhough according to practitioners (DeVall et al., 2010, 2014) using $V_{s1} = 150\ m/s$ as the normalized shear wave velocity of the first soil layer is a bit low for high-rise construction in Vancouver, but the performance of the basement walls designed for 50% and 60% PGA founded on these soil layers would still fall in the lower range of the medium response ($< 3.5\%$) category defined by ASCE-TCBRD (2010).

Table 7.2, Cases 13–16: Assess the effect of wall geometry in the form of either increasing a number of basement levels or assigning the higher top storey. To this aim the 4-level basement wall with 5.0 m top storey and total height of 13.1 m, and the 6-level basement wall with total height of 17.1 m were designed by SEABC structural engineers following the state of practice in Vancouver and were subjected to the full demand imposed by NBCC (2010).

Figure 7.1 compares the resultant maximum drift ratios of the 4-level ($H = 13.1\ m$) and 6-level basement walls ($H = 17.1\ m$) basement walls founded on two different soil profiles and confirms that within a significant range of variations, the conclusion still stands that the basement walls can be safely designed with 50–60% NBCC (2010) PGA using the modified M-O method.

Table 7.2: Summary of analyses.

Case No.	Basement wall geometry	Input motion	Method of scaling/matching	Constitutive model	Soil profile: Normalized Vs top layer (m/s)	Soil profile: Normalized Vs bottom layer (m/s)	Soil profile: Depth to impedance contrast (m)
1	4-level (11.7 m)	crustal	spectral matching	Mohr-Coulomb	200	400	12.15
2	4-level (11.7 m)	crustal	spectral matching	UBCHYST	200	400	12.15
3	4-level (11.7 m)	crustal	spectral matching	UBCHYST	200	400	17.1
4	4-level (11.7 m)	crustal	spectral matching	UBCHYST	150	250	17.1
5	4-level (11.7 m)	crustal	spectral matching	UBCHYST	150	300	17.1
6	4-level (11.7 m)	crustal	spectral matching	UBCHYST	150	400	17.1
7	4-level (11.7 m)	crustal	spectral matching	UBCHYST	200	250	17.1
8	4-level (11.7 m)	crustal	spectral matching	UBCHYST	200	300	17.1
9	4-level (11.7 m)	crustal	spectral matching	UBCHYST	250	250	-
10	4-level (11.7 m)	crustal	spectral matching	UBCHYST	250	300	17.1
11	4-level (11.7 m)	crustal	spectral matching	UBCHYST	250	400	17.1
12	4-level (11.7 m)	crustal	spectral matching	UBCHYST	300	300	-
13	4-level (13.1 m)	crustal	spectral matching	UBCHYST	200	400	13.55
14	4-level (13.1 m)	crustal	spectral matching	UBCHYST	200	400	17.55
15	6-level (17.1 m)	crustal	spectral matching	UBCHYST	200	400	18.5
16	6-level (17.1 m)	crustal	spectral matching	UBCHYST	200	400	22.5
17	4-level (11.7 m)	crustal	PGA linear scaling	UBCHYST	200	400	12.15
18	4-level (11.7 m)	crustal	Sa(T1) linear scaling	UBCHYST	200	400	12.15
19	4-level (11.7 m)	crustal	ASCE linear scaling	UBCHYST	200	400	12.15
20	4-level (11.7 m)	crustal	SIa linear scaling	UBCHYST	200	400	12.15
21	4-level (11.7 m)	crustal	MSE linear scaling	UBCHYST	200	400	12.15
22	4-level (13.1 m)	crustal	MSE linear scaling	UBCHYST	200	400	13.55
23	6-level (17.1 m)	crustal	MSE linear scaling	UBCHYST	200	400	18.5
24	4-level (11.7 m)	subcrustal	spectral matching	UBCHYST	200	400	12.15
25	4-level (11.7 m)	subcrustal	MSE linear scaling	UBCHYST	200	400	12.15
26	4-level (11.7 m)	subduction	MSE linear scaling	UBCHYST	200	400	12.15
27	4-level (11.7 m)	near-fault	MSE linear scaling	UBCHYST	200	400	12.15

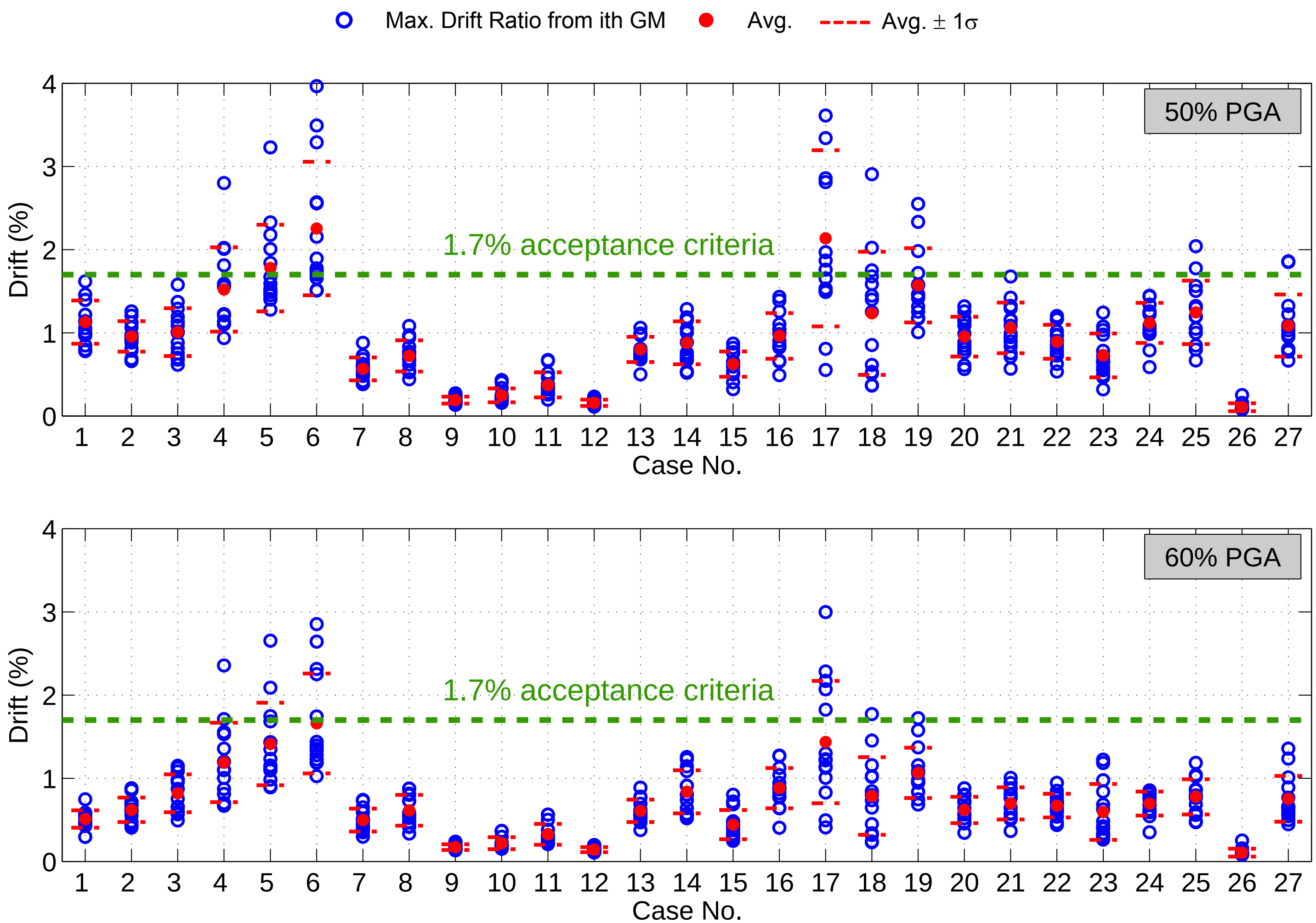

Figure 7.1: Summary of the resultant maximum drift ratio of the basement walls designed for 50% and 60% of the NBCC (2010) PGA for different cases outlined in Table 7.2.

Table 7.2, Cases 17–23: In addition to the spectrally matched accelerograms used in benchmark analyses to estimate the robust mean values of the seismic response, five linear scaling methods were adopted to capture the inherent motion-to-motion variability of the basement wall responses subjected to a suites of earthquake ground motions under the seismic demand adopted by NBCC (2010) for Vancouver. Most of the adopted linear scaling techniques were able to adequately capture the expected response of the basement wall, but the level of variability of the response in the form of the standard deviation of the resultant maximum drift ratios were reduced significantly as one moves from: (1) linear scaling the records to match the target spectrum at PGA or the natural period of the system $Sa(T_1)$; to (2) linear scaling the records to match the target spectrum over the period range using different methods such as ASCE, MSE and SIa scaling; to (3) spectrally matching the records in a time domain using the wavelet algorithm proposed by Abrahamson N.A. (1992) and Hancock et al. (2006).

Within the limitation of the sample size used in this study, discrepancy implies that the use of either linear-scaled records over a period range (SIa, MSE and ASCE methods) or spectrum-compatible records (Spectral matching) introduces a certain degree of bias in the computed structural response. Results of the analyses show that using SIa and MSE linear scaling methods lead to a mean drift ratio similar to the reference expected mean value of the response, calculated by using spectrally-matched motions, whereas ASCE scaling technique generates larger drift ratios.

Table 7.2, Cases 24–27: In order to assess the seismic performance of the basement walls in Vancouver, the input motions for these analyses should reflect three dominant seismic sources in the south-western British Columbia: shallow crustal earthquakes, deep subcrustal earthquakes and interface earthquakes from a Cascadia event. Also the effect of pulse-like near-fault ground motions which contain a short-duration pulse with high amplitude in their velocity time histories, and consequently affect the structure in a different manner than far-field records were evaluated. Therefore, in addition to the selected 14 crustal ground motions, 14 subcrustal, 14 Cascadia subduction, and 14 near-fault pulse-like records were selected and each scaled to the hazard levels proposed by NBCC (2010) using the MSE linear scaling method. As illustrated in Figure 7.1, the Cascadia subduction motions have no significant effect on the basement walls and the performance of the 4-level basement wall designed for 50% and 60% PGA subjected to subcrustal and near-fault pulse like ground motions fall into an acceptable range.

In conclusion the result of these analyses show that the behavior of the top and bottom basement levels are critical and the resultant drift ratios at these levels are significantly higher than the drift ratio of the other levels. The results as are presented in Figure 7.1 confirm that within a significant range of variations, the conclusion still stands that the basement wall founded on dry cohesionless medium dense soil can be safely designed using the modified M-O method as presently used in Vancouver but with an acceleration of 50–60% PGA instead of 100% PGA, which results in an over-designed structures. As noted in literature review (Anderson et al., 2008; Candia, 2013; Lew, 2012), even a small amount of cohesion can reduce the seismic pressure acting on the wall significantly.

7.2 Recommendations for future research

Since the purpose of this research work was to determine the seismic response of the basement walls resting on dry sandy soil deposits, further studies and some refinements are recommended to make this research work more comprehensive for practical applications. Future research work may be carried out in the following areas:

- The results presented herein are limited to the basement wall structures embedded in a dry medium dense sandy backfill soils. Fine-grained soils comprising silt and clay with substantial amount of cohesion behave differently from soils containing clean sands and can be investigated in future studies.

- There are many cities and districts exposed to seismic risk in south-western British Columbia. This study was focused on the city of Vancouver. Other cities such as Victoria and Nanaimo with high seismicity require similar assessment of seismic performances of the basement walls

- The study can be expanded to the three-dimensional (3D) analyses because of significant site economic savings that can be achieved by reducing the PGA to lower fractions. In these analyses the basement walls will be subjected to the 3D earthquake ground motions, consist of two horizontal components and a vertical component, which has generally been neglected in the design process. It has been observed in recent earthquakes that the vertical component of the ground motions may be equal or even in some cases significantly exceed the local horizontal ground motion and can have an important effect on the seismic performance of the subjected basement wall.

- This study is based on the walls meeting the safety criteria. By considering the possibility of collapse/failure for the walls, ground motions should exceed the design ground motion and therefore analyzing the basement walls using Incremental Dynamic Analysis (IDA) is recommended. IDA is a state-of-the-art method for determining the effect of increasing earthquake ground motion intensity on structural response up to collapse, following the procedure introduced by the U.S. Federal Emergency Management Agency, FEMA P695 (2009) guideline.

- Nonlinear continuum dynamic analyses of basement walls can be complex and is not a routine process. Therefore some engineers like to investigate the interaction between the wall and the backfill using p-y springs. Very little has been done to evaluate the effect of this spring approach compare to the continuum approach. Therefore, it would be worthwhile research project to evaluate the reliability of the p-y method.

Bibliography

AASHTO LRFD (2012), *Bridge design specifications*, 6th edn, American Association of State Highway and Transportation Officials, Washington, D.C.

Abrahamson, J., Bardet, R., Boulanger, J., Bray, Y., Chan, C., Chang, C. et al. (1999), 'Preliminary geotechnical earthquake engineering observations of the September 21, 1999, Chi-Chi, Taiwan earthquake'.

Abrahamson N.A. (1992), 'Non-stationary spectral matching', *Seismological research letters* **10**(1), 30.

Adams, J. and Halchuk, S. (2003), 'Open file 4459 - Fourth generation seismic hazard maps of Canada: values for over 650 Canadian localities intended for the 2005 National Building Code of Canada', *Geological Survey of Canada* .

Al Atik, L. (2008), Experimental and analytical evaluation of seismic earth pressures on cantilever retaining structures, PhD thesis, University of California, Berekeley.

Al Atik, L. and Abrahamson, N. (2010), 'An improved method for nonstationary spectral matching', *Earthquake Spectra* **26**(3), 601–617.

Al-Atik, L. and Sitar, N. (2007), Development of improved procedures for seismic design of buried and partially buried structures, Technical report, University of California, Berkeley. Final report on research supported by the San Francisco Bay Area Rapid Transit (BART) and the Santa Clara Valley Transportation Authority (VTA).

Al-Atik, L. and Sitar, N. (2009), Seismically induced lateral earth pressures: a new approach, *in* 'Proceedings of the 17th International Conference on Soil Mechanics and Geotechnical Engineering'.

Al-Atik, L. and Sitar, N. (2010), 'Seismic earth pressures on cantilever retaining structures', *Journal of Geotechnical and Geoenvironmental Engineering* **136**(10), 1324–1333.

Alavi, B. and Krawinkler, H. (2001), 'Effects of near-fault ground motions on frame structures', *John A. Blume Earthquake Engineering Center* .

Anderson, D. G., Martin, G. R., Lam, I. and Wang, J. N. (2008), *Seismic analysis and design of retaining walls, buried structures, slopes, and embankments*, NCHRP Report 611, Transportation Research Board, Washington, D.C.

Anderson, J., Bodin, P., Brune, J., Prince, J., Singh, S., Quaas, R. and Onate, M. (1986), 'Strong ground motion from the Michoacan, Mexico, earthquake', *Science* **233**(4768), 1043–1049.

Aoi, S., Obara, K., Hori, S., Kasahara, K. and Okada, Y. (2000), 'New strong-motion observation network: KiK-net', *EOS Trans. Am. Geophys. Union* **81**.

Archuleta, R. J., Steidl, J. and Squibb, M. (2006), 'The COSMOS virtual data center: A web portal for strong motion data dissemination', *Seismological Research Letters* **77**(6), 651–658.

Argyroudis, S., Kaynia, A. M. and Pitilakis, K. (2013), 'Development of fragility functions for geotechnical constructions: Application to cantilever retaining walls', *Soil Dynamics and Earthquake Engineering* **50**, 106–116.

Arulmoli, K. (2001), Earthquake simulation in geotechnical engineering: applications and research needs to improve atate of practice, *in* 'Proceedings of NSF International Workshop on Earthquake Simulation in Geotechnical Engineering', Cleveland, OH.

ASCE-TCBRD (2010), *Design of blast-resistant buildings in petrochemical facilities*, Task Committee on Blast-Resistant Design of the Petrochemical Committee of the Energy Division ASCE, 2nd edn, American Society of Civil Engineers, Reston, VA, USA.

ASCE/SEI 7-05 (2005), *Minimum design loads for buildings and other structures*, ASCE/SEI 7-05 edn, American Society of Civil Engineers, Reston, VA.

ASCE/SEI 7-10 (2010), *Minimum design loads for buildings and other structures*, ASCE/SEI 7-10 edn, American Society of Civil Engineers, Reston, VA.

Atkinson, G. M. (2009), 'Earthquake time histories compatible with the 2005 National Building Code of Canada uniform hazard spectrum', *Canadian Journal of Civil Engineering* **36**(6), 991–1000.

Atukorala, U., Puebla, H., Fernando, V., Yogendrakumar, Y., Wedge, N. and McCammon, N. (2008), Geotechnical earthquake engineering aspects of the design of foundations of the Vancouver convention center expansion project, *in* 'The 14th World Conference on Earthquake Engineering, Bejing, China'.

Baker, J. W. (2007), 'Quantitative classification of near-fault ground motions using wavelet analysis', *Bulletin of the Seismological Society of America* **97**(5), 1486–1501.

Baker, J. W. and Allin Cornell, C. (2006), 'Spectral shape, epsilon and record selection', *Earthquake Engineering & Structural Dynamics* **35**(9), 1077–1095.

Bazzurro, P. and Luco, N. (2006), Do scaled and spectrum-matched near-source records produce biased nonlinear structural responses, *in* 'Proceedings of 8th National Conference on Earthquake Engineering'.

Benuska, L. (1990), *Loma Prieta earthquake reconnaissance report*, Earthquake Engineering Research Institute.

Bertero, V. V., Mahin, S. A. and Herrera, R. A. (1978), 'Aseismic design implications of near-fault San Fernando earthquake records', *Earthquake engineering & structural dynamics* **6**(1), 31–42.

Bolt, B. A. and Gregor, N. J. (1993), Synthesized strong ground motions for the seismic condition assessment of the eastern portion of the san francisco bay bridge., Technical Report UCB/EERC-93/12.

Bolton, M. and Steedman, R. (1985), 'The behavior of fixed cantilever walls subject to lateral loading', *Application of Centrifuge Modeling to Geotechnical Design* .

Brandenberg, S. J., Mylonakis, G. and Stewart, J. P. (2015), 'Kinematic framework for evaluating seismic earth pressures on retaining walls', *Journal of Geotechnical and Geoenvironmental Engineering* **141**(7), 04015031/1–04015031/10.

Bray, J. D. and Rodriguez-Marek, A. (2004), 'Characterization of forward-directivity ground motions in the near-fault region', *Soil Dynamics and Earthquake Engineering* **24**(11), 815–828.

Britton, J., Harris, J., Hunter, J. and Luternauer, J. (1995), 'The bedrock surface beneath the Fraser River delta in British Columbia based on seismic measurements', *Current research* pp. 83–89.

Buratti, N., Stafford, P. J. and Bommer, J. J. (2010), 'Earthquake accelerogram selection and scaling procedures for estimating the distribution of drift response', *Journal of Structural Engineering* .

Callisto, L., Rampello, S. and Viggiani, G. M. (2013), 'Soil–structure interaction for the seismic design of the Messina Strait bridge', *Soil Dynamics and Earthquake Engineering* **52**, 103–115.

CAN/CSA-A23.3-04 (2004), *Design of concrete structures*, Canadian Standards Association, Mississauga, Ontario, Canada. Reaffirmed in 2010.

CAN/CSA-S6-06 (2014), *Canadian Highway Bridge Design Code*, Canadian Standards Association, Mississauga, Ontario, Canada.

Candia, G. A. (2013), Experimental and numerical modeling of seismic earth pressures on retaining walls with cohesive backfills, PhD thesis, University of California, Berkeley.

Carballo, J. E. and Cornell, C. A. (2000), Probabilistic seismic demand analysis: spectrum matching and design, Technical Report RMS-41.

CBC (2010), *International Building Code*, International Code Council (ICC), Country Clunb Hills, IL, USA.

Chiou, B., Darragh, R., Gregor, N. and Silva, W. (2008), 'NGA project strong-motion database', *Earthquake Spectra* **24**(1), 23–44.

Clague, J. J. (2002), 'The earthquake threat in southwestern British Columbia: A geologic perspective', *Natural Hazards* **26**(1), 7–33.

Clayton, C. and Symons, I. (1992), 'The pressure of compacted fill on retaining walls', *Géotechnique* **42**(1), 127–130.

Clough, G. and Fragaszy, R. (1977), 'A study of earth loadings on floodway retaining structures in the 1971 San Fernando Valley earthquake', *Proceeding, 6th World Conference on Earthquake Engineering* **3**.

Comodromos, E. M. and Pitilakis, K. D. (2005), 'Response evaluation for horizontally loaded fixed-head pile groups using 3-D non-linear analysis', *International journal for numerical and analytical methods in geomechanics* **29**(6), 597–625.

Conti, R., Madabhushi, G. and Viggiani, G. (2012), 'On the behaviour of flexible retaining walls under seismic actions', *Géotechnique* **62**(12), 1081–1094.

Coulomb, C. (1776), ‘Essai sur une application des regies des maximis et minimis a quelques problemes de statique relatifs a l’architecture’, *Memoires de l’Academie Royale pres Divers Savants* **7**.

Cundall, P. (2006), A simple hysteretic damping formulation for dynamic continuum simulations, *in* ‘Proceedings of the 4th International FLAC Symposium on Numerical Modeling in Geomechanics. Minneapolis: Itasca Consulting Group’.

Darendeli, M. B. (2001), Development of a new family of normalized modulus reduction and material damping curves, PhD thesis, The University of Texas at Austin.

Darragh, B., Silva, W. and Gregor, N. (2004), Strong motion record processing for the PEER center, *in* ‘Proceedings of COSMOS Invited Workshop on Strong-Motion Record Processing, Richmond, Calif, USA’, pp. 26–27.

Das, B. M. (1992), *Principles of soil dynamics*, PWS-KENT Publishing Company.

Day, R. and Potts, D. (1998), ‘The effect of interface properties on retaining wall behaviour’, *International journal for numerical and analytical methods in geomechanics* **22**(12), 1021–1033.

DeVall, R. (2011), Calculation of the nominal moment and shear capacities of basement walls designed for different fractions of NBCC (2010) PGA. Personal Communication.

DeVall, R. and Adebar, P. (2011), Performance criterion for typical 4-level basement wall based on curvature demand. Personal Communication.

DeVall, R., Finn, W. L., Byrne, P., Anderson, D., Naesgaard, E., Amini, A., Taiebat, M., Wallis, D., Kokan, M., Mutrie, J. and Simpson, R. (2010), Seismic design of basement walls in British Columbia. Personal Communication.

DeVall, R., Wallis, D., Finn, W. L., Taiebat, M. and Amirzehni, E. (2014), Seismic design of basement walls in British Columbia - current state of practice. Personal Communication.

Dewoolkar, M., Ko, H. and Pak, R. (2001), ‘Seismic behavior of cantilever retaining walls with liquefiable backfills’, *Journal of Geotechnical and Geoenvironmental Engineering, ASCE 127* **5**, 424–435.

Duncan, J. M. and Seed, R. B. (1986), ‘Compaction-induced earth pressures under k_0-conditions’, *Journal of Geotechnical Engineering* **112**(1), 1–22.

EduPro Civil Systems Inc. (2003), 'ProSHAKE: ground response analysis program, version 1.12, Sammamish, WA', http://www.proshake.com.

Eurocode8-EN1998-5 (2004), 'Design of structures for earthquake resistance part 5: Foundations, retaining structures and geotechnical aspects', *European Committee for Standardization* .

Federal Emergency Management Agency, FEMA P695 (2009), 'Quantification of building seismic performance factors'.

Federal Highway Administration (FHWA) (1997), Design guidance: Geotechnical earthquake engineering for highways, Volume 1 Design Principles Report No. FHWA-SA-97-076, US Department of Transportation, Washangton, DC.

Finn, W. (2000), 'State-of-the-art of geotechnical earthquake engineering practice', *Soil Dynamics and Earthquake Engineering* **20**(1), 1–15.

Finn, W. L. and Wightman, A. (2003), 'Ground motion amplification factors for the proposed 2005 edition of the National Building Code of Canada', *Canadian Journal of Civil Engineering* **30**(2), 272–278.

Finn, W., Ventura, C. E., Onur, T. and Atkinson, G. (2000), A study of seismic risk in south-western British Columbia, *in* 'Proceedings of the 6th International Conference on Seismic Zonation, Palm Springs, CA, USA'.

Gazetas, G., Gerolymos, N. and Anastasopoulos, I. (2005), 'Response of three Athens metro underground structures in the 1999 Parnitha earthquake', *Soil Dynamics and Earthquake Engineering* **25**(7), 617–633.

Gazetas, G., Psarropoulos, P., Anastasopoulos, I. and Gerolymos, N. (2004), 'Seismic behaviour of flexible retaining systems subjected to short-duration moderately strong excitation', *Soil Dynamics and Earthquake Engineering* **24**(7), 537–550.

Geraili Mikola, R. (2012), Seismic earth pressures on retaining structures and basement walls in cohesionless soils, PhD thesis, University of California, Berekeley.

Gil, L., Hernandez, E. and De la Fuente, P. (2001), 'Simplified transverse seismic analysis of buried structures', *Soil dynamics and earthquake engineering* **21**(8), 735–740.

Grant, D. N. and Diaferia, R. (2013), 'Assessing adequacy of spectrum-matched ground motions for response history analysis', *Earthquake Engineering & Structural Dynamics* **42**(9), 1265–1280.

Green, R. A., Olgun, C. G., Ebeling, R. M. and Cameron, W. I. (2003), ‘Seismically induced lateral earth pressures on a cantilever retaining wall’, *Earthquake Engineering* pp. 946–955.

Hall, J. F. (1995), ‘Northridge earthquake of January 17, 1994, reconnaissance report, vol. 1’, *Earthquake Spectra* **11**.

Hancock, J., Bommer, J. J. and Stafford, P. J. (2008), ‘Numbers of scaled and matched accelerograms required for inelastic dynamic analyses’, *Earthquake Engineering & Structural Dynamics* **37**(14), 1585–1607.

Hancock, J., Watson-Lamprey, J., Abrahamson, N. A., Bommer, J. J., Markatis, A., McCOYH, E. and Mendis, R. (2006), ‘An improved method of matching response spectra of recorded earthquake ground motion using wavelets’, *Journal of Earthquake Engineering* **10**(1), 67–89.

Hardin, B. and Drnevich, V. (1972), ‘Shear modulus and damping in soils: Design equations and curves’, *Journal of Soil Mechanics and Foundations Division, ASCE* **98**(6), 667–692.

Hardin, B., Drnevich, V., Wang, J. and Sams, C. (1994), Resonant column testing at pressures up to 3.5 MPa (500 psi), *in* ‘Dynamic geotechnical testing II’, pp. 222–233.

Hashash, Y. M., Hook, J. J., Schmidt, B., John, I. and Yao, C. (2001), ‘Seismic design and analysis of underground structures’, *Tunnelling and Underground Space Technology* **16**(4), 247–293.

Hashash, Y. M. and Park, D. (2001), ‘Non-linear one-dimensional seismic ground motion propagation in the Mississippi embayment’, *Engineering Geology* **62**(1), 185–206.

Heo, Y., Kunnath, S. K. and Abrahamson, N. (2010), ‘Amplitude-scaled versus spectrum-matched ground motions for seismic performance assessment’, *Journal of Structural Engineering* **137**(3), 278–288.

Holmes, W. T. and Somers, P. (1996), ‘Northridge earthquake reconnaissance report, vol. 2’, *Earthquake Spectra* **11**, 229–31.

Holzer, T. L. (1994), ‘Loma Prieta damage largely attributed to enhanced ground shaking’, *Eos, Transactions American Geophysical Union* **75**(26), 299–301.

Holzer, T. L., Bennett, M. J., Ponti, D. J. and Tinsley III, J. C. (1999), ‘Liquefaction and soil failure during 1994 Northridge earthquake’, *Journal of Geotechnical and Geoenvironmental Engineering* **125**(6), 438–452.

Huang, C.-C. (2000), 'Investigations of soil retaining structures damaged during the Chi-Chi (Taiwan) earthquake', *Journal of the Chinese Institute of Engineers* **23**(4), 417–428.

Huang, Y.-N., Whittaker, A. S., Luco, N. and Hamburger, R. O. (2011), 'Scaling earthquake ground motions for performance-based assessment of buildings', *Journal of Structural Engineering* **137**(3), 311–321.

Hunter, J. and Christian, H. (2001), Use of shear wave velocities to estimate thick soil amplification effects in the Fraser River delta, British Columbia, *in* 'Symposium Proceedings on the Application of Geophysics to Engineering and Environmental Problems'.

Hunter, J., Christian, H., Harris, J., Britton, J. and Luternauer, J. (1999), Mapping shear wave velocity structure beneath the Fraser River delta sediments, preliminary results, *in* 'Proceedings 8th Canadian Conference on Earthquake Engineering', pp. 101–106.

IBC (2009), *International Building Code*, International Code Council (ICC), Country Clunb Hills, IL, USA.

Ichihara, M. and Matsuzawa, H. (1973), 'Earth pressure during earthquake', *Soils and Foundations* **13**(4), 75–86.

Ishibashi, I. and Zhang, X. (1993), 'Unified dynamic shear moduli and damping ratios of sand and clay', *Soils and Foundations* **33**(1), 182–191.

Itasca (2012), *FLAC: Fast Lagrangian Analysis of Continua, version 7.0*, Itasca Consulting Group, Inc., Minneapolis, Minnesota.

Iwasaki, T., Tatsuoka, F. and Takagi, Y. (1978), 'Shear moduli of sands under cyclic torsional shear loading', *Soils and Foundations* **18**(1), 39–56.

Jaky, J. (1944), 'The coefficient of earth pressure at rest', *Journal of the Society of Hungarian Architects and Engineers* **78**(22), 355–358.

Jaky, J. (1948), Pressure in silos, *in* 'Proceedings of the 2nd international conference on soil mechanics and foundation engineering', Vol. 1, pp. 103–107.

Jones, K. C. (2013), Dynamic soil-structure-soil-interaction analysis of structures in dense urban environments, PhD thesis, University of California, Berkeley.

Kalkan, E. and Chopra, A. K. (2010), 'Practical guidelines to select and scale earthquake records for nonlinear response history analysis of structures', *US Geological Survey Open-File Report* **1068**(2010), 126.

Kalkan, E. and Kunnath, S. K. (2006), ‘Effects of fling step and forward directivity on seismic response of buildings’, *Earthquake Spectra* **22**(2), 367–390.

Kinoshita, S. (1998), ‘Kyoshin net (K-net)’, *Seismological Research Letters* **69**(4), 309–332.

Kokusho, T. (1980), ‘Cyclic triaxial test of dynamic soil properties for wide strain range’, *Soils and Foundations* **20**(2), 45–60.

Koseki, J., Tatsuoka, F., Munaf, Y., Tateyama, M. and Kojima, K. (1998), ‘Technical note-a modified procedure to evaluate active earth pressure at high seismic loads’, *Soils and Foundations* **38**, 209–216.

Kottke, A. R. (2010), A comparison of seismic site response methods, PhD thesis, The University of Texas at Austin.

Kramer, S. L. (1996), *Geotechnical Earthquake Engineering*, Prentice Hall, Inc, Upper Saddle River, New Jersey.

Kuhlemeyer, R. L. and Lysmer, J. (1973), ‘Finite element method accuracy for wave propagation problems’, *Journal of Soil Mechanics & Foundations Div* **99**(Tech Rpt).

Kurama, Y. and Farrow, K. (2003), ‘Ground motion scaling methods for different site conditions and structure characteristics’, *Earthquake engineering & structural dynamics* **32**(15), 2425–2450.

Laird, J. and Stokoe, K. (1993), ‘Dynamic properties of remolded and undisturbed soil samples test at high confining pressure’, *GR93-6, Electrical Power Research Institute* .

Lam, I. and Martin, G. R. (1986), Seismic design of highway bridge foundations - design procedures and guidelines, Technical Report FHWA/RD-86/102, Federal Highway Administration, Washington, D.C., USA.

LATBSDC (2014), *An alternative procedure for seismic analysis and design of tall buildings located in the Los Angeles region*, Task Committee on Blast-Resistant Design of the Petrochemical Committee of the Energy Division ASCE, 2014 edition with 2015 supplements edn, Los Angeles Tall Buildings Structural Design Council.

Levson, V. M., Matysek, P. F., Monahan, P. A. and Watts, B. D. (2003), Earthquake hazard mapping in British Columbia: status, demand and methodology development, *in* ‘Proceedings of Earthquake Hazard Mapping for Land Use and Emergency Planning’, pp. 37–51.

Lew, M. (2012), ‘Recent findings on seismic earth pressures’, *The Structural Design of Tall and Special Buildings* **21**, S48–S65.

Lew, M., Simantob, E. and Hudson, M. B. (1995), Performance of shored earth retaining systems during the January 17, 1994, Northridge earthquake, *in* ‘Third International Conference on Recent Advances in Geotechnical Earthquake Engineering and Soil Dynamics (1981: April 2-7; St. Louis, Missouri)’, Missouri S&T (formerly the University of Missouri–Rolla).

Lew, M., Sitar, N. and Al-Atik, L. (2010a), Seismic earth pressures: fact or fiction?, *in* ‘Proceedings of the 2010 Earth Retention Conference’, ASCE, Bellevue, Washington, pp. 656–673.

Lew, M., Sitar, N., Al-Atik, L., Pourzanjani, M. and Hudson, M. B. (2010b), Seismic earth pressures on deep building basements, *in* ‘SEAOC Convention Proceedings’, Structural Engineers Association of California, pp. 1–12.

Lilhanand, K. and Tseng, W. S. (1989), Development and application of realistic earthquake time histories compatible with multiple-damping design spectra, *in* ‘Proceedings of the 9th World conference on Earthquake Engineering, Tokyo-Kyoto, Japan’, Vol. 2, pp. 819–830.

Luco, N. and Cornell, C. A. (2007), ‘Structure-specific scalar intensity measures for near-source and ordinary earthquake ground motions’, *Earthquake Spectra* **23**(2), 357–392.

Lysmer, J. and Kuhlemeyer, R. (1969), ‘Finite dynamic model for infinite media’, *ASCE Journal of Engineering Mechanics Division* pp. 859–877.

Makris, N. and Black, C. J. (2003), *Dimensional analysis of inelastic structures subjected to near fault ground motions*, Earthquake Engineering Research Center, University of California.

Mánica, M., Ovando, E. and Botero, E. (2014), ‘Assessment of damping models in FLAC’, *Computers and Geotechnics* **59**, 12–20.

Martinez-Rueda, J. E. (1998), ‘Scaling procedure for natural accelerograms based on a system of spectrum intensity scales’, *Earthquake Spectra* **14**(1), 135–152.

McGuire, R. K. (1995), ‘Probabilistic seismic hazard analysis and design earthquakes: closing the loop’, *Bulletin of the Seismological Society of America* **85**(5), 1275–1284.

Mehanny, S. S. F. and Deierlein, G. G. (1999), Modeling and assessment of seismic performance of composite frames with reinforced concrete columns and steel beams, PhD thesis, Stanford University.

Mejia, L. and Dawson, E. (2006), Earthquake deconvolution for FLAC, *in* Hart and Varona, eds, 'Proceedings of Fourth International FLAC Symposium on Numerical Modeling in Geomechanics', Itasca Consulting Group Inc., Minneapolis, MN, pp. Paper 04–10.

Michaud, D. and Léger, P. (2014), 'Ground motions selection and scaling for nonlinear dynamic analysis of structures located in Eastern North America', *Canadian journal of civil engineering* **41**(3), 232–244.

Miranda, E. (1993), 'Evaluation of site-dependent inelastic seismic design spectra', *Journal of Structural Engineering* **119**(5), 1319–1338.

Monahan, P. A. (2005), 'Soil hazard map of the Lower Mainland of British Columbia for assessing the earthquake hazard due to lateral ground shaking', *Monahan Petroleum Consulting* .

Mononobe, N. and Matsuo, H. (1929), On the determination of earth pressures during earthquakes, *in* 'Proceedings of World Engineering Conference', pp. 176–182.

Murphy, L. M. (1973), *San Fernando, California, earthquake of February 9, 1971*, Vol. 3, U.S. Department of Commerce, Whashangton, D.C.

Naesgaard, E. (2011), A hybrid effective stress–total stress procedure for analyzing soil embankments subjected to potential liquefaction and flow, PhD thesis, University of British Columbia.

Natural Resources Canada (2012), 'Geological Survey of Canada (GSC)', http://www.nrcan.gc.ca/earth-sciences/science/geology/gsc/17100. Online; accessed: May 2012.

Nau, J. M. and Hall, W. J. (1984), 'Scaling methods for earthquake response spectra', *Journal of Structural Engineering* .

NBCC (1995), *National Building Code of Canada*, Institute for Research in Construction, National Research Council of Canada, Ottawa, ON, Canada.

NBCC (2005), *National Building Code of Canada*, Institute for Research in Construction, National Research Council of Canada, Ottawa, ON, Canada.

NBCC (2010), *National Building Code of Canada*, Institute for Research in Construction, National Research Council of Canada, Ottawa, ON, Canada.

NEHRP (2000), *NEHRP recommended provisions for seismic regulations for new buildings and other structures; Part 2: Commentary (FEMA 369)*, National Earthquake Hazards Reduction Program, Washington D.C., USA.

NEHRP (2003), *NEHRP recommended provisions for seismic regulations for new buildings and other structures; Part 2: Commentary (FEMA 450-2)*, National Earthquake Hazards Reduction Program, Washington D.C., USA.

NEHRP (2009), *NEHRP recommended provisions for seismic regulations for new buildings and other structures; Part 2: Commentary (FEMA P-750)*, National Earthquake Hazards Reduction Program, Washington D.C., USA.

NEHRP (2011), Selecting and scaling earthquake ground motions for performing response-history analyses, Technical Report Prepared for the National Institute of Standards and Technology NIST GCR 11-917-15, National Earthquake Hazards Reduction Program (NEHRP) Consultants Joint Venture, Redwood City, California.

Okabe, S. (1924), 'General theory on earth pressure and seismic stability of retaining walls and dams', *Proceedings of the Japan Society of Civil Engineers* **10**(6), 1277–1330.

Okabe, S. (1926), 'General theory of earth pressure', *Proceedings of the Japan Society of Civil Engineers* **12**(1), 123–134.

Onur, T. (2001), Seismic risk assessment in south-western British Columbia, PhD thesis, University of British Columbia.

Ortiz, L., Scott, R. and Lee, J. (1983), 'Dynamic centrifuge testing of a cantilever retaining wall', *Earthquake Engineering and Structural Dynamics* **11**, 251–268.

Ostadan, F. (2005), 'Seismic soil pressure for building walls: An updated approach', *Soil Dynamics and Earthquake Engineering* **25**(7), 785–793.

Ostadan, F. and White, W. (1998), Lateral seismic soil pressure an updated approach, *in* 'US-Japan SSI Workshop', United States Geologic Survey, Menlo Park, CA.

Park, R. and Pauly, T. (1975), *Reinforced concrete structures*, John Wiley & Sons, Inc., USA.

PEER (accessed on January 2013), 'Pacific Earthquake Engineering Research Center strong motion database', http://peer.berkeley.edu/peer_ground_motion_database.

PEER (accessed on November 2014), 'Pacific Earthquake Engineering Research Center strong motion database', http://peer.berkeley.edu/peer_ground_motion_database.

Pina, F. E. (2010), Methodology for the seismic risk assessment of low-rise school buildings in British Columbia, PhD thesis, University of British Columbia.

Pina, F., Ventura, C., Taylor, G. and Finn, W. (2010), Selection of ground motions for the seismic risk assessment of low-rise school buildings in south-western British Columbia, Canada, *in* 'Proceedings of the Ninth U.S. National and Tenth Canadian Conference on Earthquake Engineering', Toronto, ON, Canada. Paper ID: 1624, 10 pages.

Prakash, S. (1981), *Soil dynamics*, McGraw-Hill New York.

Prakash, S. and Basavanna, B. (1969), Earth pressure distribution behind retaining wall during earthquake, *in* 'Proceedings of the Fourth World Conference on Earthquake Engineering', Santiago, Chile.

Psarropoulos, P., Klonaris, G. and Gazetas, G. (2005), 'Seismic earth pressures on rigid and flexible retaining walls', *Soil Dynamics and Earthquake Engineering* **25**(7), 795–809.

Rayhani, M., Naggar, E. and Hesham, M. (2008), 'Numerical modeling of seismic response of rigid foundation on soft soil', *International Journal of Geomechanics* **8**(6), 336–346.

Reyes, J. C. and Kalkan, E. (2011), 'Required number of records for ASCE/SEI 7 ground motion scaling procedure', *US geological survey open-file report* **1083**(2011), 34.

Robertson, P., Woeller, D. and Finn, W. (1992), 'Seismic cone penetration test for evaluating liquefaction potential under cyclic loading', *Canadian Geotechnical Journal* **29**(4), 686–695.

Roesset, J. M. and Ettouney, M. M. (1977), 'Transmitting boundaries: a comparison', *International Journal for Numerical and Analytical Methods in Geomechanics* **1**(2), 151–176.

Rogers, G. (1998), 'Earthquakes and earthquake hazard in the Vancouver area', *Bulletin-Geological Survey of Canada* pp. 17–26.

S^2GM (accessed on March 2015), 'Selection and Scaling of Ground Motions, version 1.1', http://s2gm.hpcperformancedesign.com/.

Schnabel, P., Lysmer, J. and Seed, B. (1972), 'SHAKE, a computer program for earthquake response analysis of horizontally layered sites'. Report No. EERC 72-12.

SEAOC (2013), *SEAOC blue Book: Seismic design recommendations: Seismically induced lateral earth pressures on retaining structures and basement walls*, number Article 09.10.010, Structural Engineers Association of California, Sacramento, CA.

Seed, H. B. and Idriss, I. M. (1970), 'Soil moduli and damping factors for dynamic response analyses'.

Seed, H. and Whitman, R. (1970), Design of earth retaining structures for dynamic loads, *in* 'Specialty Conference, Lateral Stresses in the Ground and Design of Earth Retaining Structures', Cornell University, Ithaca, NY.

Seed, H., Wong, R., Idriss, I. and Tokimatsu, K. (1986), 'Moduli and damping factors for dynamic analyses of cohesionless soils', *Journal of Geotechnical Engineering* **112**(11), 1016–1032.

Seifried, A. and Baker, J. (2014), 'Spectral variability and its relationship to structural response estimated from scaled and spectrum-matched ground motions'.

Seismosoft (2009*a*), 'SeismoMatch, version 1.0.3', http://www.seismosoft.com/.

Seismosoft (2009*b*), 'SeismoSignal, version 4.1.2', http://www.seismosoft.com/.

Sherif, M. and Fang, Y. (1984), 'Dynamic earth pressures on walls rotating about the top', *Soils and Foundations* **24**(4), 109–117.

Sherif, M., Ishibashi, I. and Lee, C. (1982), 'Earth pressures against rigid retaining walls', *Journal of the Geotechnical Engineering Division* **108**(5), 679–695.

Shome, N. and Cornell, C. A. (1998), Normalization and scaling accelerograms for nonlinear structural analysis, *in* 'Sixth US National Conference on Earthquake Engineering, Seattle, WA'.

Shome, N., Cornell, C. A., Bazzurro, P. and Carballo, J. E. (1998), 'Earthquakes, records, and nonlinear responses', *Earthquake Spectra* **14**(3), 469–500.

Sitar, N., Mikola, R. G. and Candia, G. (2012), Seismically induced lateral earth pressures on retaining structures and basement walls, *in* 'Geotechnical Engineering State of the Art and Practice, GeoCongress 2012', ASCE, pp. 335–358.

Somerville, P. G., Smith, N. F., Graves, R. W. and Abrahamson, N. A. (1997), 'Modification of empirical strong ground motion attenuation relations to include the amplitude and duration effects of rupture directivity', *Seismological Research Letters* **68**(1), 199–222.

Stadler, A. (1996), Dynamic centrifuge testing of cantilever retaining walls, PhD thesis, University of Colorado at Boulder.

Steedman, R. S. and Zeng, X. (1990), 'The influence of phase on the calculation of pseudo-static earth pressure on a retaining wall', *Gotechnique* **40**(1), 103–112.

Steedman, R. and Zeng, X. (1991), 'Centrifuge modeling of the effects of earthquakes on free cantilever walls', *Centrifuge'91, Ko (ed.), Rotterdam: Balkema* .

Stewart, J. P., Bray, J. D., Seed, R. B. and Sitar, N. (1994), *Preliminary report on the principal geotechnical aspects of the January 17, 1994 Northridge earthquake*, Vol. 94, Earthquake Engineering Research Center, University of California, Berkeley.

Task Force Report (2007), *Geotechnical design guidelines for buildings on liquefiable sites in accordance with NBCC 2005 for Greater Vancouver Region*.

Tokida, K., Matsuo, O. and Nakamura, S. (2001), Damage of earth retaining structures in the 1999 Chi-Chi, Taiwan earthquake, *in* 'Wind and Seismic Effects: The 32 nd Joint Meeting of the U.S.-Japan Cooperative Program in Natural Resources Panel on Wind and Seismic Effects', pp. 495–512.

Towhata, I. (2008), *Geotechnical earthquake engineering*, Springer Science & Business Media.

U.S. Army Corps of Engineers (USACE) (2009), *Selection of design earthquakes and associated ground motions, EC 1110-2-6000*, U.S. Army Corps of Engineers.

User Defined constitutive Models (UDM) for the Itasca codes (2015), http://www.itasca-udm.com.

Veletsos, A. S. and Younan, A. H. (1994*a*), 'Dynamic modeling and response of soil-wall systems', *Journal of geotechnical engineering* **120**(12), 2155–2179.

Veletsos, A. S. and Younan, A. H. (1997), 'Dynamic response of cantilever retaining walls', *Journal of Geotechnical and Geoenvironmental Engineering* **123**(2), 161–172.

Veletsos, A. and Younan, A. (1994*b*), 'Dynamic soil pressures on rigid vertical walls', *Earthquake Engineering & Structural Dynamics* **23**(3), 275–301.

Vidic, T., Fajfar, P. and Fischinger, M. (1994), 'Consistent inelastic design spectra: strength and displacement', *Earthquake Engineering & Structural Dynamics* **23**(5), 507–521.

Wang, G., Youngs, R., Power, M. and Li, Z. (2013), 'Design Ground Motion Library (DGML): An interactive tool for selecting earthquake ground motions', *Earthquake Spectra* .

White, T. W., Taylor, G. W., Ventura, C. E. and Finn, W. D. L. (2008), *Overview of the bridging guidelines for the seismic retrofit of BC schools*, chapter 116, pp. 1–13.

Whitman, R. V. (1991), Seismic design of earth retaining structures, *in* 'Proceedings of the Second International Conference on Recent Advances in Geotechnical Earthquake Engineering and Soil Dynamics', St. Louis, Missouri, USA, pp. 1767–1778.

Wood, J. H. (1973), Earthquake-induced soil pressures on structures, Technical Report EERL 73-05, Earthquake Engineering Research Laboratory - California Institute of Technology, Pasadena, CA, USA.

Youd, T. L., Bardet, J.-P. and Bray, J. D. (2000), 'Kocaeli, Turkey, earthquake of August 17, 1999 reconnaissance report', *Earthquake Spectra* **16**.

Younan, A. and Veletsos, A. S. (2000), 'Dynamic response of flexible retaining walls', *Earthquake engineering & structural dynamics* **29**(12), 1815–1844.

Appendix A

Foundation Walls

A.1 Wall physical properties

W1: 4-level basement wall: 3 @ 2.7 m, top @ 3.6 m

W2: 4-level basement wall: 3 @ 2.7 m, top @ 5.0 m

W3: 6-level basement wall: 5 @ 2.7 m, top @ 3.6 m

Table A.1: Physical properties of the foundation walls

	f'_c (MPa)	f_y (MPa)	thickness (mm)	d for M^+ (mm)	d for M^- (mm)
W1	30	400	250	250-50=200	215
W2	40	400	300	300-50=250	250
W3	40	400	300	300-50=250	250

A.2 Load cases

1. Static case: active soil pressure but not less than 20 kPa compaction load. Load factor=1.5

2. Earthquake case: active pressure without compaction load + appropriate %PGA earthquake load. Load factor=1.0

3. Design case (CAN/CSA-A23.3-04, 2004): the wall is designed for whichever of the above cases governs at any point in the wall. The governing case may change along the wall height. In no case is the flexural capacity lass than that provided by minimum reinforcement.

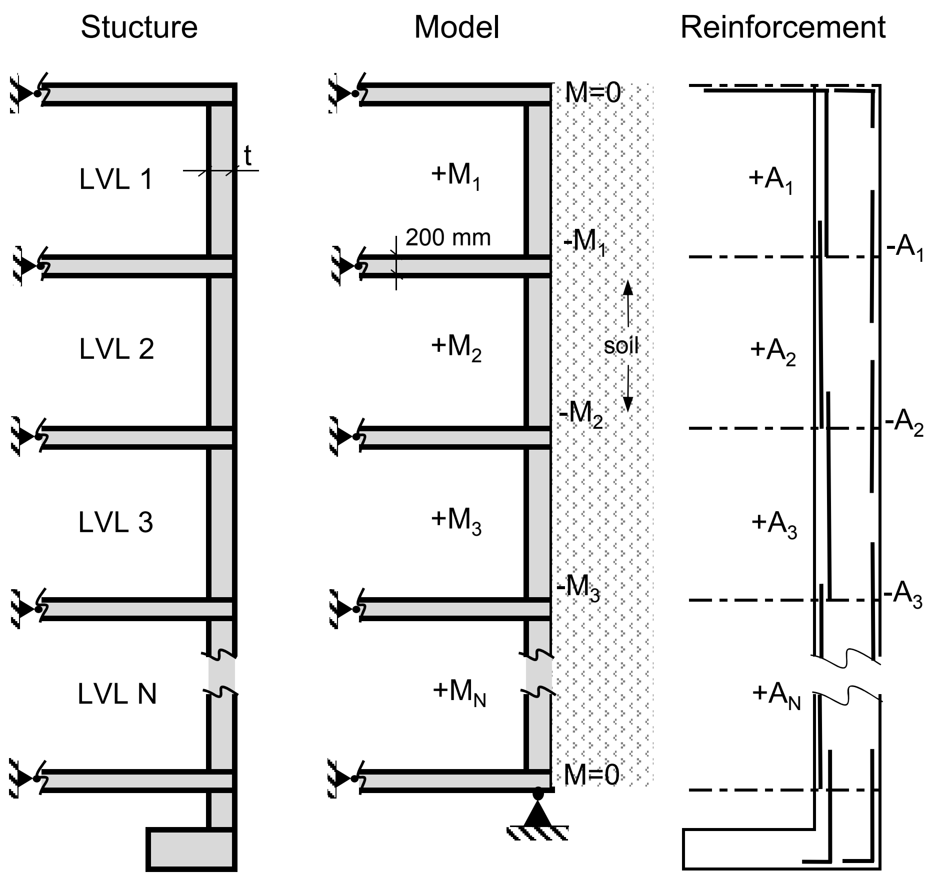

Figure A.1: The structural details of the model basement wall

In Figure A.1:

- Wall is continuous.
- Floors are 200 mm slabs, 3 m long, pinned at the end, $f'_c = 25\ MPa$ provides only ”nominal” fixity at wall to approximate pinned condition.

- 200 mm slab used to adjust wall "centre line" moments at slab/wall joint to wall "design" negative moments near top and bottom face of slab.

- Actual floor slab thickness and span lengths will vary from project to project, but for common conditions will only have a small effect on results.

- floor slabs are pinned at their ends but are fixed laterally.

- All results are for a 1 m length horizontally along the wall.

- The non-linear model that includes soil is not fixed laterally at the floors.

- The lower levels were modeled as a "box" and the floor slabs and end walls were modeled with shear and flexural stiffnesses. Various stiffnesses were assumed to develop supports for the support stiffnesses was undertaken early in this project. The effect on the foundation wall results was small and the stiffness that gave the most conservative result was used in the remainder of the study.

A.3 Moment capacity

- Calculated factored moments from governing load case $\times 1.3 \cong$ "nominal" flexural capacity.

- In no case are the moments less than the "nominal" flexural capacity based on minimum reinforcement requirements.

Table A.2: Nominal moment capacity $(kN-m/m)$ in W1

W1	Height (m)	Static No EQ.	50% PGA	60% PGA	70% PGA	80% PGA	90% PGA	100% PGA
LVL 1	3.6	0.0 +44.5 -44.5	0.0 +48.8 -59.9	0.0 +59.0 -70.6	0.0 +70.6 -82.1	0.0 +82.6 -95.5	0.0 +96.8 -109.7	0.0 +113.2 -126.2
LVL 2	2.7	-44.5 +44.5 -44.5	-59.9 +44.5 -44.5	-70.6 +44.5 -44.5	-82.1 +44.5 -44.5	-95.5 +44.5 -44.5	-109.7 +44.5 -44.5	-126.2 +44.5 -44.5
LVL 3	2.7	-44.5 +44.5 -70.3	-44.5 +44.5 -70.3	-44.5 +44.5 -70.3	-44.5 +44.5 -70.3	-44.5 +44.5 -70.3	-44.5 +44.5 -70.3	-44.5 +44.5 -70.3
LVL 4	2.7	-70.3 +63.2 0.0	-70.3 +63.2 0.0	-70.3 +63.2 0.0	-70.3 +63.2 0.0	-70.3 +63.2 0.0	-70.3 +63.2 0.0	-70.3 +63.2 0.0

Table A.3: $A_s(mm^2/m)$ in W1

W1	Height (m)	Static No EQ.	50% PGA	60% PGA	70% PGA	80% PGA	90% PGA	100% PGA
LVL 1	3.6	0.0 +500 -500	0.0 +529 -698	0.0 +635 -825	0.0 +762 -952	0.0 +909 -1121	0.0 +1015 -1311	0.0 +1248 -1524
LVL 2	2.7	-500 +500 -500	-698 +500 -500	-825 +500 -500	-952 +500 -500	-1121 +500 -500	-1311 +500 -500	-1524 +500 -500
LVL 3	2.7	-500 +500 -825	-500 +500 -825	-500 +500 -825	-500 +500 -825	-500 +500 -825	-500 +500 -825	-500 +500 -825
LVL 4	2.7	-825 +677 0.0	-825 +677 0.0	-825 +677 0.0	-825 +677 0.0	-825 +677 0.0	-825 +677 0.0	-825 +677 0.0

Table A.4: Nominal moment capacity $(kN-m/m)$ in W2

W2	Height (m)	Static No EQ.	50% PGA	60% PGA	70% PGA	100% PGA
LVL 1	5.0	0.0 +66.6 -83.8	0.0 +99.3 -119.0	0.0 +118.0 -139.0	0.0 +138.8 -161.0	0.0 +218.0 -245.6
LVL 2	2.7	-83.8 +65.0 -65.0	-119.0 +65.0 -65.0	-139.0 +65.0 -65.0	-161.0 +65.0 -65.0	-245.6 +65.0 -65.0
LVL 3	2.7	-65.0 +65.0 -77.0	-65.0 +65.0 -77.0	-65.0 +65.0 -77.0	-65.0 +65.0 -77.0	-65.0 +65.0 -77.0
LVL 4	2.7	-77.0 +66.0 0.0	-77.0 +66.0 0.0	-77.0 +66.0 0.0	-77.0 +66.0 0.0	-77.0 +66.0 0.0

Table A.5: $A_s(mm^2/m)$ in W2

W2	Height (m)	Static No EQ.	50% PGA	60% PGA	70% PGA	100% PGA
LVL 1	5.0	0.0 +615 -779	0.0 +927 -1119	0.0 +1109 -1316	0.0 +1314 -1537	0.0 +2122 -2414
LVL 2	2.7	-779 +600 -600	-1119 +600 -600	-1316 +600 -600	-1537 +600 -600	-2414 +600 -600
LVL 3	2.7	-600 +600 -711	-600 +600 -711	-600 +600 -711	-600 +600 -711	-600 +600 -711
LVL 4	2.7	-711 +611 0.0	-711 +611 0.0	-711 +611 0.0	-711 +611 0.0	-711 +611 0.0

Table A.6: Nominal moment capacity $(kN-m/m)$ in W3

W3	Height (m)	Static No EQ.	50% PGA	60% PGA	70% PGA	100% PGA
LVL 1	3.6	0.0 +65.0 -65.0	0.0 +65.0 -68.0	0.0 +78.9 -93.0	0.0 +103.0 -115.0	0.0 +155.0 -174.0
LVL 2	2.7	-65.0 +65.0 -65.0	-68.0 +65.0 -65.0	-93.0 +65.0 -65.0	-115.0 +65.0 -65.0	-174.0 +65.0 -65.0
LVL 3	2.7	-65.0 +65.0 -65.0	-65.0 +65.0 -65.0	-65.0 +65.0 -67.3	-65.0 +65.0 -73.8	-65.0 +65.0 -97.6
LVL 4	2.7	-65.0 +65.0 -65.0	-65.0 +65.0 -65.0	-67.3 +65.0 -65.0	-73.8 +65.0 -65.0	-97.6 +65.0 -65.0
LVL 5	2.7	-65.0 +65.0 -104.8	-65.0 +65.0 -104.8	-65.0 +65.0 -104.8	-65.0 +65.0 -104.8	-65.0 +65.0 -104.8
LVL 6	2.7	-104.8 +88.5 0.0	-104.8 +88.3 0.0	-104.8 +88.3 0.0	-104.8 +88.3 0.0	-104.8 +88.3 0.0

Table A.7: $A_s(mm^2/m)$ in W3

W3	Height (m)	Static No EQ.	50% PGA	60% PGA	70% PGA	100% PGA
LVL 1	3.6	0.0 +600 -600	0.0 +600 -624	0.0 +726 -860	0.0 +957 -1071	0.0 +1470 -1665
LVL 2	2.7	-600 +600 -600	-624 +600 -600	-860 +600 -600	-1071 +600 -600	-1665 +600 -969
LVL 3	2.7	-600 +600 -600	-600 +600 -600	-600 +600 -617	-600 +600 -679	-969 +600 -903
LVL 4	2.7	-600 +600 -600	-600 +600 -600	-617 +600 -600	-679 +600 -600	-903 +600 -600
LVL 5	2.7	-600 +600 -972	-600 +600 -972	-600 +600 -972	-600 +600 -972	-600 +600 -972
LVL 6	2.7	-972 +816 0.0	-972 +816 0.0	-972 +816 0.0	-972 +816 0.0	-972 +816 0.0

A.4 Shear capacity - CAN/CSA-A23.3-04 (2004)

Factored shear resistance at supports:

$$V_f = V_c = \phi_c \lambda \beta \sqrt{f_c'}\, b\, d_v \tag{A.1}$$

where, $\lambda = 1.0$, $\phi_c = 0.65$, $b = 1.0$, and $\beta = 0.21$

- For $t = 250\ mm$
  $d_v = 0.9 \times (250 - 50) = 180\ mm$
  $f_c' = 30\ Mpa$
  $V_f = V_c = 0.65 \times 0.21 \times \sqrt{30} \times 180 = 134.6\ kN/m$

- For $t = 300\ mm$
  $d_v = 0.9 \times (300 - 50) = 225\ mm$
  $f_c' = 40\ Mpa$
  $V_f = V_c = 0.65 \times 0.21 \times \sqrt{40} \times 225 = 194.2\ kN/m$

Table A.8: Nominal shear capacity

Wall	Factor Resistance (kN/m)	$\times 1.3$ (kN/m)	Nominal ($\times 1/0.65 = 1.54$) (kN/m)
250 mm	134.6	175	207
300 mm	194.2	252	299

- Walls designed for 100% PGA loading for shear.
- Shear at 50%, 60%, 70% PGA close to 100% PGA load.
- Shear reinforcement would be applied to wall to maintain thin wall thicknesses, if required.

A.5 Wall curvature and rotation capacity

Drift defined as: $\delta/(L/2) \equiv \theta$ in radians.

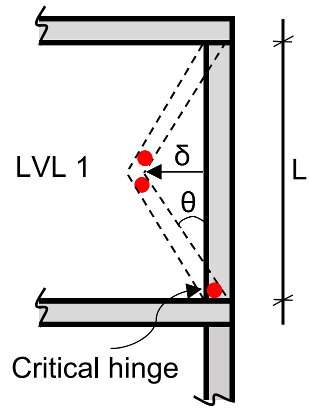

Figure A.2: Calculated θ capacity at governing section of the wall

Assumptions:

- ε_c maximum strain = 0.004.
- ε_s maximum strain = 0.05.
- ϕ_c taken as 1.0 (nominal concrete strength).
- f_y taken as 1.2×400 to approximate actual yield strength and some strain hardening.
- length of plastic hinges taken as $0.67 \times d$.
- Non-linear curve taken as elastic-perfectly plastic.

Table A.9: Drift limit

Wall	50% PGA	60% PGA	70% PGA	100% PGA
W1	0.033	0.027	0.023	0.014
W2	0.032	0.027	0.023	0.014
W3	0.035	0.035	0.034	0.020

Note:

- The recommendation by the ASCE Task Committee on Design of Blast-Resistant Buildings in Petrochemical Facilities (ASCE-TCBRD, 2010) for drift limit is 0.017 used as upper limit, which governs all of the above except for 100% PGA loads. However actual drifts for this case are very small and well within limits.

- $\varepsilon_s \leq 0.05$ cuts θ off at 0.035.